TUDelft

Delft University of Technology

Climatic Rating of Photovoltaic Modules: Different Technologies for Various Operating Conditions

Bonilla Castro, Johanna ; Schweiger, Markus ; Moser, David; Tanahashi, Tadanori ; King, Bruce H. ; Friesen, Gabi ; Haitao, Liu ; French, Roger H. ; Vogt, Malte Ruben; More Authors

Important note
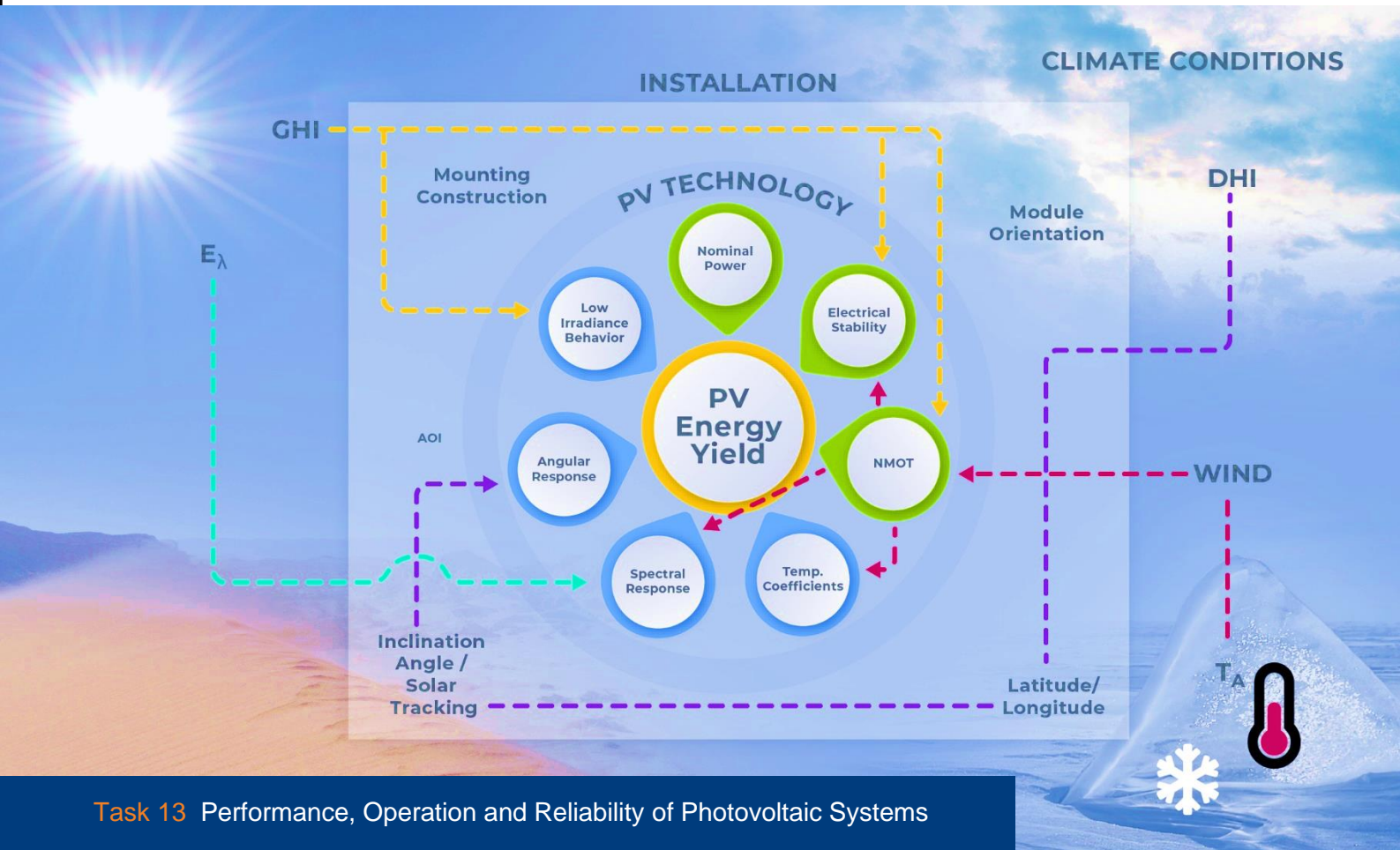To cite this publication, please use the final published version (if applicable).
Please check the document version above.

International Energy Agency
Photovoltaic Power Systems Programme

Task 13 Performance, Operation and Reliability of Photovoltaic Systems

PVPS

Climatic Rating of Photovoltaic Modules:
Different Technologies for Various Operating Conditions
2020

What is IEA PVPS TCP?

The International Energy Agency (IEA), founded in 1974, is an autonomous body within the framework of the Organization for Economic Cooperation and Development (OECD). The Technology Collaboration Programme (TCP) was created with a belief that the future of energy security and sustainability starts with global collaboration. The programme is made up of 6.000 experts across government, academia, and industry dedicated to advancing common research and the application of specific energy technologies.

The IEA Photovoltaic Power Systems Programme (IEA PVPS) is one of the TCP's within the IEA and was established in 1993. The mission of the programme is to "enhance the international collaborative efforts which facilitate the role of photovoltaic solar energy as a cornerstone in the transition to sustainable energy systems." In order to achieve this, the Programme's participants have undertaken a variety of joint research projects in PV power systems applications. The overall programme is headed by an Executive Committee, comprised of one delegate from each country or organisation member, which designates distinct 'Tasks,' that may be research projects or activity areas.

The IEA PVPS participating countries are Australia, Austria, Belgium, Canada, Chile, China, Denmark, Finland, France, Germany, Israel, Italy, Japan, Korea, Malaysia, Mexico, Morocco, the Netherlands, Norway, Portugal, South Africa, Spain, Sweden, Switzerland, Thailand, Turkey, and the United States of America. The European Commission, Solar Power Europe, the Smart Electric Power Alliance (SEPA), the Solar Energy Industries Association and the Cop- per Alliance are also members.

Visit us at: www.iea-pvps.org

What is IEA PVPS Task 13?

Within the framework of IEA PVPS, Task 13 aims to provide support to market actors working to improve the operation, the reliability and the quality of PV components and systems. Operational data from PV systems in different climate zones compiled within the project will help provide the basis for estimates of the current situation regarding PV reliability and performance.

The general setting of Task 13 provides a common platform to summarize and report on technical aspects affecting the quality, performance, reliability and lifetime of PV systems in a wide variety of environments and applications. By working together across national boundaries we can all take advantage of research and experience from each member country and combine and integrate this knowledge into valuable summaries of best practices and methods for ensuring PV systems perform at their optimum and continue to provide competitive return on investment.

Task 13 has so far managed to create the right framework for the calculations of various parameters that can give an indication of the quality of PV components and systems. The framework is now there and can be used by the industry who has expressed appreciation towards the results included in the high-quality reports.

The IEA PVPS countries participating in Task 13 are Australia, Austria, Belgium, Canada, Chile, China, Denmark, Finland, France, Germany, Israel, Italy, Japan, the Netherlands, Norway, Spain, Sweden, Switzerland, Thailand, and the United States of America.

INTERNATIONAL ENERGY AGENCY

PHOTOVOLTAIC POWER SYSTEMS PROGRAMME

IEA PVPS Task 13

Performance, Operation and Reliability of Photovoltaic Systems

Climatic Rating of Photovoltaic Modules: Different Technologies for Various Operating Conditions

Report IEA-PVPS T13-20:2020

December 2020

AUTHORS

Main Authors

Johanna Bonilla Castro, TÜV Rheinland, Cologne, Germany

Markus Schweiger, TÜV Rheinland, Cologne, Germany

David Moser, EURAC Research, Italy

Tadanori Tanahashi, AIST, Japan

Bruce H. King, Sandia National Laboratories, USA

Gabi Friesen, SUPSI, Switzerland

Liu Haitao, Institute of Electrical Engineering, CAS, China

Roger H. French, CWRU, USA

Laura S. Bruckman, CWRU, USA

Björn Müller, Fraunhofer ISE, Freiburg, Germany

Christian Reise, Fraunhofer ISE, Freiburg, Germany

Gabriele Eder, OFI, Austria

Wilfried van Sark, University of Utrecht, Netherlands

Yaowanee Sangpongsanon, CSSC, Thailand

Felipe Valencia, ATAMOSTEC, Chile

Joshua S. Stein, Sandia National Laboratories, USA

Contributing Authors

Ana Gracia-Amillo, Joint Research Centre (JRC), Ispra, Italy

Julián Ascencio-Vásquez, University of Ljubljana, Slovenia, now with: 3E, Brussels, Belgium

Carolin Ulbrich, PVcomB, Helmholtz-Zentrum Berlin, Berlin, Germany

Roland Valckenborg, TNO, Eindhoven, The Netherlands

Malte Ruben Vogt, ISFH, Germany, now with: TU Delft, Netherlands

James C. Blakesley, National Physical Laboratory (NPL), UK

Raymond J. Wieser, CWRU, USA

Elías Urrejola, ATAMOSTEC, Chile

Dorian Esteban Guzman Razo, Fraunhofer ISE, Freiburg, Germany

Editor

Ulrike Jahn, TÜV Rheinland, Cologne, Germany

TABLE OF CONTENTS

ACKNOWLEDGEMENTS

LIST OF ABBREVIATIONS

AC	Alternating current
AM	Air mass
AOI	Angle of Incidence
APE	Average photon energy
a-Si	Amorphous silicon
BG_{MOD}	Bifacial gain in terms of module DC yield
BG_{OPT}	Bifacial gain in terms of irradiance
BIPV	Building-integrated Photovoltaic (BIPV)
BiFi	Power gain per unit of rear irradiance for bifacial PV modules
BOS	Balance of system
CAPEX	Capital expenditures
CdTe	Cadmium telluride
CIGS	Copper indium gallium selenide
CSER	Climate specific energy rating
c-Si	Crystalline silicon
DC	Direct current
D_{POA}	Diffuse irradiance in plane of array
EQE	External quantum efficiency
ETA	PV module's efficiency
f	Front side of a bifacial PV module. $V_{oc,f}$, $P_{max,f}$, $I_{sc,fcancel}$
FF	Fill factor
G	Global irradiance
G_E	Equivalent irradiance (defined in IEC TS 60904-1-2)
G_{EFF}	Effective irradiance on a bifacial PV module (= G_{FRONT} + G_{REAR})
G_{POA}	Irradiance in the plane of the array (front side, also G_{FRONT})
G_{REAR}	Rear side irradiance
GPP	Green public procurement
GW	Gigawatt
HTJ	Heterojunction technology
I	Current in amper (A)
IEA	International Energy Agency
IEC	International Electrotechnical Commission
IMPP	Current at maximum power point

8

Isc	Current under short-circuit conditions. The peak current a solar panel can produce with its output shorted.
ITO	Indium tin oxide
I-V	Current voltage characteristic
KG/KGC	Köppen-Geiger climate zone (s)
KGPV	Köppen-Geiger-photovoltaic
LCOE	Levelised cost of Electricity
LPLA	Linear performance loss analysis
MPP	Maximum power point
MPR	Module performance ratio
r	Rear side of a bifacial PV module. $V_{OC,r}$, $P_{max,r}$ and $I_{sc,r}$
PSDA	Plataforma Solar del Desierto de Atacama
POA	Plane of array
PV	Photovoltaic
PR	Performance ratio
RTD	Real-time data
SR	Spectral response
SMM	Spectral mismatch
T/C	Thermocouple
T_{AMB}	Ambient air temperature
TOC	Total ozone column
UV	Ultraviolet radiation
UVA	UV-A radiation
UVB	UV-B radiation
V_{WIND}	Wind speed

EXECUTIVE SUMMARY

The photovoltaic (PV) energy rating is related to the energy yield performance of a PV module. Unlike the power rating, which is only related to the performance at a single operating point at 25°C, 1000 W/m^2, and AM1.5 spectrum (Standard Test Conditions, STC), the energy rating considers several characteristics of the PV module that affect the amount of energy produced: a) low irradiation behaviour b) temperature behaviour c) spectral response and d) angular response. These characteristics are also a function of climate and location conditions, vary over time, and differ widely from the STC. For the PV industry and its market players, accurate information on how much energy PV modules and systems can generate is crucial, and even more relevant than the power rating. In recent times the photovoltaic industry is moving from thinking about power (watt-peak) to thinking about energy (kWh), giving greater importance to the energy rating. Chapter 1 of this report examines the importance of energy classification in more detail and provides an overview of the state of the art in this area.

The energy rating aims to allow differentiation between PV modules according to their performance for typical locations. To this end, one of the most important international standardization bodies of the photovoltaic industry: The International Electrotechnical Commission (IEC), has designed the IEC 61853 series of standards *Photovoltaic (PV) module performance testing and energy rating* (Parts 1 to 4). The series provides guidelines and standardized procedures for the indoor and outdoor characterization of PV modules and the calculation of the climate-specific energy rating (CSER). The CSER is equivalent to the annual performance ratio of the PV module for a specific climate.

Part 1 deals with the measurement of PV module performance under variable irradiance and module temperature (G-T or power matrix). Part 2 contains the measurement procedures of the angular response (AR), the spectral response (SR), and the nominal module operating temperature (NMOT) of the PV modules. Part 3 lays down a methodology for the calculation of the CSER value, which uses the results from Parts 1, 2 and 4 (reference climate data sets) as input data. Currently, six climate data sets are available (temperate continental, temperate coastal, tropical humid, subtropical arid, subtropical coastal, high elevation), all of which comprise a time series of hourly data of meteorological parameters for a complete year.
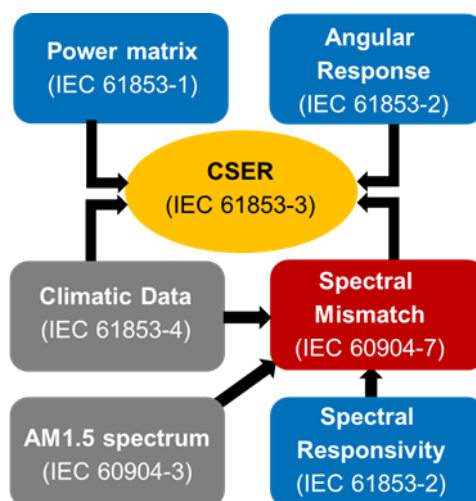
Figure 1: Methodology of IEC 61853 series for climate specific energy rating (Source: TÜV Rheinland Group).

Part 1 and Part 2 of IEC 61853 series will be discussed in Chapter 2. Specifically, Chapters 2.1 and 2.2 briefly describe the procedures for indoor measurement with a solar simulator, which is the most common practice in the PV industry. Nevertheless, procedures for outdoor measurements are also outlined in international standards and, among other advantages, can fully benefit from realistic thermal operating conditions, which is why they are discussed in Chapter 2.3. Here, Section 2.3.1 presents an approach for characterizing PV modules using two-axis solar trackers at outdoor installations. In Section 2.3.2, the challenges of the continuum cooperating conditions are addressed by extracting the IEC 61853-1 matrix from one-full year outdoor data including periods of non-optimal weather conditions. For practical purposes, Chapter 2.4 gives insights into an online dataset of nine PV modules tested according to IEC 61853 at an accredited laboratory. The new kWh thinking has not only increased the role of energy rating but has also opened the market to new technologies, such as bifacial PV modules. With this, new measuring procedures have been developed. Chapter 2.5 provides an overview of the current status of bifacial power output characterization.

It is not possible to talk about energy rating, without addressing climate classification and the efforts to understand the impact of climate on the performance and degradation of PV technologies. Therefore, Chapter 3 covers the energy meteorology in PV technologies. Chapter 3.1 discusses the most popular scheme supporting the PV community, the Köppen-Geiger (KG) climate classification, and presents other approaches to include additional photovoltaic-relevant climate variables (global irradiance, UV irradiance, and wind speed) such as the Photovoltaic Degradation Climate Zones (PVCZ), the Köppen-Geiger-Photovoltaic (KGPV) and a scheme for indoor aging testing (Project Infinity). Besides the irradiance and the temperature, the spectral distribution is one of the main influencing factors on the performance of a given PV technology, since the spectral distribution of a certain location differs from the reference global spectral irradiance defined in IEC 60904-3. Chapter 3.2 discusses this matter. Chapter 3.3 evaluates the data sets proposed by the IEC 61853-4, which contain: hourly values over a year of ambient temperature, wind speed, satellite-retrieved irradiance data of horizontal global and beam broadband irradiance, in-plane global and beam broadband irradiance, and spectrally resolved in-plane global irradiance integrated into 29 spectral bands. To give an overview of the challenges of normalizing particular climatic conditions, the case of the Atacama Desert is presented in Chapter 3.4. The comprehensive characterization required for PV technologies operating in such a harsh climate (i.e. UV radiation), is also discussed.

Chapter 4 constitutes the core of this report, as it not only explains in detail the IEC methodology for the determination of the CSER but also explains the existing approaches and practices established by recognized solar institutes. Chapter 4.1 describes step by step, the calculation of the CSER parameter using the IEC 61853-3 methodology. Even when given the equations and procedures for energy rating, practical implementation could be still challenging. Chapter 4.2 addresses this issue by presenting the results of round-robin among ten solar institutes. By using the same PV module laboratory input (Part 1 and 2 of the IEC 61853), each institution was asked to calculate the CSER. After several phases of harmonizing methods and excluding outliers, differences in the CSER value were still found amongst participants.

When it comes to measurements, whether in the laboratory or outdoors, some factors play an important role in decision making from a practical point of view: cost, time and accuracy. The reduction of measurements for the G-T matrix and the impact on the accuracy of the rating is discussed in Chapter 4.3. This reduction is not only a cost mitigation alternative but also a solution when the testing equipment does not allow measurement of the full matrix due to limitations in irradiance or temperature settings.

The need for an energy rating has caused different procedures to be developed independently by solar research institutes. Some of them are discussed in this section. Chapter 4.4 presents the Sandia Array Performance Model, which is a semi-empirical set of four principal equations that, when appropriately calibrated, reduces outdoor data into a set of coefficients that represent module performance at STC, which can be used to translate outdoor data to the IEC 61853-1 G-T matrix and be coupled with tabular weather data to perform energy predictions or ratings. Chapter 4.5 presents the approach of Fraunhofer ISE (Dirnberger et al. method), which relies on available historical data and technical datasheets of the PV module, instead of the extended laboratory measurements.

Chapter 4.6 presents the Linear Performance Loss Analysis (LPLA) from TÜV Rheinland. This approach relies on the measurements of Part 1 and Part 2 of the IEC 61853, climate datasets obtained from real measurements at outdoor locations, and equations to calculate the module performance ratio as a linear superposition of various meteorological factors. The scope of the IEC energy rating covers monofacial and single-junction PV devices, but its application cannot be easily extended to bifacial devices. These challenges and the proposal of two bifacial Standard Mounting Conditions (SMC) are discussed in Chapter 4.7.

Chapter 5 discusses issues that also need to be addressed, such as the application of energy rating to other promising PV solutions, for instance, Building-Integrated Photovoltaic (BIPV) and coloured modules. Throughout this report, the analysis has been maintained at the module level rather than the system level. Recognising how important this is, the last two sub-chapters discuss PV systems issues. Chapter 5.1 shows the results of a round robin test according to BIPV IEC 61853 with nine participating institutes from seven countries, which was carried out within the framework of the IEA PVPS Task 15.1 and in which globally identical modules, the same laboratory characterisation and a globally agreed methodology were used. Chapter 5.2 presents the results of a one-year study conducted by SUPSI PVLab, in which seven prototype modules of different colours were evaluated to understand the different technology and climatic factors impacting their real-world performance. Like any model, the IEC 61853 energy rating also has uncertainties from systematic and random errors, coming from the input data and the applied models. The main sources of uncertainties are discussed in Chapter 5.3.

The performance of photovoltaics depends on static metadata (i.e azimuth, tilt) and dynamic weather data. When it comes to obtaining global regional system performance data, Chapter 5.4 shows that, rather than finding annual performance data, a better approach is to obtain PV system metadata (module tilt and azimuth, installed capacity), and use representative, regionally resolved distributions to calculate specific annual performance distributions based on annually varying weather information. This approach could improve how national energy plans are established, installations are optimized, and give specific information about common regional installation practices. One of the biggest questions is what kind of information the energy rating has for the long-term run of PV modules and systems. To this end, it is important to understand the differences between energy rating, energy yield, and long-term performance assessment. This is discussed in Chapter 5.5. This chapter explores the long-term degradation of PV modules through a case study in Thailand.

As a whole, this report is a compendium of the current status of energy rating, ranging from input data on technologies (whether measured in the laboratory or outdoors) and on climate, to the description and evaluation of existing methods (IEC 61853 and from other solar research institutes). It also opens the discussion on the application of these methods in new technologies such as bifacial modules, BIPV and coloured PV, competitions on method uncertainties and evaluation at system level. The basic data sets for individual reader analysis are also provided.

1   INTRODUCTION

The energy generation from a photovoltaic (PV) module depends on the environmental conditions to which it is exposed during its lifetime. Usually, PV modules are tested at Standard Test Conditions (STC) where the electrical efficiency is often perceived as a conclusive indicator of their quality. STC rating is useful to compare the performance of different technologies in conditions which can be easily recreated in a laboratory environment, however it fails in giving accurate information on how much energy it can generate for long-term operations. The power output in field condition is mainly dependent on the irradiance, cell temperature, spectral response, and angle of incidence, which are functions of the time of the day, season, location and climatic conditions, and differ widely from STC conditions. Manufacturers should design PV modules optimized for various environmental conditions so that EPC contractors can choose between various options to optimize the performance of a PV plant. From a customer or investor point of view, PV module energy rating is more important than power rating. The energy rating of a module can be defined as the estimated DC energy generated in kWh per kWp per annum for a standard climate. The energy rating allows the customer to compare not only similar products from different manufacturers, but also completely different technologies. It should also provide a realistic estimated energy value for the region of installation and should be simple, accurate, repeatable, and agreed in terms of methodology for its calculation.

To include all the parameters affecting on the performance of a PV module in terms of energy generation, the International Electrotechnical Commission (IEC) has designed a standard IEC 61853 divided into four different parts. IEC 61853-1 is based on the effect of irradiance and temperature on the power rating; IEC 61853-2 deals with test procedures for measuring the effect of spectral response, incidence angle, and module operating temperature measurements, as well as the estimation of module temperature from irradiance, ambient temperature, and wind speed; IEC 61853-3 deals with the energy rating of PV modules; and IEC 61853-4 deals with climate data, which describes the standard periods and weather conditions that can be used for the energy rating calculations.

1.1 The Relevance of Energy Rating for LCOE of PV Systems and the PV Industry

As previously mentioned, from a PV installation and financing viewpoint, the energy produced during the operational lifetime is a key input element for the calculation of any economic indicator. The cost of photovoltaic electricity generation from different PV plants in the same climatic conditions can be benchmarked using the Levelised Cost of Electricity (LCOE). For the calculation of the LCOE, the most important parameters are of economic and financial nature (i.e. the Cost of Capital, the Capital Expenditures (CAPEX), and the Operational Expenditures (OPEX)) and of technical nature (i.e. lifetime, utilisation rate, degradation). The value of the LCOE is then used to determine whether a PV project is bankable or not also in comparison with other projects (e.g. in PPA tenders). However, PV modules are rated and sold according to their power measured at standard testing conditions (STC), and not based on their energy output during their lifetime. Consequently, scientists have worked on procedures to rate PV modules according to their output energy (or energy yield) rather than STC power. These procedures are usually referred to as "energy rating". The aim of the energy rating is to enable a significant differentiation between PV modules according to their yield for typical locations, so that users have better information for selecting the optimal module type for their purposes. The series of standards IEC 61853 aims to establish "IEC requirements for evaluating PV module performance based on power (watts), energy (watt-hours) and performance ratio". The IEC

requirements will support the needs during initial yield assessments in defining standard weather data sets covering different climatic regions and standard performance assessment at PV module level in terms of angle of incidence (AOI) effects, spectral response, and operating temperature.

The Energy Rating methodology has already proven itself as successful also in the recommendation given by the preparatory study for the feasibility of Ecodesign, Energy labelling, EU Ecolabel, and Green Public Procurement (GPP) requirements for PV modules and systems [1]. Specifically, the Ecodesign suggested requirements for modules electricity yield states that the module energy output (yield) expressed in kWh/kWp and calculated according to IEC 61853-3 for each of the three reference EU climate zones shall be declared by the manufacturer.

In Report Uncertainties in Yield Assessments [2] we have demonstrated the importance of the initial assumptions in a yield assessment with the choice in data input and modelling steps that can have a very important impact on the probability of exceedance, e.g. on the P50/P90 values. Although this is a clear indication of the importance of the internal knowledge and skills of each yield assessor in a particular climate and/or technology, a standardized approach in evaluating the energy output of PV modules could be beneficial in competing tenders and/or in situations where the main need of the investor/PV project developer is limited to the best choice in PV module technology.

As a result of all the above mentioned considerations, the criteria for the selection of a PV module should shift from a power-based rating to a more accurate and climate specific rating based on the expected lifetime expected yield, e.g. energy-based rating or "energy rating". In conclusion, deeper knowledge in energy rating can have multiple benefits for:

- Manufacturers as they can demonstrate how their products perform in specific climates and thus cost optimise the process
- EPC and yield assessors as they can better understand the climate dependent behaviour of PV modules and thus provided more accurate yield assessment and lifetime yield prediction
- Policymakers and regulators, as they can introduce more accurate calculation for the requirements on life time electricity yield for example in ecodesign requirements.

1.2 Literature Review of Published Research on PV Module Energy Rating

To supply a realistic estimation of the yearly performance of a PV module installed at different climate conditions, the PV module energy rating (MPR) has been defined as "normalized energy collection for the reference climatic profile" in the international standards published by International Electrotechnical Commision (IEC), through the discussion over 20 years [3–7] MPR is referred to as "Climate Specific Energy Rating (CSER)", in these standards (IEC 61853-1, -2, -3, and -4). That is, MPR (CSER) is a dimensionless indicator to express the ratio of PV module output (watt-hours) to the maximum output (watt-hours) expected under the reference climatic conditions. This CSER parameter is calculated from the power rating data (which are comprised of the performance data obtained at various temperatures and in-plane irradiance intensities), the PV performance data depending on incident light characteristics (angle of incident, spectrum) and temperature of PV module, and the hourly weather datasets including ambient temperature, wind speed, and irradiation characteristics. As described in our

previous report [8], some approaches to clarify the differences between the actual MPR observed at various locations/technologies and the respective calculated-MPR has have been proposed so far (reviewed in [9]). In this section, the MPRs reported in the published articles have been collected, and meta-analyzed to extract the features on MPR under various PV technologies and climates

Over 100 work of literatures have been identified on the energy yields of PV modules with various technologies at numerous locations since 1990s (the activities in the last century were summarized in [10]. The number accounts for a literature database search with the combination of subject words (e.g., photovoltaic* × "performance ratio*" × "energy yield*"). However, in most of the reports, the performance characteristics were only taken from the label attached to the deployed PV modules and not actually determined or measured (i.e. in the laboratory) prior to outdoor deployment. These reports provide a valuable estimation to elucidate the real energy yield in the individual locations and the performance ratio under the specific situations such as high irradiance condition, however, the MPR could not be precisely estimated, depending on the data collected under the unfavourable conditions (e. g., low irradiance condition). Among all publications, five reports could be examined to meta-analyze the MPR features, in which the energy rating data in South Asia, North America, Middle East and Europe were included (Table 1) [11–15].

Table 1: Locations (on MPR estimation) selected from the literature.

Country	City	Latitude	Longitude	KG Climate*	Reference
UK	near Glasgow	56.00	-4.00	Cfb	[13]
UK	Norwich	52.70	1.09	Cfb	[11]
Netherlands	Utrecht	52.10	5.20	Cfb	[12]
Germany	next Berlin	52.00	14.00	Cfb	[13]
Germany	Cologne	50.92	6.99	Cfb	[14]
Germany	Breisach	48.00	7.59	Cfb	[11]
Italy	near Milano	45.00	9.00	Cfa	[13]
France	near Avignon	44.00	5.00	Csa	[13]
Italy	Ancona	43.47	13.07	Csa	[14]
India	Gurgaon	28.62	77.07	Cwa	[15]
Spain	near Ubeda	38.00	-3.25	BSk	[13]
India	Leh	34.15	77.56	BWk	[15]
USA	Tempe	33.42	-111.91	BWh	[14]
Egypt	Rafah	31.20	34.30	BWh	[13]
India				B**	[15]
India	Chennai	12.98	79.99	Aw	[14]
India				A**	[15]

*KG climate indicates the climate zone defined in Köppen-Geiger climate classification [16].

**These climate zones were described in the reference [15] as "Hot & Dry" and "Hot & Humid" for B and A, respectively. Other climate zones were determined by the literature [16] and relevant web sites [17].
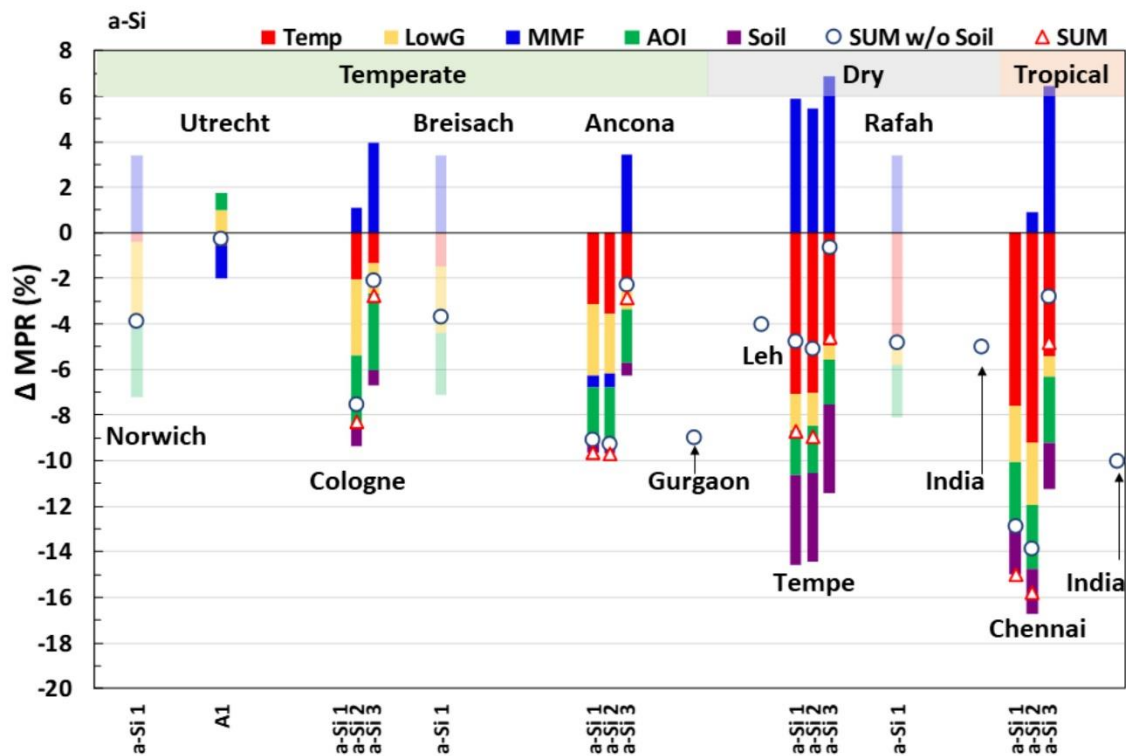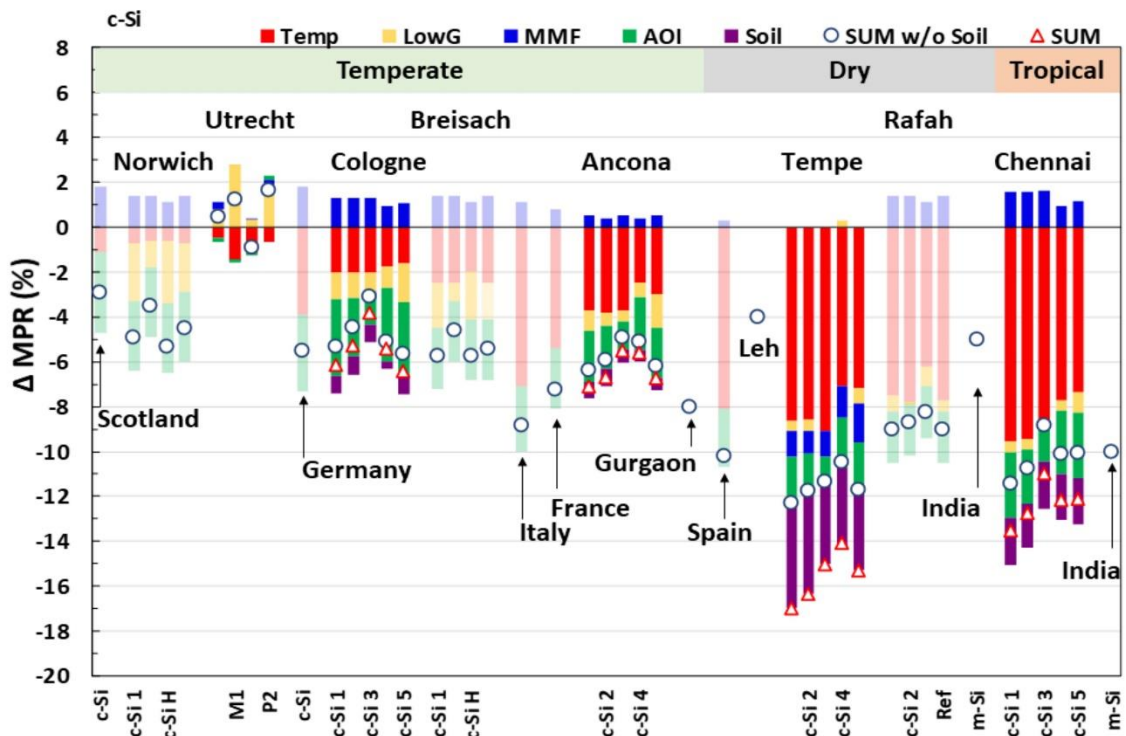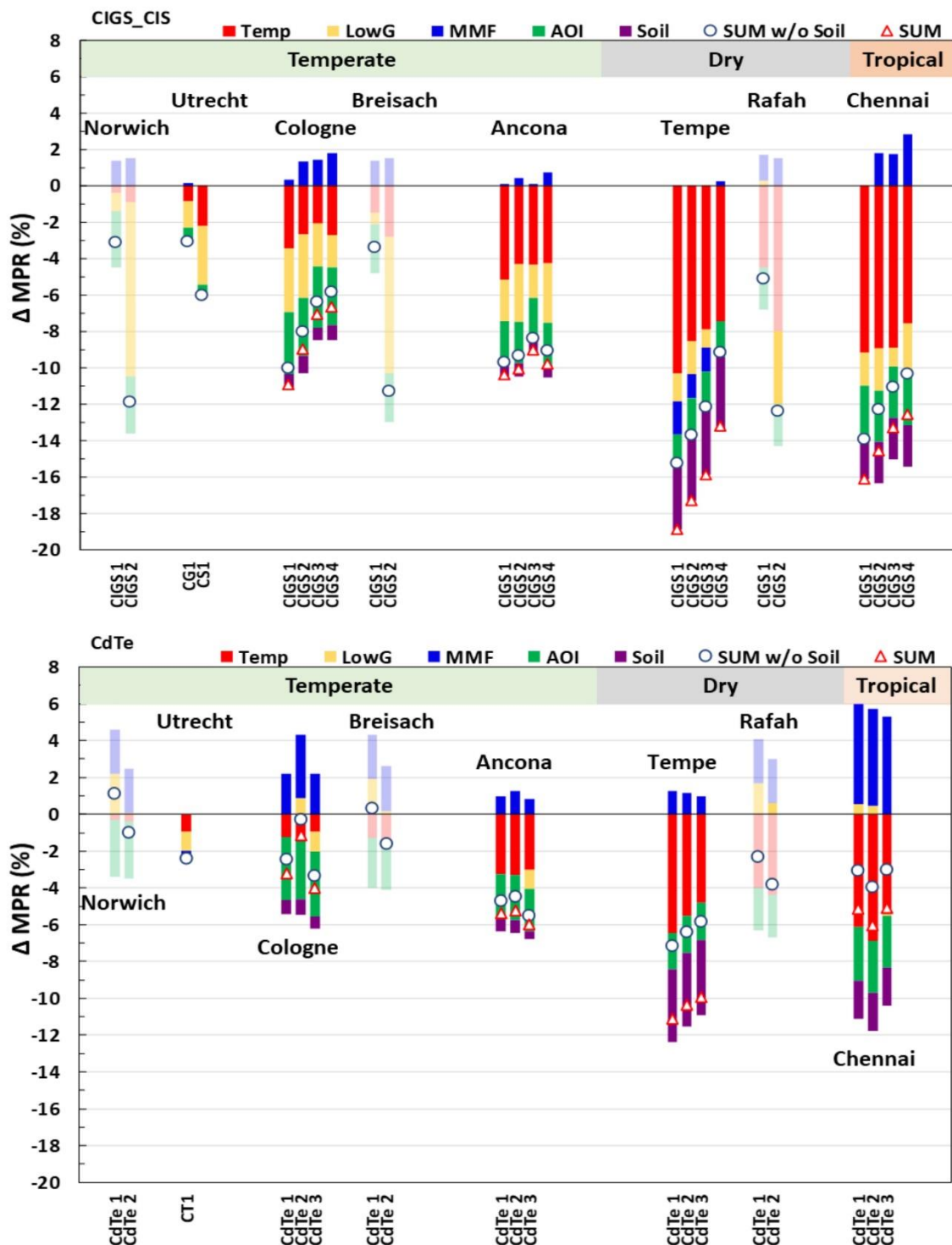
Figure 2: Difference in MPR estimated from the indoor measurement data, based on the weather data at the respective locations. The climate zones (tropical, dry and temperate) are corresponding to climate zones (A, B, and C, respectively) defined in Köppen-Geiger climate classification. The bars with semi-transparent colours indicate the data without outdoor observation (Source: Adapted from [11–15]).

MPR is mainly varied depending on two factors (irradiance and temperature). For the irradiance, the energy generation in a PV module is heavily impacted by the spectral mismatch (which is indicated as MMF and the angle of incidence (AOI), as well as its intensity (which is denoted as LowG (Figure 2). Since the temperature of PV modules are affected by the ambient temperature, wind speed, and irradiance, the output is changed in accordance with the temperature coefficients owing to the respective PV modules.

Figure 2 summarizes the differences in MPR (ΔMPR), which have been reported so far [12–15, 18] for four different PV technologies. This ΔMPR is estimated from the indoor measurement data (power rating and other characteristics), based on the weather data at the respective locations. Some common MPR features beyond the achievements in the individual reports are shown in Figure 2, e.g., sum ΔMPR (without that depending on soiling) is near consistent in each climate zone, irrespective of data source, in crystalline silicon (c-Si) PV modules. This deviation in MPR is largely attributed to that of local temperature, indeed, ΔMPR caused by temperature in the PV modules installed in Hot & Dry and Tropical climate zones is about twice against that in temperate climate zone. The effect of temperature is larger in hot climate, regardless the PV technologies of the investigated PV modules. The contribution of AOI to ΔMPR has similar extent, irrespective of climate and PV technology. Furthermore, the effect of low irradiance on MPR is near consistent (positive impact), although there are clear differences among the different PV technologies. We should note that the large positive-deviation due to spectral mismatch effect (SMM) is observed in the PV modules with amorphous silicon (a-Si) and cadmium telluride (CdTe) technologies, in particular in Hot & Dry and Tropical climate zones. The small positive effect with SMM is also detected in other PV modules, while the intensity does not depend on the climate zones where the PV modules are installed (although the negative SMM effect detected in Tempe, the causes of this estimation is unknown).
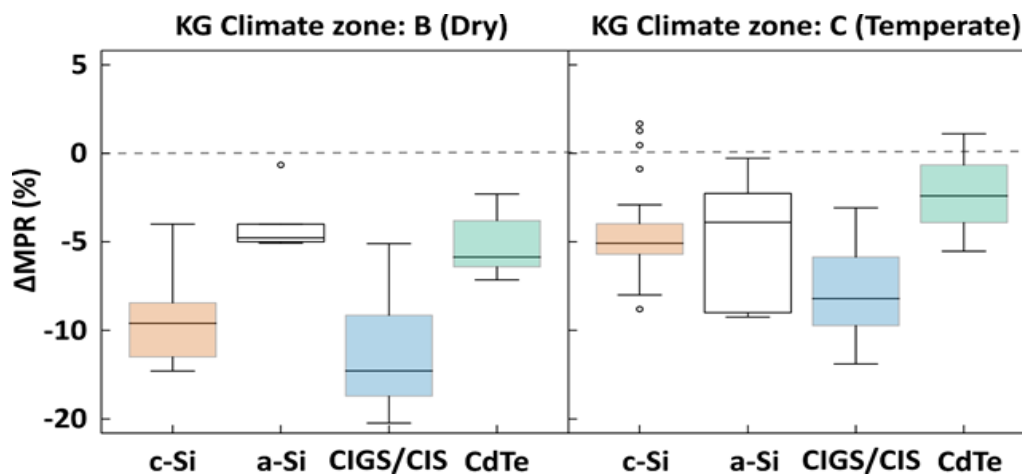
Figure 3: Difference in MPR among PV modules with four technologies, in the respective climate zone (Source: Adapted from [11–15]).

MPR is thus a tool that can provide not only a realistic estimate of the performance of a PV specific technology at various climate conditions, but also that of various PV technologies at a specific climate zone. For this viewpoint, total ΔMPRs of PV modules with four PV technologies are compared between two climates [Hot & Dry (B) and Temperate (C)]. As shown in Figure 3, it is likely to reveal that similar ΔMPRs among four technologies are confirmed in temperate climate zone, although ΔMPRs of PV modules with c-Si and CIGS/CIS technologies are slightly large in Hot & Dry climate zone. These larger ΔMPRs in c-Si and CIGS/CIS technologies are caused by the absence of positive SMM effect found in a-Si and

CdTe technologies, unlike the common effects of other environmental factors (temperature, low irradiance, and AOI) across all technologies (Figure 4). However, it should be noted that these results derived from the published data with a certain amount of uncertainty, as discussed in our previous report [8].
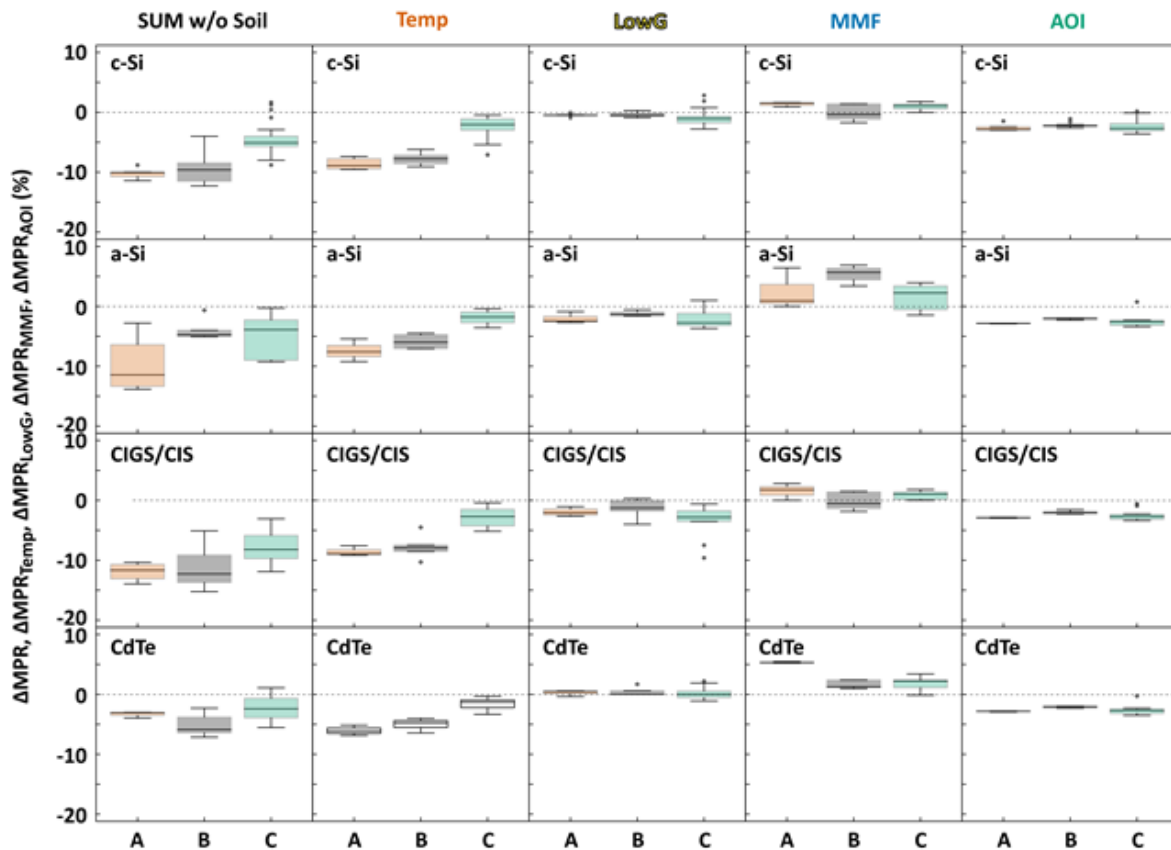
Figure 4: Impact of environmental factors on the MPR. A, B, and C in the horizontal axis indicate the Köppen-Geiger climate zones (tropical, dry and temperate), respectively (Source: Adapted from [11–15]).

Uncertainty on MPR depends on the uncertainties related to measured environmental data, power rating data, and estimation of effective irradiance and module temperature, as well as that in the estimation procedure to find the performance at desired irradiance and temperature. A lot of approaches to reduce these uncertainties have been reported [18–33] and some advanced procedures are introduced in the following chapters of this report. In addition, it has been suggested that the effect of degradation during outdoor exposure should be taken into consideration for the reduction of uncertainty in energy rating [11, 15, 34]. Besides the uncertainty, the climate classification must be improved from the classical Köppen-Geiger climate zone, because this classical climate zones definition is specific for vegetation grow in a given climate classification region. Recently, two proposals on the climate classification for PV performance have been published, based on the factors concerning energy rating [35–38]. On energy rating, these novel classification systems would provide a clear relationship between PV technology and climate zone.

2 ELECTRICAL PERFORMANCE CHARACTERIZATION OF PV MODULES

The electrical performance of PV modules at various operating conditions can be characterized either outdoor under natural sunlight (see Chapter 2.3) or indoor using artificial light sources (see Figure 5).

Figure 5: Solar simulators for PV modules, left: pulsed, right: steady state (Source: TÜV Rheinland Group).

PV module electrical performance ratings are most commonly represented by a single set of values for current, voltage and maximum power given at standard test conditions (STC) of 25°C, 1000 W/m^2 and AM1.5 spectrum. Since test conditions in natural sunlight cannot be controlled, the use of a solar simulator for performance characterization is the most common practice in the PV industry. However, procedures for outdoor measurements are also lined up within international standards (see Chapter 2.3).

The IEC 61853 standard, Parts 1 and 2, provide the guidelines for the performance measurements relevant to energy rating and will be described in this chapter.

Chapter 2.5 will also discuss the existing procedures for the characterization of bifacial PV modules.

2.1 Indoor Test Methods IEC 61853-1

2.1.1 Low irradiance behaviour

To measure the performance at different irradiances the light source may be either a pulsed or steady state solar simulator. When variating the irradiance between 100 W/m² and 1100 W/m² (see Figure 6), as stipulated in part one of the energy rating standard [3], special care has to be taken to keep constant spectral irradiance conditions and to fulfil the required specifications regarding the homogeneity of irradiance for each setting as described in the standard for solar simulators [39]. In practice, this can be achieved by neutral grate filters in combination with varying the distance between the light source and the test sample. Implementing glass filters or reducing the power of the simulators can influence the spectral distribution and may induce negative measuring artefacts.
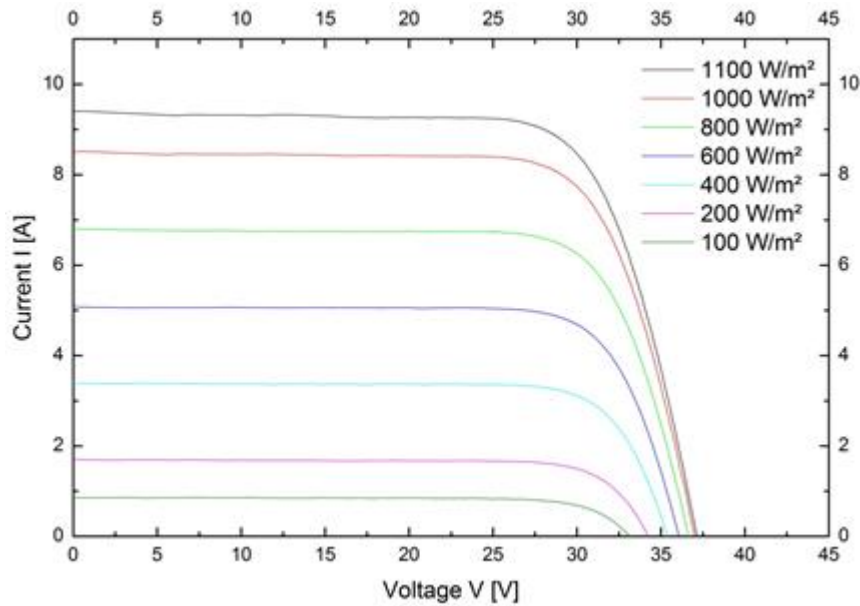
Figure 6: I-V curves of crystalline PV module measured at seven different irradiances with a class A⁺A⁺A ⁺solar simulator (Source: [40]).

The main goal of this measurement is to determine any non-linearity of the sample`s efficiency with irradiance. The low irradiance behaviour (see Figure 7d) is calculated as

$$\eta_{Rel.} = (P_{Max,Meas.} 1000 W/m^2)/(G_{Meas.} P_{Max,1000 W/m^2}) \cdot$$

(1)

The performance at low irradiances depends more on the manufacturing processes and PV module design than on cell technology. Generally, desired is a highly parallel resistance to reduce losses at low irradiances and a low series resistance to reduce losses at high currents. The performance can strongly vary between PV module types and necessarily must be tested in the laboratory. Values between 80% and 100% at 100 W/m² have been observed. A typical value for a good performing sample is 95% at 100 W/m². The higher the efficiency curve the better for the specific energy yield (kWh/kW_p).
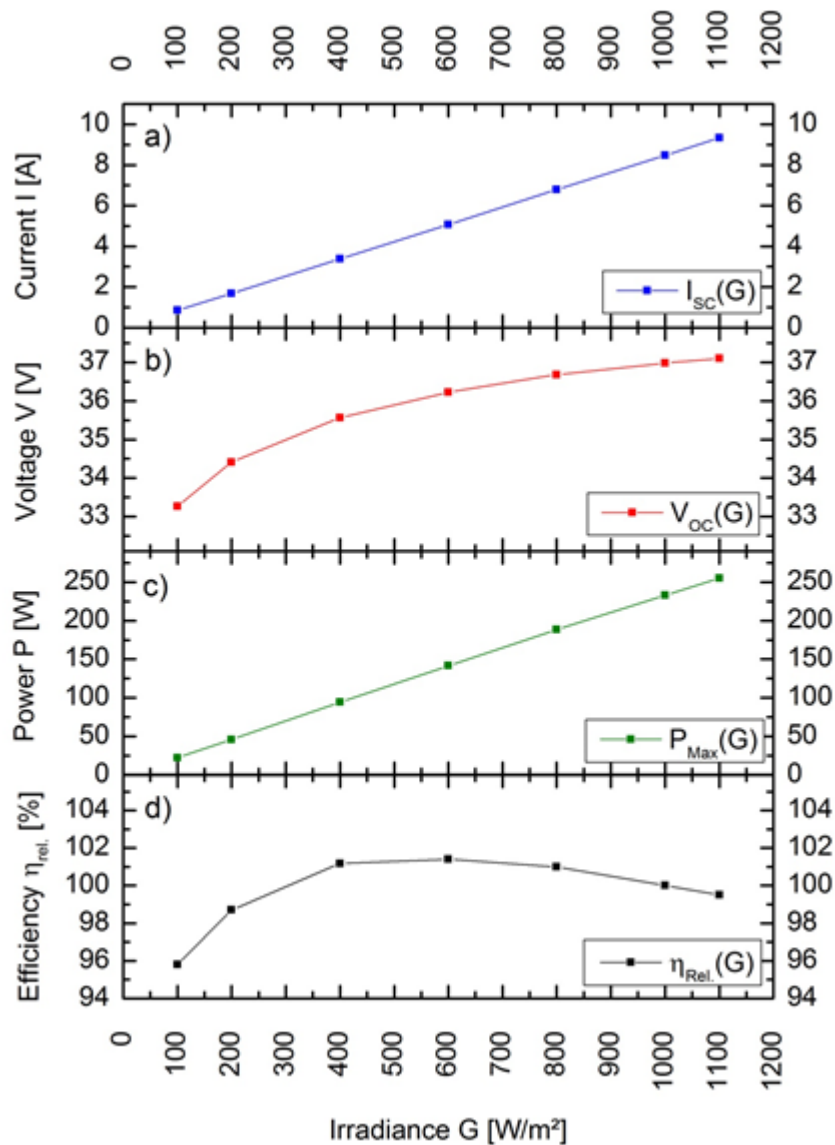
Figure 7: I-V curve characteristics of a crystalline PV module measured at seven different irradiances (Source: [40]).

2.1.2   Temperature behaviour

When measuring the electrical performance at different temperatures special care has to be taken on homogeneous and stable device temperatures. In practice, different PV module temperatures in the range of 15°C to 75°C, as stipulated in part one of the Energy Rating Standard [3], are reached by heating champers implemented directly into the solar simulators` tunnel. The temperature itself is measured by averaging four Pt100 or infrared sensors as described in the standard. The goal of this measurement is to determine the devices' performance in dependency on temperature (see Figure 8).
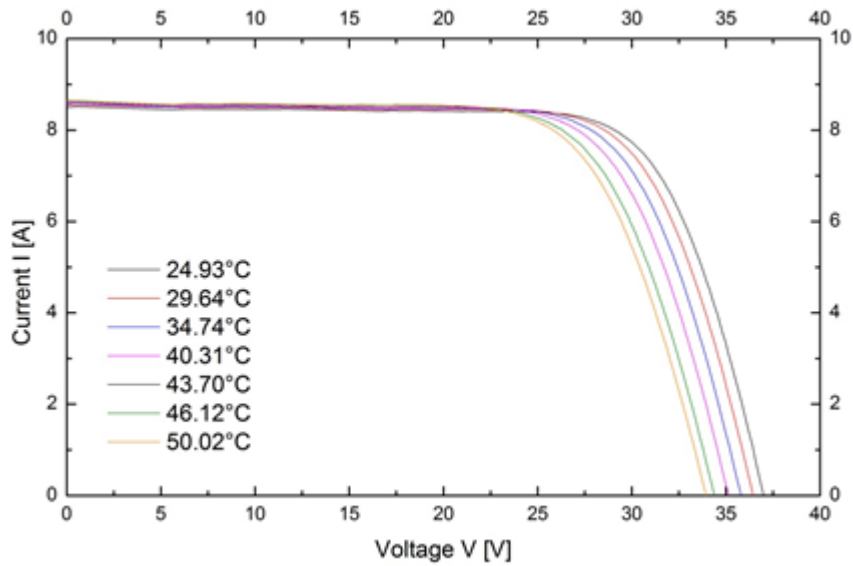
Figure 8: I-V curves of crystalline PV module measured at different temperatures and an irradiance of 1000 W/m² (Source: [40]).

The temperature coefficient of P_{Max} is called γ and is negative (-%/K). It is calculated out of the slope γ_{abs} (W/K) of the linear regression (see Figure 9) normalized by the power P_{STC} at 25°C as

$$P(T) = \gamma_{abs}T + b; \qquad \gamma = \gamma_{abs}/P_{STC}.$$

(2)

The temperature coefficient γ is a decisive factor for temperature-driven energy yield losses during field operation. For high yields it should be as low as possible. The temperature coefficients depend more on cell technology than on manufacturing processes or PV module design. Best values can be achieved by thin-film PV modules (a-Si, CdTe) with values in the range of -0.23%/K to -0.39%/K. For c-Si technologies, γ can be found in the range of -0.35%/K, for high-efficiency c-Si technologies, to -0.43%/K.
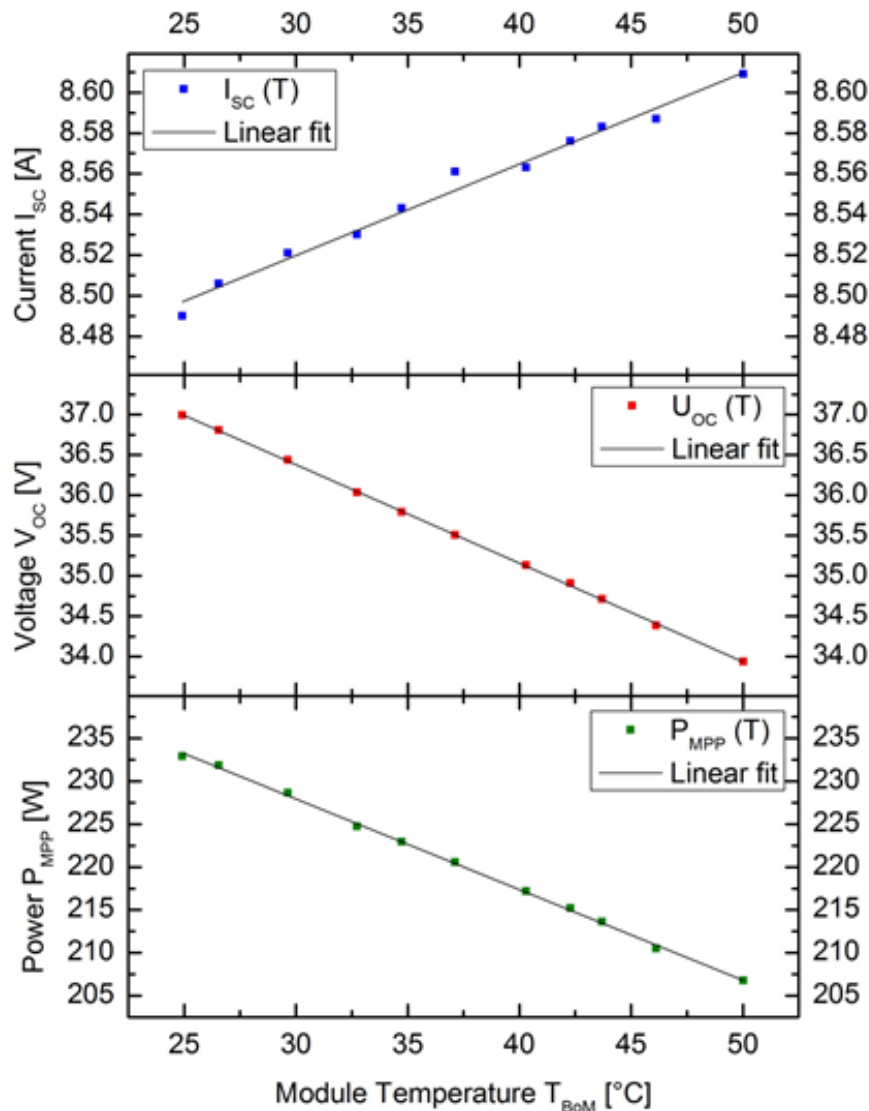
Figure 9: Dependence of I_{SC}, U_{OC}, P_{Max} of crystalline module on temperature with linear fit to determine temperature coefficients α, β, and γ (Source: [40]).

2.1.3 The irradiance-temperature (G-T) performance matrix

The IEC 61853-1 [3] specifies a combination of the different operating irradiance and temperatures to determine the so-called irradiance-temperature (G-T) performance matrix, also known as power matrix. The power matrix is a set of 21 module power measurements at various levels of irradiance between 100 and 1100 W/m² and module temperature from 15 to 75°C, as shown in Table 2. The norm allows multiple methods to populate the G-T matrix and the idea behind the given values is to cover all possible options of operation in the field.

Table 2: Irradiance and module temperature levels applied to obtain the power matrix, as defined in Part 1 of the IEC 61853 standard series.

Irradiance (W/m^2)	Module temperature (°C)			
	15	25	50	75
1100	NA	✓	✓	✓
1000	✓	✓	✓	✓
800	✓	✓	✓	✓
600	✓	✓	✓	✓
400	✓	✓	✓	NA
200	✓	✓	NA	NA
100	✓	✓	NA	NA

(NA: not applicable)

The total amount of bins in the matrix is a compromise between the effort to take a measurement of P_{mpp} and the accuracy. It has been decided to take four settings of T_{mod} and seven settings of G_{POA}. Thereafter a common-sense filter has been applied and six extreme bins less likely to occur in the field have been cancelled from the matrix. Ending up with (7x4=28 minus 6=) 22 bins that must be measured by the manufacturer.

2.2 Indoor Test Methods IEC 61853-2

2.2.1 Spectral response

The spectral response (SR) describes the efficiency of the PV module depending on the wavelengths of the light source. It is mainly driven by the cell technology and its bandgap, but is also strongly affected by cell quality, anti-reflection coatings, embedding materials and front glass.

To measure the spectral response of PV modules, as requested in Part 2 of the Energy Rating Standard [4], a measuring device with an adjustable narrow-bandwidths light source is needed. This can be either achieved by solar simulators combined with transmission filters or a grating monochromator (see Figure 10).

Figure 10: System for spectral response measurements of full-size PV modules (Source: TÜV Rheinland Group).

Crystalline Silicon cells are active in the wavelength range from 275 nm to 1190 nm (Figure 11). The great variety of spectral response curves within the same technology makes it difficult to generalize the spectral behaviour for all technologies. Thus, it must be measured in the laboratory for each PV module type and spectral shifts must be considered for accurate power ratings.

To quantify the impact of spectral shifts on the PV module`s performance in comparison to AM1.5 [41], a spectral mismatch correction factor (SMM) according to IEC 60904-7 [42] can be calculated (Figure 11). The SMM is calculated from the spectral irradiance $E(\lambda)$ of the solar simulator, the AM1.5 reference spectrum and the spectral responses of a reference sensor and device under test as

$$SMM = \frac{\int E_{Am\,1.5}(\lambda) \cdot SR_{ref}(\lambda)\delta\lambda}{\int E_{Simulator}(\lambda) \cdot SR_{ref}(\lambda)\delta\lambda} \times \frac{\int E_{Simulator}(\lambda) \cdot SR_{sample}(\lambda)\delta\lambda}{\int E_{AM\,1.5}(\lambda) \cdot SR_{sample}(\lambda)\delta\lambda} \qquad (3)$$

A SMM > 1 means the cell received more effective irradiance than it would at perfect AM1.5 conditions, while for SMM < 1 it is less than aspired. Having calculated the SMM, the underlying irradiance of the measured I-V curve can be corrected.
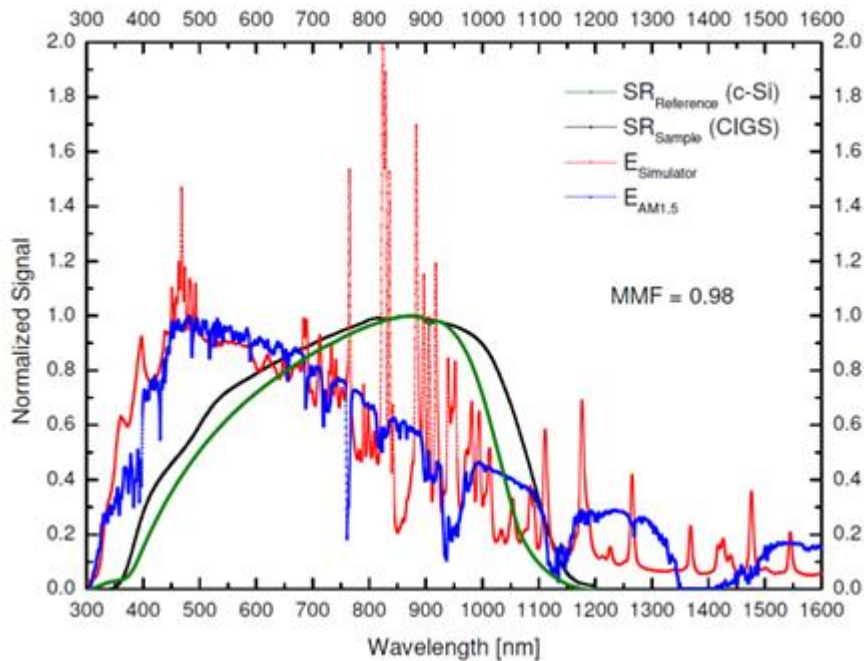
Figure 11: Spectral response of c-Si reference cell and CIGS sample with AM1.5G standard spectrum and spectrum of pulsed solar simulator, resulting SMM: 0.98 (Source: [40]).

2.2.2 Angular response

The angular response describes the dependence of the PV module efficiency on the incidence angle of the illuminating irradiance. The angular response curve is mainly driven by the front glass of the PV module. Deeply structured glass or glass with anti-reflection coating can achieve a better transmission as well as a better angular behaviour than non-treated front glass. Nevertheless, when quantifying possible yield gains due to front glass optimization, possible impacts on the soiling behaviour must be considered.

The main goal of this measurement, as requested in part two of the energy rating standard [4] is to determine reflection losses at high angles (>40°). Therefore, the measurement signal must be normalized to the cosine to exclude impacts coming from geometrics while tilting the sample (Figure 12). The measured current I_{SC} depending on the angle of incidence θ is normalized as

$$\tau_{rel}(\theta) = \frac{I_{SC,STC}(\theta)}{\cos(\theta) \cdot I_{SC,STC}(\theta)} \tag{4}$$

When determining the angular response of full-size PV modules with solar simulators, the biggest challenge to solve is the volume inhomogeneity of the light source when tilting the sample from -90° to +90°. A solution can be the non-destructive approach described in [43].
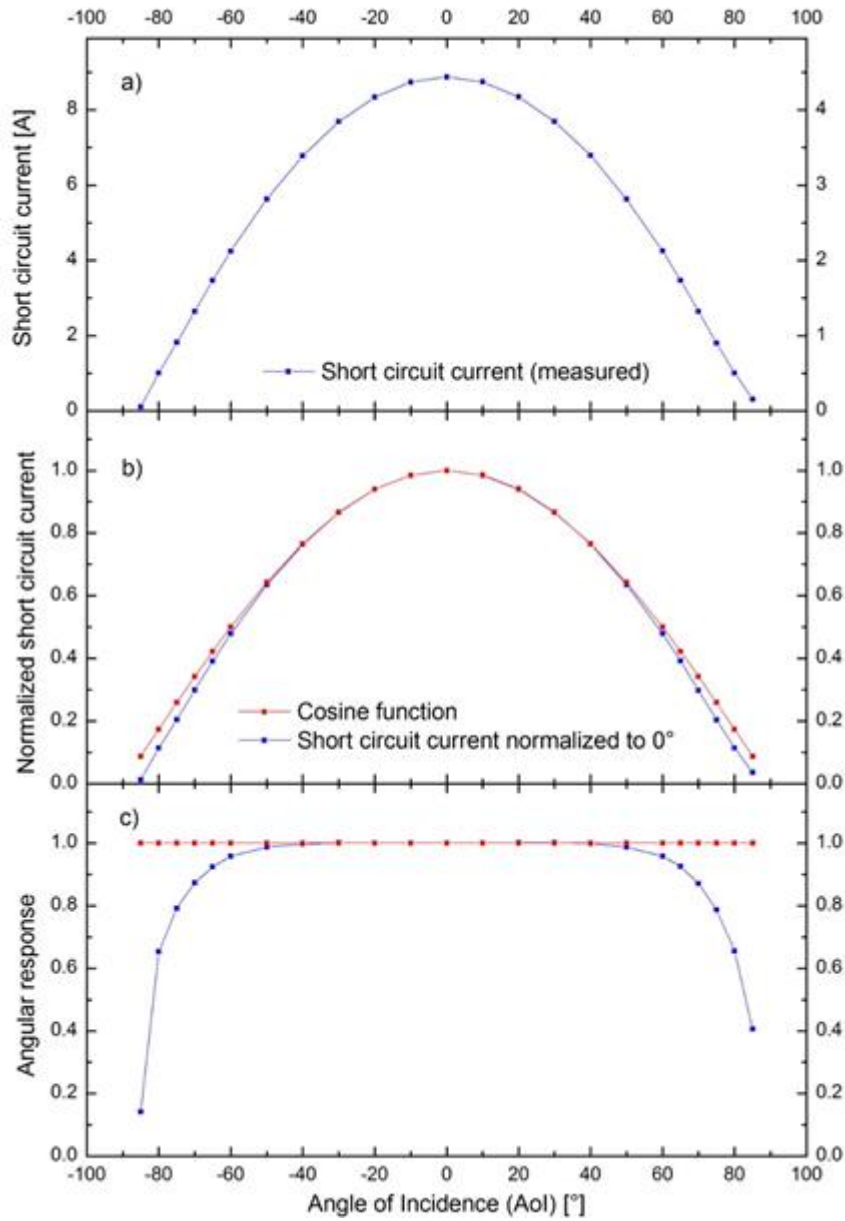
Figure 12: Measurement procedure for angular response, a) ISC measurement, b) Normalization of measurements to normal incidence, c) Reference to cosine function (Source: [40]).

2.2.3 Nominal module operating temperature (NMOT)

The temperature of the module (T_{mod}) is predominantly a function of the ambient temperature (T_{amb}), the wind speed (V_{Wind}) and the total solar irradiance (G) incident on the active surface of the module, and has an direct impact on the energy yield generation of a PV module.

The temperature difference ($T_{mod} – T_{amb}$), however is largely independent of the ambient temperature and is linearly proportional to the irradiance at levels above 400 W/m².

The module temperature is modelled by:

$$T_{mod} - T_{amb} = \frac{G}{u_0 + u_1} \tag{5}$$

Where the coefficient u_0 accounts for the influence of the irradiance and u_1 describes the wind impact. This two factors are site-specific and shall be evaluated for different locations.

The Nominal Module Operating Temperature (NMOT) describes the nominal operating module temperature at an irradiance of 800 W/m² and an ambient temperature of 20°C, therefore is calculated as:

$$NOMT = (T_{mod} - T_{amb})_{@\ 800\frac{w}{m}\text{and 2.1 m/s}} + 20°C \tag{6}$$

The ($T_{mod} – T_{amb}$) @ G=800 W/m² and V_{Wind}=2.1 m/s is found with a linear regression.

For the characterization the complete installation layout is described in the IEC 61853-2 standard. The tested modules (s) shall be mounted in a tilted installation of 37.5°± 2.5°, at least 0.6 m above the ground and installed with other modules to reflect thermal conditions of modules in an array.

To compensate the variations of temperature due to sky temperature, ground temperature, etc. a correction of up to 5°C may be applied. For this, two reference modules are placed next to the device under test (one on either side). The reference modules shall have been characterized for >6 months to derive Nominal Module Operating Temperature (NMOT). The two reference modules and the device under test are characterized during the same period and the average deviation from the 6-month NMOT values for the two reference modules is applied to the NMOT measurement for the device under test.

2.3 Outdoor PV Module Characterization

As mentioned, the electrical performance ratings of current, voltage and power of PV modules are most commonly determined at STC and indoors on a solar simulator under controlled conditions. Those ratings have been used for ages and suit the purpose of nameplate of the product. To cover more real operating conditions, the IEC 61853-1 performance matrix expands upon this point measurement to include 21 additional points in irradiance/temperature space (see Section 2.1.3). While the G-T performance matrix is achievable with specialized solar simulators with integral temperature control, both the spectral response and the angle of incidence (AOI) characterization on the full-size PV module level present challenges and therefore not commonplace. Therefore, in addition to the indoor method (61853-1 Chapter 8.2) also aligns two procedures for outdoor characterization using natural sunlight:

- 61853-1 Chapter 8.3, natural sunlight with tracker
- 61853-1 Chapter 8.4, natural sunlight without tracker

Outdoor characterization can also leverage realistic thermal operating conditions inherent to the testing to calibrate irradiance/wind speed models, which can in turn be used to calculate nominal module operating temperatures (NMOT).

Further, light soaking or preconditioning can be conducted in situ before the start of characterization. For products that display metastability (e.g. thin-film technologies), significant relaxation in the absence of light during testing is avoided, producing more representative characterization results. Finally, for products with non-standard form factors, such as building-integrated panels, outdoor testing may be the only solution possible.

Outdoor characterization is not without its limits. Testing can be limited by the accessibility of appropriate weather, making it a seasonal activity. The availability of equipment is another factor. Depending on the selected method, a tracker will be or not needed, but in addition. Outdoor irradiance measurements and appropriate weather instruments (wind-speed, barometric pressure, ambient temperature, etc.) are required. These instruments are common to laboratories involved in researching photovoltaic systems outdoors, but may not be practical for laboratories in urban or space-constrained settings.

Measurements tend to encompass a continuum of operating conditions rather than the tidy, discrete points prescribed by IEC 61853-1. Extended duration tests can suffer from "too much data." As such, outdoor testing is commonly paired with an appropriate performance model for the technology under test or at least translation equations such that the IEC 61853-1 matrix can be reproduced.

In this Section, 2.1.3 presents an approach for characterizing PV modules using two-axis solar trackers at outdoor installations.

In Section 2.3.2 the challenges of continuum operating conditions will be approached by extracting the IEC 61853-1 matrix from one-full year outdoor data and including all measuring points, even during periods of non-optimal weather conditions, as restricted in the standard.

2.3.1 Outdoor PV module characterization: Using two-axis solar trackers

A. Introduction

Outdoor characterization utilizing a two-axis solar tracker is an alternative method that circumvents the limitation of module full size AOI, or IAM due to the non-uniformity/divergence of indoor light sources. Given suitable weather, operating conditions spanning the 61853-1 matrix and beyond are possible. Spectral conditions ranging from AM0.85 to > AM7.0 are possible. AOI response can be measured deterministically, taking advantage of the uniformity and collimation of natural sunlight.

In this chapter, equipment and procedures for outdoor module characterization on a two-axis solar tracker will be described. Procedures include normal incident or "on-sun" characterization, which forms the bulk of the data from outdoor testing, along with "off-sun" or Angle of Incidence (AOI) testing. An optional, on-sun thermal test is also presented. In the event that the on-sun thermal test is omitted, temperature coefficients must be extracted from on-sun electrical performance data. Detailed measurement procedures and data reduction are too lengthy to present here and are instead presented in [44].

B. Equipment

Characterization is performed outdoors on a two-axis solar tracker. Modules are instrumented with resistance temperature devices (RTD's) or thermocouples (T/C) attached to the back of the module, and then mounted on the tracker. The majority of measurements are performed with the module held normal to the sun. Current-voltage (I-V) characteristics are measured with sufficient accuracy to extract I_{sc}, V_{oc}, I_{MPP} and V_{MPP} at a minimum. These parameters can be used to fit "point models" such as the Sandia Array Performance Model [45]. Full I-V curves may be required for calibration of mechanistic performance models such as the single-diode model [46].

Figure 13: Two-axis solar tracker used for PV module characterization. A variety of different form factors and cell technologies can be characterized simultaneously.

The following equipment is used for conducting these tests;

1. Solar tracker

    - Test plane for mounting the module and reference irradiance sensors
    - Tracking system capable of keeping the module normal to the sun during the measurement procedure.
    - Off-tracking capability to controllably steer the tracker over a range of 0° – 90° Angle of incidence (AOI) between the module plane of array (POA) and the sun during AOI characterization

2. Irradiance sensors mounted on the test plane

    - Broadband instrument for measuring global plane of array irradiance (typically a pyranometer), preferably calibrated for angle of incidence response
    - Broadband instrument for measuring the diffuse GPOA irradiance (typically a shaded pyranometer) [47], (optional, see Chapter 4.4 for more details)

3. Weather Station

    - Pyrheliometer measuring Direct Normal Irradiance (DNI), typically mounted on a separate two-axis tracker
    - Wind speed and direction at 10 meters height
    - Ambient air temperature
    - Barometric pressure (optional, for use in calculating absolute, pressure adjusted air mass)

4. Capability for measuring and logging module current-voltage (I-V) characteristics in rapid succession, at a rate of 2 scans/minute and preferably at 4 scans/minute or faster.
5. Means of measuring the average temperature of the PV module under test to ±1°C. The average temperature is typically determined from measurements of three or four temperature sensors, typically either Pt-100 RTDs or Type-T T/C's.
6. Opaque material to shade the module (optional thermal test only). This allows the module to cool to near ambient temperature prior to the start of the measurements.
7. Insulation to be added to the back surface of the module (optional thermal test only). Insulation improves the temperature uniformity across the module and increases the temperature range that can be achieved during the test.

C.   On-sun electrical performance measurements

On-sun or normal incident electric performance measurements form the bulk of the data from outdoor testing. These measurements are best performed over a wide range of weather conditions (Table 3 and Table 4). When clear sky conditions do not occur for full days, data from multiple days may be merged. For crystalline silicon modules, this practice is generally acceptable. However, care must be exercised when characterizing any module type that displays significant metastability or relaxation overnight. In addition to data collected during clear sky conditions, the equivalent of several days of data during all sky conditions is required (Table 4). Preferably, these data represent both overcast conditions in which the irradiance is stable, as well as transient partly cloudy conditions.

Table 3: Clear Sky Ambient Conditions.

Parameter	Required	Preferred
GNI	800 - 1050 W/m^2	600 - 1200 W/m^2
DNI/GNI	> 0.85	> 0.90
Air Mass	1.5 – 5.0	1.0 – 7.0
Wind Speed	0 - 4 m/s	0 - 10 m/s
Min. Test duration	600 min./2 days	1200 min./3 days

Table 4: Cloudy or All-Sky Ambient Conditions.

Parameter	Required	Preferred
GNI	200 - 400 W/m^2	100 - 500 W/m^2
DNI/GNI*	0 – 0.85 (< 0.05)	
Min. Test Duration	200 min./1 day	1200 min./3 days

* a range of conditions are preferred; however, the bulk of the measurements should occur at DNI/GNI< 0.05

The module is held normal to the sun for the duration of the electrical performance test while I-V curves are recorded. A data collection frequency should be selected to ensure adequate data across the range of conditions, typically every two minutes. Irradiance is checked before and after each IV sweep to ensure that irradiance was stable over the I-V sweep time. The I-V curve is discarded when irradiance is determined to have changed during the I-V curve sweep. This check can be built into the data collection system or performed in post-processing. The module is preferably held at maximum power between I-V curves to produce the most representative operating conditions.

D.   Angle of incidence testing

Reflection losses are characterized through Angle of Incidence (AOI) testing. AOI testing often may be considered optional for modules utilizing a plain glass cover sheet lacking and antireflective coating or texture because an accurate general-purpose model is available [48, 49]. Between the electrical, thermal and AOI tests described in this chapter, the AOI test presents the greatest challenge due to the requirements for tracker articulation; commercial two-axis solar trackers frequently lack the controls and range of motion appropriate to index a module fully off-sun (e.g. 90°) during the preferred test conditions near solar noon. However, with careful planning and procedure development, it is possible to work around these limits [47].

Stable, clear sky ambient conditions are required during the test (Table 5), preferably near solar noon. The module should be on sun for a minimum of 30 minutes before initiating an angle of incidence test to ensure thermal stability at the beginning of the test. The module is initially tracked normal to the sun for 10 minutes while I-V curves and module temperature are recorded (~ 4 scans/minute). The tracker is then gradually indexed to a range of incidence angles from 0° to 90°. Ideally, the tracker will have a deterministic control system such that prescribed incidence angles can be achieved (i.e. 0°, 5°, 10°, etc.). Often this is not the case and incidence angle must be calculated from recorded sun position and tracker position.

Tracker rotation is preferably towards and beyond zenith rather than across the horizon, to minimize irradiance variation from ground reflections [47].

Table 5: Ambient Conditions for AOI and Thermal Tests.

Parameter	Required	Preferred
Global Normal Irradiance (GNI)	800 - 1200 W/m^2	950 - 1050 W/m^2
Variation in GNI	± 2.5%	± 0.5%
DNI/GNI	> 0.85	> 0.90
Air Mass (Absolute, pressure adjusted)	1 - 2	1.4 - 1.6
Wind Speed	< 4 m/s	< 2 m/s
Ambient Temperature	> 0°C	> 10°C

E. On-sun thermal test to determine PV module temperature coefficients

Thermal characterization is performed to determine temperature coefficients for I_{sc}, I_{MPP}, V_{oc}, and V_{MPP}. This procedure requires no prior knowledge regarding the electrical performance characteristics of the module being tested. Stable ambient conditions are required during the test (Table 5).

The module is covered with an opaque sheet and allowed to cool to ambient temperature. Once at ambient (to within ~ 6°C) the back of the module is thermally insulated to improve temperature uniformity and increase the maximum temperature reached during the test. I-V curves and module temperatures are then measured rapidly (~ 4 scans/minute) with the tracker normal to the sun. The cover is removed and heated to an equilibrium temperature. A typical test requires approximately 30 minutes once the cover has been removed. Linear regression analysis is then performed to determine voltage and current temperature coefficients. The temperature coefficient for power can either be determined directly or calculated from measured temperature coefficients for I_{MPP} and V_{MPP}.

2.3.2 Outdoor PV module characterization without trackers: Extracting IEC 61853-1 Matrix from outdoor measured data

The G-T or Power matrix has been used before by other authors [48–50] to understand the performance of various PV technologies.

This section summarizes the findings of Valckenborg [51] by extracting the IEC 61853-1 matrix from outdoor measurements, in which the following setups without trackers where used:

- BIPV façade module
- c-Si and CIGS module in façade
- In-house developed modules IBC and n-PERT mounted at fixed-rack, south facing and 30° tilt.

The outdoor method without tracker (Chapter 8.4 in [2]) has been used as starting point. However, for research purposes, all measurement points have been included, ignoring the restriction of the standard in which it is recommended to use only periods of full sun with minimal disturbance of clouds and wind. In addition, a measurement period of almost a full year has been considered. This is significantly longer than the minimum period of 3 days recommended in the standard.

A.   Visualization

Visualization with 2D-colour plots of a specific parameter of interest (VOC, V_{mpp}, I_{sc}, I_{mpp}, FF, PR or even AOI or spectral properties) as a function of the G_{POA}-T_{mod} matrix has proven to be a powerful tool. Additional statistics on all points within each bin makes it easier to filter out measurement points that could have been disturbed by power outage on measurement equipment, unexpected irradiance mismatch, or other issues which are common for 24/7 outdoor research.

B.   Results

The following results correspond to the values captured from a vertical mounted BIPV-module at test facility SolarBEAT in Eindhoven, the Netherlands [50]. The BIPV-module is part of a round-robin action of the IEA PVPS Task 15 (Enabling Framework for the Acceleration of Building Integrated Photovoltaics, BIPV), which has been performed in the period from the end of 2017 until the end of 2019. The setup and first results of this round-robin and the glass/glass-BIPV-modules were described in detail in [51, 52]. The resulted P_{mpp}-is shown in Figure 14.
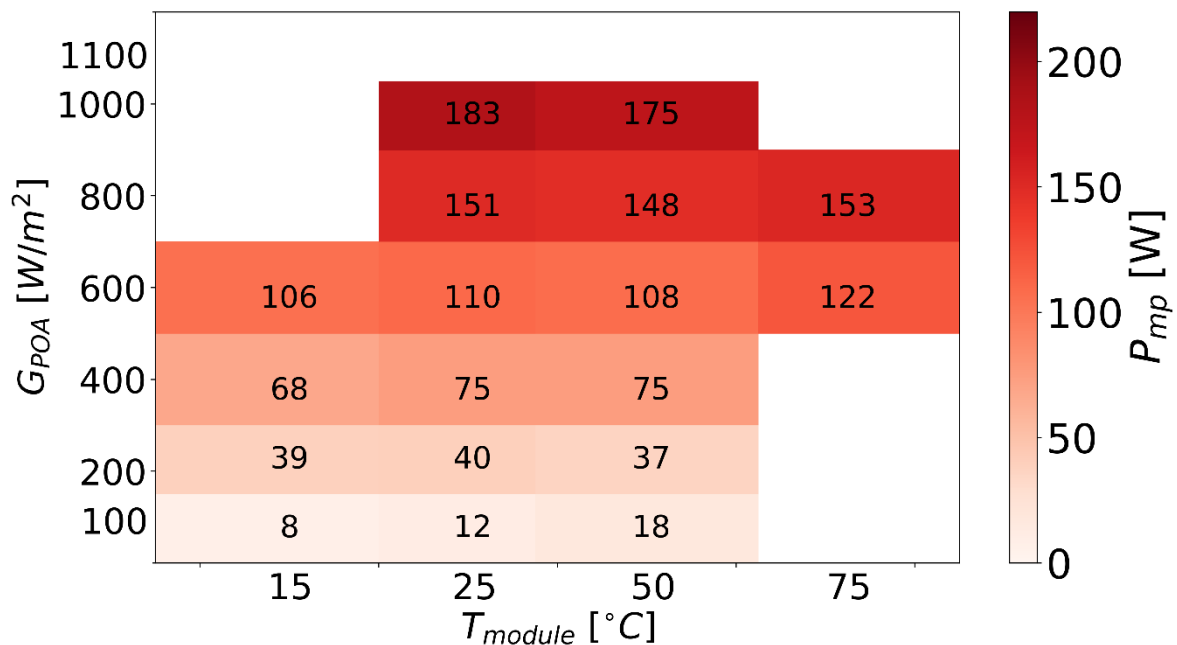
Figure 14: Results of round robin BIPV façade module- P_{mpp} as a function of T_{mod} and G_{POA}. The red colour bar is defined till the rated power at STC, which is 219 W_p for this module.

There are a couple of unexpected findings in this P_{mpp}-matrix, which will be revealed by using additional visualization and another tooling. First, we analyze the number of datapoints in each

bin, see Figure 15. Due to limited measurement accuracy, it is a good practice to take a threshold number of data points as a criterion for including a bin in the P_{mpp}-matrix plot. A too low threshold makes the matrix 'noisier' and a too high threshold will throw out interesting data. We found a compromise at n=5 for the dataset of this BIPV module and will use this threshold for all graphs in this paragraph. As can be seen in Figure 15, the bin with STC has just 14 data points in one full year. This might be very striking; however, one should note that a façade in Northwest-Europe will have only very few hours per year with G_{POA}=1000 W/m². And during these strong sunshine hours, the T_{mod} increases rapidly, especially because of the thermal insulation on the back.
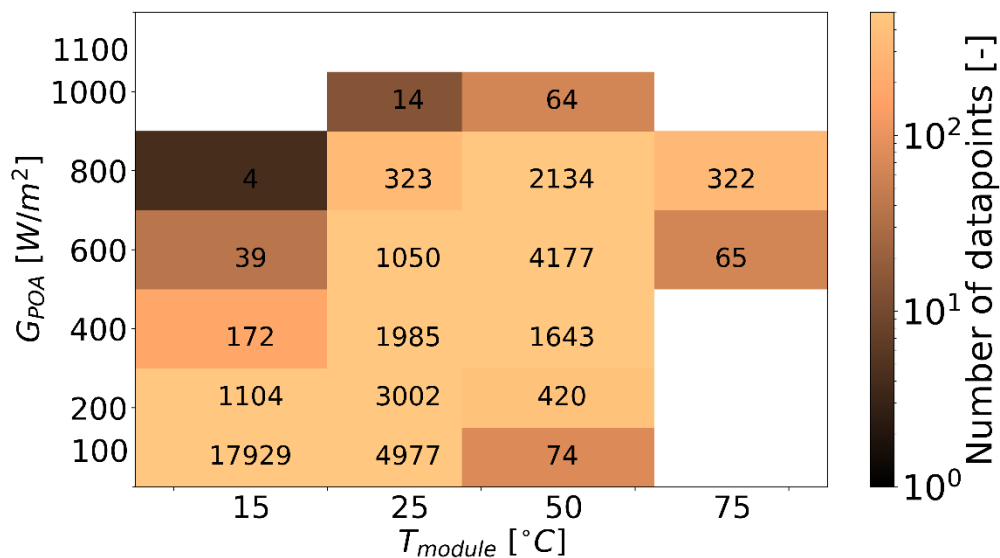
Figure 15: Number of data points as a function of T_{mod} and G_{POA}. The colour bar is scaled logarithmically to be able to distinguish better between all the bins.

Next, we are interested in the amount of irradiation per bin, because that will reveal which bins are the most contributing to the yearly yield, e.g. how much contribution is expected from the left corner bin (100 W/m² and 15ºC) with a huge amount of data points. This H_{POA}-matrix is plotted in Figure 16. For this graph, there is no need to set a threshold because bins that are populated with only a few data points will also have a very low H_{POA} and blend away in the background colour. The most contributing weather conditions (and bins) are clear at a glance.
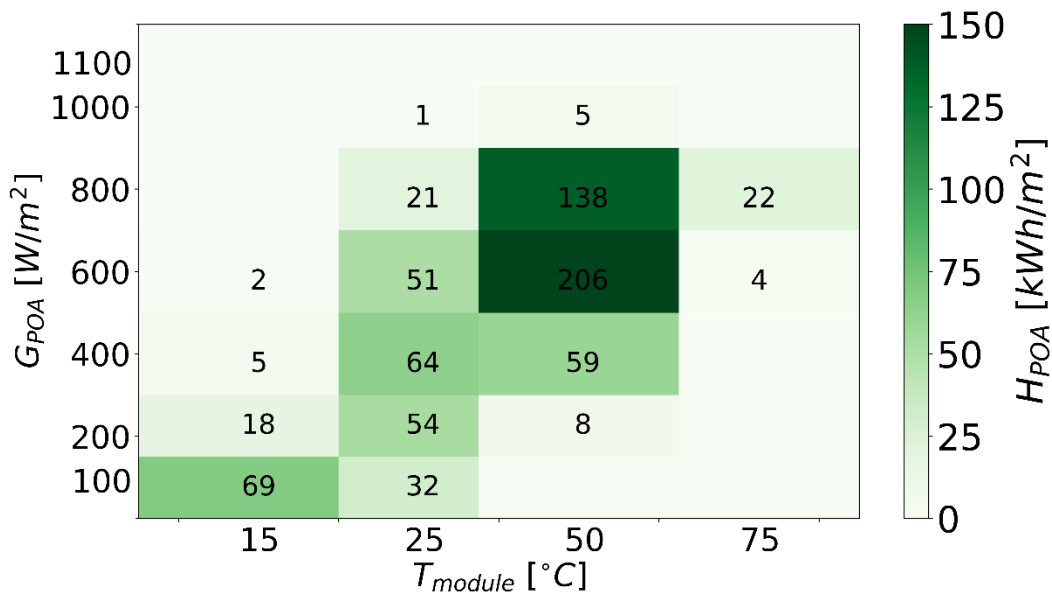
Figure 16: Irradiation H_{POA} in [kWh/m²] as a function of T_{mod} and G_{POA}. The green colour bar is scaled linearly to give an intuitive contribution to total period irradiation.

As PV is very linear in G_{POA} we expect that the specific yield of the module looks quite similar. In Figure 17 the specific yield is plotted using the same colourbar as Figure 16.
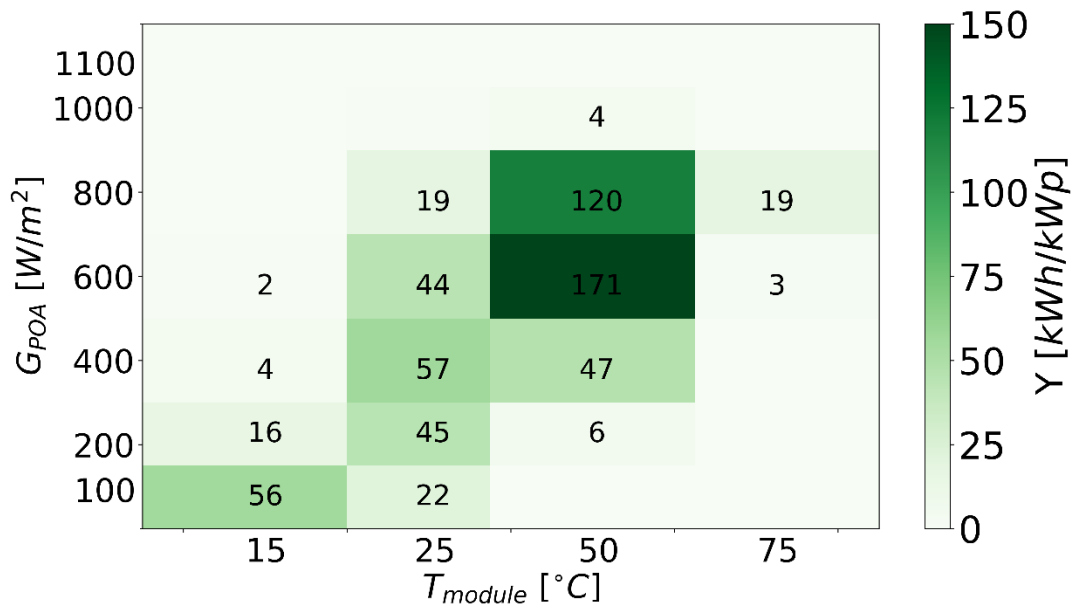
Figure 17: Specific Yield Y in [kWh/kW$_p$] as a function of T_{mod} and G_{POA}. The green colour bar is scaled linearly to give an intuitive contribution to total period yield.

The P_{mpp}-matrix bins on the row of G_{POA}=600 W/m² show a local maximum of 122 W_p, which is difficult to understand as normally P_{mpp} is decreasing with increasing T_{mod}. Therefore, we add statistics for each bin, see Figure 18.
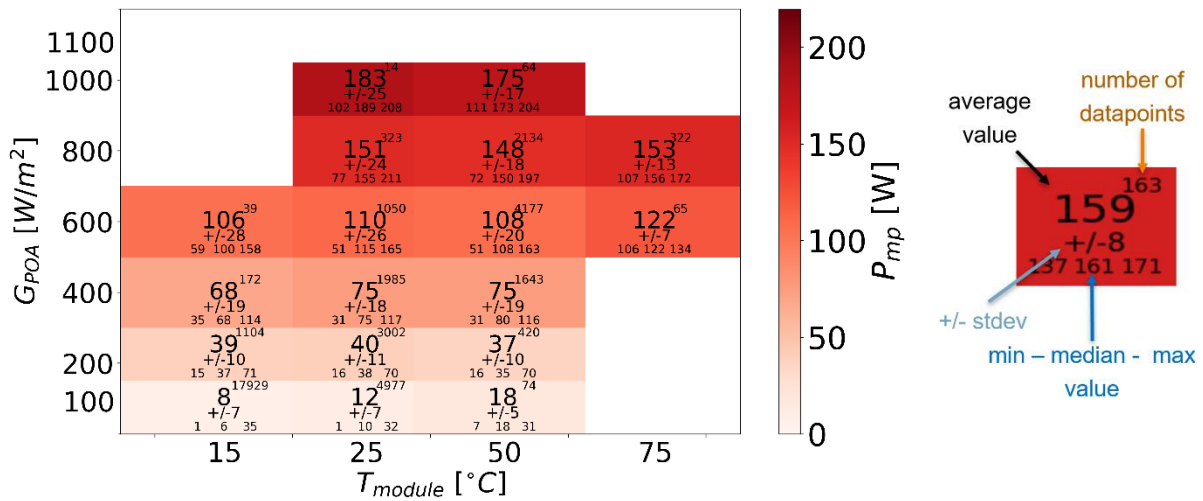
Figure 18: Left part: statistics added to each bin. Right part: An explanation of the additional statistical parameters.

With this statistic, we could eliminate unexpected outliers (caused by spikes and data gaps). The graphs shown in this paper are the versions after filtering the outliers. Data points that are still weird are mostly caused by local shading effects which are difficult to eliminate. Note that the minimum value is just one data point, and the same holds for the maximum value. However, the standard deviation (stdev in Figure 18) should be reasonable in line with the expected spread based on the boundaries of the bin.

Thereafter, the number of bins was increased in both directions to create a smoother graph (Figure 19). Still the results were not completely satisfying for the behaviour that the P_{mpp} for low temperatures ($T_{mod} < 15^oC$) which seem to be 'too low'.

To quantify this qualitative observation, the PR matrix is the best graph to check this hypothesis (Figure 20).
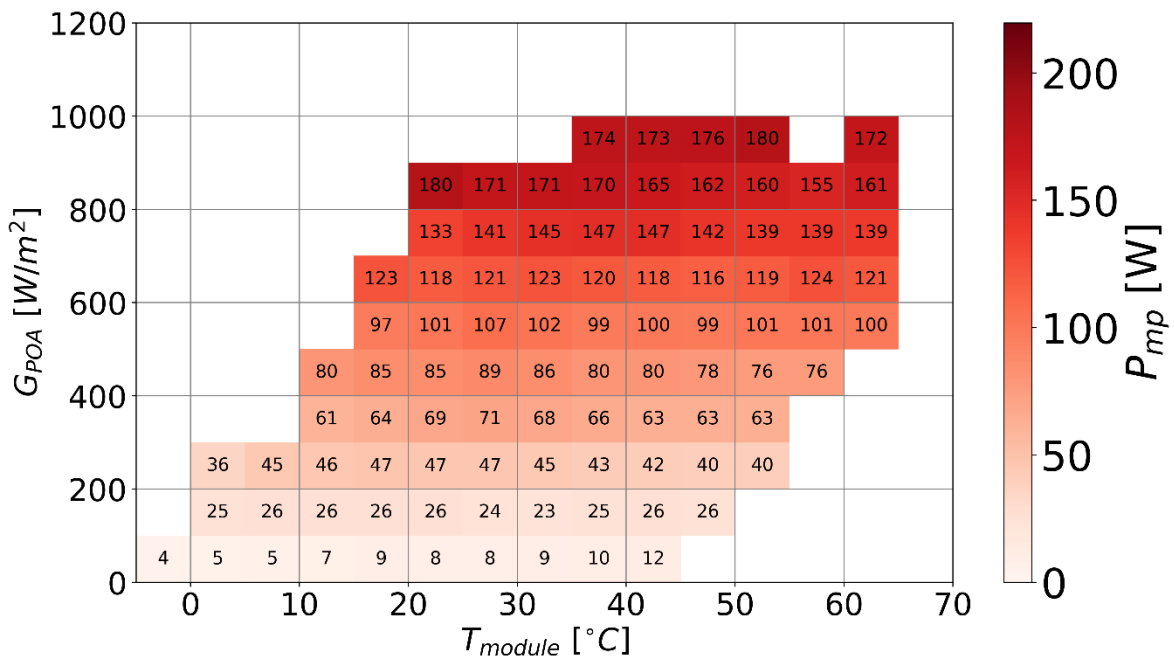
Figure 19: P_mpp as a function of T_mod and G_POA. Bin sizing not according to the norm but set equidistant at 100 W/m² and 5⁰C.

$$\text{Figure 19: } P_{mpp} \text{ as a function of } T_{mod} \text{ and } G_{POA}.$$
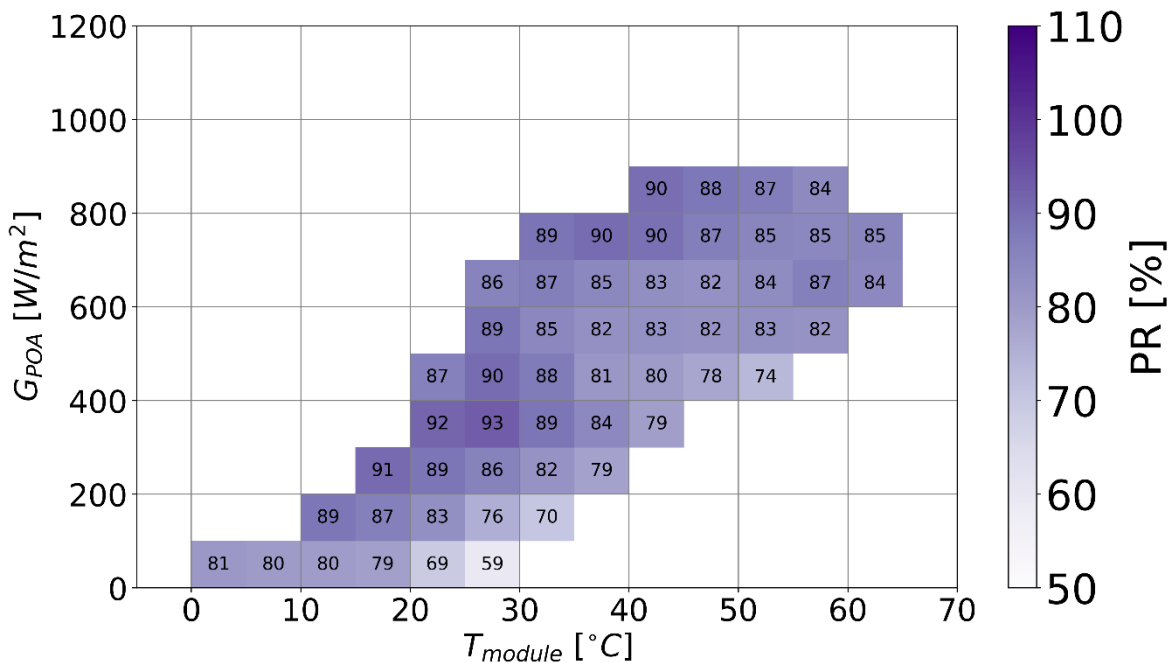
Figure 20: PR as a function of T_mod and G_POA with the fine binning. The additional threshold applied, please refer to text.

An additional threshold (on top of criterium n> 5) has been applied while composing Figure 20: only bins that contribute more than 0.5% to the full year specific yield are included. Looking at Figure 20, we see a much better understandable trend in which PR is always decreasing with increasing T_mod. One other remaining observation in Figure 20 cannot be neglected: the PR for

all lowest bins with 100 W/m^2 is significantly lower than expected. We proposed the hypothesis that these irradiation levels are reached in a façade mostly during shallow angles of sun light. Therefore, we calculated the AOI for each measurement point, and visualized the result in the same matrix graph, see Figure 21.
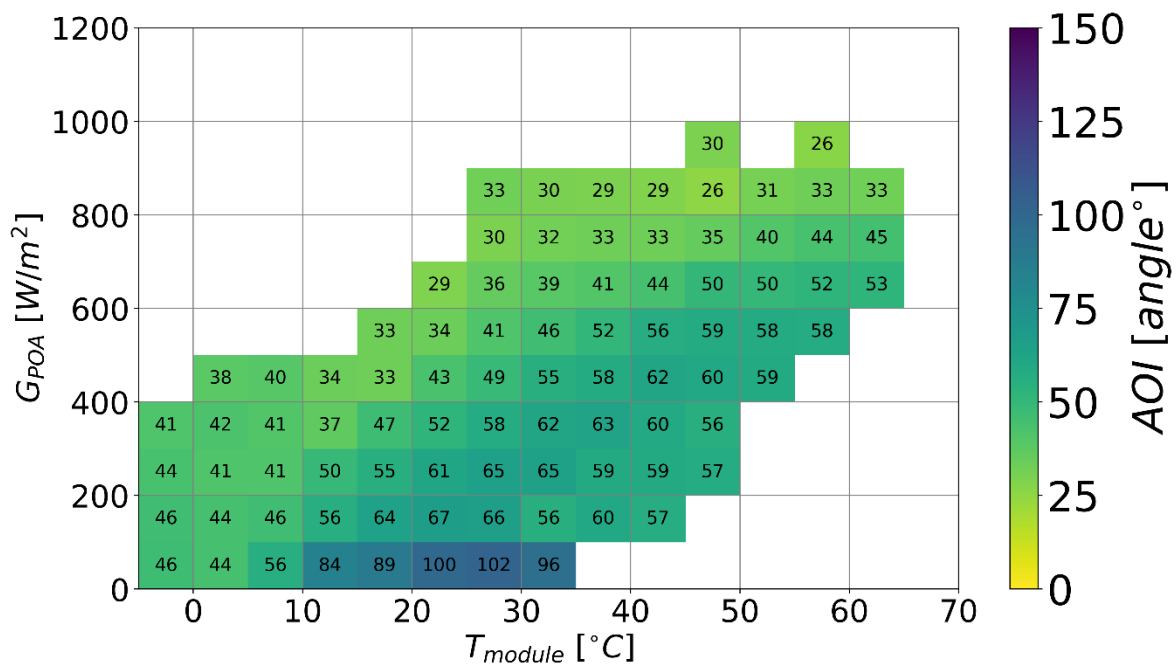
Figure 21: AOI as a function of T$_{mod}$ and G$_{POA}$ with the fine binning.

Please note that for AOI > 90º, the sun is behind the PV module, and hence all irradiance on these moments will be in the form of diffuse light. The effect of AOI on the module power is called Incidence Angle Modifier (IAM), which is a monotonic decreasing function of AOI from 1 till 0. We were not in the possibility to measure this IAM-function (the correct way to do so is specified in 61853-2). However, a general assumption for the IAM suits our purpose to get a quantitative feeling if AOI-effects are large enough to explain the lower power of the 100 W/m^2-bins. The ASHRAE-function with b$_0$=0.05 [53] has been applied to each measurement point. Thereafter the statistics on the IAM of each bin is plotted.

Figure 22 clearly shows how strong the shallow sunlight hours (high AOI-values) are expected to decrease the module power.
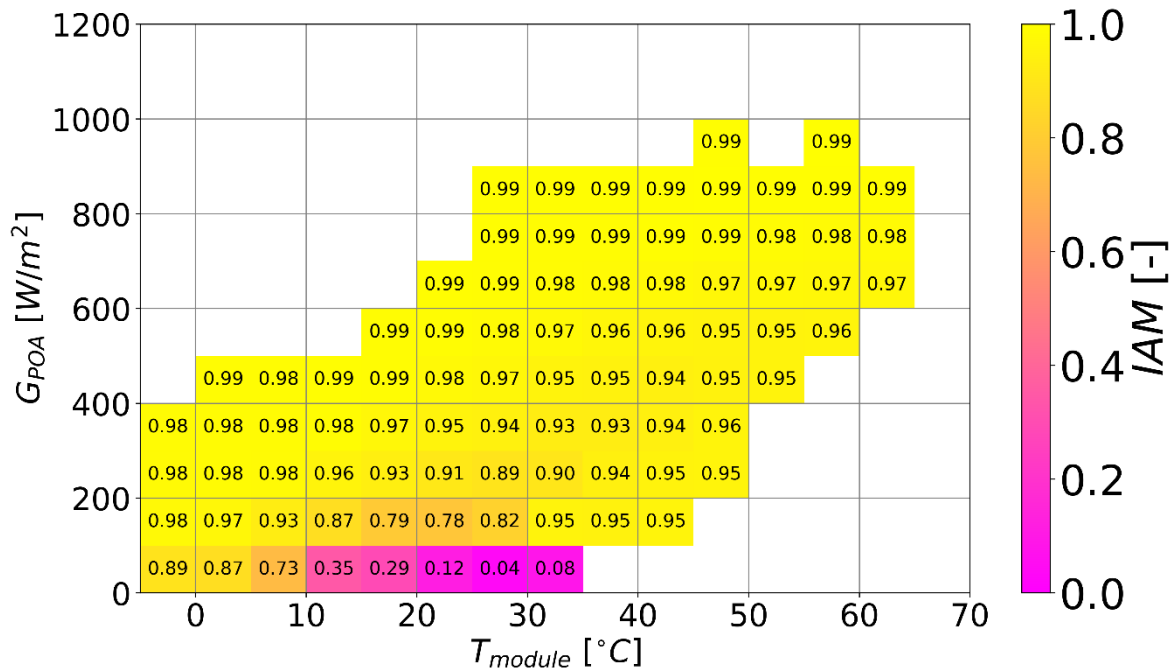
Figure 22: IAM (calculated from the ASHRAE-function) as a function of T_mod and G_POA with the fine binning.

The new visualization including statistics is demonstrated to three use cases [50]. Also within the phase 2 of IEA PVPS Task 15, which started in March 2020, these tools will be used to analyze full-year BIPV module measurement data from seven test sites over the world.

2.4 IEC 61853-1 Matrix Data Sets

Sandia National Laboratories sent a group of nine PV modules to CFV Labs in Albuquerque, New Mexico USA to be tested according to IEC 61853-1. The results of these tests have been made available on the PV Performance Modelling Collaborative website [54]. A list of these modules is given in Table 6.

Table 6: Sandia modules tested to IEC 61853-1.

Manufacturer	Model	Cell technology
Jinko Solar	JKM260P-60	Multi-c-Si
LG	LG320N1K-A5	N-type Mono-Si
Panasonic	VBHN325SA 16	HIT Mono-Si
Canadian Solar	CS6K-270P	Multi-c-Si
Canadian Solar	CS6K-275M	Mono-Si

Hanwha Q-Cells	Q.PLUS BFR-G4.1 280	Multi_Si PERC
Hanwha Q-Cells	Q.PEAK-G4.1 300	Mono-Si PERC
Mission Solar	MSE300SQ5T	Mono-Si PERC
Itek Energy	IT-360-SE72	Mono-Si PERC

All matrix testing was performed by CFV Labs (formerly CFV Solar), an ISO 17025-accredited test lab, in conformity with IEC 61853-1:2011 § 8.1. The modules were characterized in late 2019 under contract to Sandia.

All nine PV modules were preconditioned by outdoor exposure at open circuit for at least 40 kWh/m^2 of insolation and electroluminescence images were taken prior to matrix testing. Module performance at STC was measured according to IEC 61215-2:2016 MQT 06.1.

The matrix flash measurements were made using an AAA Halm pulse-type solar simulator with irradiance controlled with a co-planer Fraunhofer WPVS type reference cell that meets the requirements of IEC 60904-1:2015. A spectral mismatch factor of 1.0 was used as there were no EQE data available for any of the modules. External quantum efficiency (EQE) is the ratio of the number of charge carriers collected by the solar cell to the number of photons of a given energy shining on the solar cell from outside. An integrated thermal chamber varied the module temperature with a laminar air flow, and the module temperature was monitored at four points with calibrated RTDs having uncertainties of ± 0.13°C. For each measurement, the max-min temperature spread was less than 1.5°C.

The test points cover irradiances from 100 to 1100 W/m^2, and temperatures from 15 to 75°C. In addition to the test points defined in IEC 61853-1:2011 § 8.1, measurements were obtained at five additional points at low irradiance/high-temperature combinations (200/50, 100/50, 400/75, 200/75, and 100/75). The irradiance was varied by adjusting the voltage applied to the Xenon arc lamp. The spectral match remains class A or better for all irradiances. Reported points are an average of three I-V curves at each irradiance/temperature condition.

The monitor cell was mounted at a location outside the thermal chamber and was not co-planar with the test module. The monitor cell sensitivity was adjusted to reproduce the P$_{mpp}$ measured at STC on the test module.

For each module there is a data report and a PVsyst 6 PAN file available for download [54]. The PAN files were prepared using CFV Labs's PANOpt® in-house software, which calculates PVsyst 6 single diode model parameters optimized to the matrix measurements. Starting with the measured values of I$_{sc}$, V$_{oc}$, I$_{mpp}$, V$_{mpp}$, I$_{sc}$, and an R$_s$ value calculated from the I-V curves with the Swanson method, the PANOpt® solver iterates over a given parameter space for R$_s$, R$_{sh}$, RshG0 until the PVsyst 6 model-predicted P$_{mpp}$ values over the Performance Matrix points match the measured values (average of three samples) with minimum error. PAN file model accuracy is reported for each module in its data report.

2.5 Characterization of Bifacial PV Modules

2.5.1 Output power characterization

Due to power gain driven by the rear irradiance driven for bifacial PV modules, more characteristic parameters, such as the bifaciality coefficient and BiFi (quantity which indicates the power gain per unit of rear irradiance) should be considered besides the characteristic parameters of traditional monofacial modules like I_{sc}, V_{oc} and P_{max}. The procedures for determining these parameters are described in the IEC TS 60904-1-2 [55].

The technical specification includes procedures by means of a solar simulator and under natural light. For the procedures with a solar simulator two options are described: the single-side illumination and the double side illumination, as shown in Figure 23.
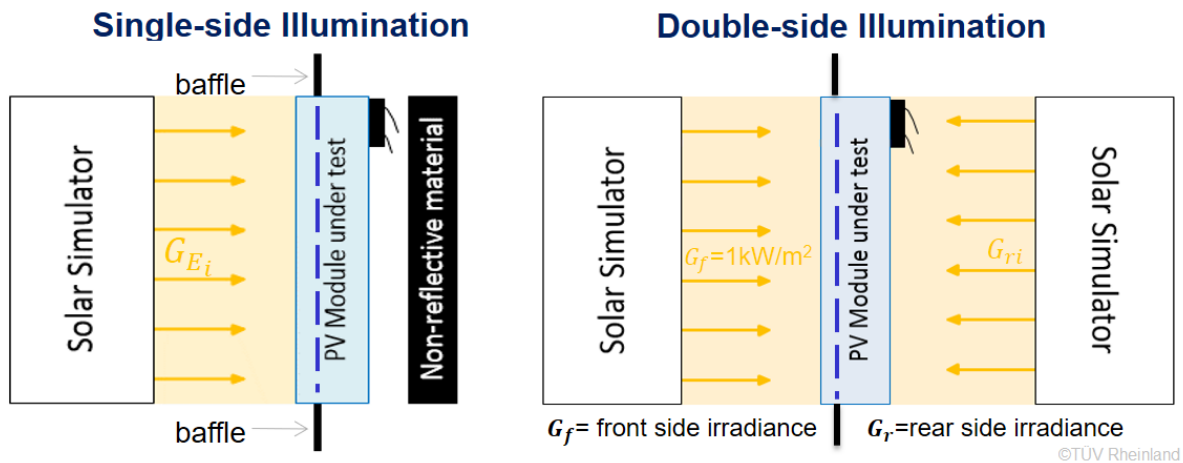
Figure 23: Output power characterization of bifacial PV modules: Approaches with a solar simulator.

The differences and the parameters of the bifacial module are described in Table 7.

Since 2018, the bifacial module have been gradually developed and widely used in China, to regulate the performance evaluation method of bifacial module in the market of China, dozens of photovoltaic companies and third-party laboratories jointly initiated and formulated the China PV Industry standard 1619-2018 (Measurement procedures for current-voltage characteristics of bifacial photovoltaic (PV) modules) [56]. The International Electrotechnical Commission (IEC) published the IEC TS 60904-1-2 in 2019. Table 8 summarizes the similarities and differences between Chinese industry standard and IEC standard in three different test environments such as single-side illumination, bifacial illumination and outdoor

Table 7: The parameters of the bifacial module defined in IEC TS 60904-1-2 [55].

Parameters	Description
The I-V characteristics of front side and rear side of bifacial module I_{scf}, V_{ocf}, P_{maxf} I_{scr}, V_{ocr}, P_{maxr}	The procedure for the measurement of the *I-V* characteristics of a bifacial PV device is based on the same basic principles as in IEC 60904-1, but requires some additional considerations and also provides supplementary characteristics specific to bifacial devices.
Bifacialities Coefficients φ_{Isc}, φ_{Voc}, φ_{Pmax}	Property expressing the ratio between the main characteristics of the rear side and the front side of a bifacial PV device quantified by specific bifaciality coefficients which can be determined by: $$\varphi_{Isc} = \frac{I_{scr}}{I_{scf}}$$ $$\varphi_{Voc} = \frac{V_{ocr}}{V_{ocf}}$$ $$\varphi_{Pmax} = \frac{P_{maxr}}{P_{maxf}}$$
Bifacial Factor φ	φ is the minimum value between the Isc and the Pmax bifaciality coefficients φIsc and $\varphi Pmax$.
The I-V characteristics of bifacial module considering rear irradiance driven power gain yield I_{sc}, V_{oc}, P_{max}	a) In the case of bifacial illumination: with G_r= 1000 W/m^2 on the front side plus at least two different rear side irradiance levels G_r; b) In the case of single sided illumination: with at least two different equivalent irradiance levels G_E on the front side according to G_{Ei}= 1000 W/m^2 + $\varphi \cdot$ G_{ri}; $\varphi = Min(\varphi_{P_{max}}, \varphi_{I_{sc}})$
The rear irradiance driven power gain yield BiFi	The slope derived from the linear fit of the P_{max} versus G_r data series, This linear least squares fit shall be forced to cross the P_{max} axis at P_{maxstc} and its non-linearity shall be considered in the uncertainty estimation

Table 8: Comparison of IEC and CQC standards for energy rating of bifacial module.

Test items		Standards	
		IEC TS 60904-1-2	China PV Industry Standard 1619-2018
Bifaciality coefficient φ		$\varphi = \min(\varphi_{Isc}, \varphi_{Pmax})$	
Determination of the rear irradiance driven power gain yield	Double sided illumination	G_f= 1000 W/m^2 on the front side plus at least two different rear side irradiance levels G_r	-
	Single sided illumination	equivalent irradiance levels G_{Ei} on the front side according to $G_{Ei} = 1000\ W/m^2 + \varphi \cdot G_{ri}$	
		At least two levels of irradiance should be tested i = 1, 2, 3,…; $0 \leq G_{r1} < 100$ W/m^2, 100 W/m$^2 \leq G_{r2} < 200$ W/m^2 and 200 W/m$^2 \leq G_{r3}…$	At least the rear irradiance of 50 W/m^2, 100 W/m^2,150 W/m^2, 200 W/m^2 should be tested
	Outdoor	The non-uniformity of irradiance on the rear side shall be below 10% which should be measured by at least 5 points besides the reference device used for the irradiance measurement on the rear side；A distance of 0,5 m to 1,0 m between the bottom edge of the device and the ground is recommended	

-		Test conditions: Irradiance ≥ 800 W/m², module temperature: 25 ± 1℃). The I-V characteristics of bifacial should be measured at front irradiance 1000 W/m² (or corrected to the irradiance value), and the rear irradiance G_r should be selected at least four levels of the rear-side irradiance $G_{r, 50}$ $G_{r, 100}$ $G_{r, 150}$ $G_{r, 200}$). If the irradiance of the ear side cannot be obtained, the linear interpolation method can be used.
BiFi, the rear irradiance driven power gain yield.	The rear irradiance driven power gain yield, BiFi, is the slope derived from the linear fit of the P_{max} versus G_r data series	-

2.5.2 The energy rating of PV modules based on IEC standards

At present, the series standards of IEC 61853 clarify the test requirements for monofacial PV modules of power rating at various temperatures and irradiances, the test procedures for environment parameters (such as spectral responsivity, incidence angle and module operation temperature measurements) and standard reference climatic profiles. According to these standards, the climatic specific energy rating of monofacial module for a complete year at maximum power operation for different reference climate can be calculated. However, for bifacial module, besides the IEC TS 60904-1-2 for output power characterization, the energy rating of bifacial module has not been further clarified. The IEC standards concerning about energy rating of monofacial module and bifacial module are listed as follows, it can be seen that the IEC standards for energy rating calculations are mainly for monofacial modules.

Table 9: Comparison of existing IEC standards for energy rating of bifacial module and monofacial module.

Parameter/characteristics	Monofacial module	Bifacial module
Pmax	IEC TS 60904-1	IEC TS 60904-1-2
Bifaciality	———	IEC TS 60904-1-2
Power rating at various temperatures and irradiance	IEC 61853-1	X
Spectral responsivity	IEC 60904-8	X
Incidence angle	IEC 61853-2	X
Module operation temperature	IEC 61853-2	X
Energy rating calculation method	IEC 61853-3	X

2.5.3 An outdoor experiment of energy rating for bifacial PV module

Until now, the outdoor test of bifacial module mainly focuses on the research of the irradiance of rear side and the rear irradiance driven power gain yield. Factors such as the solar elevation angle, height of mounting rack and the albedo will have greater impacts on the rear side irradiance of the bifacial module.

At the same time, the non-uniformity of the rear irradiance plays an important role when calculating the equivalent irradiance and consequently for the energy rating of bifacial PV modules. For the rear irradiance driven power gain yield, current research shows that the power gain of bifacial module increases with the height of mounting rack of module, but has less relationship with tilt angle of module [57].

For the research of determination of equivalent irradiance, in [58] it was compared the differences of energy rating between monofacial and bifacial modules. In this research, when only using the irradiance of front side of bifacial module to calculate the performance ratio (PR) , the result is quite different from that of monofacial module, which is 11% higher during the period of high irradiance (700-1100 W/m^2), and it is 20% higher than that of monofacial module at low irradiance situation, which is even much higher at situation of low irradiance and high temperature (40%). By using the equivalent irradiance, which is determined by the equation as:

$$G_E = G_f + \varphi \cdot G_r \qquad\qquad (7)$$

In that case, the performance ratio of bifacial module is more consistent with that of monofacial module.

According to [58], the results of performance ratio vary greatly by using different calculation methods, However, there is no standard for energy rating of bifacial module currently, and the key point of performance ratio calculation of bifacial module is to determine the value of the irradiance involved in the calculation process, and when using the equivalent irradiance to calculate performance ratio, the uniformity of the rear irradiance and the applicability of bifaciality coefficient in outdoor condition need to be considered.

The Institute of Electrical Engineering, Chinese Academy of Sciences has established an outdoor testing platform in Baoding, Hebei Province, China, which is used to carry out the energy rating experiments of bifacial modules, the testing platform information is as follows:

Table 10: Testing platform information.

Location:	N 38 ° 55'38.77 '' E 115 ° 26'7.18 ''
Climate type:	Warm climate
Ground:	White concrete
Test equipment:	Pyranometers, I-V tracer
Nominal parameters of tested module (P_{max}):	Monofacial module: 310 W Bifacial components: 330 W, 345 W
Measurement parameters:	Front/rear irradiance of the module (collection interval: 5 s); I-V characteristics of module (collection interval: 5 min)

Figure 24: Testing platform in Hebei province of China.

For the calculation of the performance ratio of bifacial module, three different methods are used here to determine the irradiance parameter involved in the calculation, which are:

1. Only the irradiance of front side is used for performance ratio calculation;

2. Adopt the bifaciality coefficient defined in the IEC TS 60904-1-2 to calculate the equivalent irradiance, and use the equivalent irradiance to calculate performance ratio; GE=Gf+ϕ·Gr

3. Using the sum of irradiance of both sides as irradiance involved in the performance ratio calculation.

According to the statistics of the irradiance change of the front and rear sides, the curve of the irradiance change in one day is drawn as follows:
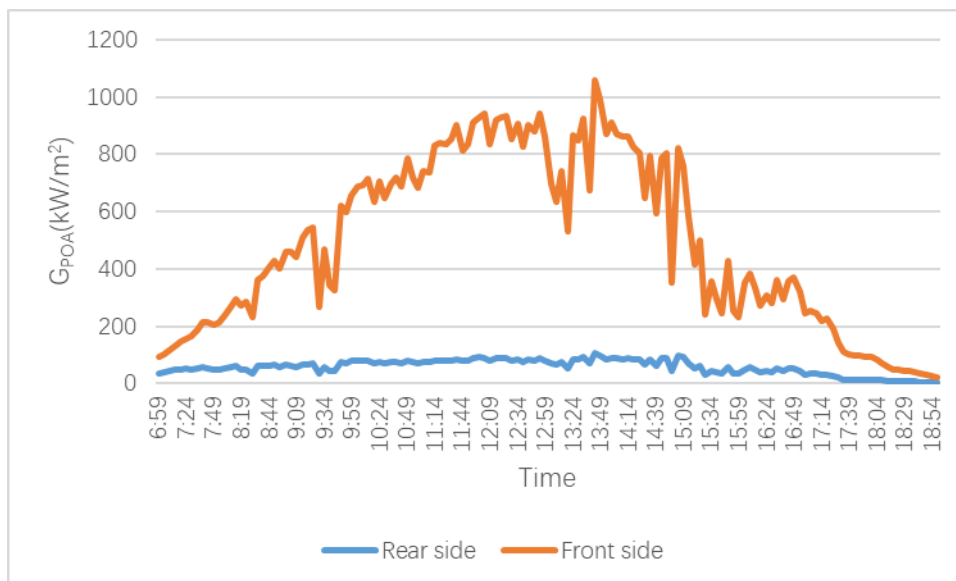
Figure 25: Real-time irradiance changes on the front and rear sides of bifacial module.

The comparison of performance ratio of bifacial module under different irradiance calculation methods and monofacial are shown in Figure 26. It can be seen that for different irradiance calculation methods, although the trend of performance ratio changes in one day is relatively consistent, but because the rear irradiance is not considered under the first method, the performance ratio calculation result is greater than 100%, and compared with the calculation method considering the rear irradiance, the calculation result without considering the rear irradiance is about 10% higher.

From morning to noon, the performance ratio of the bifacial module is higher than that of the monofacial module, while in the afternoon, the performance ratio of the bifacial module considering the rear irradiance is slightly lower than that of the monofacial module. The preliminary analysis shows that it is caused by the irradiance uniformity of the rear side. Due to the oblique sunlight in the afternoon, the part of the rear side which is closed to the ground could be shaded, so the irradiance of high position is higher than that of the lower position which is shaded, and when the pyranometer is placed at the higher position of the module, the measured irradiance of the rear side would be higher than the actual value, resulting in the lower performance ratio of the bifacial module.

For the calculation of performance ratio of bifacial PV modules, although the calculation method is the same as for monofacial samples, due to the power gain generated by the rear side to determine the effective irradiance has become the key. Figure 27 shows a comparison of the PR by choosing different approaches of irradiance selection.

On the one hand, for the calculation of equivalent irradiance, the influence of rear irradiance uniformity should be considered. In addition, when the bifaciality coefficient of module defined

in IEC TS 60904-1-2 is used to calculate the equivalent irradiance, it is necessary to consider whether the bifaciality coefficient measured under indoor experimental conditions is suitable for the irradiance calculation under outdoor test conditions.
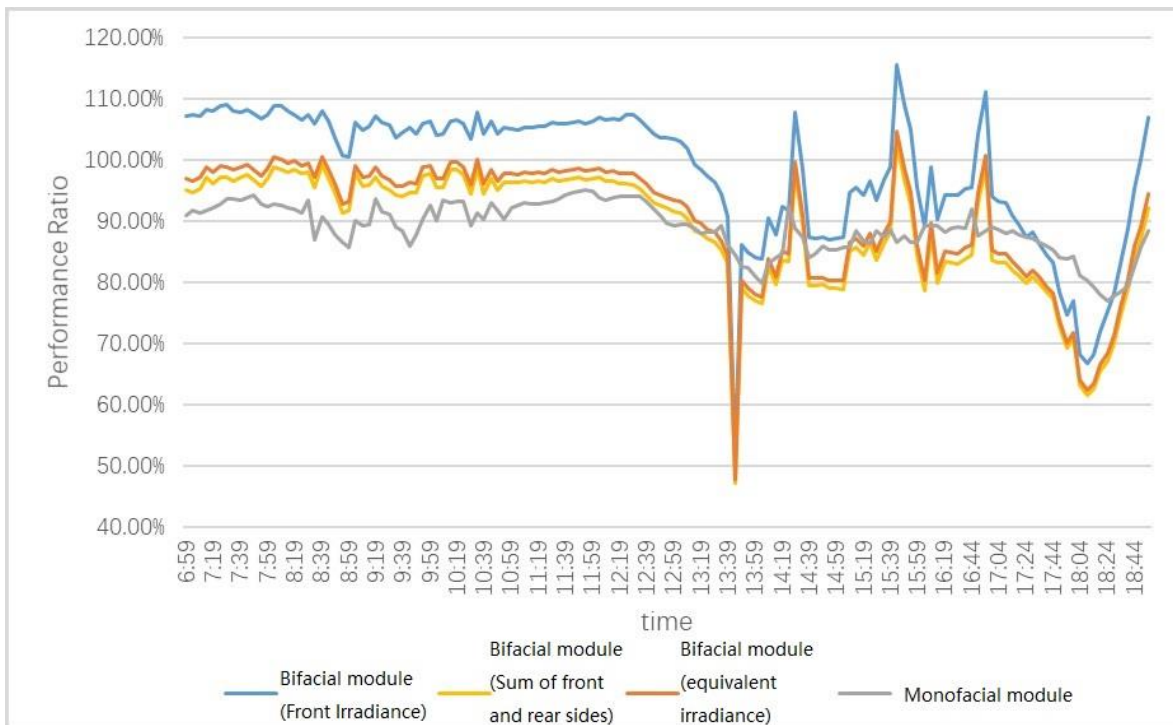
Figure 26: Comparison of PR between bifacial module and monofacial module.
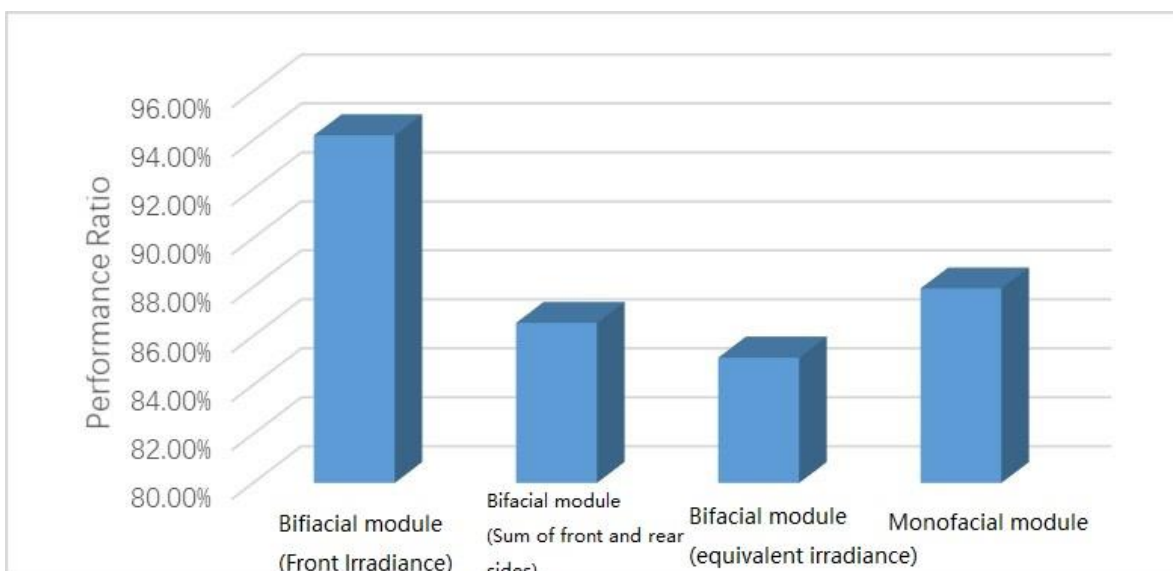
Figure 27: PR of bifacial module and monofacial module in one day.

It should also be noted that the rear irradiance of the bifacial module varies according to the height of the module to the ground, the material of the ground, shading and other factors, so the performance ratio of the bifacial module is not only related to the climate area, but also to

the surrounding environment and installation layout of the module. Therefore, how to determine the influence of support height and other detail factors on the performance ratio calculation results of bifacial module in typical climate areas is also a key point to be considered.

Comparison of field climatic data

The field environmental data is analysed as follows:
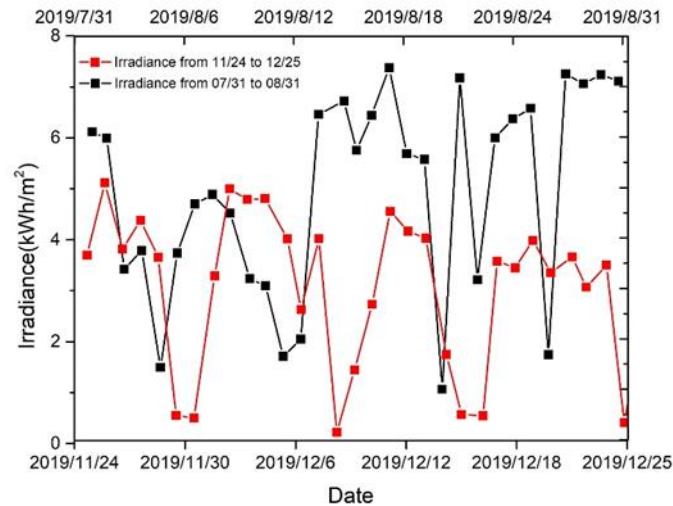
Figure 28: Comparison of daily irradiance in different seasons.

By comparing the front irradiance of modules in different months, it can be found that the accumulated irradiance in summer is significantly higher than that in winter.
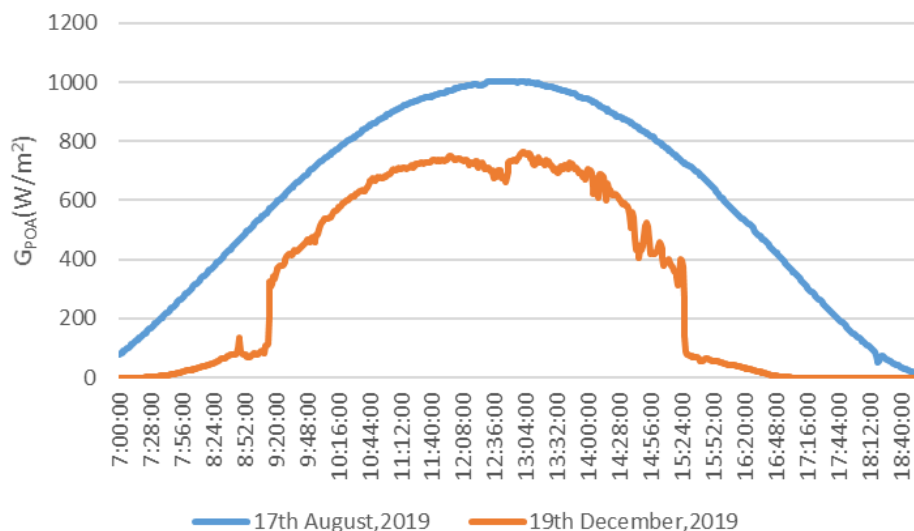
Figure 29: Irradiance Change of one day in different seasons.

Based on the analysis of the meteorological data from August 2019 to December 2019, line charts of the irradiance amount changes are drawn as shown in Figure 30. It can be seen from the charts that the daily accumulated radiation amount on the front side of the module is much higher than that on the rear side of the module when the irradiation resources are good in

sunny days. In the case of poor irradiation resources in cloudy days, the difference between the accumulated daily irradiation amount on the front and rear of the module is smaller.
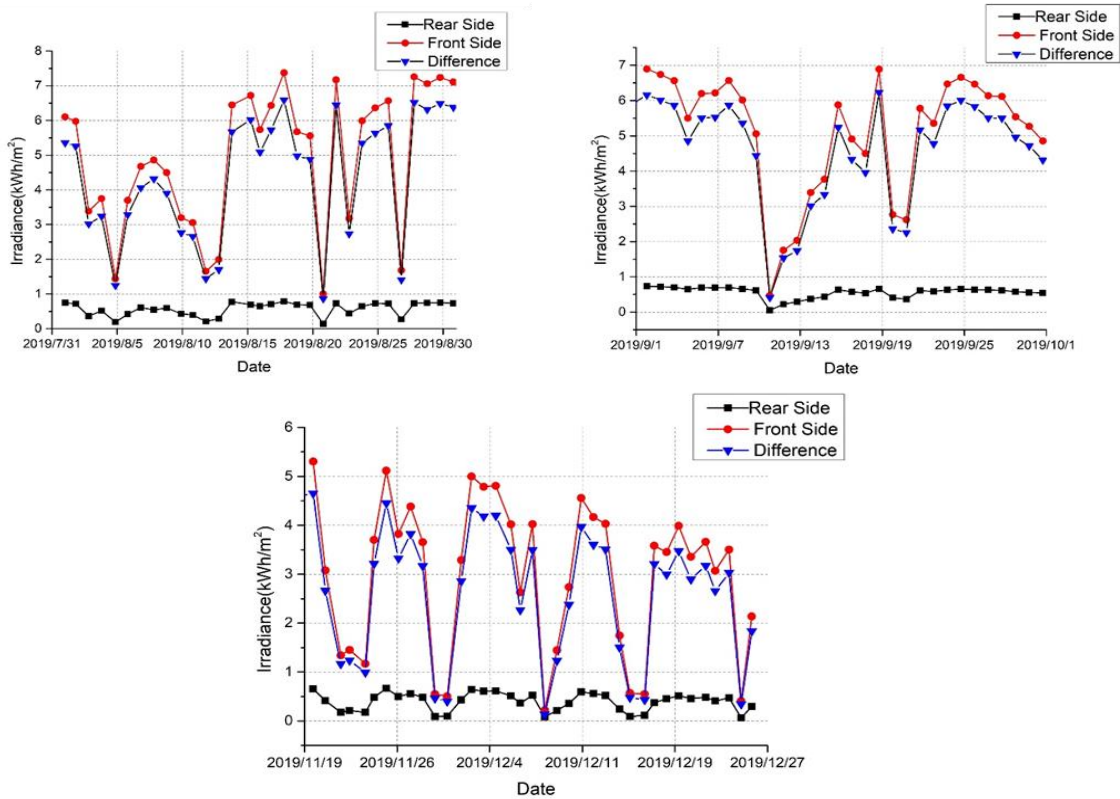
Figure 30: Daily radiation variation between the front and rear sides.

The data collected in August and September of the bifacial module (nominal power: 345 Wp) is analysed as follows, the daily performance ratio of bifacial module is calculated by the performance ratio calculation formula as:

$$PR = \frac{\sum_{i=1}^{N} P_i}{\sum_{i=1}^{N} G_i} \cdot \frac{G_{STC}}{P_n} \tag{8}$$

P_i: Measured power of module G_i: Measured irradiance

G_{STC}: Irradiance under STC P_n: nominal power of module
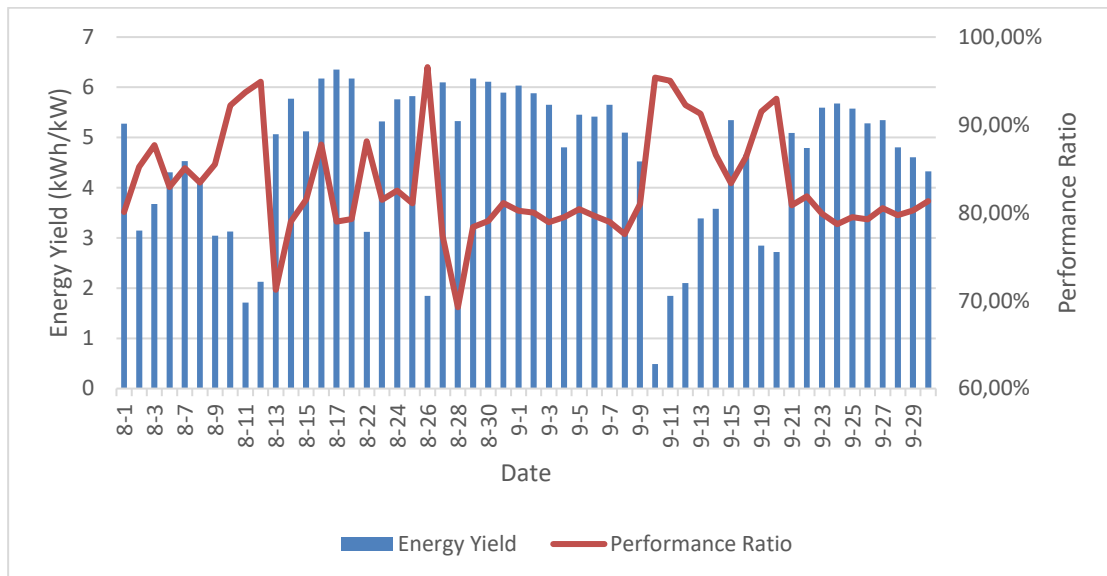
Figure 31: Power generation capacity & PR of bifacial module.

The daily power generation of the bifacial module with the nominal power of 345 W is generally about 2 kWh when the sun resource is abundant, and that of bifacial module in cloudy days is about 0.5 kWh. At the same time, comparing the single-day performance of the bifacial module, it can be found that when the sun resource is abundant and the daily power generation of the module is high, the performance ratio of module is generally about 80%; when the daily power generation of the bifacial module is low, the single-day performance ratio of bifacial module is increasing instead.

3   ENERGY METEOROLOGY IN PV TECHNOLOGY

3.1 Climate Zone Systems and Defining PV Specific Climate Zones

As global installations of photovoltaic modules spread, a greater understanding of climatic stressors is warranted to increase module component lifetime.

Climatic Zone ratings have arisen as a convenient classification for the general weather patterns in a specific location. In general, most systems classify climate based on the annual temperature and humidity of a region. The main differences between climate zone classifications are the criterion of classification for each region and the stressors used in the classification.

3.1.1   Köppen-Geiger climate zones

The most commonly used stressors for climate classification are temperature and humidity. Climate classification systems benefit from being widely accepted and used in many fields. The Köppen-Geiger classification is used most often. This system, first introduced in 1884 by Walidmir Köppen [59], was improved upon by Rudolf Geiger in 1951 [60]. The Köppen-Geiger classification (KGC) divides the world into five main climatic groups, A, B, C, D, E, (Equatorial, Arid, Warm Temperate, Snow, and Polar respectively). The main groups are then divided into classifications with the addition of two more letters. The two additional categories are Precipitation (W, S, f, w, sm) and Temperature (h, k, a, b, c, d, F, T,). The criterion for each classification group is based on the type of foliage that can grow in a specific region [59]. So, the Dfa climate is a snowy climate with year round precipitation and a hot summer. Although the criteria are based on foliage growth, they are determined by yearly measurements of variance temperature and precipitation. For example, the D climate has an average temperature of < 3°C during its coldest month. The current criteria for classification can be seen in Table 17. The climate classification is updated regularly to represent current climatic conditions [16, 61]]. There are multiple current Köppen-Geiger maps generated with different sources of satellite weather data [60, 62–64]

Additionally, higher resolution maps of climate are approaching 1km resolution at the equator [65]. In addition to increasing the resolution and data quality used in classification, groups have also refined the criterion for classification. Peel et al. have refined the criterion for main climate classification using suggestions from Russel et al. [63, 65, 66]. The threshold value classifying C/D climates has been increased from -3°C to 0°C. Beck et al. have made slight adjustments to the precipitation zones [63].The precipitation zone for the B climate has been changed to describing whether or not 70% of the precipitation falls in the summer or winter months. Finally, the precipitation zones for the C & D climates have been made mutually exclusive by providing s when the majority of precipitation falls in the winter and w otherwise.

The use of KG in the PV industry also is present in essential publications of the field. Many groups use the Köppen-Geiger in the classification of sample exposure [67–72] Jordan et al. built an extensive database of over 11000 degradation rates worldwide to evaluate the relationship among the degradation rates and climate zones based loosely on KG and defined as desert, hot & humid, moderate, and snow [73]. The study of operating conditions of PV modules under different climates was carried out by Kohl et al., where four specific locations with ground measurements were named maritime, moderate, arid, alpine, and tropical, also based on the KG scheme [74]. Within the Infinity project, Eder et al. designed a comprehensive classification for indoor tests, which is related to real climate conditions by matching the KG climate zones tropical, arid, moderate, and alpine [75].

Even though the basis of the KG scheme is not directly related to the performance and degradation of PV technologies, it provides a logical definition of climate zones as human beings know them. For example, KG defines well the desert areas (high temperature and low precipitation), which in general identify locations with harsh conditions or polar regions known as places with shallow temperatures and high possibilities of snowfall along the year. However, no standard has been defined, and the climate zones differ from one group to another. As a result of this, scientific groups work on different approaches to define relevant climate zones for PV technologies.

3.1.2 INFINITY climate-specific accelerated aging test procedures

In the frame of the INFINITY project, G. Eder et al. proposed a first approach to relate the degradation modes of PV modules to specific climate zones [75]. They designed a climate classification for indoor testing procedures based on the main KG climates zones.

The matrix defines the climates Moderate (with five subzones), Tropical (x3), Arid (x3), and Alpine (x3). For each climate zone, different duration and magnitude of the stresses are indicated. The aging tests include as stresses: temperature, humidity, irradiation, dynamic mechanical loads, thermal cycles, salt, and sand.

3.1.3 The Köppen-Geiger-Photovoltaic climate classification scheme

As an extension and simplification of the KG scheme, in [38], the solar resource was included as a new layer of the KG scheme. Using global gridded data, temperature, precipitation, and irradiation were combined to create the Köppen-Geiger-Photovoltaic (KGPV) scheme with 12 climate zones defined by two letters. The first letter (*TP*-zones) is based on the criteria of the KG CZ. It is important to note that the main climate zones have been relabelled and the Arid zone (B) in the traditional scheme has been divided into the main climates: B-desert and C-Steppe in the new scheme. Thus, *TP*-zones are defined as: A-Tropical, B-Desert, C-Steppe, D-Temperate, E-Cold, and F-Polar climates. The second letter (*I*-zones) considers the level of global horizontal irradiation, and it defines four different zones: L-Low, M-Medium, H-High, and K-Very High irradiation zones. The criterion to divide the *I*-zones is given by 1130 kWh/m^2 between L-M, 1560 kWh/m^2 between M-H, and 2070 kWh/m^2 between H-K.

The KGPV scheme also includes a selection of the most relevant climate zones depending on the population density and the land-surface ratio, reducing the number of zones to 12 out of 24 possibilities. The result of the KGPV climate classification is illustrated in Figure 32, and available online as Mendeley dataset.

Table 11: The Köppen-Geiger Climate Classification Criterion. This table along with certain yearly values of temperature and precipitation can be used to calculate any location`s climate classification. P_{smin}, P_{wmin}, P_{smax}, and P_{wmax} represent the minima and maxima of the precipitation for summer and winter seasons. T_{min}, T_{max}, T_{ann}, and T_{mon} are the minima, maxima, annual, and monthly temperatures, respectively. Temperature values are in °C and precipitation is measured in mm of water. Additionally, the Pth variable is calculated for the B- arid zone based on the annual temperature. See Kottek et.al [16].

Group	Type	Sub-Type	Description	Criterion
A – Tropical $T_{min} \geq +18°C$	f		Rainforest	$P_{min} \geq 60$ mm
	m		Monsoon	$P_{ann} \geq 25 (100-P_{min})$ mm
	w		Savanna	$P_{min} < 60$ mm in winter
B – Arid $P_{ann} < 10\ P^{th}$	w		Desert	$P_{ann} \leq 5\ P^{th}$
	S		Steppe	$P_{ann} > 5\ P^{th}$
		h	Hot	$T_{ann} \geq +18°C$
		k	Cold	$T_{ann} < +18°C$
C - Temperate $-3°C < T_{min} < +18°C$	s		Dry Summer	
	w		Dry Winter	$P_{smax} > 10\ P_{wmin}$, $P_{wmin} < P_{smin}$
	F		Without dry season	Not Cs or Cw
		a	Hot Summer	$T_{max} \geq +22°C$
		b	Warm Summer	$T_{max} < +22°C$, $4\ T_{mon} \geq +10°C$
		c	Cold Summer	$T_{max} < +22°C$, $4\ T_{mon} \geq +10°C$, $T_{min} > -38°C$
D – Cold (Continental) $T_{min} \leq -3°C$	s		Dry Summer	$P_{smin} < P_{wmin}$, $P_{wmax} > 3\ P_{smin}$, $P_{smin} < 40$ mm
	w		Dry Winter	$P_{smax} > 10\ P_{wmin}$, $P_{wmin} < P_{smin}$
	F		Without dry season	Not Ds or Dw
		a	Hot Summer	$T_{max} \geq +22°C$
		b	Warm Summer	$T_{max} < +22°C$,

				$4\ T_{mon} \geq + 10°C$
	c	Cold Summer		$T_{max} < +22°C$, $4\ T_{mon} < + 10°C$, $T_{min} > - 38°C$
	d	Very cold Winter		$T_{max} < +22°C$, $4\ T_{mon} < + 10°C$, $T_{min} \leq - 38°C$
E – Polar	T		Tundra	$T_{max} \geq 0°C$
$T_{max} < +10°C$	F		Frost (ice cap)	$T_{max} < 0°C$

Calculation of Pth for the B – arid Climate Zone

P^{th}	$2\{T_{ann}\}$	if at least 2/3 of the annual precipitation occurs in winter
	$2\{T_{ann}\}+28$	if at least 2/3 of the annual precipitation occurs in summer
	$2\{T_{ann}\}+14$	otherwise
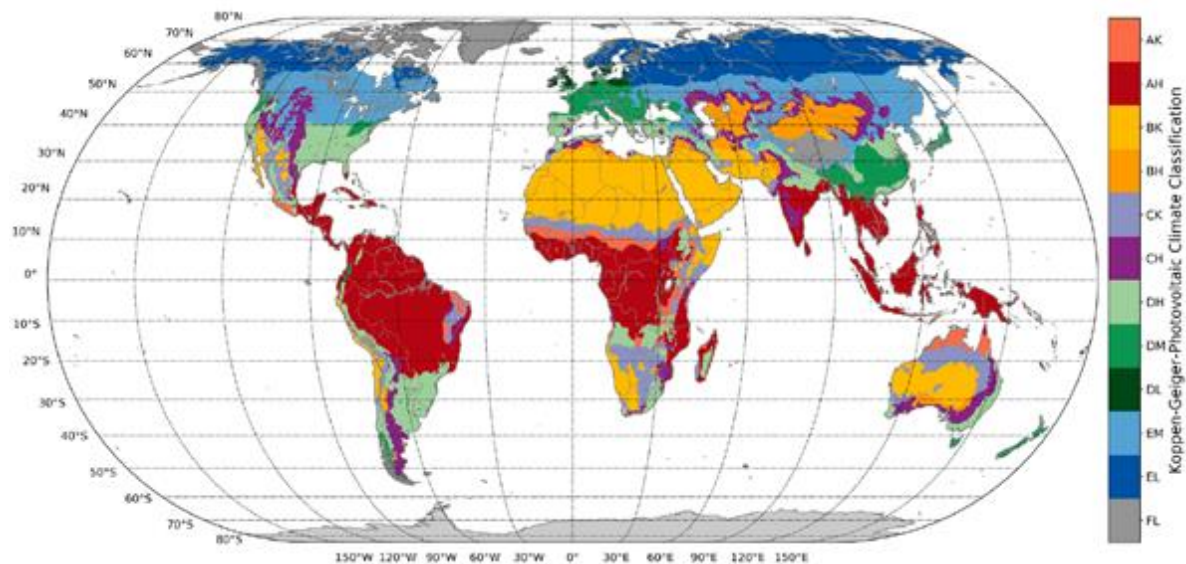
Figure 32: Köppen-Geiger-Photovoltaic climate classification with the 12 most relevant climate zones (Antarctica excluded). The first letter indicates the Temperature-Precipitation (TP)-zones: A-Tropical, B-Desert, C-Steppe, D-Temperate, E-Cold, and F- Polar. The second letter indicates the Irradiation (I)-zones: K-Very High, H-High, M-Medium, and L-Low irradiation (Source: [76]).

The KGPV climate zones have also been related to simulated degradation rates of PV modules. In [20], the degradation rates of a monocrystalline Silicon PV module are calculated worldwide using a physical model proposed by Kaaya et al.[76] based on temperature, UV

irradiation, and relative humidity. In Figure 33, the spatial distribution of degradation rates per each KGPV zone reflects explicit probabilities of high climate stress on PV modules in Tropical and Steppe climates, as well as low natural degradation in colder regions.
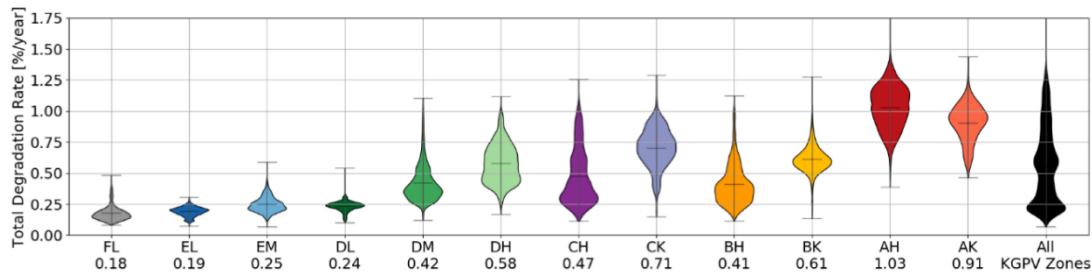
Figure 33: Spatial distribution of the total degradation rates in view of the KGPV climate zones. The average of total degradation rate per climate zone is indicated below each label in %/a (Source: [20]).

3.1.4 Photovoltaic degradation climate zones

An alternative scheme to assess the impact of climate variables on PV modules has been proposed by T. Karin et al. [35]. This climate classification scheme is based on specific stressors: Arrhenius-weighted mean module temperature, mean module temperature rate of change as a measure of thermal cycling, extreme low ambient temperature, wind stress, specific humidity as a measure of damp heat, and UV exposure. This scheme sets thresholds for each climate stressor (temperature, humidity, and wind) and gives a letter key for each. The so-called "Photovoltaic Degradation Climate Zones" (or PVCZ) defines the ones by a first letter depending on Arrhenius-weighted module temperature, calculated for different mounting configurations and activation energies, and a second letter determined by the mean specific humidity level.

A friendly tool is available online (https://pvtools.lbl.gov/pv-climate-stressors) [77] to visualize and obtain the main climate variables and climate zones.

3.1.5 Improvements and extension of the Köppen-Geiger climate classification with satellite weather data from 357 PV sites

Recently, Wieser et al. [78]. have evaluated the Köppen-Geiger climate classification with satellite weather data from 357 PV sites The assigned climate zones were found to be generally very accurate. The measured weather variables for each climate zone were observed to agree with the criterion laid out for each classification. As a slight modification, Wieser et al. have suggested increasing the threshold values that divide the temperature zones for B, C and D climates. By increasing the threshold values for the Bh/Bk, Ca/Cb and Da/Db split by 1°C to 2°C the criteria would better reflect the actual clustering of the temperature values for the specific climate zone (Figure 34).

Wieser et al. have suggested replacing the precipitation classification with a measurement of moisture condensation as well as implementing the irradiance categories proposed by Ascencio-Vasquez et al. [38]. Moisture condensation is more strongly correlated with the degradation of modules than precipitation. This effect was seen during the outdoor exposure of PET films [71].

The frequency of moisture condensation on the backside of modules can be calculated from module temperature, relative humidity, and ambient temperature. No clear relationship between the assigned precipitation category and the amount of days with condensation was found. Therefore, Wieser et al. has created four categories based on the annual amount of days with dewing based on 25th, 50th and 75th quartiles.

There is ongoing research to integrate the KGPV Irradiance class onto the actual KG climate zones.
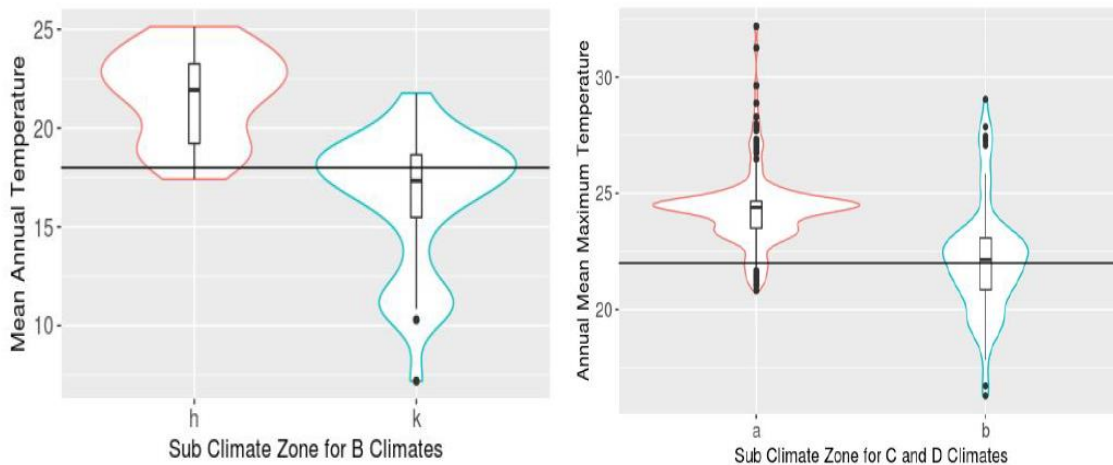
Figure 34: the distribution of Annual Mean Maximum Temperature for the B, C and D climates. The horizontal line represents the current criterion for classification. There is a significant overlap between the Temperature zones.

3.1.6 Climate zones determination tools

Many groups have compiled tables for the determination climate zones. The Köppen-Geiger climatic zones can be determined quickly and efficiently by using the kgc R package available on the Comprehensive R Archive Network (CRAN) [79]. Additionally, the Köppen-Geiger Photovoltaic Climate zones can be found as an open dataset hosted by Mendeley [80]. The Photovoltaic Degradation Climate Zones can be found online [77] to visualize and obtain the main climate variables and climate zones.

3.1.7 Conclusion

Climate classifications are needed to aggregate locations with similar climate stresses, and in this way, help to understand how the climate can affect the performance and degradation of PV technologies. The most popular scheme is known as the Köppen-Geiger climate classification. The scheme splits the Globe into five different main climates, and it has been the starting point and support for several research projects in the PV community.

However, the KG scheme only includes temperature and precipitation. For this reason, different approaches to creating specific climate zones for PV technologies have been developed, including climate variables such as global irradiance, UV irradiance, and wind speed. In the frame of the Infinity project, a scheme for indoor aging testing was proposed considering four main climates. For global approaches, the PVCZ scheme aims to understand the degradation of PV modules based on the Arrhenius law, and the KGPV scheme extends the KG climate classification by including irradiation as a new layer of the map.

The efforts to understand the impact of the climate on the performance and degradation of PV technologies show important progress, but still, the correlation with field-observed degradation modes are needed.

Climate classification presents a multifaceted problem, in which solutions have to balance specificity, accuracy, simplicity, and applicability.

3.2 Spectral Distribution and PV Performance

The reference global spectral irradiance for power rating and also for energy rating is defined in IEC 60904-3, for an air mass of 1.5 (AM1.5G) and a solar spectral irradiance of 1000 W/m² at a zenith angle of 48.19° on a 37° tilted surface. Under operating conditions in the field, the spectral irradiance distribution differs from the theoretical standard spectrum. An example of these differences is shown in the following figure, where the AM1.5 reference spectrum is compared to the real one-year spectrum measurements at four different location [40].
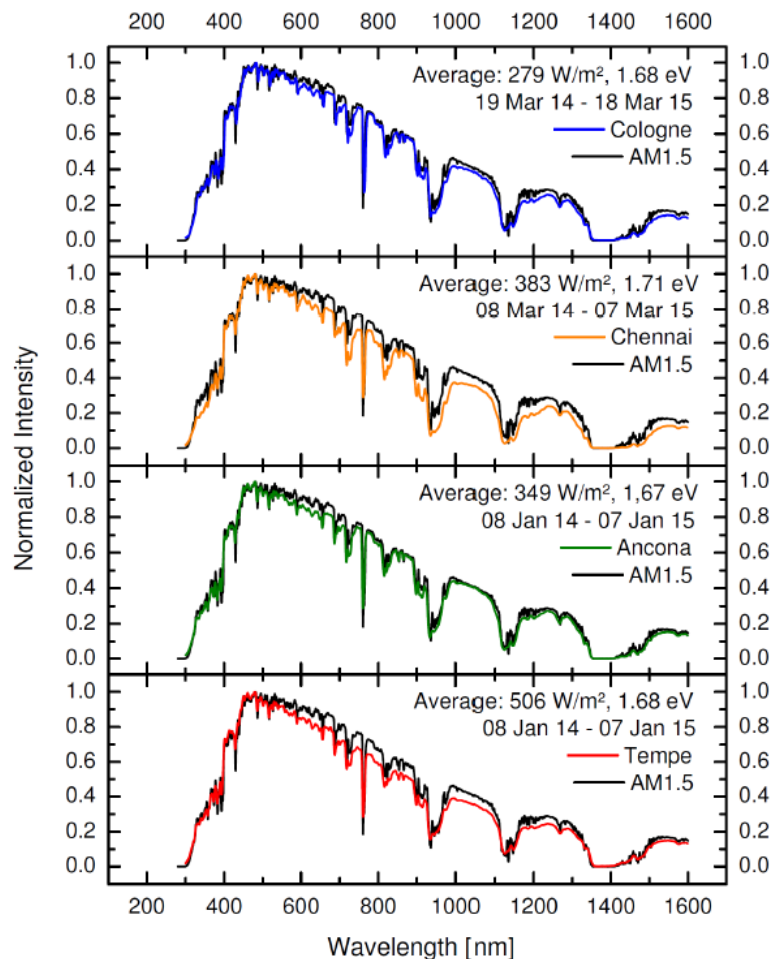
Figure 35: Average annual solar spectral irradiance of four test sites compared to AM1.5 spectral irradiance (Source: [40]).

This deviation of the local spectra from the standard does have an influence on the energy yield and performance, the extent depending on the respective installed PV technology [81]. Indeed, the spectral distribution is considered one of the main influencing factors on the performance of a given PV technology at a specific location besides illumination intensity and

temperature [28]. Recently, Lindsay et at. [82] reported the importance of considering spectral and angular effects in the modelling of PV power plants. The predicted PV performance can differ from the real performance by up to 15% considering only the *global horizontal* irradiance. The local spectra are also a source of uncertainty in business models of energy projects [83].

To rate the influence of the spectral changes on the PV module performance, some indicators have been introduced and applied in literature, see the review by Rodrigo et al. [84] who list in a structured overview the indexes and methods that assess the spectral effects on different PV technologies. Some of the given indexes are device-independent as the well-known Average Photon Energy (APE). Some indicators consider the devices' specifics. For a detailed description on the single parameters and the respective formulas along with the advantages and disadvantages of each parameter, see [84].

The APE reduces the spectral distribution being a function of the wavelength to a single number [85]. It calculates the average photon energy of spectra within a defined wavelength band (λ_{Min} and λ_{Max}) Therefore the integral of the spectral irradiance Ei (λ) is divided through the numerically integrated photon flux density ϕi (λ) and the conversion factor qe is the elementary electric charge.

$$APE = \int_{\lambda_{Min}}^{\lambda_{Max}} E_i(\lambda)d\lambda / q_e \int_{\lambda_{Min}}^{\lambda_{Max}} \phi_i(\lambda)d\lambda \tag{9}$$

The number gives information on the blueshift or redshift of a solar spectrum to the reference spectrum at standard test conditions (STC). An increase of the APE of the incident spectrum, i.e. a blue-rich spectrum, leads to an increase in the performance ratio of wide-bandgap PV modules, such as a-Si modules and a decrease for lower-bandgap modules [86]. A decrease in the APE has the opposite effect. However, poly-Si PV modules under test seem to be less sensitive to spectral changes. Their performance ratio varied less than 5% over the incident spectra. Similarly, Schweiger et al. [87] report that single junction PV modules based on crystalline silicon and most CI(G)S modules have been proven to be relatively stable under spectral distribution changes under their specific investigated local (Cologne, Germany) experimental circumstances. The same study reports on gains in the spectral factor of less than 3% in a-Si and 1% in CdTe.

Recently, similar results were found for three sites in Japan with slightly different representative APE's [88].The measured spectra and calculated and irradiance weighed spectral current gains/losses relative to STC (and to single crystalline silicon solar cells) show an annual spectral gain for CIS, cadmium-telluride (CdTe), perovskite and a-Si PV technologies (roughly between around 1% (CIS) and up to 7% (a-Si) – depending on the location) whereas there was found a tiny spectral loss (below 1%) for single-crystalline silicon back contact (BC), and heterostructure-with-intrinsic-thin-layer (HIT) PV technologies. For an overview based on other studies until 2017, see [84]. It is worth mentioning, that the global uniqueness of the APE for its representation of a spectral distribution is under discussion among different researchers [89–91]. In different studies it was shown that spectra with the same APE value applied to the same technology result in different performance indicators [22, 88, 92, 93].

An intuitive way to quantify the spectral shift or Spectral Mismatch (SMM) induced by a local spectrum compared to a standard spectrum is to compare the respective short circuit currents, I_{sc}'s. The incident solar spectrum has, therefore, to be known. The currents can be calculated using the spectral response (SR) or can be determined experimentally. The Spectral Mismatch and the Spectral Factor (SF) both give a percentage of gain or loss on the short-

circuit current due to a spectral variation to the spectrum at STC for a particular technology (the first indicator additionally using a reference).

A deviation from the standard spectrum introduces uncertainty in the prediction of annual energy yield which can range from less than 1% to up to 8.8% (for the high bandgap material a-Si) depending on location and module technology [84]. This uncertainty can be even higher, up to 15% for daily energy yield predictions for CdTe modules [94]. More and more time series of experimental spectral data, as well as models, are available to reduce that uncertainty.

A study performed by Ascencio-Vásquez et al. [38] presents a worldwide mapping of PV system performance for clear days based on the Köppen-Geiger climate classification. This classification is made only for c-Si and considers the spectral mismatch using an empiric method which depends on the clearness index and the AM to obtain a POA effective global horizontal irradiance. Climate variations due to the prognosed climate change until 2100 are also considered. Belluardo et al. [95] simulated spectra over a broad range of 124 considered locations worldwide. Losses in the spectral factor are found to be up to 3% and gains of up to 2% for the annual yield for c-Si technologies – as a maximum depending on the investigated locations. For the thin-film technologies, CdTe and CIGS the gains or losses are larger, and largest for a-Si with 10% for losses and gains. For thin-film technologies they found a latitudinal pattern (losses in the North, gains in the tropics), contrary to the homogeneity that was found for c-Si. These authors also explicitly discourage the use of APE due to the data dispersion.

While experimental spectral long-time data are scarce, satellite-based spectral irradiance data are available from sources like CMSAF or NREL, for example. Huld and Amillo, 2015 [96] report gains and losses in the same range as Belluardo et al. for cSi and CdTe modules in a worldwide study based on satellite data. Note that this general result does not hold according to [96] in high-elevation and low-temperature areas. The authors assume that the larger reduction of ca. -8% for both technologies and predicted for those regions is due to the fact that there the air has very low water vapour content.

Tandem solar cells are affected by spectral changes as the single cells are often series-connected and the current is limited. A decrease in the incident spectrum in a wavelength range relevant to one subcell results in a lower current. That lower current – if it ends up being the least – limits the overall current of the tandem stack regardless of any possible gain in another subcell. Simulations comparing different locations corresponding to a range also of the Köppen climate classification [97] calculate an average of 3.5% decrease in annual yield of perovskite/CIGS tandems mainly due to the influence of local spectra. This was concluded from a comparison of two terminal (series connection, thus, spectral changes limit overall current) versus four terminal tandem modules. Liu et al. [98]suggest to adapt the current matching of tandem solar cells to the local illumination conditions to minimize losses.

Beyond the above cited literature, some models and algorithms that aim at predicting the output power considering the spectral distribution are being developed and published on thin film [99–101] and multi-junction (also bifacial) modules. Note that a spectral impact factor (SIF) is also introduced in the literature, it corresponds to an irradiance-weighted average of the spectral mismatch factor [102]. This factor has been also been called *Spectral gain & loss* factor in a recent publication [88].

3.3 Data Format and Reference Data Sets

An accurate estimation of the energy yield of a PV system requires long-term climatological and solar resource data of the location in order to take into consideration weather patterns and

inter-annual and year-to-year variability of the weather conditions [8]. On the contrary, an energy rating study whose objective is to provide an unbiased comparison of the performance of different PV devices, can be performed considering a shorter time series dataset, as long as it is representative of the area considered.

In 2018, the International Electrotechnical Commission (IEC) completed the standard series 61853 "*Photovoltaic (PV) module performance testing and energy rating*" with the publication of Part 4 entitled "*Standard reference climatic profiles*". These standardized datasets provide the necessary climatic information over one year to perform the energy-rating analysis at any location. They comprise six different climatic profiles that represent the environmental conditions affecting PV systems installed worldwide.

The final result from applying IEC 61853 is a Climate Specific Energy Rating (*CSER*) value for each climate profile. *CSER* is a dimensionless parameter corresponding to the ratio of the energy yield estimated for the working conditions defined in each standard dataset to the energy yield that would be obtained if the module efficiency was that measured under STC. A more detailed description of the *CSER* is provided in Chapter 4.1. The standard reference datasets are the scope of the present section.

Two main aspects have to be considered when defining standardized climatic datasets for energy rating studies [13]:

    a) How much data, in terms of variables and length of the time series to include, and
    b) Since the climate profiles are based on real data, which set of geographical locations have to be used to represent the full range and geographical variation of the performance of PV devices worldwide.

The variables included in the datasets are the result of the equilibrium between the models used for the energy rating estimation and the data available. Both elements have to be appropriate and unbiased for all technologies in order not to favour or penalize certain technologies. At the same time, they must be able to provide accurate and realistic information to the user.

Even though there are many methods in the scientific bibliography to model the performance of a PV device, those included in any international standard are a compromise between simplicity and accuracy. The latter is in most cases limited by the required input data. For example, the development of methods for analysing satellite-based data that provide estimates of the spectrally resolved irradiance at a continental scale has enabled the implementation of a spectral correction factor in the energy rating method used in IEC 61853, which gives a better estimate of the irradiance effectively absorbed by the PV device. Previously, this spectral effect, which has a significant impact on the performance of PV devices, could not be considered systematically. As stated in [96], the estimated energy yield from c-Si and CdTe devices can, with or without considering spectral effects, vary by up to 6% depending on the location.

The IEC energy rating methodology also takes into consideration the thermal behaviour of the PV device, by calculating the operating temperature as a function of irradiance, ambient temperature and wind speed. This was possible due to the availability of datasets for the said climatological variables at a continental scale.

Regarding the size of the datasets, in the first drafts of the IEC 61853 standard, the use of standard days was considered. These standard days represented extreme conditions to generate an umbrella around all possible operating environments. The six proposed days were: Low-Irradiance-Low-Temperature (LILT), Medium-Irradiance-Medium-Temperature (MIMT), Medium-Irradiance-High-Temperature (MIHT), High-Irradiance-Low-Temperature (HILT), High-Irradiance-High-Temperature (HIHT) and Normal-Irradiance-Cool-Environment (NICE).

However, these standard days do not provide a good estimate of the energy yield of any site, which should be the basis of an energy rating, as they were not sufficiently representative of the climatic conditions for most sites as shown in [103]. Even considering location-specific typical days would not give a proper indication of the working conditions either, and the use of very short periods may favour one technology over another. Therefore, even though there are energy rating studies based on the results obtained considering only various days [104] a minimum period of one year was adopted for the IEC standard in order to obtain repeatable and reliable ratings. This is supported, as shown in [96], by small year-to-year variability of the module performance ratio, similar parameter to the *CSER*, in nearly all regions considered (Africa and most of Europe and Asia), which are representative of most of the environments where PV systems are installed worldwide. On this basis it was agreed that one year of hourly data contain all relevant information to perform reliable energy rating studies.

The second aspect to consider in selecting the standard datasets is the definition of the different climatic regions. In contrast to the traditional climatic regions such as those in the Köppen-Geiger classification [105], which are strongly influenced by precipitation and its effect on vegetation, or the differentiation proposed by the European Solar Radiation Atlas based on the yearly average clearness index [106] for PV energy rating purposes the reference climates need be based on the performance of the PV modules. Taking into consideration only the irradiation or the clearness index would not be descriptive enough, as temperature, for example, has an important role in the performance of PV devices.

If a PV device obtains the same *CSER* at two locations, the energy yield from identically configured PV systems at the two locations will differ in proportion to the difference in the available annual irradiation in both sites. Therefore, in these cases, an estimation of the performance based on data from one of the sites can then be used to estimate the performance at another site by scaling for the yearly total irradiance. Thus, the definition of a reference climatic dataset should guarantee similar PV performance (*CSER* or performance ratio) over the corresponding geographical region. This region should be identified based on long-term data (10 years or more). Then the year selected as reference should provide performance values as close as possible to the average performance over the multiyear time period. Finally, a suitable site, representative of the entire region or climatic zone has to be identified. The irradiation from this representative site may be used to estimate the yield of any other site within the same climatic region.

Following the previous steps, [103] identified seven different climatic regions in Europe, with a difference in the performance of c-Si modules between regions of about 1%, with the module performance ratio varying between 0.88 and 0.96. A similar variation was observed for the CdTe technology although with higher values (0.93-1.05). The standard deviation (SD) on the performance in the different regions showed low values between 0.1% and 0.6%, whereas that of the irradiance varied between 1.5% and 4%. This indicates that considering one year of data is sufficient. An analysis of the impact of using synthetic datasets created with the statistical properties of the full time series, concluded that the rating of the PV devices was not affected.

Similarly, but applying a more complex PV performance estimation method and considering the effects applied in the IEC 61853, the authors in [13] identified five different regions in Europe for c-Si and CdTe modules. The variability in the input data results in an uncertainty in the estimated performance ratio of 2%. Therefore, as authors conclude, the standard climate reference datasets should be defined to guarantee differences not lower than this value.

Taking these results into consideration, the IEC 61853-4 considers six reference climatic profiles to represent the most common climatic conditions that PV installations may encounter

worldwide. They are named tropical humid, subtropical arid, subtropical coastal, temperate coastal, temperate continental and high elevation (above 3000 m).

Each dataset contains hourly values over a year of ambient temperature, wind speed, satellite-retrieved irradiance data of horizontal global and beam broadband irradiance, in-plane global and beam broadband irradiance, and spectrally resolved in-plane global irradiance integrated into 29 spectral bands of different width as specified in the datasets. Besides these variables, the solar elevation angle and the angle of incidence between the sun and the normal to the surface of the module are also provided.

At present, the scope of the energy rating IEC 61853 standard covers single-junction monofacial devices. If in the future, other devices such as bifacials are to be considered, the standard datasets may have to be modified or extended. The new variables will depend on the methodology used to model the performance of the new devices and the availability of data at a global scale.

3.4 Module Characterization Considering Atacama Desert Conditions

3.4.1 Indoor characterization of PV modules

The energy rating standards IEC61853 Parts 1–4 provide a method for differentiating the expected performance of photovoltaic modules under real-world conditions. It combines a comprehensive set of measurements on modules with a numerical model to produce performance ratings for different reference climates [107].

The Atacama Desert presents particular conditions that pose several challenges in the selection of photovoltaic modules and in the operation of photovoltaic power plants. One of the main challenges is the solar spectrum: the solar spectrum of Atacama Desert does not completely correspond to the ASTM G173 spectrum (Figure 36), which is often recommended by IEC standards to assess the effect of the radiation in modules and other components of photovoltaic power plants.

The main differences between both spectrums lie in the range of the UVA and UVB, being more notorious in the UVA range. The key factors responsible for these spectral differences are 1) the elevation above sea level; 2) the number of days with clear skies due to the absence of cloud cover and, hence, a low diffuse radiation fraction; 3) the small aerosol optical depth; 4) the small total ozone column (TOC); and 5) the small water vapour column. This finding indicates that the technologies to be installed in Atacama Desert should be designed/selected to support considerable energy in the UVA range so that the modules' energy rate is not diminished.
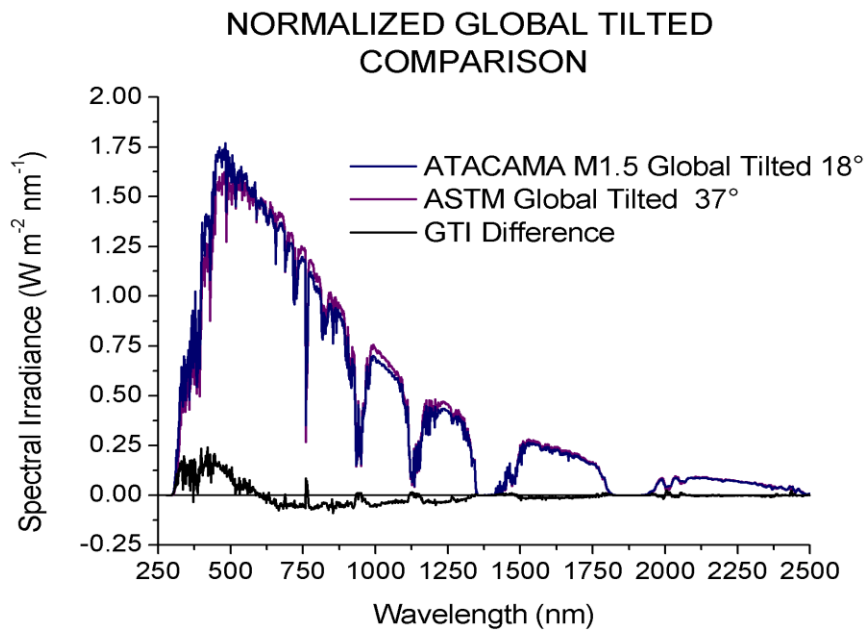
Figure 36: Comparison of both the ASTM G173 and the normalized Atacama Desert solar spectrum [108].

To cope with the issues posed by the solar spectrum of the Atacama Desert, ATAMOSTEC has developed both indoor and outdoor testing methodologies to determine whether a particular module technology is adequate for being installed in a photovoltaic power plant. Since IEC 61853 standards do not adequately represent the conditions of the Atacama Desert (an in general several high radiation high altitude desert regions), its procedures for indoor module testing have been slightly modified and additional tests have been added so as the modules are subject to the expected UV radiation indices in real operating conditions [109]. Figure 37 displays the procedure proposed by ATAMOSTEC for the indoor assessment of photovoltaic modules considering the conditions of the Atacama Desert. As it can be noticed, the proposed procedure gives as outputs the performance of the modules assessed considering the expected UV radiation dose plus corrosive environment found in the desert (UV + salt mist); the expected UV dose plus the temperature oscillations (UV + PTC); and the expected UV dose plus the damp heat and the highly accelerated stress test (UV + DH/HAST). These tests allows to determine whether the assessed technology has the potential to reach an expected PV module lifespan of 25 years or more (in the near future it is expected to determine the features that increase or decrease a module's potential). The motivation for estimating modules' lifespan lies in the fact that current technologies are highly sensitive to UV radiation, and therefore it is expected that under Atacama Desert conditions their lifespan is shortened. It is important to remark that the focus of ATAMOSTEC is on bifacial module technologies. Nevertheless, the proposed procedure can also be applied to assess monofacial technologies.
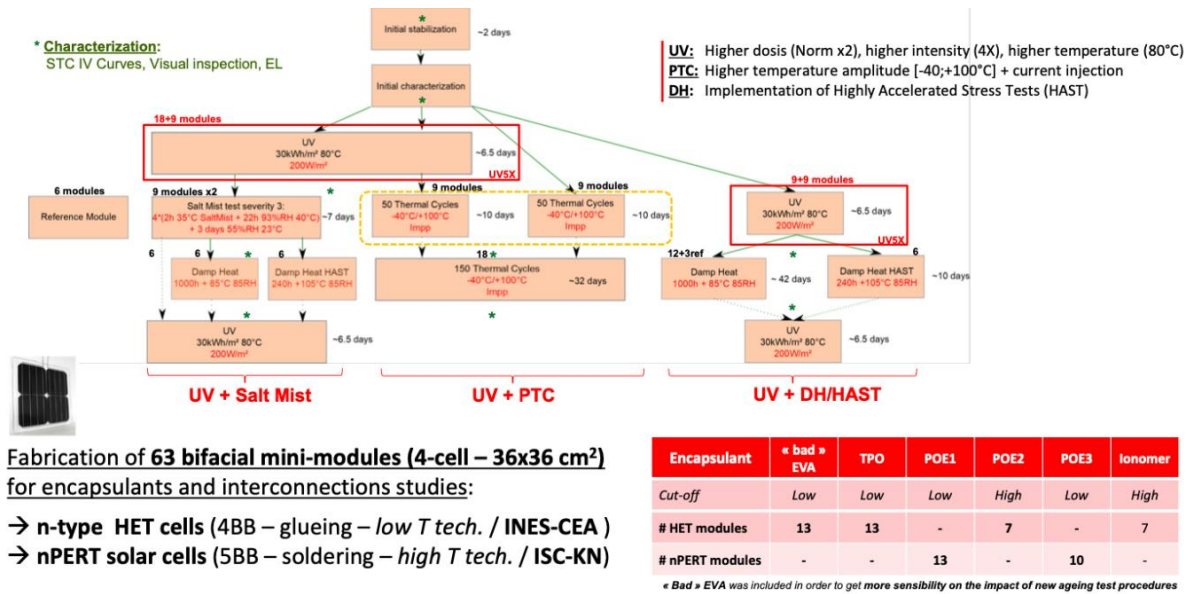
Figure 37: Block diagram of the proposed procedure for indoor module testing taking into account the environmental conditions of the Atacama Desert. Source: [109].

As a complement to radiation, the procedure shown in Figure 37 also allows us to determine the effect of soiling, corrosive environments and a combination of the two, on the energy rating of the modules. These additional tests, combined with the UV test, are also important for module characterization since the Atacama Desert has 1) temperature oscillations that range from -10ºC to 30ºC within a day (e.g. at the PSDA); 2) environmental humidity that ranges from 20% to 100% during a day (that combined with the temperature oscillations produce water condensation), and 3) presence of salts that combined with humidity could affect the performance of the modules due to rusting or water condensation within the modules. Figure 38 presents the performance of different bifacial technologies. Specifically, heterojunction and nPERT modules with different encapsulants were evaluated. From the evaluation, it can be concluded that heterojunction modules with high cut-off encapsulants performed better than the remaining technologies. Nevertheless, these remarks must be validated in outdoor conditions, such as at the PSDA.
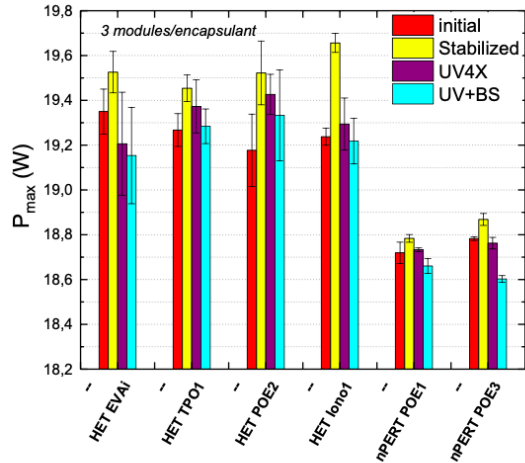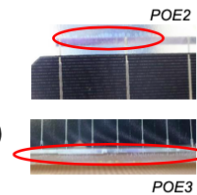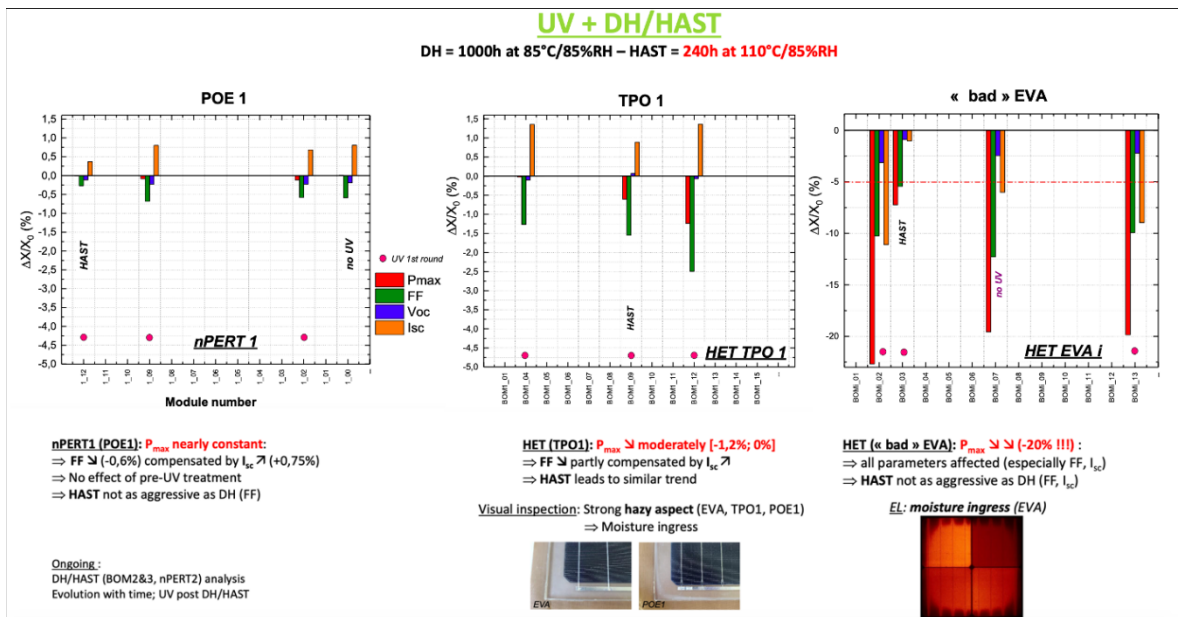
Figure 38: Assessment of heterojunction and nPERT modules with different encapsulants, following the modified indoor testing procedure (Source [109]).

3.4.2 Outdoor characterization of PV modules

As a complement of the indoor module assessment, ATAMOSTEC has also conducted out-door characterization in its outdoor solar testing facility. As in the indoor testing facilities, the PSDA is used to test commercial and non-commercial photovoltaic modules in order to rank them for their implementation at utility scale power plants. In addition, advanced O&M practices, mounting structures, and inverter technologies are considered for being analysed in desert conditions. Figure 39 shows the current PSDA facilities. These facilities are composed by the state-of-the-art instrumentation for assessing meteorological conditions; tilted and vertical structures, and tracking systems fully instrumented for module testing at real environmental conditions; and mini module mounting structures to assess new module concepts. As it can be seen, the PSDA facilities allow to validate the results obtained from the indoor test, and also evaluate the adequateness of a module technology for a specific application at either utility or niche scale.

Figure 39: Current facilities at the Atacama Desert solar platform.

Currently, at the PSDA bifacial PERC+, nPERT and HJT, monofacial PERC technologies are being tested (taking the PERC technology as baseline/reference). From the results obtained so far, it can be concluded that in average the bifacial technologies have an extra energy gain of about 11%, for the fixed mounting structures. In the case of the tracking system, as expected an extra gain of about 31% is achieved for both: monofacial and bifacial technologies. Hence, combining bifacial module technologies with single axis tracking systems it has been achieved an extra energy gain of about 44%. This extra gain was achieved with an average measured albedo, in Atacama Desert, of about 30% (natural albedo, i.e., the soil was not modified during the tests). Figure 40 illustrates how the aforementioned results relate one with another. These results are in concordance with those obtained from the indoor characterization, for the energy production. Concerning the effect of UV radiation in the module performance, it is still too early to risk a final conclusion. Nonetheless, to date, none of the modules installed in the desert have exhibited any degradation mechanism taking place on them. It is important to clarify that the modules are being tested at the PSDA from January 2020.
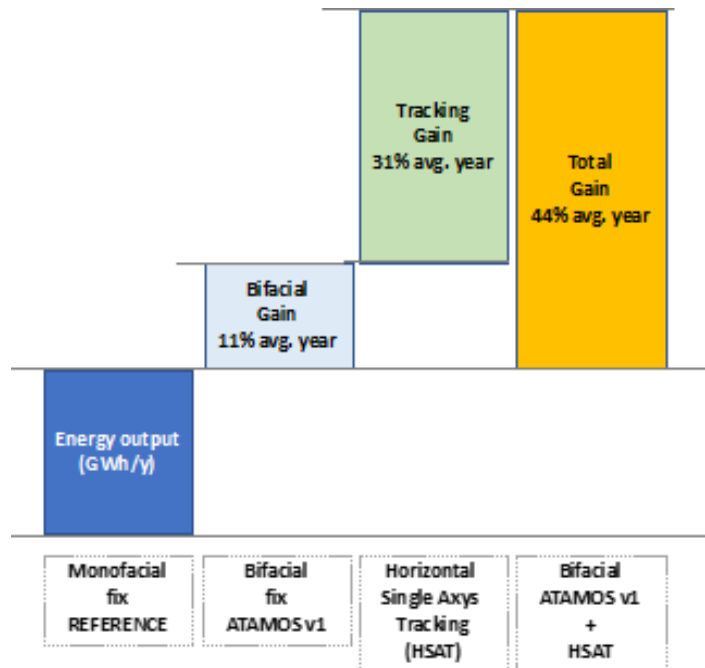
Figure 40: Relationship between the measured gains of the different technologies currently tested at the PSDA.

4 ENERGY RATING OF PV MODULES

The evaluation, rating, and pricing of photovoltaic modules are commonly assessed based on the maximum power output measured at Standard Test Conditions (STC) defined by a cell temperature of 25°C and an in-plane irradiance of 1000 W/m^2 with a spectral content as specified in IEC 60904-3 [41]. However, the electricity produced over the lifetime of a PV module and the subsequent Levelized Cost of Electricity (LCOE) and return on investment derive from working conditions far from those standard ones, as they depend on location, climatic conditions and installation. Therefore, the scientific community has developed methods to perform a more meaningful and unbiased comparison of PV devices (defining performance surfaces or matrixes of each device) based on the estimated energy output considering predefined environments representative of real operating conditions. This comparison or energy rating is intended to be able to differentiate between devices, and therefore fundamentally depends on the characteristics of the modules.

There are various energy rating methodologies in the scientific bibliography, such as those developed by Sandia (PVUSA) [110] or TÜV Rheinland (LPLA) [14]. Furthermore, in 2018 the International Electrotechnical Commission (IEC) completed the standard series IEC 61853 on PV module energy rating [3–6]. Even though all of these methodologies are based on an energy yield estimation over predefined working conditions, the model used to estimate the power output and the effects considered differ. For example, in addition to the effects quantified by the IEC 61853 methodology, the LPLA method takes into consideration soiling, while PVUSA estimates the AC energy yield taking into account the performance of the inverter. Besides, this latter method applies to different types of installations, from small arrays to utility-scale installations, while the IEC standard refers the calculations to a single module.

A detailed description of these and other energy rating methods, including a comparison with the IEC 61853 methodology is presented in this chapter.

4.1 According to IEC 61853-3

The International Electrotechnical Commission (IEC) Standard series 61853 "*Photovoltaic (PV) module performance testing and energy rating*" provides PV manufacturers, installers and buyers a tool to obtain a simple but realistic estimate of the performance of a PV module at different climatic conditions. The final output of the standard, the Climate Specific Energy Rating (*CSER*) parameter, can be used to compare the performance of different PV technologies or modules in a more meaningful way than by just comparing the output power declared by the manufacturer and measured at Standard Test Conditions (STC), which are almost never met under real working conditions. The dimensionless *CSER* parameter is, in fact, calculated as the ratio of the estimated energy output of a PV module under certain climate conditions to the energy output that would have been obtained if the module efficiency would have been the one measured under STC.

The calculation of the energy rating *CSER* is based on one year of hourly data which, even though could be representative of the conditions of a certain climatic region, it would not be enough to provide an accurate estimation of the energy yield of a PV installation in a specific location. For that purpose, data for that specific site and installation would be required including climatic data for several years and information about the possible presence of shadows, snow, or dust on the modules, as well as information about the installation configuration, such as orientation and inclination angles. In addition, for an accurate prediction of the total energy yield, the effects of degradation and ageing of the PV modules and other components of the

PV system should be considered as well. On the contrary, the purpose of the IEC 61853 standard series is to provide a realistic estimation of the energy rating of a PV module located in a generic site with defined climatic conditions where the modules are installed facing the equator with an inclination angle of 20°. The estimation methodology defined in the energy rating standard may be applied to calculate the energy yield of a real PV module installation, provided losses due to the presence of obstacles, dirt or snow and the effects of degradation are taken into consideration. However, these and other effects such as light-induced changes or thermal annealing, which should be considered for an accurate energy yield estimation, are not defined nor considered in the IEC energy rating standard.

The IEC 61853 standard series, completed in 2018 with the publication of the final two parts, defines a methodology to estimate the performance of PV modules considering real working conditions defined by six datasets representative of the major climatic conditions PV installations will likely encounter worldwide. These climatic datasets are defined in Part 4 of the standard [6], while the models to estimate the PV performance are described in Part 3 [5]. Part 1 and Part 2, published respectively in 2011 and 2016 [3, 4], describe the procedures to test and measure the relevant characteristics of the PV modules under evaluation to obtain the input data required by the models applied in Part 3. These data, which are described in Chapter 2 of the present report, include a matrix of maximum output power under various levels of irradiance and module temperature (Part 1), the spectral responsivity of the PV device, the reflectance of the surface of the module and the module's thermal properties (Part 2).

The methodology described in IEC 61853-3 to estimate the PV module output under real working conditions takes into consideration various effects. The first one quantifies the effect of the angle of incidence between the solar radiation and the normal to the module in the reflected irradiance. This irradiance is not transmitted to the active material, and consequently does not contribute to the power generation. The second effect is related to the spectral responsivity of the module that determines the irradiance effectively absorbed by the active material. The last effect evaluated is the temperature behaviour, since the temperature of the module, along with the received irradiance, is one of the main factors that most significantly affect the power generation.

In fact, the complete IEC 61853-3 methodology is the concatenation of various steps focused on modelling the above-mentioned effects to obtain for every hour of the complete reference year of the climate datasets two sets of data:

- The in-plane irradiance, broadband and spectrally resolved, corrected for both angle of incidence (AOI) and spectral effects to define the effectively absorbed irradiance (G_{corr}),
- The module's temperature (T_{mod}) estimated using the ambient temperature (T_{amb}), the wind speed (v) and the in-plane irradiance corrected for angle of incidence effects only ($G_{corr,\ AOI}$).

These two sets of hourly values, the effective irradiance and the module temperature (G_{corr}, T_{mod}) are used to estimate the power output from the efficiency values derived from the power matrix obtained in part 1 of the standard (applying interpolation, and extrapolation when necessary). The power matrix is a set of module power measurements at various levels of irradiance between 100 and 1100 W/m^2 and module temperature from 15 to 75°C, as shown in Section 2.1.3.

The complete methodology to estimate the *CSER* for the PV module under consideration for each reference climate is shown in Figure 41. The models applied in the various steps are described in the following sections.
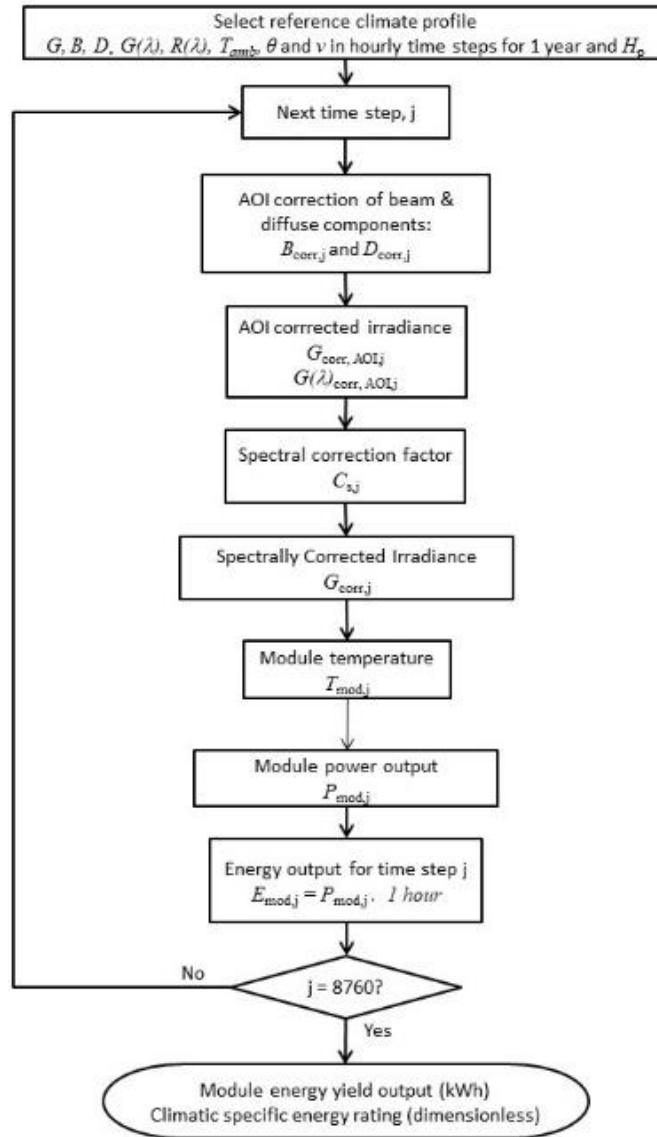
Figure 41: Complete methodology to obtain the Climate Specific Energy Rating for the PV module under consideration, for every reference climate profile (Source: Adapted from: [5]).

4.1.1 Angle of incidence effects

The first step is the quantification of the AOI effects by means of the model developed by Martin and Ruiz [48, 111]. The model applies a different correction to the beam (*B*) and diffuse (*D*) irradiances as shown in Eq. (10) and Eq. (11), respectively.

$$B_{corr,j} = B_j \cdot \left[\frac{1 - exp\left(-\frac{\cos\theta_j}{a_r}\right)}{1 - exp\left(-\frac{1}{a_r}\right)} \right] \tag{10}$$

$$D_{corr,j} = D_j \cdot \left\{ 1 - exp\left[-\frac{1}{a_r}\left(\frac{4}{3\pi}\left(\sin\beta + \frac{\pi - \beta - \sin\beta}{1 + \cos\beta}\right) + (0.5a_r - 0.154)\left(\sin\beta + \frac{\pi - \beta - \sin\beta}{1 + \cos\beta}\right)^2 \right) \right] \right\} \tag{11}$$

Where B_j and D_j are, respectively, the uncorrected in-plane broadband beam and diffuse irradiance of hour j, and θ_j is the incidence angle between the normal to the PV module and the sun for the same hour j. All these values are tabulated in the datasets provided in Part 4 of the standard. β is the inclination angle of the module, expressed here in radians, which is fixed at 20° and a_r is the empirical factor obtained in Part 2 from the analysis of the AOI experimental measurements. The IEC standard does not provide reference values for the a_r parameter, as its value depends on the device under test's configuration and coating. However, some values are reported in [48] for the devices analyzed in this study. The a_r parameter ranges from 0.136 for air/glass/a-Si:H/Ag modules to 0.179 for air/glass/triple coat./Si devices. The higher the a_r value is, the more irradiance is reflected back into the atmosphere as it reaches the surface of the module.

The sum of $B_{corr,\,j}$ and $D_{corr,\,j}$ is the global in-plane broadband irradiance corrected for AOI effects ($G_{corr,\,AOI}$), which is used to define the AOI correction coefficient to be applied to the global in-plane spectrally resolved irradiance, $R(\lambda)$, and estimate the corresponding AOI corrected values ($G(\lambda)_{corr,\,AOI}$), required for the spectral correction effect estimation. The $R(\lambda)$ values are also provided in the reference climate datasets.

4.1.2 Spectral correction effects

The second step estimates the effectively absorbed irradiance, taking into account the spectral responsivity of the PV module material. An hourly spectral correction factor is calculated, C_s, as in Eq. (12) and applied to estimate the corrected in-plane irradiance for both angle of incidence and spectral effects, G_{corr}, see Eq.(13)

$$C_{s,j} = \frac{1000 \cdot \int SR(\lambda) \cdot G(\lambda)_{corr,AOI,j} \, d\lambda}{G_{corr,AOI,j} \cdot \int SR(\lambda) \cdot R_{STC} d\lambda} \tag{12}$$

$$G_{corr,j} = C_{s,j} \cdot G_{corr,AOI,j} \tag{13}$$

Where $SR(\lambda)$ is the spectral responsivity measured at different wavelengths as defined in Part 2 of the standard according to IEC 60904-8 [112], $G(\lambda)_{corr,AOI,\,j}$ is the global in-plane spectrally resolved irradiance corrected for AOI at the hour j and R_{STC} is the spectral intensity for the standard test condition spectrum AM1.5G (IEC60904-3 [41].

4.1.3 Effects of temperature of the module

In addition to the in-plane irradiance corrected for AOI and spectral effects (G_{corr}), the operating temperature of the module (T_{mod}). is also required for the estimation of the PV power output

(P_{mod}). T_{mod} is calculated using the model suggested by Faiman [113] where the module temperature depends on the received irradiance corrected only for AOI effects ($G_{corr, AOI}$), the ambient temperature (T_{amb}) and the cooling effect of the wind (v), as shown in Eq. (14).

$$T_{mod} = T_{amb} + \frac{G_{corr,AOI}}{u_0 + u_1 \cdot v} \tag{14}$$

The model uses two thermal parameters, u_0 and u_1, which are obtained with the methodology described in Part 2 of the standard, whilst T_{amb} and v are provided in tabulated form in the climatic datasets of Part 4. Similarly to the a_r parameter used to quantify the reflected irradiance, the IEC standard does not provide default values for the two coefficients used in the thermal model, u_0 and u_1. Estimated values of both coefficients for a series of a-Si, CIS, CdTe and c-Si devices are reported in [114]. The u_0 and u_1 values for the c-Si module are 30.02 and 6.28, respectively. While for the CdTe the calculated coefficients are 23.37 and 5.44.

4.1.4 Output power

Considering the hourly values of T_{mod} and G_{corr}, the hourly power output (P_{mod}) is obtained by bilinear interpolation, or extrapolation, of the efficiency values derived from the power matrix measured in Part 1.

It is known that for some of the six reference climatic datasets, at some times the working conditions of the PV modules fall outside the irradiance and temperature range covered by the power matrix (See Section 2.1.3), so extrapolation is required. Most of these situations correspond to low temperature and/or irradiance levels (G_{corr} <100 W/m^2 and/or T_{mod} <15°C). The IEC 61853-3 provides the equations to apply extrapolation under these circumstances.

From the hourly power output, the hourly energy output (E_{mod}) is derived assuming a constant performance over every hour. The sum of these hourly values is the annual module energy output, $E_{mod, year}$, used in the estimation of the dimensionless parameter *CSER* (See Eq.(15)).

$$CSER = \frac{E_{mod,year} \cdot G_{ref}}{P_{max,STC} \cdot H_p} \tag{15}$$

Where G_{ref} is equal to 1000 W/m^2 as the irradiance applied at STC to measure the maximum power at STC ($P_{max, STC}$). H_p is the yearly global in-plane irradiation provided in Part 4 for every reference climatic region.

To illustrate the energy rating values that can be obtained for the different reference climates, the complete methodology has been applied to several generic technologies. The thermal coefficients used (u_0 and u_1) are shown in Table 12. Due to the lack of specific data for every technology regarding the AOI effects, an a_r of 0.155 was considered for all devices. For information about the spectral response data and power matrix values used for every technology, refer to the authors of [7].

Table 12: Thermal coefficients (u_0 and u_1) used to estimate the *CSER* [7].

	c-Si	CdTe	a-Si	OPV
u_0	26.91	23.37	25.71	26.91
u_1	6.2	5.44	4.26	6.2

The obtained *CSER* values are shown in Figure 42. (Values from [7]). As expected, the performance of the crystalline silicon technology (c-Si) is significantly affected by the high temperatures of the tropical and subtropical climates. Under these conditions, the performance, compared to that of STC conditions can be reduced by more than 10%, as shown in Figure 42. In contrast, the tropical humid climatic conditions enhance the performance of the amorphous silicon technology (a-Si) to the extent that it would perform better than expected by the power output measured under STC conditions.

As an example of the emerging PV technologies, the organic PV device (OPV) included in the analysis shows good performance in the two warmer reference climates but its performance is significantly diminished under lower irradiance conditions like those characteristics of the temperate coastal climate. A detailed characterization of this device can be found in [115] where the onset of power is visible after approximately 100 W/m² of irradiance indicating a poor low irradiance performance.
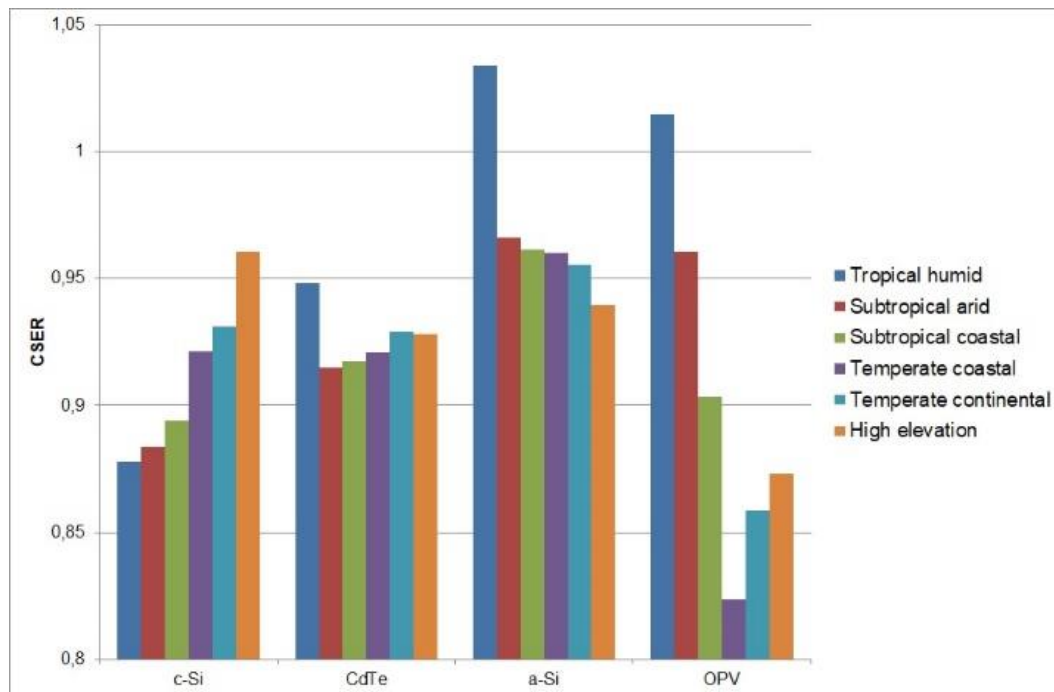
Figure 42: *CSER* calculated for four different PV technologies at the six reference climates defined in IEC 61853-4 (Source: [7]).

Results shown in Figure 42 reflect clear differences in the behaviour of most of the considered devices in the six reference climates. While the performance of the CdTe device is more stable over the different climates (3.6%), the difference between the performance at the best and

worst climatic conditions for the c-Si, a-Si and OPV device is 9.5%, 10% and 23.2% respectively. These values show the importance of selecting the best-suited PV technology for every location. In this regard, the trend under the subtropical and temperate climates is the same for the c-Si and CdTe devices, with an increased performance towards colder climates, whilst the opposite is observed for the a-Si device.

Under the same climatic conditions, the highest differences between devices (17%) is observed under the tropical humid climate characterized for higher temperatures and irradiance levels, which can have opposite effects on some technologies. Whilst the most uniform behaviour is observed under the subtropical coastal climate, with a maximum deviation between devices of 7.5%. Under the temperate climate, the *CSER* values of the c-Si and CdTe devices are very similar due to the various effects taken into consideration in the modelling of the power output. However, when the wind and the spectral content of the incidence irradiance are not considered, the performance of these two technologies can differ by more than 10% [116].

In addition to [116], there are other examples of energy rating and theoretical energy yield prediction studies in the scientific bibliography. Nevertheless, in most cases different methodologies are applied, taking into consideration different effects for the power output estimation, and considering as well different climatic datasets to the ones described in the IEC 61853. In [116], in addition to CdTe and c-Si modules, $CuInSe_2$ and $Cu(In\text{-}Ga)(Se,S)_2$ were analysed. Without considering spectral effects and the cooling effect of the wind, the performance variation between the CIS and c-Si devices in Europe is below 2.5%, while between CdTe and c-Si this difference goes up to 12%, which is higher than the variations plotted in Figure 42. Despite the differences in the performance estimation, the values obtained for the c-Si technology in Europe vary between 0.87 and 0.97, in line with the results shown in Figure 42 for the reference climates representative of the European climatic conditions.

The linear performance loss analysis (LPLA) method [14], which is described in detail in Chapter 4.6, was applied to different thin film devices including CdTe, CIGS and a-Si; and various types of silicon devices like poly c-Si with different coating, mono c-Si with heterojunction and back-contacted mono c-Si n-type basis cells. The variation between the devices with the best and worst performances go from 30% in warm locations with high insolation levels to 15% in temperate locations, which is higher than the differences plotted in Figure 42. Reported differences within the devices of the c-Si and CdTe technologies are smaller, around 4% and 2% respectively. The variation is higher between the a-Si and CIGS devices. Various c-Si devices were compared in [117] and differences in the estimated power output were below 2%. However, the variability between devices increased to almost 4% under low irradiance conditions. Similar conclusions were found by [118] comparing various devices of c-Si and mc-Si. The former presented higher variability than the mc-Si devices, especially below 200 W/m^2, and better performance.

The authors obtained a maximum difference in the estimated energy yield for the two-mainstream silicon-based modules of 5%. The methodology applied is very similar to the one defined in the IEC 61853 standard between, in that it also considers light induced degradation. Most of the considered effects in the IEC standard were considered by [11] but using different equations. The module performance ratio (*MPR*), which is similar to the *CSER* parameter of the IEC standard, of eight different devices of four different technologies was calculated, including high efficiency c-Si devices, CdTe, CIGS and a-Si modules. Differences in the *MPR* were only significant between different technologies with clear different characteristics. The performance of the c-Si devices was very similar to each other. None of the above-mentioned studies considered the reference standard datasets defined in IEC 61853-4 [6], which were selected to represent distinctive weather conditions, as described in Chapter 3.4. Now that the

complete standard series is available, further analysis of new devices and fast-evolving PV technologies is required.

Overall, the *CSER* values provide a tool to compare different PV technologies and differentiate between products of the same technology in a simple way that is more representative of the real performance than the maximum power output at STC. This can help PV installers identify the most appropriate technology or device for the climatic conditions of the location of interest.

However, it should be noted here that the scope of the IEC standard covers mono-facial and single-junction devices of any PV technology, including prototypes. Due to the required input data and the models used, the application of the energy rating standard cannot be easily extended to bifacial devices until albedo and bifaciality effects are defined. For multi-junction devices, a method to account for limiting junction effects due to varying spectral conditions has been elaborated [119], but a method is not specifically defined in the energy rating standard. Therefore, the extension of the energy rating standard's scope to include bifacial and multi-junction devices would require new data, experimental setups to obtain those and new methods to account for the various effects (irradiance and temperature-dependent behaviour, spectral effects and AOI effects) on these other PV technologies. In this regard, the IEC's Technical Specification IEC-TS 60904-1-2 [55], published in 2019, sets the foundations for a possible future methodology to obtain power matrix measurements on bifacial devices.

Another limitation of the IEC energy rating standard regards the technologies with significant non-linearity in the characteristics modelled, such as the performance at low irradiance levels. Results should be taken with caution, due to the different effects taken into consideration, for devices whose efficiency is affected by long-term exposure to outdoor conditions, as results may be misleading. Devices lacking long-term stability would obtain overestimated ratings concerning to real lifetime performance. These and other possible sources of uncertainties in the IEC energy rating methodology are further discussed in Chapter 5.3.

4.2 Round Robin of Different Implementations of the PV Module Energy Rating Standard IEC 61853-3

The IEC 61853 standard series "Photovoltaic (PV) module performance testing and energy rating" aims to provide a standardized measure for PV module performance, namely the Climate Specific Energy Rating (CSER) as defined in Part 3 [5]. However, the specific implementation of the calculation is left to the user (details see Chapter 4.1), and some steps in the calculation procedure leave room for interpretation. Additionally, there is no reference parameter set and no solution included in the standard, which could be used to verify the correct implementation of the CSER calculation. This may lead to deviations between different implementations. Thus, a round robin of the PV module energy rating standard IEC 61853-3 was conducted [120]. Researchers from different organizations provided ten different implementations of the standard with one being open source [121]. In the following, the results and lessons learnt from the round robin are summarized.

For phase one, TÜV Rheinland experimentally determined the PV module input parameters required for the CSER calculation and provided them to the other participants. Each participant then calculated the CSERs without knowledge of the other participant's results. The resulting CSER values as well as important intermediate results of the calculation procedure from each participant were available to everyone afterwards. The relative differences for each calculation step were analyzed and discussed.

The CSER results relative to the median of each climate profile for the first phase are shown at the top of Figure 43. Participants E1 or H1 had the highest CSER for all climate profiles,

while I1 had the lowest values. Additionally, the order of the participants is not the same in every profile. Table 13 lists absolute and relative difference between the CSER values. For all phases, the tropical humid profile had the highest deviations for both, which is 0.133 for absolute difference and 0.039 as the standard deviation in phase 1. If this CSER difference 0.133 is taken relative to the median CSER value of this climate profile the result is 14.7%. Even for the climate profile with the best agreement the relative difference between participants' CSER for the same module is 6.8%, which is comparable to the difference in CSER between different module technologies as shown in Figure 42. For the energy rating calculation to be more comparable between participants, further investigation is clearly needed.

In-depth analysis of the intermediate results revealed two kinds of sources for the deviations. One kind was coding errors such as missed brackets or signs. The other was different interpretations of the standard, one of these was related to the angular correction. IEC 61853-3 uses the angular loss model of Martin and Ruiz [48, 111], whose single fit parameter is the angular loss coefficient a_r. It is obtained by fitting it to the measured IAM(θ) as defined in [4]. However, the mathematical fit method is not defined in the standard. Five participants performed least-square fit resulting in an $a_r = 0.14571$. While other participants used other methods such as the mean absolute deviation approach resulting in higher a_r values. The impact of these differences is about 0.002 in CSER.

For phase two of the round robin, it was decided to use $a_r =0.14571$ in all implementations to remove this fitting difference and focus on other steps. Additionally, participants had access to all the results of phase 1 to improve their implementations.
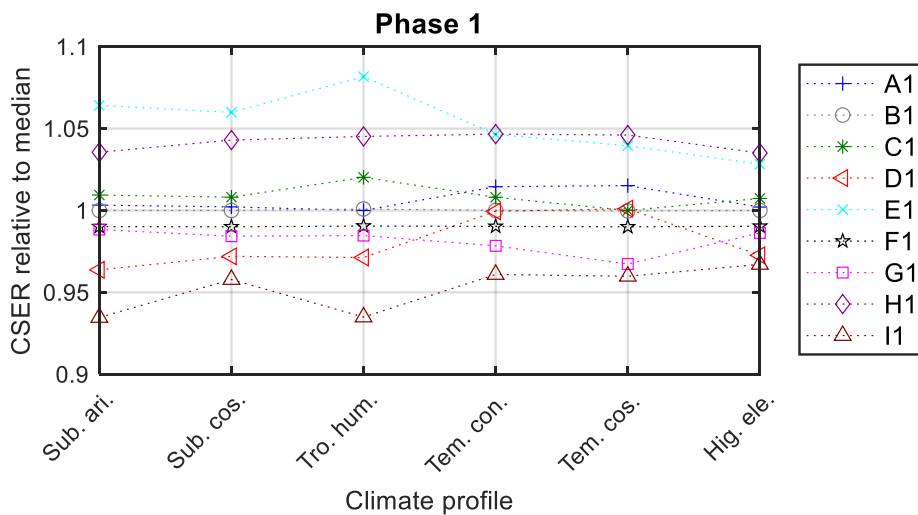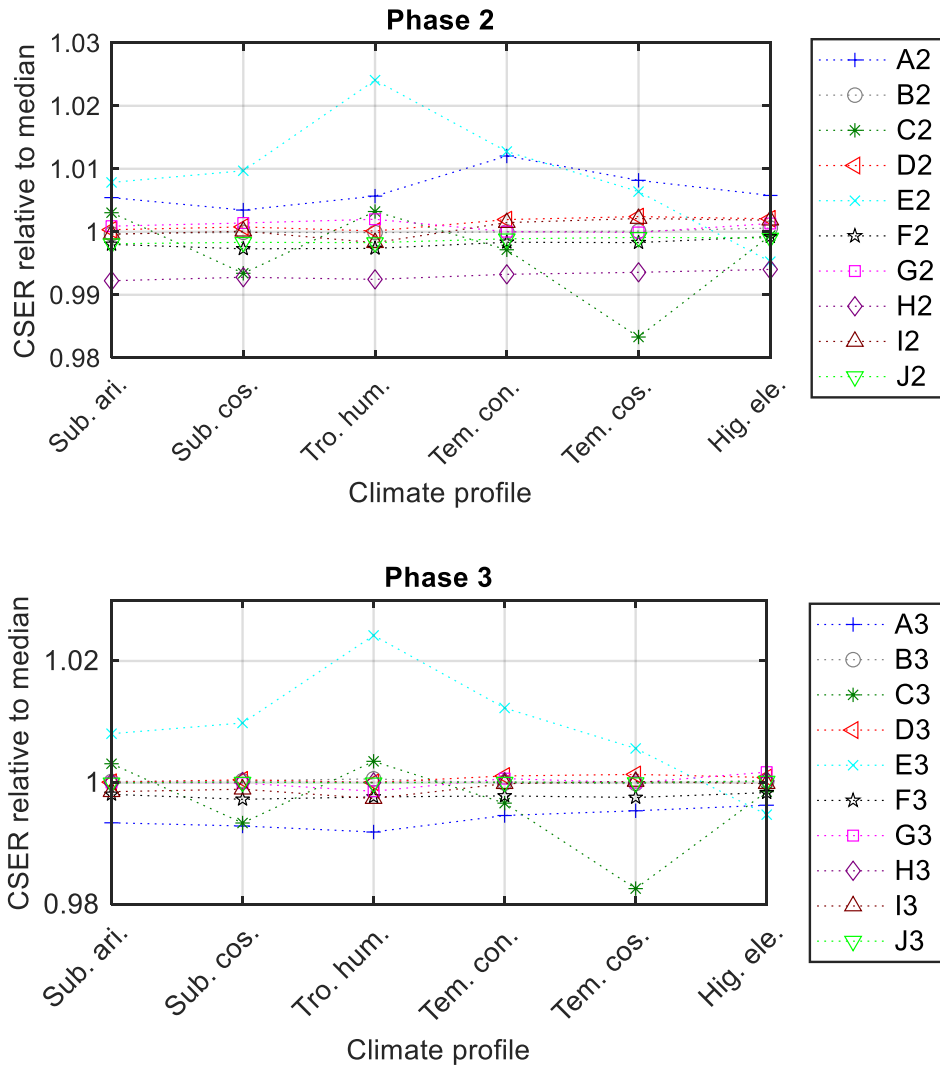
Figure 43: The CSER relative to the median of each climate profile in each phase. Please note that J1 was excluded due to the use of input parameters from a different module.

Table 13: The absolute difference of CSER values and the difference relative to the median of CSER values for each climate profile for all three phases.

Climate profile	Absolute CSER difference			CSER difference relative to the median CSER value [%]		
	Phase 1	Phase 2	Phase 3	Phase 1	Phase 2	Phase 3
Subtropical arid	0.117	0.014	0.013	12.9%	1.6%	1.5%
Subtropical coastal	0.098	0.016	0.016	10.2%	1.7%	1.7%
Tropical humid	0.133	0.029	0.029	14.7%	3.2%	3.2%
Temperate continental	0.084	0.019	0.017	8.6%	1.9%	1.8%
Temperate coastal	0.085	0.024	0.023	8.6%	2.5%	2.3%
High elevation	0.067	0.012	0.007	6.8%	1.2%	0.7%

The results for phase 2 are shown in the center of Figure 43, where the CSER values are given relative to the median for this phase. The biggest change is signified by the change in the y-axis range, which is due to the four-fold reduction of the absolute difference to 0.029 (3.2%). The difference was driven by the four outliers, A2, C2, E2 and H2. After excluding those four outliers the largest absolute difference between the other six participants is 0.0042 (0.46%).

Further analysis of the intermediate results showed that differences in the spectral correction step were the source for the outliers as well as the largest source for the difference between the other six participants. The challenge in the spectral correction step is that the irradiation is provided in the 29 bands by the standard, while the spectral response was measured in steps of 5 nm and the reference spectrum AM1.5g spectrum [41] is provided in steps of 0.5 nm, 1 nm or 5 nm depending on the wavelength region. To perform the spectral correction, all of them have to be interpolated and numerically integrated. However, the exact method for this is not defined in the standard [5], which opens the door to different interpretations.

For phase three of the round robin, it was decided to use a_r =0.14571 in all implementations and to use a common method for interpolation and integration.

The CSER results relative to the median of each climate profile are shown at the bottom of Figure 43 for the third phase. While participant H3 improved the calculation to join the other six participants, A3, C3, and E3 still had large differences in the spectral correction. The absolute difference of phase 3 was 0.029 (3.2%). The difference was driven by the three outliers A3, C3, and E3. After excluding those three outliers the largest absolute difference between the other seven participants is 0.0037 (0.38%).

In conclusion, the practical implementation of IEC 61853-3 is more complicated than one might expect as demonstrated by the initial comparison with differences of 0.133 (14.7%) in CSER. In the third phase of the intercomparison, the differences are less than 0.029 (3.2%) in CSER. After excluding the remaining three outliers the largest absolute difference between the other seven participants is 0.0037 (0.38%).

4.3 Reduced Matrix Measurements

The IEC 61853-1 performance matrix described in Section 2.1.3 is made of 22 points measured in the range of 100 to 1100 W/m^2 and module temperatures from 15°C to 75°C (Figure 44a). A reduced matrix with fewer points is measured when: the module performance is linear according to IEC 60904-10 [122], the testing equipment do not allow measurement of the full matrix due to limitations in irradiance or temperature settings or the testing costs has to be reduced.

The reduced matrix measurement, depicted in Figure 44b and described in the IEC 61853-1 standard can be only applied as an alternative to the full matrix measurement (Figure 44a) when the module performance is linear according to IEC 60904-10. This simplified procedure allows measuring the dependence on irradiance at one single fixed temperature, usually 25°C, whereas the dependence on temperature has to be measured at two fixed irradiances, one between 800 W/m^2 and 1000 W/m^2 and the second between 100 W/m^2 and 300 W/m^2.

a) Full Matrix accord. to IEC 61853-1				
Irradiance	Temperature			
W/m^2	15°C	25°C	50°C	75°C
1100		X	X	X
1000	X	X	X	X
800	X	X	X	X
600	X	X	X	X
400	X	X	X	
200	X	X		
100	X	X		

b) Simplified matrix accord. to IEC 61853-1				
Irradiance	Temperature			
W/m^2	15°C	25°C	50°C	75°C
1100		X		
1000	X	X	X	X
800		X		
600		X		
400		X		
200	X	X	X	X
100		X		

c) Cross-matrix accord. to IEC 60891				
Irradiance	Temperature			
W/m^2	T_{min}	25°C	…	T_{max}
1100		X		
1000	X	X	X	X
800		X		
600		X		
400		X		
200		X		
100		X		

d) Measurements for IEC 61215-1				
Irradiance	Temperature			
W/m^2	T_{min}	25°C	…	…T_{max}
1100				
1000	X	X	X	X
800			NMOT	
600				
400				
200		X		
100				

Figure 44: Different matrix configurations for module performance according to IEC testing standards.

Very often the temperature coefficients are not measured at low irradiance and the temperature and irradiance dependencies are measured only at 1000 W/m² or respectively 25°C. The reduced matrix is here identified as cross shaped matrix (Figure 44c). Module datasheets, databases and simulation tools like e.g. PVSyst are generally limited to this type of data. An extension of these to the IEC 61853 standard is of course envisaged for the future, but it is still not the rule.

Another typical situation is the one shown in Figure 44c, where only the data requested by the IEC 61215 standard for module qualification are available. It consists of the temperature coefficient measurement, the measurement at STC and 200 W/m² and the performance at NMOT (MQT04, MQT06 and MQT07).

4.3.1 Overview of existing interpolation/correction methods

To perform an energy rating according to IEC 61853-3 with these reduced matrices an extrapolation of the measured points is needed. The standard approaches available to do this are here summarised. It has to be considered that the accuracy of the extrapolated data depends strongly on the accuracy of the applied approach and that in some cases it can be worse than the measurement accuracy. It can be the case especially for low irradiances or high temperatures and for modules with non-linear behaviour. In this case, the measurement of the full power matrix is preferred. The accuracy of different methods and its impact on the climate specific energy rating CSER are discussed in more detail in the next paragraph. The propagation of the measurement error is also analysed there.

The two main standards describing extra/interpolation procedures are the IEC 61853 and the IEC 60891. The methods can be roughly divided into linear interpolation methods and single diode model-based methods. Some of the methods are limited to the translation of module power or performance ratio whereas others are based on the translation of the full I-V curves. Table 14 lists only the methods which can be used for the extrapolation of the energy rating matrix. The four approaches described in the standards differ in applicability (range of validity) and input data requirements (distribution of measured data).

The first method is the original linear interpolation method according to IEC 61853-3, introduced in Section 4.1.4. The power output is modelled by bilinear interpolation of the performance ratio between points on the measured matrix. The method is less accurate in the case of extrapolation and in particular when applied to reduced matrices like cases c and d, where far extrapolation is required.

The second method corresponds to the correction procedure 3 in IEC 60891. It is generally used for interpolation between three IV curves chosen within a reduced matrix. It does not require correction parameters as input. It can be applied already with two current-voltage curves, which determine the limits to which the temperature and irradiance correction can be applied. With a minimum of four IV-curves measured at the extremes, the full matrix can be determined.

Table 14: Within IEC standards proposed correction methods for the inter-/extrapolation of a power matrix for energy rating purposes.

Correction procedure	Correction parameters	Min. input values required for the extrapolation of the power matrix accord. IEC61853-3	Reference

1	Bi-linear interpolation of performance ratio	none	-	Measurement of full power matrix accord. IEC 61853-1	*IEC 61853-3* *standard procedure*
2	Linear interpolation applied to IV-curves	none	-	2-4 I-V curves at the extremes of the value to be interpolated.	*IEC 60891 ed.03 correction procedure 3*
3	Temperature correction of P_{max} with average temperature coefficient	γ_{high}, γ_{low}	- -	Measured temperature coefficient at high and low irradiance Measured irradiance dependency in the range of 100-1100 W/m² at fixed temperature	*IEC 61853-1* *simplified procedure*
4	IV-curve correction based on semi-empirical 1 diode model	α_{rel}, β_{rel}, k', R'$_s$, B$_1$ and B$_2$	- -	Measurement of min. 4 I-V curves at 1000 W/m² and over the range of at least 30°C. Measurement of min. 4 I-V curves at 25°C and in the range of 100-1100 W/m².	*IEC 60891 ed.03* *correction procedure 2*

Both linear interpolation methods can lead to discontinuities as the maximum power point is sensitive to measurement noise and the choice of IV curves. Different combinations of I-V curves are possible depending on the type of available input matrix. There are more than 1000 different combinations of I-V curves possible from the measurements provided by the full IEC 61853 performance matrix (case a).

The third method, applied in case b to extrapolate the full matrix from a simplified matrix measured according to IEC 61853-1, foresees that when the deviation of the relative temperature coefficients determined from the two irradiance levels is less than 10% for the open-circuit voltage and less than 15% for maximum power, the average of the two temperature coefficients can be used to fill out the missing points of the matrix. This very specific case applies only to linear modules.

The last method, IEC 60891 procedure 2, is based on a simplified one-diode model, which was improved by Monokroussos et al. [123] to take into account non-linearities of the open-circuit voltage and temperature dependence of series resistance. The improved model was implemented into edition 3 of the standard [124]. The latest version of the correction procedure is described by the following two equations:

$$I_2 = \frac{G_2}{G_1} \cdot I_1 \cdot \frac{\left(1 + \alpha_{rel} \cdot (T_2 - 25°C)\right)}{\left(1 + \alpha_{rel} \cdot (T_1 - 25°C)\right)} \tag{16}$$

$$V_2 = V_1 + V_{oc,stc} \cdot \left[\beta_{rel} \cdot \left(f(G_2) \cdot (T_2 - 25°C) - f(G_1) \cdot (T_1 - 25°C)\right) + \frac{1}{f(G_2)} - \frac{1}{f(G_1)}\right]$$
$$- R'_{s1} \cdot (I_2 - I_1) - k' \cdot I_2 \cdot (T_2 - T_1) \tag{17}$$

where, $f(G) = \frac{V_{oc,stc}}{V_{oc}(G)} = 1 + B_1 \cdot ln\left(\frac{1000 Wm^{-2}}{G}\right) + B_2 \cdot ln^2\left(\frac{1000 Wm^{-2}}{G}\right)$

and $\quad R'_{s1} = R'_s + k' \cdot (T_1 - 25°C)$.

I_1, V_1	current and voltage of the measured I-V curve;
I_2, V_2	current and voltage of the target I-V curve;
G_1	measured irradiance;
G_2	target irradiance;
T_1	measured temperature of the DUT;
T_2	target temperature of the DUT;
$V_{oc,stc}$	open-circuit voltage at STC;
V_{oc1}	measured open-circuit voltage;
α_{rel} and β_{rel}	relative short-circuit current and open-circuit voltage temperature coefficients, of the DUT measured at 1000 W/m^2.
B_1	irradiance correction factor for open-circuit voltage
B_2	irradiance correction factor for open-circuit voltage which accounts for non-linearity of V_{OC} with irradiance scaling;
R'_S	internal series resistance of the DUT;
R'_{S1}	internal series resistance at temperature T1;
k'	temperature coefficient of the internal series resistance R'_s.

The semi-empirical translation equations (16) and (17) contain six correction parameters: Besides the relative temperature coefficients for short-circuit current (α_{rel}) and open-circuit voltage (β_{rel}) an additional temperature coefficient (κ') is needed which accounts for changes of the internal series resistance (and fill factor) with temperature. The two parameters B_1 and B_2 describes the irradiance dependency and corrects the open-circuit voltage. B_1 is linked with the diode thermal voltage D of the p-n junction and the number of cells n_s serially connected in the DUT, whereas B_2 takes into account non-linearities of V_{OC} which can occur at lower irradiances.

In the case of linearity, B_2 can be set equal 0. The correction parameters has to be determined from a set of measured I-V curves. Some laboratories add the correction parameters already as output to their test reports. This correction method has the advantage that it can be used over a large range of irradiance levels. As will be shown in a later example, it is so the most appropriate method to extrapolate a cross shaped matrix.

Besides these four methods described in the standards, the measured performance matrix can be also fitted to other generic models. The fitted model does not necessarily pass through all the measured data points, unlike interpolation methods. They have the advantage of being tolerant to random noise, but the disadvantage that they are only valid when the chosen model is a good description of the real module behaviour. This introduces the possibility that they will fail for some module types. An example used for energy rating is the "Mechanistic Performance Model" developed by [125].

4.3.2 Impact of interpolation/correction methods on the accuracy of energy rating

Blakesley et al. [107] used a computational simulation approach to study the impact of measurement error on the accuracy of energy rating using different interpolation methods and different choices of reduced sets of measurements. More detail is given below, but the general conclusions were that:

1. The accuracy of the energy rating is dominated by measurement error for a realistic laboratory setup. The choice of interpolation method/correction procedure has only a minor impact relative to the unavoidable measurement uncertainty.

2. Given the impact of measurement error, the number of data points measured in the performance matrix can be greatly reduced without a significant impact on the accuracy of the energy rating provided that these points are well chosen. A minimum of six data points is needed for good results.

It is important to note that these conclusions apply only to the energy rating of modules; the choice of interpolation method and use of reduced matrices can have a very large impact on the ability to accurately model instantaneous power output (see Figure 45).

The benefits of this approach are that it allowed the simulation of a large number of possible modules (1000 modules), including modules of different types. By repeatedly sampling measurement errors, a statistical analysis of measurement error was possible. Four different interpolation approaches have been investigated using this approach including the first three methods listed in Table 14 (bilinear interpolation, simplified method, and linear interpolation of I-V-curves) and the Mechanistic Performance Model (MPM) of Ransome and Sutterlüti [125].
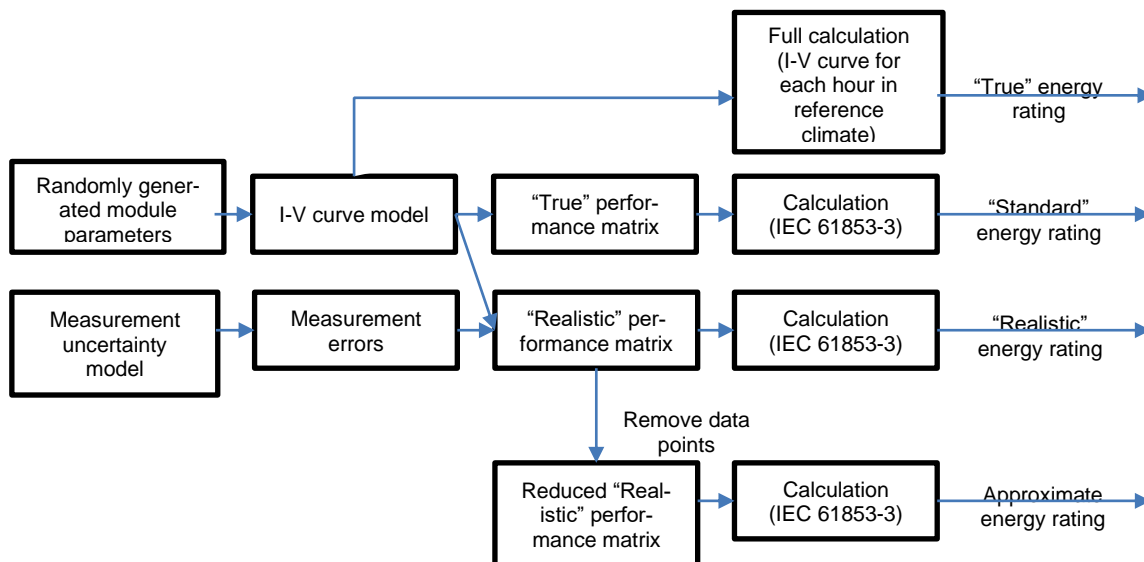
Figure 45: Schematic diagram of the computational method used to assess the accuracy of different interpolation methods and reduced performance matrix configurations (Source: Adapted from [107]).

The benefits of this approach are that it allowed the simulation of a large number of possible modules (1000 modules), including modules of different types. By repeatedly sampling measurement errors, a statistical analysis of measurement error was possible. Four different interpolation approaches have been investigated using this approach including the first three methods listed in Table 14 (bilinear interpolation, simplified method, and linear interpolation of I-V-curves) and the Mechanistic Performance Model (MPM) of Ransome and Sutterlüti [125].

Figure 46 provides examples of the output of these interpolation functions for the case of a single CIGS-like module measured with realistic measurement error. It shows how measurement error can be amplified by extrapolation to conditions outside of the measured performance matrix. However, for energy rating purposes these errors are effectively averaged over one year's worth of data, greatly reducing the impact of random errors.
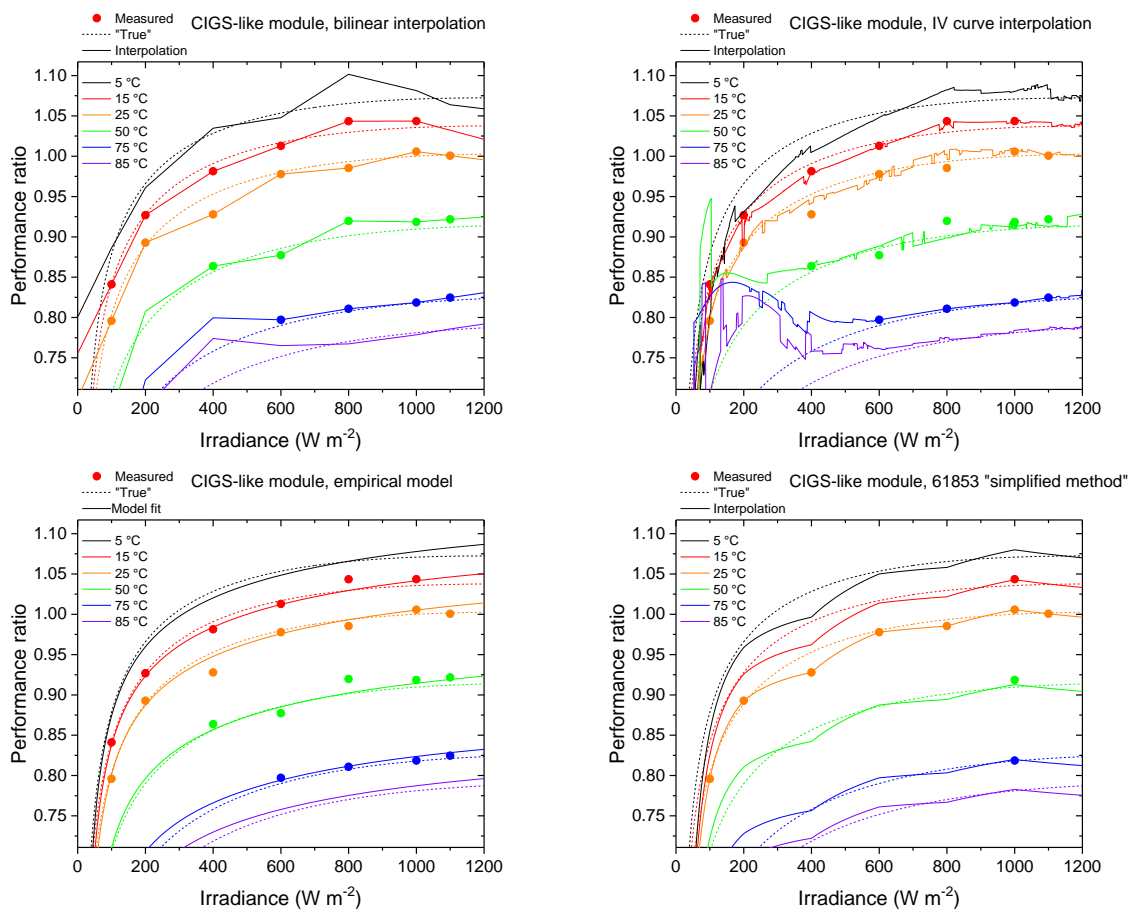
Figure 46: An example of the impact of noise on different interpolation methods for a single simulated CIGS-like module. Dashed lines show the true behaviour of the module in the absence of measurement error. The dots show example performance matrix measurements according to IEC 61853-1 with simulated measurement errors. The solid lines show the output when interpolation is performed using the simulated measurements as inputs.

Random and systematic errors in measurement of the performance matrix and the choice of interpolation method impact the accuracy of the calculated annual energy yield according to the energy rating model 61853-3. Figure 47 shows how the accuracy of the energy yield metric depends on this choice. The error bars illustrate the range of likely values relative to the "true" energy yield that would be obtained with perfect interpolation and no measurement error. The

results demonstrate that there is little difference in overall uncertainty between the choice of bilinear interpolation or empirical models. On the other hand, the IV curve interpolation model performs very well for crystalline silicon modules (c-Si), but failed for Cadmium Telluride (CdTe) modules. The reason for this is that the assumptions of the IV curve model can break down for modules whose behaviour is not well described by a single-diode model. The "simplified method" of IEC 61853-1, using a reduced set of measurements performs as well as the full-matrix measurement for the linear crystalline silicon modules but introduces a small bias in energy rating when applied to slightly non-linear CdTe modules. These results suggest that there is sufficient redundancy in the full performance matrix to suppress the effects of random measurement errors.
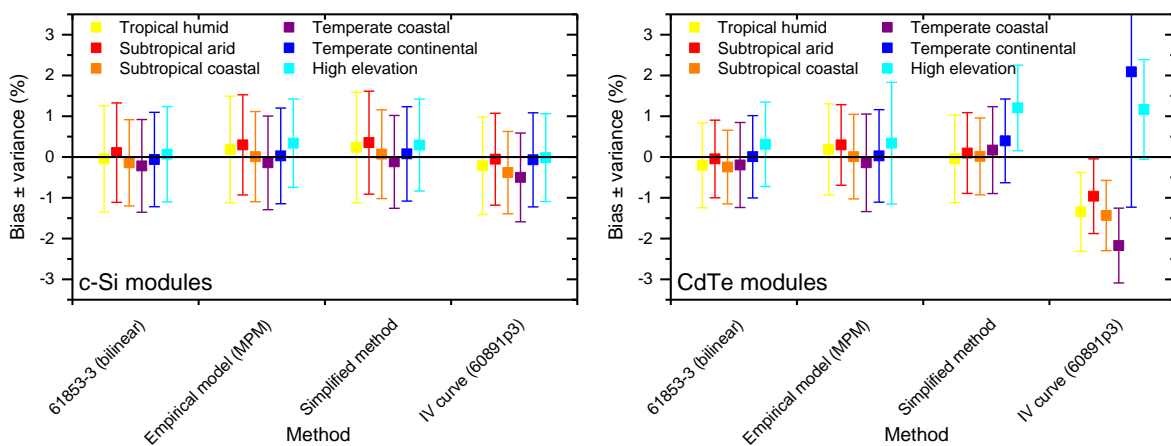
Figure 47: Statistical analysis of error in energy rating resulting from all sources when full performance matrices are measured using simulated modules and simulated measurement errors. The symbols show mean bias in energy rating and error bars denote one standard deviation. Different colours are used for each of the six reference climates contained in IEC 61853-4. Four different interpolation methods were compared. 1000 modules of each type were simulated. Left: monocrystalline silicon modules. Right: Cadmium telluride modules.

4.3.3 Example of an extrapolation of cross-shaped matrix with IEC 60891 procedure 2

The following section shows how the IEC 60891 correction procedure 2 (see Table 14 method 4) can be applied for the extrapolation of a cross-shaped matrix to a full energy rating matrix. Figure 48b) shows an example of a measured power matrix of a commercial PV module with 60 PERC cells. The ten I-V curves depicted in Figure 48a) corresponds to the values highlighted in the matrix. By translating these to STC the 6 correction parameters α_{rel}, β_{rel}, k', B_1, B_2, and R_s' are determined. Figure 48c and d) show the translated IV curves and respectively its deviation achieved with the iteratively determined parameters. The correction parameters fulfil the IEC 60891 requirement of max ±0.5% deviation in P_{max} over the whole irradiance and temperature range.

a)
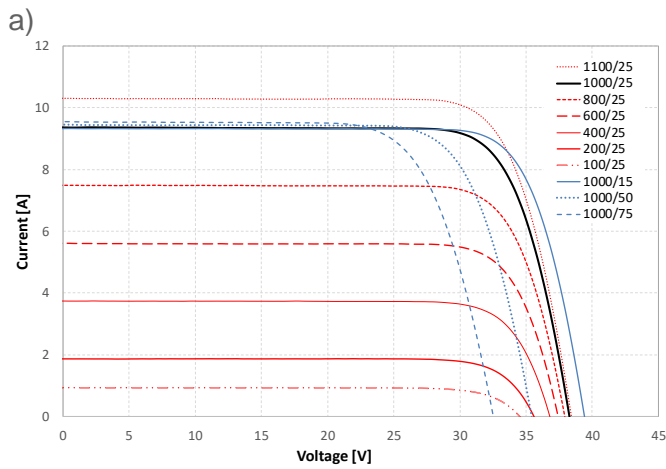
b)

G/T	15	25	50	75
1100		307.72		
1000	291.06	280.21	252.10	223.66
800	232.71	223.83	201.70	179.03
600	173.97	167.21	150.57	133.51
400	114.66	110.30	99.08	x
200	55.92	53.70	x	x
100	26.59	25.77	x	x

c)

αrel=0.0004
βrel=-0.003
k'=0.0022
B1=0.0435
B2=0.0018
Rs'=0.192
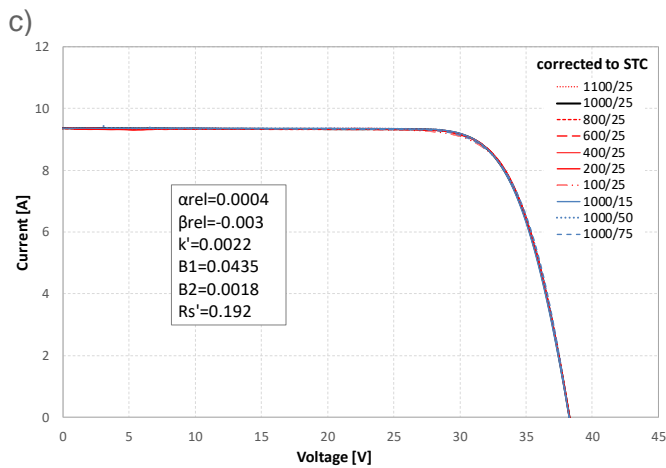
d)

G/T	15	25	50	75
1100		-0.11%		
1000	-0.02%	0.00%	-0.14%	-0.50%
800		-0.03%		
600		0.01%		
400		0.04%		
200		-0.08%		
100		-0.94%		

Figure 48: a) and b) Example of power matrix values in [W] of a commercial PERC PV module together with the 10 measured IV-curves corresponding to the cross shaped matrix used for the determination of the correction parameters. c) and d) Correction parameters (α_{rel}=0.0004; β_{rel}=-0.003; k'=0.0022; B_1=0.0435; B_2=0.0018; R'_s=0.19) obtained by translating the 10 IV-curves and the relative deviation in power.

Figure 49 shows how the error propagates when applying the same correction parameters to determine the full energy rating matrix. The deviation of the calculated power versus the measured power values, shown in Figure 48b, is therefore analysed. The full matrix can be either obtained by applying a temperature correction (horizontal translation) or irradiance correction (vertical translation). Figure 49a) and b) shows the deviations for the two respective approaches.

a)

G/T	15	25	50	75
1100			-0.07%	-0.17%
1000				
800	-0.11%		0.13%	0.38%
600	-0.29%		0.34%	0.89%
400	-0.22%		0.64%	
200	-0.24%			
100	1.78%			

b)

G/T	15	25	50	75
1100			-0.06%	-0.03%
1000				
800	-0.13%		0.23%	0.66%
600	-0.28%		0.51%	1.29%
400	-0.21%		0.81%	
200	-0.30%			
100	0.80%			

Figure 49: Relative deviation of the translated power respect to the measured power for a) a pure vertical translation (irradiance correction) and b) a pure horizontal translation (temperature correction).

For the vertical translation, the error is well below 0.9% over the whole matrix, except for the power value at 100 W/m² where the error is reaching 1.8%. The deviation remains however significantly below the typical measurement uncertainties for maximum power, which ranges from of 1-4% [107, 126, 127] depending on the irradiance level and the laboratory at which the measurement is performed. Figure 49b) shows the results of the horizontal translation. As expected due to the limitation that the temperature correction parameters are applicable in a limited range of approx. ±30% of the irradiance at which the temperature coefficients are measured, the deviations are increasing below 800 W/m². Translations over a larger temperature range are more affected than the translation from 25°C to 15°C. In the last case, the error remains below 0.9% for all irradiances. The horizontal translation can be so applied at very low irradiances in alternative to the vertical translation.

The following section shows how a combination of a vertical/horizontal translation applies to a set of commercial modules with different crystalline silicon cell technologies (poly, mono, PERC, PERT, HJT) and module characteristics. The nine crystalline silicon module matrices measured by CFV Labs described in Chapter 2.4 have been processed with the same procedure.

Table 15: IEC 60891 Coefficients of Sandia Modules Described in Chapter 2.4.

Model	Techn	α_{rel}	β_{rel}	B_1	B_2	R_s'	k'
JKM260P-60	Multi-c-Si	0.038%	-0.338%	0.0439	0.0026	0.165	0.0013
CS6K-270P	Multi-c-Si	0.039%	-0.332%	0.0415	0.0022	0.154	0.0012
Q.PLUS BFR	Multi-Si PERC	0.038%	-0.315%	0.0411	0.0022	0.210	0.0012
CS6K-275M	Mono-Si	0.035%	-0.334%	0.0419	0.0022	0.160	0.0013
Q.PEAK-G4.1 300	Mono-Si PERC	0.033%	-0.319%	0.0382	0.0018	0.278	0.0011
MSE300SQ5T	Mono-Si PERC	0.033%	-0.323%	0.0379	0.0017	0.198	0.0009
IT-360-SE72	Mono-Si PERC	0.036%	-0.311%	0.0406	0.0020	0.240	0.0015
LG320N1K-A5	N-type Mono-Si	0.030%	-0.318%	0.03828	0.0017	0.220	0.0010
VBHN325SA	HJT	0.025%	-0.229%	0.04217	0.0022	0.430	0.0040

Table 15 gives an overview of the module specifications of the nine investigated modules to-gether with the IV-correction parameters determined according to IEC 60891. The I-V curves required for this analysis were generated with the PAN files available together with the power matrices.

An irradiance correction (vertical translation at fixed temperature) is applied to all values, except for the low irradiance values @15°C of MOD1, MOD2, MOD3, MOD5, MOD6, MOD8 and MOD9 where the determination of the correction parameters exceeded the 0.5%. In this case a temperature correction is applied instead to the IV curve measured at 100 W/m² and 25°C. Figure 50 shows the deviation of the extrapolated values with respect to the measured values for all nine modules, whereas Figure 51 shows the mean bias error and standard deviation error of all modules.

The largest error is of 0.64%. The standard deviation is increasing with decreasing irradiance and reaches up to 0.54%. The results are in line with the observations made by Blakesley et al. [107].

MOD1	JKM260P-60 260 W			
G/T	15	25	50	75
1100		0.19%	0.20%	0.20%
1000	-0.01%	0.00%	0.13%	0.45%
800	-0.31%	-0.32%	-0.32%	-0.32%
600	-0.49%	-0.49%	-0.49%	-0.47%
400	-0.45%	-0.45%	-0.42%	
200	0.19%	0.21%		
100	-0.41%	2.11%		

MOD2	CS6K-270P 270W			
G/T	15	25	50	75
1100		0.18%	0.19%	0.20%
1000	0.03%	0.00%	0.03%	0.26%
800	-0.27%	-0.28%	-0.30%	-0.31%
600	-0.40%	-0.42%	-0.45%	-0.46%
400	-0.36%	-0.37%	-0.39%	
200	0.17%	0.16%		
100	-0.34%	1.93%		

MOD3	Q.Plus BFR-G4.1 280W			
G/T	15	25	50	75
1100		0.13%	0.13%	0.14%
1000	0.02%	0.00%	0.04%	0.24%
800	-0.18%	-0.18%	-0.19%	-0.18%
600	-0.22%	-0.22%	-0.22%	-0.18%
400	-0.11%	-0.10%	-0.06%	
200	0.43%	0.46%		
100	-0.38%	2.18%		

MOD4	CS6K-275M 275W			
G/T	15	25	50	75
1100		0.11%	0.10%	0.07%
1000	0.02%	0.00%	0.03%	0.21%
800	-0.21%	-0.19%	-0.15%	-0.09%
600	-0.36%	-0.33%	-0.22%	-0.08%
400	-0.46%	-0.39%	-0.18%	
200	-0.39%	-0.25%		
100	0.20%	0.40%		

MOD5	Q.Peak BLK G4.1 300W			
G/T	15	25	50	75
1100		0.12%	0.12%	0.11%
1000	0.06%	0.00%	0.00%	0.27%
800	-0.20%	-0.19%	-0.18%	-0.15%
600	-0.34%	-0.32%	-0.27%	-0.20%
400	-0.40%	-0.36%	-0.25%	
200	-0.28%	-0.20%		
100	-0.40%	0.62%		

MOD6	MSE300SQ5T			
G/T	15	25	50	75
1100		0.10%	0.11%	0.12%
1000	0.05%	0.00%	0.05%	0.41%
800	-0.13%	-0.13%	-0.14%	-0.15%
600	-0.15%	-0.16%	-0.17%	-0.17%
400	-0.13%	-0.13%	-0.11%	
200	0.11%	0.13%		
100	-0.28%	1.38%		

MOD7	IT-360-SE72			
G/T	15	25	50	75
1100		0.08%	0.06%	0.03%
1000	0.03%	0.00%	0.04%	0.27%
800	-0.13%	-0.12%	-0.07%	-0.01%
600	-0.23%	-0.19%	-0.08%	0.07%
400	-0.30%	-0.23%	-0.01%	
200	-0.31%	-0.16%		
100	0.15%	0.37%		

MOD8	LG320N1K-A5 320W			
G/T	15	25	50	75
1100		0.08%	0.07%	0.06%
1000	0.04%	0.00%	0.03%	0.33%
800	-0.12%	-0.11%	-0.09%	-0.05%
600	-0.18%	-0.16%	-0.10%	0.00%
400	-0.25%	-0.20%	-0.05%	
200	-0.23%	-0.13%		
100	-0.42%	0.54%		

MOD9	N325SA16 325W			
G/T	15	25	50	75
1100		0.11%	0.09%	0.06%
1000	0.00%	0.00%	0.03%	0.11%
800	-0.20%	-0.18%	-0.12%	-0.05%
600	-0.33%	-0.29%	-0.15%	0.02%
400	-0.44%	-0.35%	-0.08%	
200	-0.42%	-0.24%		
100	0.22%	0.48%		

Figure 50: Relative deviation of the translated power with respect to the measured power for nine commercial modules.

	Mean bias error			
G/T	15	25	50	75
1100		0.10%	0.04%	-0.04%
1000	0.03%	0.00%	0.05%	0.29%
800	-0.17%	-0.14%	-0.03%	0.11%
600	-0.26%	-0.19%	0.01%	0.27%
400	-0.25%	-0.16%	0.11%	
200	-0.10%	0.12%		
100	-0.04%	1.20%		

	Standard Deviation			
G/T	15	25	50	75
1100		0.05%	0.07%	0.12%
1000	0.05%	0.00%	0.07%	0.13%
800	0.08%	0.07%	0.12%	0.21%
600	0.15%	0.12%	0.21%	0.40%
400	0.31%	0.23%	0.28%	
200	0.54%	0.67%		
100	0.31%	1.70%		

Figure 51: Mean bias error and standard deviation of the energy rating power matrix values of nine commercial modules.

4.3.4 Accuracy and costs of reduced energy rating measurements

Based on the results of the survey of accredited laboratories done by Blakesley *et al.* [107] it was also possible to build a picture of the indicative typical relative costs of different components of energy rating, reproduced in Figure 52, as well as a breakdown of the typical sources of uncertainty when the full performance matrix is used. The analysis confirmed that random

errors in measuring the performance matrix measurement are suppressed, and that the final uncertainty is dominated by systematic errors such as calibration of the reference cells. Taken together, these results indicate that estimating energy rating from a reduced set of measurements can provide a result with similar accuracy but reduced cost relative to measuring the full matrix.
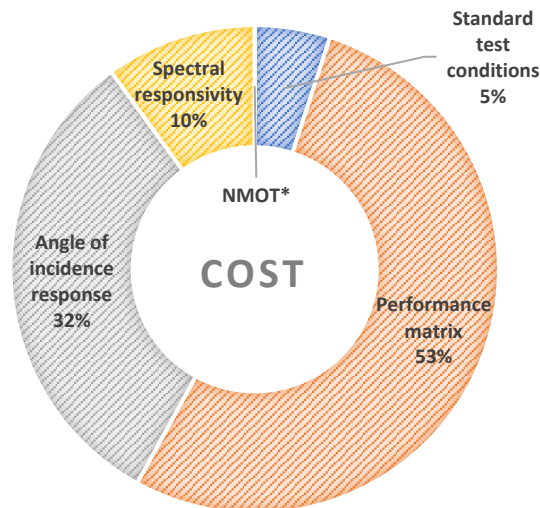
Figure 52: Indicative relative contributions to the cost of performing a complete set of energy rating measurements according to IEC 61853-1&2. *The cost of measuring the nominal module operating temperature (NMOT) parameters was not included (Source: [107]).

To demonstrate this, the accuracy and cost were evaluated for more than 1000 different scenarios of reduced measurement matrices using both linear interpolation and an empirical model to interpolate and extrapolate from measurement points. The results, shown in Figure 53, indicate that it is possible to reduce the number of measurement points in the performance matrix without significant loss of accuracy in the evaluation of energy rating provided that the measurement points are well chosen. Reducing the number of points to this degree approximately halves the cost of measuring the performance matrix. The bias between different technology types is also influenced strongly by the number and choice of measurement points, as some combinations are better able to capture nonlinear behaviour. Comparing two different interpolation methods, the general behaviour is very similar. The empirical modelling approach was more tolerant to poor choices of measurement points, but was also more prone to technology bias when good choices of measurement points were used.
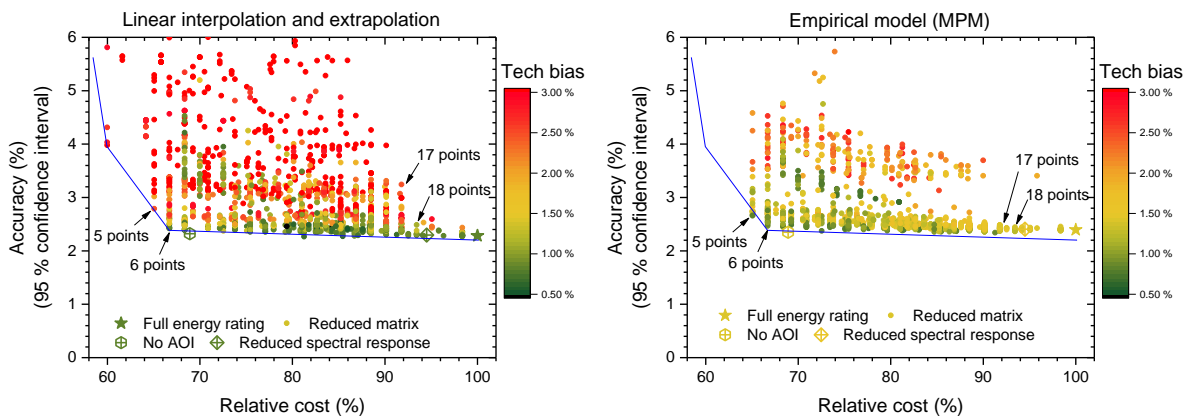
Figure 53: Accuracy (expressed as 95% confidence interval in the value of $E_{mod,year}$) in the calculation of energy rating from using performance matrices with a reduced number of measurement points compared to those required by the IEC 61853-1 standard. Left: Using linear interpolation between measurement points. Right: Using an empirical model fitted to measured points. Results are plotted against the relative total cost of energy rating, which includes the cost of angular and spectral response measurements. The colour indicates the magnitude of bias between different module types. Calculations were based on a cohort of 1000 randomly generated simulated modules of mixed technology type using uncertainty and cost models from a survey of test and measurement laboratories (Source: [107]).

The best performing of these measurement scenarios are depicted in Figure 54. There are a number of alternative strategies that yield similar results for a given number of points. As a general rule, it is necessary to perform one set of measurements at a low temperature (*e.g.* 15°C) including low and medium irradiances and one at a high temperature (50°C or 75°C) including medium and high irradiances. With six or more measurement points, most of the relevant nonlinear behaviour can be captured.

Eight measurement points				
Irradiance	Temperature			
W/m²	15°C	25°C	50°C	75°C
1100				
1000	X		X	
800	X		X	
600				
400	X		X	
200	X			
100	X			

Seven measurement points				
Irradiance	Temperature			
W/m²	15°C	25°C	50°C	75°C
1100				
1000	X		X	
800	X		X	
600	X		X	
400				
200	X			
100				

Six measurement points					Five measurement points				
Irradiance	Temperature				Irradiance	Temperature			
W/m^2	15°C	25°C	50°C	75°C	W/m^2	15°C	25°C	50°C	75°C
1100			X		1100				X
1000	X		X		1000				
800	X		X		800	X			X
600					600				
400					400	X			
200	X				200	X			
100					100				

Figure 54: Examples of the best measurement scenarios (scenarios with the lowest 95% confidence interval for energy rating error) of all of the scenarios shown in Figure 53. Crosses indicate conditions where measurements are taken, grey boxes indicate measurements not taken. Here the best scenarios for eight, seven, six and five measurement points respectively are shown.

Besides performance matrices, as explained in Chapter 4.1 before, the energy rating also requires the measurement of spectral responsivity, angle-of-incidence (AOI) response and nominal module operating temperature (NMOT) parameters according to IEC 61853-2, which contribute considerably to the total cost. The standard allows the use of AOI measurements to be shared for similar modules, avoiding the need to repeat this measurement. The effects of this were considered in Figure 54, where it was found that cost could be reduced by more than 30% without significant loss of accuracy by excluding AOI measurements. Similarly, it was found that 5% of the total energy rating cost could be saved by reducing the number of data points measured in the spectral responsivity measurements without significant loss of accuracy. These cost savings can be combined with the reduction of performance matrices to six points, providing an accurate estimate of standard energy rating for only about 1/3 of the total cost.

4.4 Calibration and Application of the Sandia Model to PV System Energy Predictions

4.4.1 Introduction

As discussed in Chapter 2.3, rather than the tidy, discrete points prescribed by IEC 61853 for indoor characterization, outdoor measurements tend to encompass a continuum of operating conditions. In addition to irradiance and temperature, these measurements also commonly span a range of other variables affecting PV performance, principally spectrum, solar incident angle and wind speed. As such, outdoor testing is commonly paired with an appropriate performance model for the technology under test or at least translation equations such that the 61853-1 matrix can be reproduced.

The Sandia Array Performance Model [45] is a semi-empirical set of four principal equations that, when appropriately calibrated, effectively reduces outdoor data into a set of coefficients that a) represent module performance at STC, b) can be used to translate outdoor data to the IEC 61853-1 performance matrix and c) can be coupled with tabular weather data to perform energy predictions or ratings under arbitrary conditions. These four principal equations are supplemented by sub-models describing spectral response, cell temperature, and reflection loss. While efforts have been made to calibrate the model using fixed-tilt data [128], the most complete and reliable method continues to utilize data from a two-axis solar tracker [129]. The use of a two-axis tracker facilitates the separation of the measured performance data into normal incident or "on-sun" conditions and angle of incidence or "off-sun" or conditions. This in turn facilitates the assessment of module performance as a function of primary environmental variables, separate from the accompanying incident angle response associated with off-axis reflection losses.

Procedures for characterizing modules outdoors on a two-axis tracker are summarized in Chapter 2.3: Outdoor PV Module Characterization using Two-Axis Solar Trackers and [44]. In this chapter, analysis procedures for calibrating the SAPM from outdoor module characterization will be described. The procedures are separated into normal incident or "on-sun" characterization, which forms the bulk of the data from outdoor testing, and "off-sun" or Angle of Incidence (AOI) testing. Analysis of an optional, on-sun thermal test is also presented. In the event that a discrete on-sun thermal test is omitted, temperature coefficients must be extracted from on-sun electrical performance data. Details of the data reduction are too lengthy to present here and are instead presented in [44].

4.4.2 Sandia array performance model overview:

The Sandia Array Performance Model consists of four primary equations describing short circuit current, open circuit voltage, current at MPP and voltage at MPP. The equation for short circuit current is the core component of the model as it is used to calculate Effective Irradiance (E_e), which is used in all remaining equations. The model also includes intermediate points along the IV curve, I_x and I_{xx} shown below in Figure 55. These points were originally included to support modelling of battery-based systems in which PV modules may operate off of the MPP. In practice, these points are rarely used and are not addressed here.
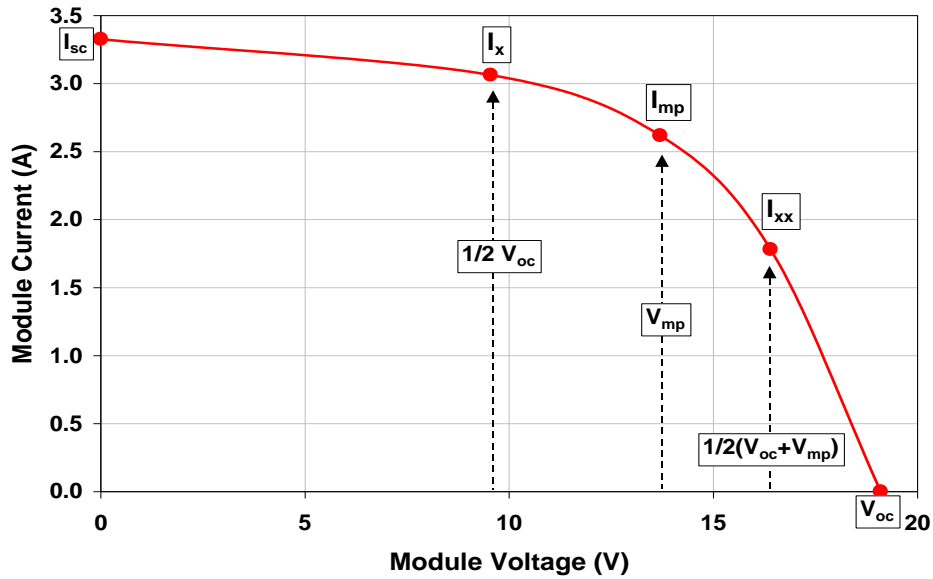
Figure 55: Model points on the IV curve described by the Sandia Array Performance Model (reproduced from [45]).

A.   Primary equations

The equation for I_{sc} is given by

$$I_{sc} = I_{sco}f_1(AM)\left[\frac{G_{poa}}{G_0}\right]\left[1 + \hat{\alpha}_{Isc}[T_c - T_0]\right] \tag{18}$$

where the function $f_1(AM)$ is a dimensionless polynomial function linking the influence of air mass to photo-generated current.

$$f_1(AM) = a_0 + a_1(AM) + a_2(AM)^2 + a_3(AM)^3 + a_4(AM)^4 \tag{19}$$

Effective irradiance, used for all remaining calculations, is given by:

$$E_e = \frac{I_{sc}}{I_{sco}\left[1 + \hat{\alpha}_{Isc}[T_c - T_0]\right]} \tag{20}$$

The remaining primary equations then are

$$V_{oc} = V_{oco} + N_s\delta(T_c)\ln(E_e) + \beta_{Voc}[T_c - T_0]$$

$$I_{mp} = I_{mpo}[C_0 E_e + C_1 E_e^2]\left[1 + \hat{\alpha}_{Imp}[T_c - T_0]\right] \tag{21}$$

$$V_{mp} = V_{mpo} + C_2 N_s\delta(T_c)\ln(E_e) + C_3 N_s[\delta(T_c)\ln(E_e)]^2 + \beta_{Vmp}[T_c - T_0]$$

where $d(T_c)$, the thermal voltage per cell, is given by

$$\delta(T_c) = \frac{nk[T_c + 273.15]}{q} \tag{22}$$

Finally, cell temperature T_c is rarely known, whereas module temperature T_m is measured directly during outdoor characterization. A simple one-dimensional thermal conduction model is used to calculate cell temperature from module temperature,

$$T_c = T_m + \frac{G_{POA}}{G_0}\Delta T \tag{23}$$

where ΔT is the temperature difference between a cell and module back surface at solar irradiance of 1000 W/m² (typically assumed to be 3°C).

B. Thermal model

Module temperature may be linked to ambient temperature, T_a through the "wind speed" equation,

$$T_m = T_a + G_{POA}e^{a+bW} \tag{24}$$

C. Angle of incidence

Reflection losses during "off-axis" operations are represented by an Angle of Incidence (AOI) function. G_{poa} in Eqn (1) may be decomposed into beam and diffuse components, where only the beam component, G_b is affected by reflection losses through the function $f_2(q)$. The diffuse utilization term f_d, is commonly treated as being unity.

$$G_{poa} = G_b f_2(\theta) + f_d G_{diff} \tag{25}$$

In the classical formulation of the SAPM, angle of incidence is represented by an empirical 5th order polynomial.

$$f_2(\theta) = b_0 + b_1(\theta) + b_2(\theta)^2 + b_3(\theta)^3 + b_4(\theta)^4 + b_5(\theta)^5 \tag{26}$$

However, any number of other mathematical functions such as the ASHRAE [130], physical [46], or Martin and Ruiz [48] can be used. Deterministic measurement at prescribed incident angles as described in Section 2.3.1 facilitates the use of a lookup table coupled with nearest-neighbour interpolation, eliminating the need to apply a model

4.4.3 Model calibration procedures

Currently, there are two approaches to calibrating the primary equations of the model. The older, classical method relies on the piecewise solution of each primary equation, using data sets tightly constrained to specific environmental conditions. Here, the on-sun thermal test is required to determine temperature coefficients prior to calibrating the primary equations. The newer and preferred method utilizes the simultaneous solution of each primary equation via multivariate regression analysis and does not require a separate on-sun thermal test. In this method, all coefficients of each primary equation are solved without constraint. The ambient temperature/wind speed and Angle of Incidence models are calibrated independently of which method is chosen to calibrate the primary equations.

Independent of which calibration method is chosen, two data sets are required to calibrate the primary equations. The first is a "clear sky" data set, spanning conditions given in Table 3 of Chapter 2.3, while the second is an "all sky" data set that merges the Clear Sky data set with

a data set spanning the Cloudy conditions given in Table 4 of the same chapter. The Clear Sky data set is used exclusively to calibrate the primary equation for I_{sc}, while the All Sky data set is used to calibrate all remaining primary equations. The need for the Clear Sky data set for I_{sc} is driven by the air mass function, $f_1(AM)$, a proxy for spectral correction. I_{sc} is not correlated to air mass under cloudy conditions, particularly diffuse, overcast conditions. Separate data sets are required to calibrate the angle of incidence and optional temperature coefficients (conditions given in Table 5 of Chapter 2.3). All data should be quality checked and filtered before analysis. The calibration of I_{sc} can in principle be done with any type of irradiance instrument. However, the instrument type and accuracy propagate into the model coefficients. A broadband thermopile-based pyranometer is recommended as the general choice for model calibration. However, if it is known in advance that model predictions will be referenced to irradiance from an alternate instrument, e.g., a reference cell or silicon photodiode, then model coefficients can be developed with that type of instrument in mind. The magnitude of I_{sco} may be affected by the choice of instrument, but the effect will primarily be seen in calibration of the air mass function, which serves as a proxy for spectral effects including mismatch to the reference device.

D. Classical Solution Method

The classical method builds on fitting procedures developed in parallel with the development of the model and relies on a piecewise solution of each primary equation, using data sets tightly constrained to specific environmental conditions [45]. The most recent method was described in detail in [44]. Principally, temperature coefficients are first determined for I_{sc}, I_{mp}, V_{oc}, and V_{mp}. Using measured module temperature, each measured point on the IV curve can then be translated to a common reference temperature, traditionally 50°C. This reduces the equation for I_{sc} to a product of normalized irradiance, the unitless air mass function, and a scaling factor (I_{sco}) and the remaining primary equations to a set of polynomials varying only with effective irradiance.

In the original solution method, I_{sco} was found by filtering the clear sky data set to a narrow range of irradiance centred about 1000 W/m^2 and a narrow range of air mass centred about AM1.5. The remainder of the I_{sc} clear sky data set was then irradiance corrected and normalized by I_{sco}. Coefficients for the air mass function, $f_1(AM)$ were then found by polynomial regression of this data set onto air mass. As with I_{sco}, the remaining principal factors, I_{mpo}, V_{oco} and V_{mpo} can be found from the filtered clear sky data set. The remaining terms for each primary equation are then found from the all-sky data set. The equation for I_{mp} is solved by regression onto effective irradiance, while equations for V_{oc} and V_{mp} are solved by regression onto the natural log of effective irradiance.

While this method is satisfying in that it yields "STC" parameters from measured data close to reference conditions, it can suffer from insufficient data near these conditions, resulting in bias errors that propagate into the rest of the model. The more recent method [131] eliminates use of the narrow clear sky data set centred about 1000 W/m^2 and AM1.5. Using the clear sky data set, I_{sc} is first irradiance corrected and then directly regressed onto Ama using a 4th order polynomial. I_{sco} is found by solving this polynomial at AM1.5. Normalizing the polynomial coefficients by I_{sco} then produces the unitless $f_1(AM)$. The remaining primary equations are then solved similarly, using the all sky data set.

E. Simultaneous Solution Method

The simultaneous solution method builds upon the more recent classical method. Here, multivariate regression analysis is applied to the full set of IV curves collected under a range of environmental conditions to solve the primary equations for SAPM [131]. This method has a

distinct advantage over the classical method, in that the separate thermal test is eliminated. Beyond reducing complexity, it allows temperature coefficients to be calibrated under steady-state conditions that better reflect those of an operational PV array. This can be particularly beneficial for PV cell technologies that display metastability [132]. Further, the determination of temperature coefficients for voltage has traditionally assumed a diode factor of 1. For crystalline silicon modules tested near 1000 W/m^2, this assumption is unlikely to introduce error. However, for testing conducted away from this condition and for thin-film modules, this assumption may introduce error. As with the classical solution method, the equation for I_{sc} is solved first, using the Clear Sky data set. Solution to this equation yields I_{sc} at STC (I_{sco}), the air mass function, $f_1(AM)$ and temperature coefficient α_{Isc}. This equation can be challenging to solve simultaneously because of the 4th order polynomial term commonly used to represent the effect of airmass. In practice, it may be more efficient to solve the equation iteratively until convergence is obtained for I_{sco}, $f_1(AM)$ and α_{Isc}. Once this equation is calibrated, the Effective Irradiance, E_e, is calculated using measured I_{sc} and module temperature from for the All Sky data set. The remaining equations are then solved as above but including the temperature coefficients as unknowns.

F. Thermal model

The thermal model provides a link between ambient weather conditions and module temperature. While it is not necessary to solve this equation in order to solve the primary equations, it is a useful component for applying measured weather data to system analysis via the SAPM. Eq. (24) is rewritten as

$$\ln\left(\frac{T_m - T_a}{G_{POA}}\right) = a + bW \tag{27}$$

This can be solved simply to determine the a and b coefficients using either the Clear Sky or All Sky data sets.

G. Angle of incidence

Procedures for measuring AOI response were described in Section 2.3. This analysis differs from the others described in this procedure, in that a separate data set from deterministic testing is required. AOI analysis is typically conducted after calibration of the primary SAPM equations, such that the air mass function and temperature coefficient for I_{sc} are known. Incident angle response is found by first correcting the measured I_{sc} for temperature and optionally, spectrum.

$$I_{sc,Tr,AM1.5} = \frac{I_{sc}}{f_1(AM)[1 + \hat{\alpha}_{Isc}[T_c - T_0]]} \tag{28}$$

A reference condition, I_{scr}, is then found at 0° incident angle.

$$I_{scr} = \frac{1}{n}\sum\left[I_{sc,Tr,AM1.5}\left[\frac{G_0}{G_{DNI} + G_{diff}}\right]\right]_n \quad @\ AOI = 0° \tag{29}$$

Normalized I_{sc} (Nisc) is then found by removing cosine losses from each measured value and normalizing by I_{scr}.

$$Nisc = \left[\frac{G_0}{G_{DNI}\cos\theta}\right]\left[\frac{I_{sc,Tr,AM1.5}}{I_{scr}} - \left[\frac{G_{diff}}{G_0}\right]\right] \tag{30}$$

Multiple measurements obtained at each incident angle are then averaged and tabulated. When the tracker control system facilitates repeatable testing at prescribed incidence angles, measured values can be averaged across multiple days. This is the currently preferred approach. If desired, the tabulated data set may then be fit to the 5th order polynomial (Eq. (27)) to yield the classical $f_2(\theta)$ function. Historically, this function worked well enough for plain glass cover sheets, but the presence of a modern anti-reflective coating can induce instability and oscillation in the polynomial. Constraining the slope of the function to be 0 at 0° incident angle can dampen the oscillation.

H. Temperature coefficients (optional)

Procedures for measuring temperature coefficients were described in Section 2.3. As with angle of incidence, this analysis differs from the others described in this procedure, in that a separate data set from deterministic testing is required. When performed, temperature coefficient analysis is conducted prior to calibration of the primary SAPM equations. Ideally, characterization would be performed at exactly 1000 W/m^2, however this is rarely possible with outdoor characterization. Measured points are therefore translated from the measurement condition back to the 1000 W/m^2. Traditionally, this analysis does not rely on coefficients from the primary analysis and instead assumes either linear or logarithmic response to irradiance for current and voltage, respectively. It further assumes a diode factor of 1, which can introduce error in temperature coefficients for voltage, particularly for thin film modules.

Both I_{sc} and I_{mp} are translated assuming linear, directly proportional response to irradiance,

$$I_{1000} = I\left[\frac{G_0}{G_{poa}}\right] \tag{31}$$

Both V_{oc} and V_{mp} are translated assuming logarithmic response to irradiance,

$$V_{1000} = V - N_s\delta(T_c)\ln\left(\frac{G_{poa}}{G_0}\right) \tag{32}$$

Each translated value is then regressed linearly onto (T_c-25). The resulting slope is the temperature coefficient. Note in the SAPM that temperature coefficients for current are traditionally used in dimensionless units of 1/°C, while temperature coefficients for voltage are used in engineering units of V/°C.

4.5 ISE Model vs IEC 61853-3

The increment on PV market around the globe demands to PV simulation tools to perform at high accuracy and precision for different climate conditions, technologies and grid conditions. In addition, international standardization strives for comparable yield assessment outputs adapted to these conditions and a more reliable prediction to gain confidence in investments. In response to this demand, PV Module simulation tools must be adapted to the new market requirements. This chapter presents a summary of a previously developed approach for PV module simulation and compares it to the IEC energy rating approach.

4.5.1 PV module energy rating simulation

As mentioned in Chapter "4.1 According to IEC 61853-3" of this report, the International Electrotechnical Commission (IEC) has published a PV module simulation model in 2011: International Standard IEC 61853 (see [133]). Six different reference climate profiles have been defined in IEC 61853-4 (see [134]) to simulate the PV module behaviour under different outdoor conditions. The reference climate profiles are representative of global regions relevant to the PV industry. Each standard reference climate profile consists of one-year of data in hourly increments, including the following parameters: ambient temperature, irradiance, wind speed at module height, sun position, and solar spectrum.

For all the climate profiles and PV module simulations, the following PV system conditions are defined: Fixed open rack, equator-facing, and 20° inclination angle.

To make the PV module energy rating technology-specific, the methodology is divided mainly into four correction and calculation steps:

1. Angle of incidence (AOI) effects
2. Spectral correction effects
3. PV module temperature
4. PV module efficiency (ETA) and output power

The four steps will be described in detail within this section.

1. Angle of incidence (AOI) effects

To accurately simulate the behaviour of a PV module at any time of the day, it is important to describe PV module light transmission properties at different AOI. As [135] describes, the diffuse irradiance in plane of array (D_{POA}) is calculated based on Eq.(33), together with the data from the climate profiles, defined in [134].

$$D_{POA} = G_{POA} - I_{POA} \tag{33}$$

After that, DPOA and the direct irradiance in POA (IPOA) are corrected for solar incident angle as indicated in equations 1 and 2, respectively of Chapter "4.1 According to IEC 61853-3" of this report. The use of these equations requires the effective light transmission into the PV model (AOI response ar) at different incident angles to be calculated beforehand, as explained in [136]. Finally, the angular corrected POA (plane of array) global irradiance is calculated as described in Eq. (34).

$$G_{POA,AOIcorr} = D_{POA,corr} + I_{POA,corr} \tag{34}$$

2. Spectral correction effects

Different locations around the planet present diverse radiation wavelengths and spectral properties. Therefore, a description of the PV module response at different solar irradiance levels is indispensable. The spectral correction factor (C_s) of the PV module is calculated as described in Eq. (12) of section "4.1 According to IEC 61853-3" of this report. Previous to this step, two sub-steps have to be performed. On the one hand, spectrally resolved G_{POA} in a set of discrete wave-bands, included in the standard reference climate profiles, has to be also AOI corrected as shown in Eq.(35). On the other hand, the PV module spectral responsivity ($S(\lambda)$) has to be measured for different wavelengths, as [136] shows. Finally, the spectrally corrected G_{POA} is calculated as described in Eq. (13) of section "4.1 According to IEC 61853-3".

$$G(\lambda)_{POA,AOIcorr} = \frac{G_{POA,AOIcorr} * G(\lambda)_{POA}}{G_{POA}} \tag{35}$$

3. PV module temperature

One of the most important factors for an accurate PV module performance description is the temperature dependency. A PV module, in normal operation, is exposed to different outdoor conditions. Different technologies have a different response to temperature changes, therefore the temperature coefficients ($u0$, $u1$) of the module have to be calculated before as described in [136]. These coefficients describe the operating temperature of the module as a function of the irradiance and ambient temperature. The module temperature (T_{mod}) is calculated as defined in Eq. (14) of section "4.1 According to IEC 61853-3". The wind speed, extracted from [134], is considered as described by the Faiman Method [113].

4. PV Module efficiency and output power

Finally, PV module output power is calculated as described in section 4.1.4 [137] as bilinear interpolation. The calculation is based on T_{mod}, G_{POA} spectrally corrected and PV module efficiency (ETA) at different irradiances and temperatures generated from [133].

4.5.2 ISE approach: Dirnberger et al. model

A model to simulate the PV module output power was proposed by Dirnberger in 2015 [11]. In contrast to the IEC energy rating model, Dirnberger et al. method does not require expensive and comprehensive laboratory measurements to model PV module response at different outdoor conditions. As an alternative, Dirnberger et al. is based on available historical data and technical datasheets of the PV module.

Dirnberger et al. method proposes five main calculation steps to be followed instead of four:

1. Reflection losses

2. Spectral losses

3. PV module temperature

4. PV module efficiency at 25°C

5. PV module efficiency and output power

1. **Reflection losses**

The magnitude of the losses depends on the position of the sun on the specific location, the tilt and azimuth angles for the particular PV module, and the ratio of I_{POA} and D_{POA}. Therefore, in this approach reflection losses are calculated separately for I_{POA} and D_{POA}.

In the case of I_{POA}, AOI and module reflection behaviour are combined for each time step, and the position of the sun is considered for the given tilt and orientation angles. While in the case of D_{POA}, as described in [11], 3.5% losses are assumed for all time steps. AOI between 50° and 60° is assumed as an average thus the diffuse part is considered as isotropic.

Finally, G_{POA} reflection losses are the sum of I_{POA} and D_{POA}, considering already the reflection losses for both.

2. **Spectral losses**

For the spectral losses calculation, a spectral factor is considered in a straightforward way as indicated the section 3.3 of [11].

3. **PV module temperature**

PV module temperature is calculated in a simplified way following Eq. (36). Unlike the energy rating model, in Dirnberger et al. model wind speed is not explicitly included and a typical value of 25K for free-standing modules is considered for all PV module types regardless of the module's technology.

$$T_{mod} = T_{amb} + 25K \frac{G_{POA}}{1000W/m^2} \tag{36}$$

4. **PV Module Efficiency at 25 °C**

To calculate the relative efficiency at 25 °C Dirnberger et.al. model proposes a model developed by Heydenreich [138]. PV module efficiency irradiance response has been simplified and described only by three parameters: a, b and c. Parameters a, b, and c can be derived from two independent sources, as explained in [8]: technical datasheets of a PV module, which is normally a certified description of the PV module and its properties and flasher laboratory measurements.

Eq.(37) defines PV module ETA response at different irradiance levels.

$$\eta(G_{POA}, T_{STC}) = aG_{POA} + b\ln(G_{POA} + 1) + c\left(\frac{\ln^2(G_{POA} + e)}{G_{POA} + 1} - 1\right) \tag{37}$$

5. **PV module efficiency and power output**

As a final step, the PV module efficiency at any given temperature and irradiance level is calculated as described by Eq.(38). The efficiency (or power) temperature coefficient (γ) of the PV module can be calculated before as an empirical value derived from long-term monitoring data or it can be derived from technical datasheets.

$$\eta(G_{POA}, T_{mod}) = \eta(G_{POA}, T_{STC})\big(1 + \gamma(T_{mod} - T_{STC})\big) \tag{38}$$

Output Power is calculated with instantaneous relative ETA to the ETA at STC, the Irradiance, and the PV module's nominal power.

4.5.3 Models comparison

This section is divided in two sub-sections. The first sub-section compares step by step the results of IEC energy rating [133, 134, 136, 137] and Dirnberger et.al. [11] model simulations, using the tropical humid climate data set from [134]. The second sub-section presents the results of the two simulation models describing the PV module's behaviour under the other five different locations proposed in the IEC as reference climates [134].

For both sub-sections, a PV module with the following characteristics has been selected:

- Nominal power measured at STC: 259 W
- Area: 1.607 m^2
- Technology: Poly-Si
- Measured efficiency temperature coefficient: -0.42%

For this section, spectral responsivity of the PV module ($S(\lambda)$) is considered as 1 for all the wavelengths and AOI response (a_r) is 0.16. Faiman Method thermal coefficients are the ones determined in [113] for silicon modules. Steps 1 to 4 from the IEC energy rating model were calculated using the pvpltools-python IEC 61853 open-source implementation module, available on github.com [139].

In recent publications [140], Heindenreich model has also been compared with bilinear interpolation model (step 4 from IEC energy rating model). This publication ([140]) offers an alternative model to Heidenreich and bilinear interpolation models, which aims to achieve better results.

A. PV module simulation

Figure 56 shows a comparison of the first step of both models. On the left, a four-day simulation and on the right, a correlation of the results of the first step of both models. As can be seen, there is no considerable difference in the results of the two approaches.

Figure 56: First step simulation results from both models. On the left side, a comparison of a four-day simulation after losses and corrections. On the right side, a correlation between both models first step.

Figure 57 shows the simulation results of the "spectral losses" (second step) from both models. On the left the results of a four-day simulation after losses and corrections. On the right a

correlation of the second step results. Similar to step one difference between the results are not considerable.
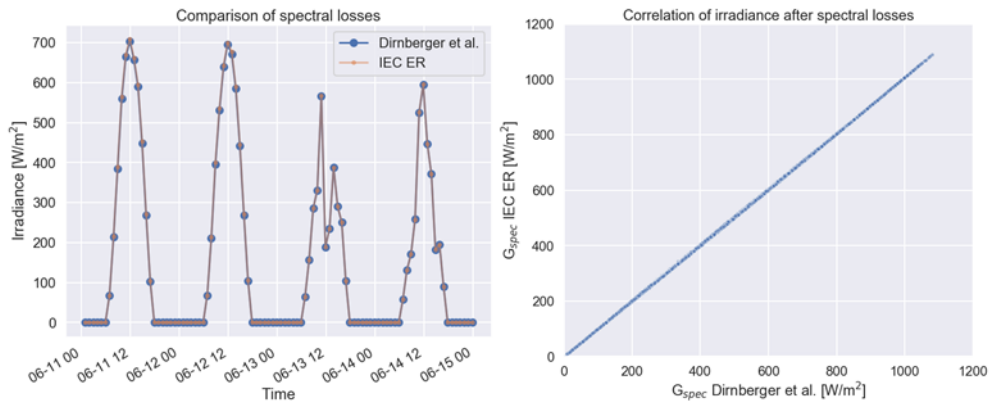
Figure 57: Results of spectral losses simulations from both models. On the left side, the comparison of a four-day simulation after the losses and corrections. On the right side, a correlation between the results of both models at the second step.

The results of the "PV module temperature" (step 3) of both models can be observed in the following figure. In contrast to the two previous steps, in this step the difference between the results of both models is evident. As Figure 58 shows, on the left, higher T_{mod} values are calculated with the IEC energy rating model. Larger differences can be observed in T_{mod} above 25°C on the right of Figure 58.
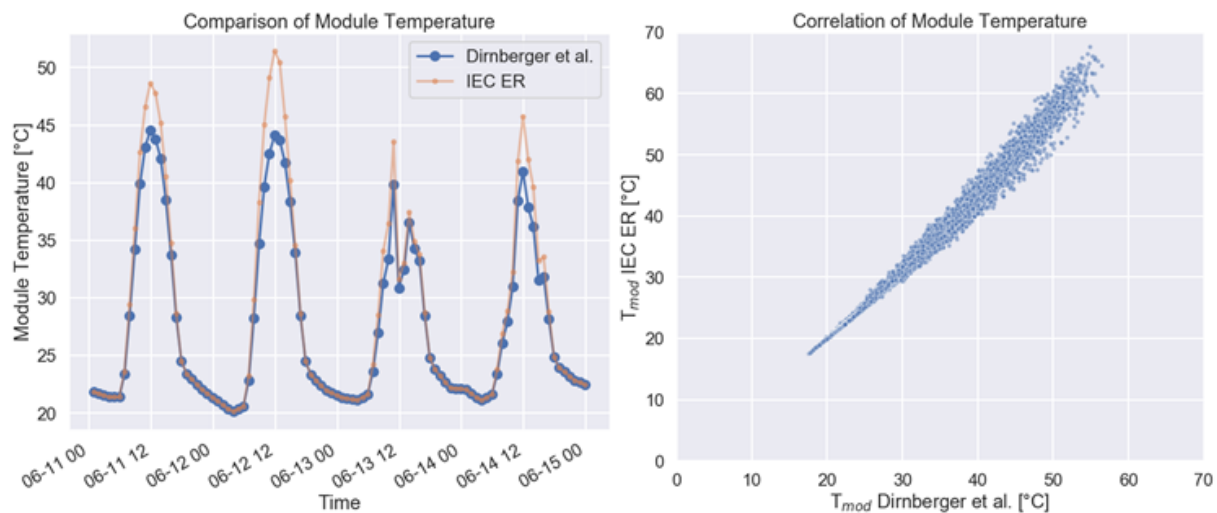
Figure 58: Third step simulation results from both models. On the left side, the comparison of a four-day simulation results after losses and corrections. On the right side, a correlation between both models third step.

In order to calculate the instantaneous power of Dirnberger et al. model, the three coefficients of Heydenreich model have to be calculated. Measurements from CalLab PV Modules – Fraunhofer ISE have been considered for this step. Figure 59 shows a fitted curve based on the Heydenreich model and the measured values with the following coefficients values:

- a = 0. 007268
- b = -12.455229
- c = -187.738543
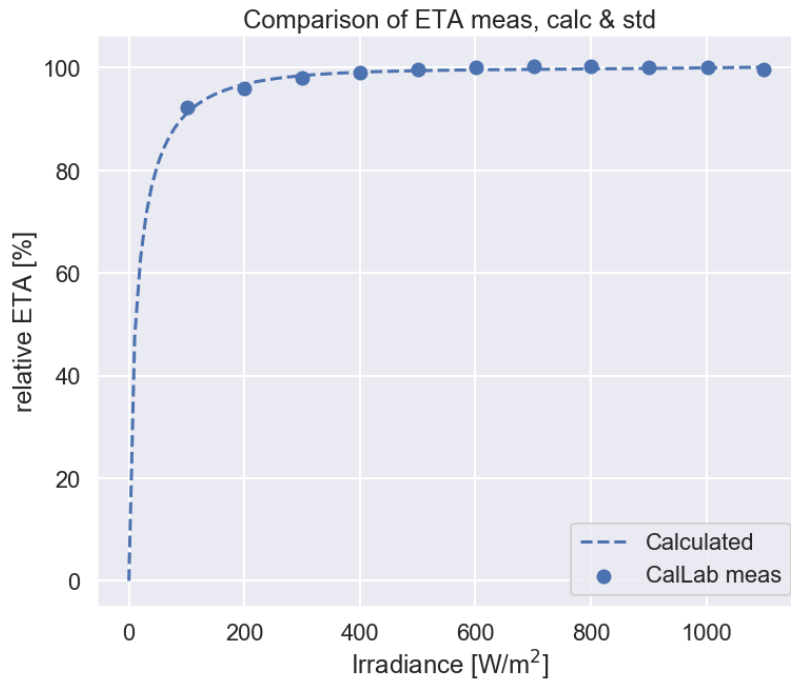
Figure 59: Heydenreich model's parameters fitting curve. Blue points indicate the measurement values and the blue dotted line represents the fitted curve.

The PV module simulated output power can be compared by plotting the results of the last step of each model. Figure 60 shows the difference between the simulated output power of both models. On the right, a difference in the correlation when the output power is higher than 150 W can be seen, which may obey the differences obtained at higher temperatures.
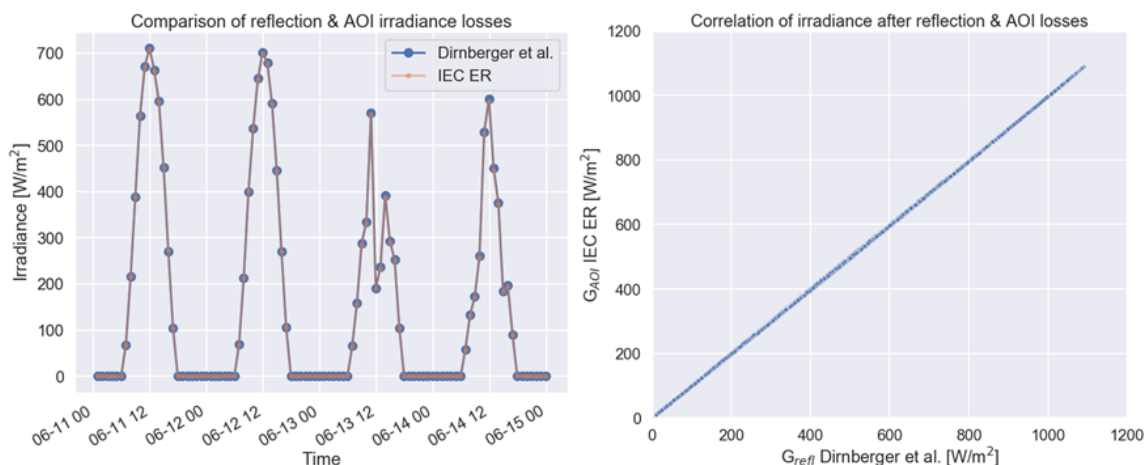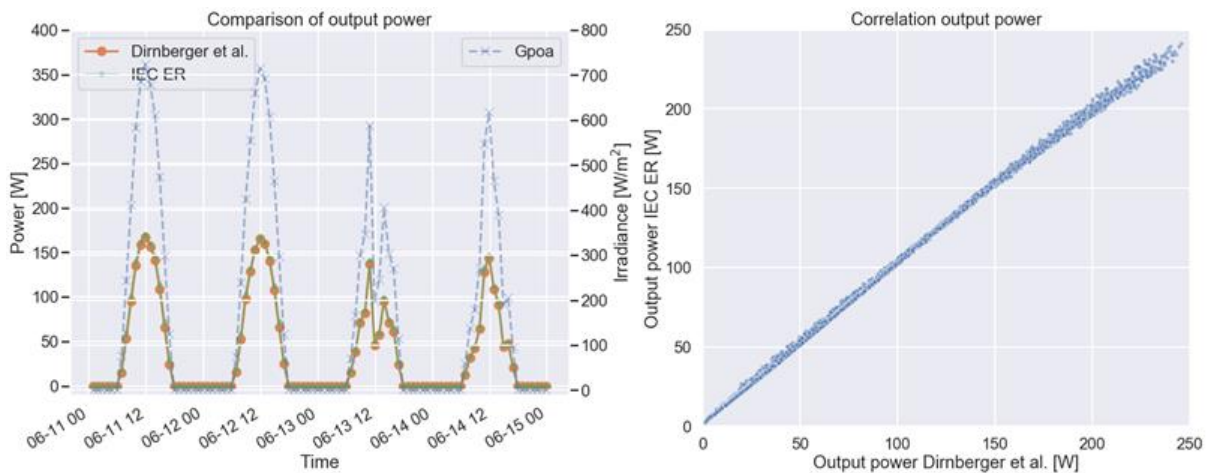

Figure 60: Last step results from both models. On the left side, the comparison of the four-day simulation results after the losses and corrections. On the right side, a correlation between both models last step.

Figure 61 shows an ETA comparison of the results of a four-day simulation from both models. The blue line represents results from Dirnberger et.al. approach. In orange line the results from Energy Rating model are shown. In red dotted line the mean values of ETA measured by CalLab PV Modules – Fraunhofer ISE are represented.
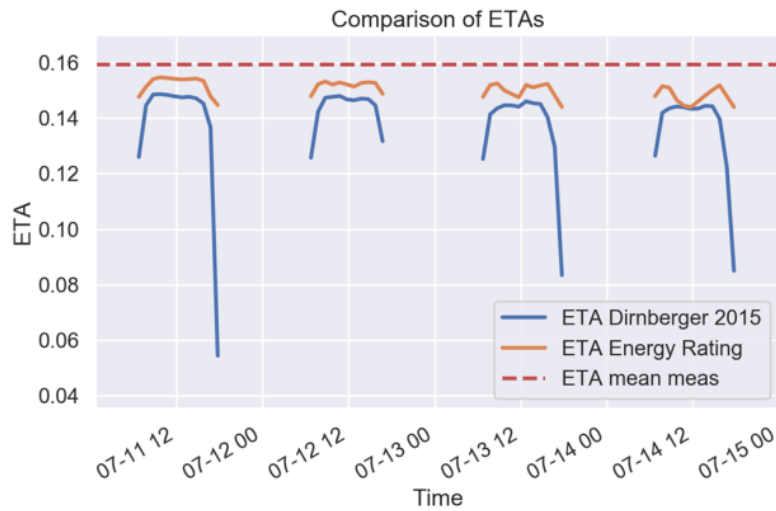
Figure 61: Four-day ETA results from comparison from both models.

To quantify the difference of both models, a relative loss to G_{POA} of each simulation step from both models is calculated. Figure 62 shows the G_{POA} losses and differences on each simulation step within both models.
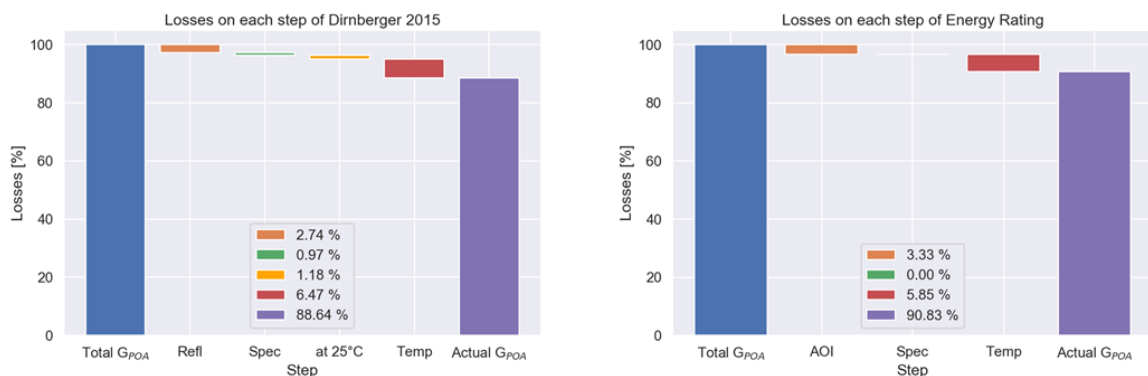
Figure 62: Relative loses to the G_{POA} tropical humid climate. On the left, the losses from Dirnberger 2015 model. On the right side, the losses from Energy Rating model.

B. PV module behaviour under different conditions

Relative losses to G_{POA} at different reference climate profiles. Negative sign means gains. This is shown in the following figures:

- **Subtropical arid (desert)**
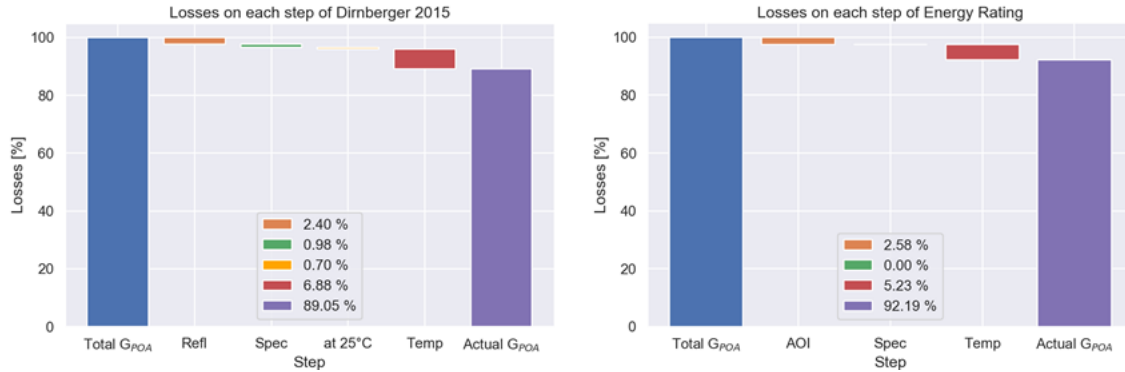
Figure 63: Relative loses to the G$_{POA}$ subtropical arid climate. On the left, the losses from Dirnberger 2015 model. On the right side, the losses from Energy Rating model.

- **Subtropical coastal**
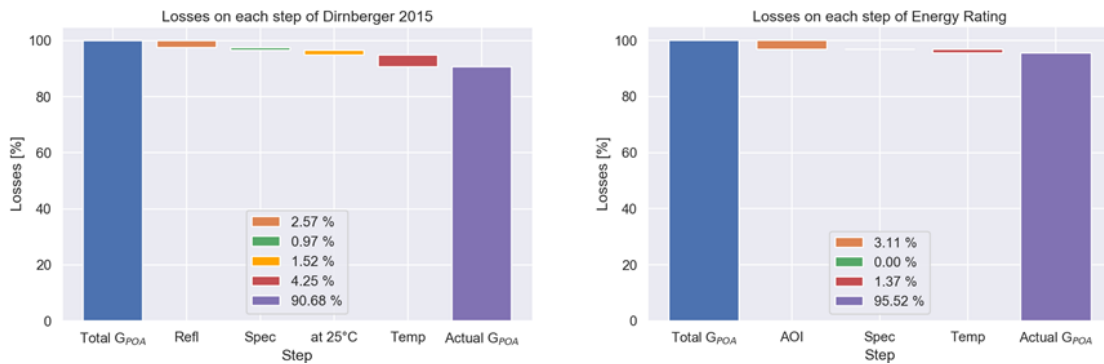
Figure 64: Relative loses to the GPOA subtropical coastal climate. On the left, the losses from Dirnberger 2015 model. On the right side, the losses from Energy Rating model.

- **Temperate coastal**
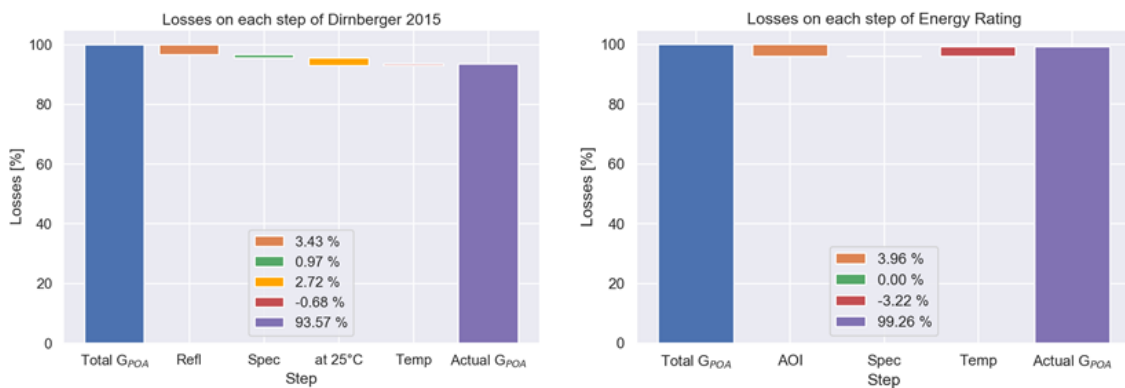
Figure 65: Relative loses to the GPOA temperate coastal climate. On the left, the losses from Dirnberger 2015 model. On the right side, the losses from Energy Rating model.

- **High elevation (above 3 000 m)**
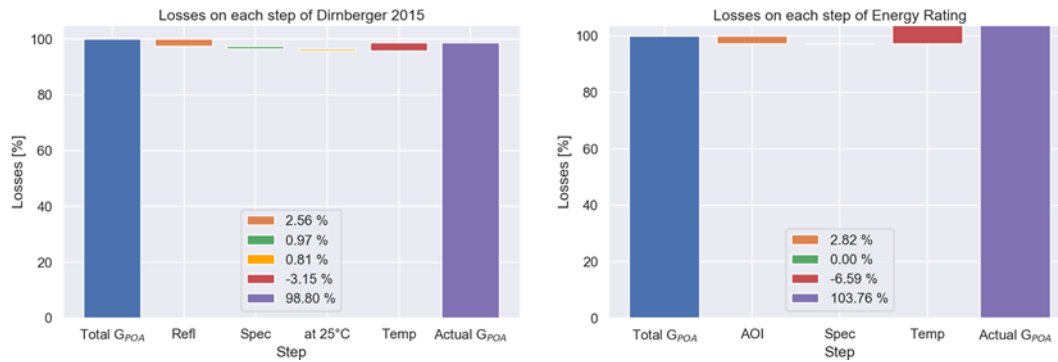
Figure 66: Relative loses to the GPOA high elevation climate. On the left, the losses from Dirnberger 2015 model. On the right side, the losses from Energy Rating model.

- **Temperate continental**
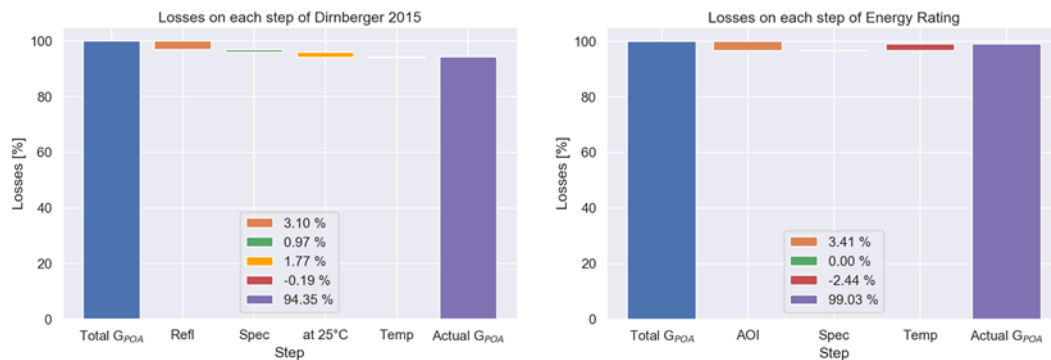
Figure 67: Relative loses to the GPOA temperate continental climate. On the left, the losses from Dirnberger 2015 model. On the right side, the losses from Energy Rating model.

- **Abbreviations**

D_{POA}	Diffuse irradiance in Plane of Array
I_{POA}	Direct irradiance in Plane of Array
a_r	PV Module's AOI response
C_s	Spectral correction factor
$S(\lambda)$	PV Module's spectral responsivity
$u0, u1$	Faiman Model Thermal coefficients
T_{mod}	PV Modules Temperature
a, b, c	Heydenreich model's coefficients

4.6 Linear Performance Loss Analysis - An Alternative Energy Rating Approach

4.6.1 Introduction

The standards IEC 61853 Part 1 and Part 2 are powerful tools to characterize all energetic relevant electrical characteristics of PV modules in a reproducible and comparable way [3, 4]. PV module technologies with good measurement results perform well in most cases for every climate as long as they stay electrically stable. The rating to different climate zones (Part 3 of the standard [5] and also the reference climate data itself (Part 4 [6]) are still in discussion.

The Linear Performance Loss Analysis (LPLA) is an alternative energy rating approach. It follows the PV module measurements defined in Part 1 and Part 2 of the IEC 61853 energy rating standard. Whereas, the G-T-matrix input data needed for the energy rating calculations can be reduced. Furthermore, the weather data sets have a different structure and are short compared to Part 4. The underlying calculations themselves differ clearly from Part 3. The main differences of LPLA to Part 3 are more simple calculations, defined operation states and its suitability for bifacial technologies. The focus of LPLA is more on the PV module performance relative to STC efficiency than on the high-resolution simulation-like calculation of hourly P_{MPP} values as defined in the standard. This opens space for several advantages as described in the following.

The underlying results of this study go back to the "PV-Klima"-project, a national funded research project to investigate various PV module technologies in five climate zones. Out of the indoor and outdoor data gathered an energy rating approach was developed called Linear Performance Loss Analysis (LPLA). The main results regarding the LPLA approach are published in [40] and [9].

4.6.2 Approach

The module performance ratio (MPR) is a well-accepted factor to describe and compare the energy yield performance of PV modules for specific operating conditions. It is independent of the nominal power and the local annual insolation. This makes it possible to compare PV modules` performance with different STC power for locations with different sun hours. Generally, the focus of energy rating approaches is to identify differences that result from the relative climate profile of different locations and not from available sun energy or STC power. This means influences on the yield performance with regards to average device temperatures, percentage of low irradiance operation, impact of spectral shifts and angular effects are of main interest. To which extent the meteorological profile (which has to be given as reference) impacts the energy yield performance of PV modules depends on their electrical characteristics measured in the laboratory.

The Linear Performance Loss Analysis (LPLA) gives a validated approach which considers all relevant influencing factors to calculate the Module Performance Ratio (MPR) of a PV module for defined operating conditions as

$$MPR_{CALC} = 1 + \Delta MPR_{TEMP} + \Delta MPR_{LIRR} + \Delta MPR_{SMM} + \Delta MPR_{AOI} + \Delta MPR_{SOIL} + \Delta MPR_{BIFA} \qquad (39)$$

This allows us to quantify, compare and rate each impact factor individually. The individual loss (and gain) factors express the deviation of outdoor performance to the efficiency at stand-

ard test conditions (for STC the MPR is 100%). The MPR is interpreted as a linear superposition of various meteorological impact factors. Note that the loss terms ΔMPR implies that losses are defined by negative numbers and gains by positive numbers. Although second-order effects are neglected, a difference of less than ±3% between rating result and measurement could be demonstrated for most PV module technologies investigated [9]. While a great portion (typically ±1.5%) of this deviation still can be attributed to uncertainties coming from the measured STC power influencing the measured MPR results.

As input data serves PV module data, determined according to IEC 61853-1 and -2. The following measurements are needed:

a) Preconditioning acc. IEC 61215

b) Spectral response measurement acc. to IEC 61853-2

c) Measurement of incident angle modifier (IAM)

d) Reduced matrix measurements acc. to IEC 61853-1 (G: 100-1100 W/m² at 25°C only)

e) Temperature coefficients acc. to IEC 61215 (at 1000 W/m² only)

f) NMOT acc. IEC 61853-2

A. Temperature losses:

The temperature losses ΔMPR$_{TEMP}$ are calculated out of the temperature coefficient of the nominal power (TC: γ) and the operating temperature of the device for a certain climate. The TC is measured in the laboratory, the operating temperature in the field. The ΔMPRTEMP shall be calculated as

$$\Delta MPR_{TEMP} = \gamma\left(\overline{T_{BoM,G}} - 25°C\right) \tag{40}$$

Whereas,

$$\overline{T_{BoM,G}} = \frac{\int_T T_{BoM} G_{PoA} dt}{\int_T G_{PoA} dt} \tag{41}$$

is the average annual device temperature weighted with irradiance. The magnitude of temperature losses for different climates is illustrated in Figure 68.
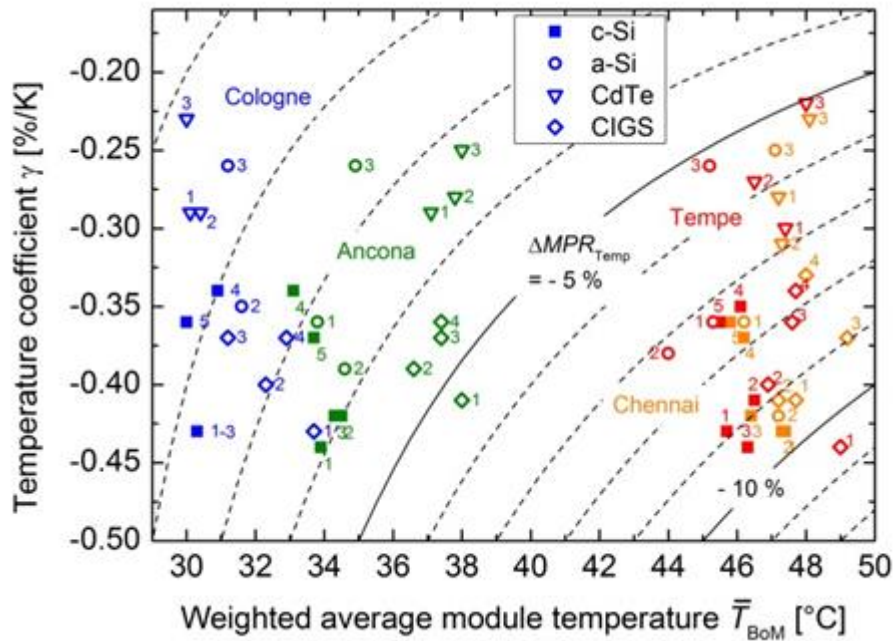
Figure 68: Temperature coefficient γ and irradiance weighted average module temperature for the different PV module technologies at the four locations (colour coded, blue: Cologne, green: Ancona, red: Tempe, orange: Chennai). The temperature-related performance differences ΔMPR_Temp is shown by iso-lines from ΔMPR_Temp =- 1% to - 12% (Source: [40]).

Since is not available for the samples to rate, it must be extrapolated out of the NMOT value. The device temperature can be calculated out of the reference temperatures NMOT$_{REF}$ and T$_{REF}$ given for each reference climate as

$$T_{DUT} = T_{REF} \cdot \frac{NMOT_{DUT}}{NMOT_{REF}}$$ (42)

B. Low irradiance losses:

While the photocurrent is linear to the irradiance, most PV modules show a non-linear dependency of power on irradiance. Thus, it is important to know how much solar energy is insulated at which irradiance. The ΔMPR$_{LIRR}$ shall be calculated as

$$\Delta MPR_{LIRR} = \left(\frac{\int_T p(G_{PoA}) G_{PoA} dt}{\int_T G_{PoA} dt} \right) - 1$$ (43)

Whereas,

$$p(G_{PoA}) = \frac{P_{Max,Meas} G_{STC}}{P_{Max,STC} G_{Meas}}$$ (44)

is the low irradiance behaviour measured in the laboratory for seven irradiances from 100 to 1100 W/m² at 25°C.

C. Spectral losses or gains:

The impact of shifts in the spectral distribution of sunlight are considered by the spectral mismatch factor according to IEC 60904-7 [42] using AM1.5 reference spectral irradiance E_{STC} according to IEC 60904-3 [41] as reference irradiance. The ΔMPR_{SMM} shall be calculated as

$$\Delta MPR_{SMM} = \frac{\int \overline{E_{SUN}(\lambda)} \cdot SR_{DUT}(\lambda) d\lambda}{\int \overline{E_{SUN}(\lambda)} \cdot SR_{REF}(\lambda) d\lambda} \times \frac{\int E_{STC}(\lambda) \cdot SR_{REF}(\lambda) d\lambda}{\int E_{STC}(\lambda) \cdot SR_{DUT}(\lambda) d\lambda} - 1 \tag{45}$$

Further inputs are the average annual spectral irradiance E_{SUN}, the spectral response of the pyranometer SR_{REF} and the spectral response of the device under test SR_{DUT}. Note that daily and seasonal impacts may outrange annual impacts since summer and winter blue and red shifts can compensate each other on an annual basis.

D. Angular losses:

The angular losses are calculated for various angles. Therefore, the energy for various angular bands are calculated out of the sum of the direct component and the diffuse component of sunlight. For the diffuse portion, a linear distribution of the half-space of the sky can be assumed. For the direct portion, the direct irradiance measurements where cosine corrected with the angle of incidence to receive the direct irradiance in plane of array. The angular response of the pyranometer including glass dome is considered to meet ideal cosine behaviour. The ΔMPR_{AOI} shall be calculated as

$$\Delta MPR_{AOI} = \left(\frac{\int_T p(AOI) G_{PoA}(AOI) dt}{\int_T G_{PoA} dt} \right) - 1 \tag{46}$$

Whereas,

$$p(AOI) = \frac{I_{SC,Meas}(AOI)}{I_{SC,STC} \cdot \cos(AOI)} \tag{47}$$

is the angular response of the flat sample with deviation to cosine behaviour due to reflectance measured in the laboratory.

E. Gains due to bifacial operation:

The gains due to bifacial operation are considered by the available energy coming from the rear side and the bifacial coefficient of the device under test. To receive representative rear insulation, albedo values per site specifically for their climate can be given as constants. The ΔMPR_{BIFA} shall be calculated as

$$\Delta MPR_{BIFA} = \varphi_{Pmax} \frac{H_{rear}}{H_{front}} \quad (48)$$

Where φ_{Pmax} is the bifacial coefficient according to IEC TS 60904-1-2 [55] calculated as

$$\varphi_{Pmax} = \frac{P_{max,rear}}{P_{max,front}} \quad (49)$$

No bifacial gain can be considered for monofacial PV samples ($\Delta MPR_{BIFA}=0$).

F.   Impact of soiling:

The annual losses due to soiling depend strongly on seasonal events as rain or sandstorms as well on the cleaning procedure. Thus, for the annual losses due to soiling a constant must be considered for each climate. Note different soiling factors can be necessary for PV modules with anti-soiling coating or deeply structured front glass.

G.   Further aspects:

The rated operational efficiency η_{OP} can be calculated out of the measured efficiency at STC and the rated MPR_{DUT} as

$$\eta_{OP} = MPR_{DUT} \times \eta_{STC,Lab} \quad (50)$$

The LPLA approach rates the samples based on their performance in the field relative to their performance at STC. To prevent a good energy rating for samples with lower power than stated on the datasheet, the STC power must be controlled separately. In general, the stated STC power should reflect the average in the production line. If this is not the case a power correction factor can be applied to the rating results if needed.

Another practical application of LPLA can be the short term analysis of outdoor performance. In Figure 69 the measured fluctuations in monthly PV performance is illustrated. Applying the LPLA method for temperature and spectral effects reveal reasons for seasonal MPR changes.
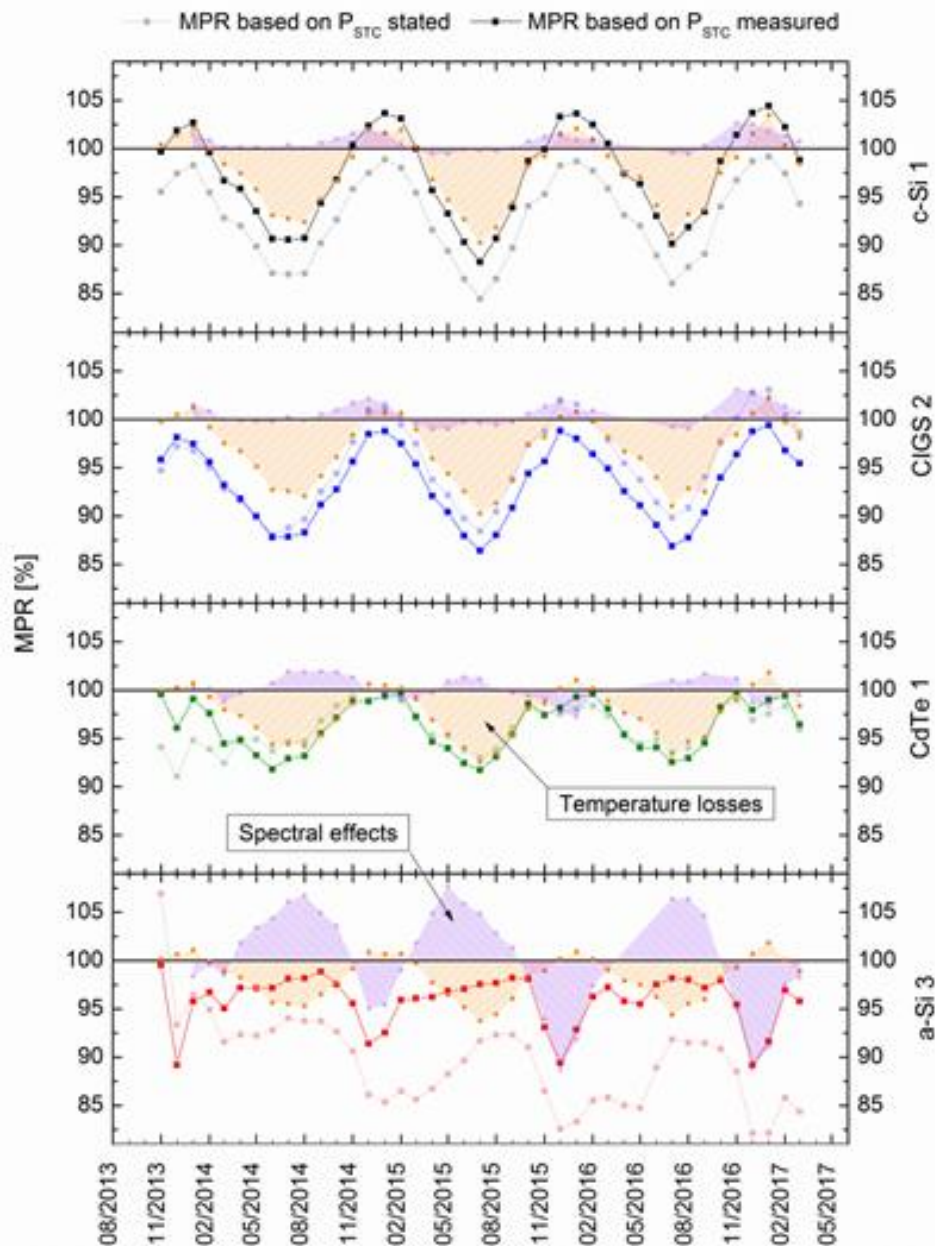
Figure 69: Monthly module performance ratio of four PV module types based on stated PSTC in comparison with MPR based on monthly measured PSTC, deviation to 100% means yield losses or gains, the shares of temperature (orange) and spectral effects (purple) are visualized, test site Ancona, Italy [Source: [14]).

4.6.3 Simplified use case

In this chapter, LPLA is demonstrated in the simplest form, on only one page, for a standard polycrystalline PV module operating under optimal conditions in Ancona, Italy (13°N/80°E, 35 m above sea level). Optimal mounting conditions mean optimal tilt angle facing south, no shading, and low device temperatures due to detached mounting. The individual ΔMPR loss factors are calculated one after another and summarized (see example of report in Figure 70).

Loss factor	ΔMPR_{TEMP}	$+\Delta MPR_{LIRR}$	$+\Delta MPR_{MMF}$	$+\Delta MPR_{AOI}$	$+\Delta MPR_{SOIL}$	$+\Delta MPR_{BIFA}$	$= MPR_{CALC}$
Result	-3.83%	-0.82%	0.56%	-2.43%	-0.50%	0.00%	**92.98%**

ΔMPR_{TEMP}:

γ_{DUT} (%/K)	$\overline{T_{REF}}$ (°C)	ΔMPR_{TEMP}
-0.43	33.9	**-3.83%**

ΔMPR_{LIRR}:

Irradiance range (W/m²)	H(G) Italy (08.01.2014 – 07.01.2015)	PV module $p(G_{PoA})$	$p(G_{PoA})$ x H(G) Italy
15 - 150	5.95%	0.947	0.056
150 - 250	6.38%	0.970	0.062
250 - 350	6.62%	0.985	0.065
350 - 450	6.61%	0.999	0.066
450 - 550	7.00%	1.000	0.070
550 - 650	8.04%	1.000	0.080
650 - 750	9.64%	1.000	0.096
750 - 850	11.78%	1.000	0.118
850 - 950	12.68%	1.000	0.127
950 - 1050	16.37%	1.000	0.164
1050 - 1400	8.73%	0.996	0.087
Σ	100 % (= 1291 kWh/m²)	ΔMPR_{LIRR}	**-0.82%**

ΔMPR_{MMF}:

	ΔMPR_{MMF}	**+0.56%**

ΔMPR_{AoI}:

Angular range (°)	H(AOI) Italy (08.01.2014 – 07.01.2015)	PV module $p(AOI)$	REF $p(AOI)$ x H(AOI) Italy
90	0.00%	0.00	0.00%
85	0.56%	0.14	0.08%
80	1.19%	0.65	0.78%
75	1.92%	0.79	1.52%
70	2.79%	0.87	2.44%
65	3.64%	0.92	3.36%
60	4.63%	0.96	4.44%
55	5.63%	0.97	5.48%
50	6.56%	0.99	6.48%
45	7.31%	0.99	7.26%
40	8.12%	1.00	8.10%
35	8.99%	1.00	8.98%
30	10.45%	1.00	10.46%
25	8.74%	1.00	8.75%
20	8.53%	1.00	8.53%
15	8.70%	1.00	8.70%
10	7.48%	1.00	7.47%
5	3.62%	1.00	3.62%
0	1.14%	1.00	1.14%
Σ	100 % (= 1249 kWh/m²)	ΔMPR_{AOI}	**-2.43%**

Figure 70: Example of repot results for energy yield calculation based on the LPLA Method for a standard c-Si sample operating in Italy.

4.6.4 Conclusions

With LPLA an alternative energy rating method was presented. The approach is optimized for practical application and suitable for all non-concentrating PV module technologies including bifacial. The advantages of this method are simplified energy rating calculations and easy to compile weather data sets which are short and robust to missing data. It still follows the PV module characterization part 1 and 2 of the IEC standard whereas the matrix can be reduced. The independent analysis of all impact factors enables a classification of PV modules performance. A future PV module energy rating classification based on this method could look similar to the classification of solar simulators according to IEC 60904-9 [39]. For example, a PV module with a classification of CBABBC would describe a PV module with unsatisfactory temperature behaviour (C), average low irradiance performance (B), superior spectral gains (A), average angular and soiling losses (B,B), and no bifacial operation (C). However, the operating temperature (NMOT) as well as the electrical stability of electrical parameters still must be tested in the field. The validation of this method by other institutes is pending and reference data sets have to be established and internationally agreed.

4.7 Energy Rating of Bifacial PV Modules

4.7.1 What is new with bifacial modules

As explained in Chapter 4.1, the climate specific energy rating (CSER) defined in the IEC 61853-3 of monofacial PV modules normalizes the annual DC yield of a single PV module $E_{MOD,YEAR}$ to its maximum output power at STC (P_{STC}) and the annual in-plane irradiation H_{POA} (see Eq. (15) in Section 4.1.4).

This is – beside the differences in variable names – quite similar to the definition of the Performance Ratio (PR) in IEC 61724-1 [141], which deals with monitoring of complete PV systems:

$$PR = \left({E_{out}}/{P_0} \right) / \left({H_i}/{G_{i,ref}} \right) \qquad (51)$$

If all components besides the module would be excluded from a PR evaluation, this formula is identical to the CSER definition. Therefore, the CSER value is sometimes also denoted as DC-PR or Module PR (MPR).

Generally seen, the MPR depends on the environmental conditions G_{POA}, T_{AMB}, V_{WIND}, and a specific set of PV module properties:

$$MPR = f (G_{POA}, T_{AMB}, V_{WIND}, \text{module properties}) \qquad (52)$$

Module properties are (typically) determined in the laboratory and are specific to one single module type. The calculation procedure in IEC 61853-3 then connects these properties to defined meteorological conditions.

Any influence of other system components (as seen in real life) is excluded. This is obvious for inverters and cabling, but excludes as well any influence from the mounting geometry. There is no row-to-row shading, instead, PV modules are assumed to be exposed to perfectly homogeneous illumination. Also, there is no influence of the number of modules mounted above each other on module temperature. As only exception, ground albedo is considered intrinsically, as the typical transposition models from G_{HOR} to G_{POA} account for a fraction of reflected irradiance on a tilted plane of array. Here, most probably a default value of 20% was used for all calculations behind the standard data sets.

Up to now, the Energy Rating procedures defined in IEC 61853 are valid for monofacial (standard) PV modules only. The procedures enable comparison and an assessment of expected DC yield for a given PV module operated in one of the six climatic regions. As seen above, there are several simplifications in the energy rating process for monofacial PV modules already. Even more simplifications are necessary with bifacial PV modules – this will be explained in the remainder of this introduction.

At a first glance, the changes to the MPR definition – when moving to bifacial modules – look simple, thus MPR = f (G_{FRONT}, **G_{REAR},** T_{AMB}, V_{WIND}, **more** module properties).

The rear side irradiance G_{REAR} and a number of properties specific to bifacial PV modules are added to the previous formula.

The determination of additional module properties appears rather straight forward. Several measurements need to be repeated for the rear side of the module. Some values are then to be calculated from measurements, e.g. the bifaciality factor φ. For more details, see also the discussion of bifacial module characterization in Chapter 2.5.

The challenges appear with the proper determination of G_{REAR}. With monofacial PV modules, an estimation of the total irradiance received by the module plane (G_{POA}) is easy. Transposition procedures to calculate irradiance levels received on tilted planes were developed, validated and agreed on decades ago. They include irradiance contributions from the sun, the sky and from ground reflection. The choice of a specific model or procedure makes a difference, but a small difference in the range of 1% to 2% in annual irradiation only.

With bifacial PV modules, rear side irradiance G_{REAR} and its homogeneity depends on

- Albedo (reflectivity) of the ground
- Height of PV modules above ground
- Tilt angle of PV modules
- Row-to-row distance of PV modules (and/or size of PV generator)
- Structural elements of the mounting system

Therefore, even identical PV modules at the same site can perform quite differently, depending on system design factors. A bifacial PV module's yield no longer depends on module properties only, but on system properties as well.

Table 16 gives examples for the variability of bifacial gain – the ratio of rear side contribution to front side yield – for a number of realized bifacial PV systems. Differences in bifacial gain up to a factor of two may easily be reached for identical bifacial PV modules in similar mounting modes. This is much bigger than the variability in well-known transposition models for G_{POA}, so, small modelling uncertainties are negligible compared to actual impacts from system layout.

Table 16: Bifacial gain values for several realized PV systems featuring quite similar bifacial modules. BG$_{MOD}$ denotes the additional DC yield related to the front side yield.

Type	Height	Tilt	Albedo	GCR	BG$_{MOD}$	Remark
	m	°				
ground mounted	0.7	30	0.20	0.43	5%	(1)
ground mounted	1.0	30	0.20	0.40	8%	(2)
ground mounted	0.5	30	0.20	0.40	9%	(3)
ground mounted (agro PV)	4.0	5	0.20	0.66	13%	(2)
ground mounted (vertical)	0.0	90	0.20	n/a	80%	(4)
roof top	0.1	20	0.40	0.40	6%	(5)
roof top	0.3	20	0.40	0.40	11%	(5)
roof top	0.5	20	0.40	0.40	14%	(5)
roof top	0.3	20	0.20	0.40	6%	(5)
roof top	0.3	20	0.40	0.40	11%	(5)
roof top	0.3	20	0.60	0.40	16%	(5)
pole mounted	5.0	60	0.20	n/a	24%	(6)

Remarks: Height means the distance of lower module edge to ground; GCR means ground cover ratio, the ratio of module area to ground area; (1) 3 modules in landscape mode; (2) 1 module in landscape mode, mounting structure not considered; (3) 2 modules in portrait mode; (4) single row, BG$_{MOD}$ is 9% only when compared to 30° south and monofacial; (5) mounting structure not considered; (6) used e.g. in small off-grid applications.

The mounting conditions also influence the homogeneity of rear side irradiance – in two different ways. At first, the homogeneity of rear side irradiance levels per PV cell depends on the mounting geometry. Typically, higher irradiance levels are observed at the module (or module table) edges, lower levels at the centre of PV modules or tables. The edges typically have a greater view angle towards bright sections of the ground or towards the diffuse sky light, therefore, they see more light than the inner parts of a module or module table.

Secondly, homogeneity depends on the design of the mounting structures. Structural elements like beams or rails close to the rear surface of a module cause a kind of local shading of diffuse rear side irradiance, which adds to the cell performance mismatch caused be the geometrical inhomogeneity.

Figure 71 gives an example of both types of inhomogeneity. Rear side irradiance decreases from both edges towards the centre of the module table, while a few PV cells in the centre see an (uncommon) increase of irradiance. With this specific design of a one axis tracker, direct sunlight is reflected from the central torque tube and increases rear side irradiance in this region.
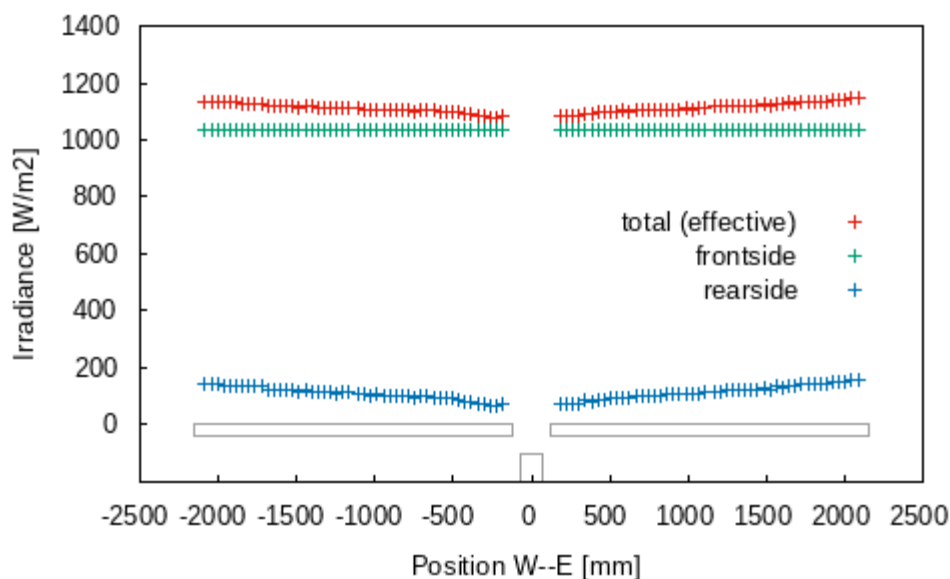
Figure 71: Irradiance levels across two modules mounted in portrait mode on a horizontal single-axis tracker for one exemplary time step (noon on June 21st). Rear-side irradiance shows a mostly linear decrease from the edge towards the centre of the tracker table. With this special design, reflections on the centre tube lead to an increase of irradiance levels close to the inner edge of the modules.

As a summary, the single new quantity G_{REAR} makes a big change to the prediction or assessment of module performance. It is not a purely meteorological quantity but depends on system properties on several scales. Ground cover ratio and height above ground have a more general influence on rear side irradiance levels, while the structural design even affects rear side irradiance on cell level. A clear distinction between module properties and environmental conditions is not possible anymore. As any Energy Rating procedure should be a rather simple procedure, a number of simplifications or even restrictions need to be introduced. These simplifications and restrictions will be discussed in detail in Section 4.7.4 on IEC 61853-4.

4.7.2 Necessary changes to the four parts of IEC 61853

Despite the challenges discussed in the introduction above, an extension of IEC 61853 towards bifacial PV modules is currently under discussion. A good fraction of this effort has been and is still covered by the EU EMPIR project "PV-Enerate: Advanced PV Energy Rating" (see https://www.pv-enerate.ptb.de). The working groups involved in this project aim to provide input to the IEC technical committee 82 "Solar photovoltaic energy systems" to support the update of the standard. The extensions discussed in PV-Enerate are presented in the following.

IEC 61853-1 Irradiance and temperature performance measurements and power rating

The PV-Enerate specialists propose bifacial PV module power measurements according to the G_E-Method as defined in IEC TS 60904-1-2 [55]. This method utilizes the concept of equivalent irradiance levels (G_E) on the front side only, leading to the same I_{SC} as a given combination of front side and rear side irradiance levels, as explained in Chapter 2.5. Using this cost-saving approach, a matrix of measurements of module power as a function of (G_E; T_{MOD}) can be measured similar to the procedure for monofacial modules.

However, the range of measurements needs to be extended to higher irradiance levels, as G_E may exceed 1100 W/m² easily when calculating total irradiance on bifacial modules with several of the reference data sets.

IEC 61853-2 Spectral responsivity, incidence angle and module operating temperature measurements

Both the spectral response measurements and the AOI dependency measurements may be performed independently on both module sides (with the other side being covered or facing towards a dark laboratory environment). The determination of the thermal parameters u0 and u1 remains as defined in IEC 61853-2, using the outdoor method.

IEC 61853-3 Energy rating of PV modules

The correction for the angle of incidence (AOI) may be performed independently for both module sides. A problem is the proper definition of the AOI for the rear side irradiance, as it cannot be related to the solar position. Ideally, a generalized AOI could be defined on the basis of an averaged and/or weighted AOI of all contributions of reflected irradiance. This concept is sometimes used for the diffuse fraction of front side irradiance on PV modules, but not yet agreed on for the bifacial case.

The spectral correction may be performed independently for both sides as well. Part 4 of the standard is then assumed to provide spectrally resolved irradiance data for both sides of the module.

After these corrections, the effective total irradiance on both module sides may be calculated as $G_{EFF} = G_{FRONT} + G_{REAR}$. Please note that a similar approach known from bifacial yield estimations, using $G_{EFF} = G_{FRONT} + \varphi\, G_{REAR}$, would not be adequate here. The bifacialty factor φ must have a direct influence on MPR or CSER, this influence would be cancelled out if φ would be included in the irradiation resource already.

Module operating temperature T_{MOD} may be calculated from total irradiance G_{EFF} as with the existing procedure, and also module power P_{MOD} may then be derived from the matrix of measurements (G_{EFF}; T_{MOD}) in the defined way for each time step. This finally leads to the annual DC yield $E_{MOD,YEAR}$ of a bifacial PV module.

Another decision is pending concerning the calculation of the resulting CSER value. For monofacial PV modules, the module DC yield is referred to in-plane (= front side) irradiation E_{POA}. If E_{POA} (= E_{FRONT}) would be the reference for bifacial PV modules too, then CSER values greater than one would be expected. To keep CSER values smaller than one and comparable to those of monofacial modules, the annual DC yield would need to be referred to the effective total irradiance H_{EFF}. It is a question of philosophy whether CSER values above one may represent an extended yield from a PV module of the same physical size or whether efficiency values (comparing output to input) should stay below one at any time.

IEC 61853-4 Standard reference climatic profiles

For both monofacial and bifacial PV modules, irradiance in plane of array (G_{POA}) is determined by PV module mounting conditions. For the monofacial case, IEC 61853-3 defines a single standard mounting condition for all six climatic regions under consideration, literally "... facing the equator with an inclination angle of 20 degrees." [5] Accordingly, IEC 61853-4 provides time series of G_{POA} (and other quantities) for this single condition and each of the six regions [6].

As explained in the previous sections, the total annual irradiation received by bifacial PV modules depends on more parameters than tilt angle only. How to deal with this large number of influences? As energy rating shall assess module properties only, any influence from any possible system design must be excluded. The only way to achieve this is to standardize the system design, i.e. to restrict possible application cases to a very small number of different layouts.

Such exemplary mounting conditions may be defined as "Standard Mounting Conditions (SMC) for bifacial PV modules". Then, G_{FRONT} and G_{REAR} may be provided for these conditions similarly to G_{POA} in the existing version of IEC 61853-4. This approach is detailed in the following sections.

4.7.3 "Standard Mounting Conditions" and simplifications

Several mounting options/cases were discussed as candidates for Standard Mounting Conditions (SMC). The most prominent options were:

- Fixed tilt ground-mounted (typical albedo 20%) (quite close to the existing definition for monofacial modules)
- Fixed tilt mounted on a flat roof featuring a bright roofing membrane (typical albedo 60%)
- Horizontal single-axis tracked (typical albedo 30%) (currently a big share of the market for bifacial PV modules)
- East-west facing vertical mounted (typical albedo 20%) (e.g. noise barriers, agricultural PV)

Every single option requires a new meteorological data set of remarkable size, so the number of options was finally reduced to two mounting strategies: the fixed-tilt option on flat roofs and the vertical east-west option. Figure 72 presents examples of bifacial PV systems of such kind.

Figure 72: Examples for the two standard mounting conditions selected for bifacial PV module energy rating. Left: fixed installation on a flat roof, tilt angle = 20°, albedo = 60%. Right: vertical east-west facing installation on agricultural ground, albedo = 20%. *Photos: Christian Reise, Next2Sun.*

Of course, there is a mutual influence between the PV modules in a large PV generator. For monofacial PV systems, this influence typically is limited to mutual shading between several rows of modules. The existing standard for monofacial modules excludes shading by definition. A single unshaded PV module is assumed, this would be true as well for a module in the first row of a large PV generator.

With bifacial PV systems, also shading or non-shading of the surrounding ground area is relevant. A single PV module mounted at fixed-tilt will receive more rear side irradiance than a module in the middle of a row of modules. However, the module-in-a-row scenario is far more relevant for real-life operation than a single module. So, a central module in a single long row of modules is proposed as a reference case.

For each of the two SMC, one albedo value, one height above ground, and one setting for any other parameter are defined. All kinds of variations (leading to a large variability of bifacial performance, see the introduction to this chapter) are left to system specific yield estimations outside the scope of IEC 61853.

4.7.4 Preparation of additional reference data sets

To avoid most of the modelling effort and the related ambiguities when using the IEC 61853 series of standards, a time series with hourly values of G_{POA} and other input quantities is delivered as part 4 of the standard. In total, each of the six existing data sets comprises 44 columns already:

- Timestamp
- Ambient temperature
- Wind speed at module height
- Sun elevation & incidence angle
- Global horizontal irradiance
- Direct horizontal irradiance
- Global in-plane irradiance @ 20°
- Direct in-plane irradiance @ 20°
- Spectrally resolved global in-plane irradiance in 32 spectral bands

The extended data sets for use with bifacial PV modules might provide 78 or even 142 additional columns:

- Wind speed at rooftop height
- Sun incidence angle for three new surface orientations
- Global east vertical irradiance
- Direct east vertical irradiance
- Global west vertical irradiance
- Direct west vertical irradiance
- Global rear side irradiance @ 20°
- Direct rear side irradiance @ 20°
- Spectrally resolved global irradiance in 32 spectral bands for one or three new surface orientations

One major task was to provide irradiance values for the new module orientations – vertical east and west and rear side of a 20° tilted module. Global and direct components of horizontal irradiance are provided with the existing data sets, but standard transposition models (Perez, Klucher, or others) do not work perfectly for vertical planes. For the rear surface of a tilted module, these models do not work at all.

Therefore, for the yield prediction of bifacial PV systems, either view factor methods or ray tracing methods are in use. As the latter is typically more accurate (for the sake of computing time), a ray tracing approach was selected to create the first test data sets for an extension of IEC 61853-4.

Ray tracing calculations were carried out for the six one-year time series (one per climatic region) and for many sensor points, representing each cell of a PV module in the centre of a single row of modules. No mounting structures were considered in this step to keep the general validity of the data sets. The final values of G_{FRONT} and G_{REAR} were then determined by simple spatial averaging. Using an electrical model of the PV cells, the string topology, and the bypass diodes would have led to more realistic results, but would limit the procedure to one specific module design. Different modules might deal differently with shading and inhomogeneity in irradiance, so plain averaging is a clear, but necessary simplification.

At the writing of this report, test data sets were under preparation. Typical annual sums of several irradiance values are given in Table 17 and Table 18.

How (and even whether) to supply spectrally resolved data, especially for the rear side of a tilted module, is still under discussion. There are publications on the spectral composition of reflected sunlight [142–144], but it seems to be difficult to derive a generalized procedure from existing information.

For a test phase, the existing spectrally resolved data will be used for the other surface orientations as well.

The preparation of wind speed data for the roof-top scenario also is still under discussion. Either additional hourly values or a correction factor or formula to the existing values might be provided.

Table 17: Annual values of front and rear side irradiance for the fixed-tilt case. BG$_{OPT}$ denotes the additional irradiance received on the rear module surface, the optical bifacial gain, as a fraction of front side irradiance.

#	Latitude	Region	G_{HOR} kWh/m²	G_{FRONT} kWh/m²	G_{REAR} kWh/m²	BG_{OPT}
1	01°00' S	Tropical humid	1716	1669	448	0.27
2	33°30' N	Subtropical arid	2051	2311	497	0.21
3	33°22' N	Subtropical coastal	1352	1476	344	0.23
4	56°00' N	Temperate coastal	876	994	236	0.24
5	34°00' N	High elevation	1897	2157	473	0.22
6	57°00' N	Temperate continental	1074	1287	282	0.22

Table 18: Annual values of front and rear side irradiance for the vertical east-west case. BG$_{OPT}$ denotes the additional irradiance received on the rear module surface, the optical bifacial gain, as a fraction of front side irradiance.

#	Latitude	Region	G$_{HOR}$ kWh/m²	G$_{FRONT}$ kWh/m²	G$_{REAR}$ kWh/m²	BG$_{OPT}$
1	01°00' S	Tropical humid	1716	875	816	0.93
2	33°30' N	Subtropical arid	2051	1203	1066	0.89
3	33°22' N	Subtropical coastal	1352	701	710	1.01
4	56°00' N	Temperate coastal	876	552	548	0.99
5	34°00' N	High elevation	1897	1046	1057	1.01
6	57°00' N	Temperate continental	1074	687	659	0.96

4.7.5 Conclusions

The additional yield of bifacial PV modules depends on several PV system properties – other than with monofacial modules, where module orientation is the only prominent system specification. While Energy Rating for monofacial modules is restricted to one single module orientation (20° tilt and facing towards the equator), it is proposed to restrict Energy Rating for bifacial modules to two single system layouts named Standard Mounting Conditions (SMC). These SMC comprise a fixed system tilted at 20° on a high albedo ground and a vertical east-west facing system on natural albedo.

The overall approach (module characterization plus simple calculus using a time series of G$_{POA}$ readily provided with the standard) may be kept in place with bifacial Energy Rating, as long as specific time series of front and rear side irradiances are provided. Some parts of the standard need to be amended or extended accordingly.

Of course, the restriction to two SMCs implies severe simplifications, any dependency of bifacial gains on albedo, height, or tilt angle cannot be considered. Also, inhomogeneity of rear side irradiance is not considered at all, despite its dependency on mounting geometry and racking structures.

According to this approach, an extension of the existing standard series IEC 61853 is under discussion in IEC TC 82. A number of open issues still need to be solved, among them the rear side AOI definition and some assumptions on the spectral distribution of rear side irradiance.

The differences in the yield of real bifacial PV systems may vary by more than 10% for identical PV modules, just depending on rather simple environmental and design parameters like albedo, mounting height, and ground cover ratio. These variations are much bigger than most of the expected performance (or CSER) differences of different module brands and types. Therefore, the value of bifacial PV module Energy Rating – when compared to individual yield predictions – might be less pronounced than with monofacial PV modules.

5 ARISING FIELDS OF RESEARCH

5.1 Special Operating Conditions of BIPV Modules

Building-integrated Photovoltaic (BIPV) devices have to fulfil specifications both, from the building and the electrical sector as they act as construction material and as electricity-producing devices. Besides those fundamental requirements, the aesthetical appearance of a BIPV-module in the façade of a building or the roof-shape of a town is of high importance [145]. Within IEA PVPS Task 15 "Enabling Framework for the Acceleration of BIPV", a joint action (a special type of round robin test) was initiated to compare the performance of identical glass-glass BIPV elements at outdoor tests facilities in different climates [51] , nine participating institutions from seven countries in Europe and Asia agreed on such a joint round robin action. Identical glass/glass BIPV elements with crystalline Si-cells were produced by ertex solartechnik GmbH, pre-characterized in the certified test laboratory of the AIT – Austrian Institute of Technology GmbH and shipped to the nine selected outdoor test sites. A monitoring procedure was developed and harmonized with all participants [51]. The constructive requirements for the test stands were based on the façade setup of the reference building (ventilated curtain wall, cold façade) and were taken into account by all participating institutions. The outdoor monitoring of the round robin action started in November 2017 was finished end 2019. Identical module-design combined with an accorded monitoring method and constructive boundaries allowed for the analysis of the influence of geographical and climatic conditions on the performance of the BIPV elements. The calculated performance ratios were related to the pre- and post-installation measurement results in a reference lab under standard test conditions STC (AM1.5, 1000 W/m², 25°C) [52]

First, the monitoring data were merged, processed and filtered for further analysis. MATLAB® was used as a software tool, aiding to build up a database of the acquired measurement data. Analysis of the available measured data has been performed) [52] in terms of

1) distribution (frequency) of the module temperatures and the in-plane irradiation at the outdoor test locations (see Figure 73)
2) time-series of mean daily performance ratio coefficients (PR) of all monitored days
3) median and quartiles in box plots of all daily PR per test module
4) comparison of ambient and module temperatures
5) yield matrix plots (see Figure 74) showing the relative yield of the investigated modules over module temperature and irradiance
6) time series of monthly yield at the test sites

The daily PR coefficients were calculated as the ratio of the specific yield in kWh/kW (with the rated power in kW at STC) in relation to the specific insolation reference yield in kWh/m²/1 kW/m² (using the STC irradiance of 1 kW/m² as the reference). If a temperature correction is applied on the daily PR values, the specific yield values were corrected using module temperature values and the relative modules power temperature coefficient of -0.37%/°C.
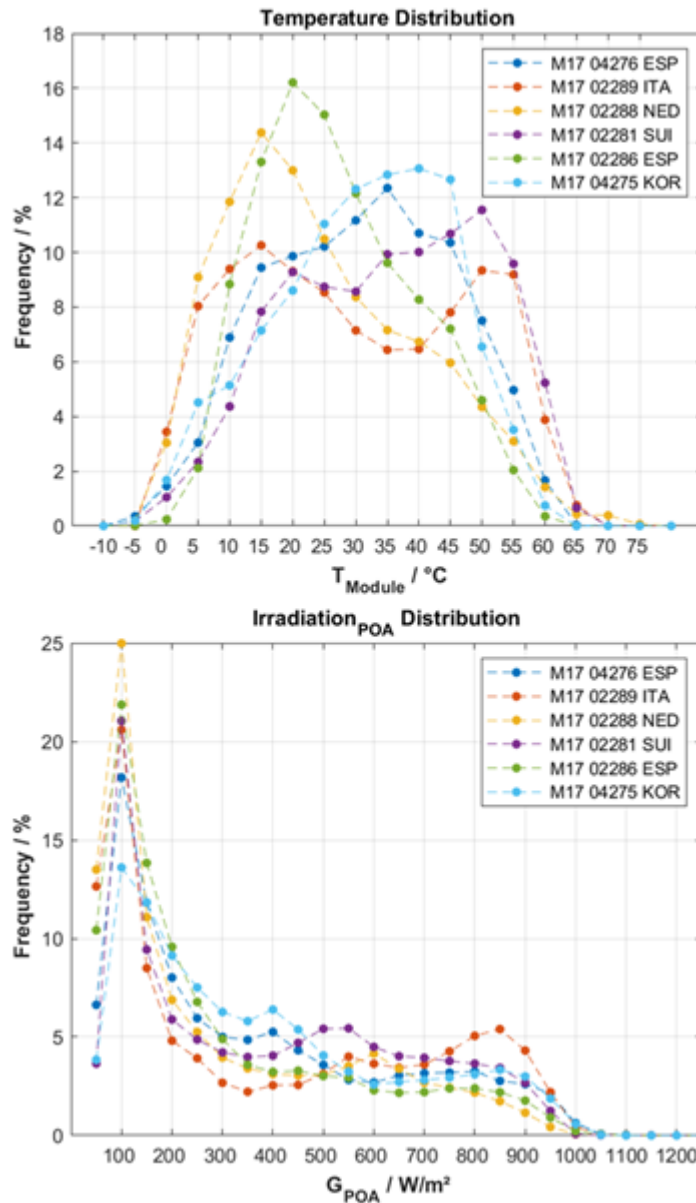
Figure 73: Distribution of the module temperature (top) and the in-plane irradiation (bottom) in 50 W/m² bins starting with the bin around 50 W/m² measured at the outdoor test locations.

Temperature is, besides irradiance, one of the most important factors in terms of module performance. In Figure 74, the measured distributions in module temperature (T_M) and in-plane of array irradiance (G_{POA}) measurements are compared for the different locations.
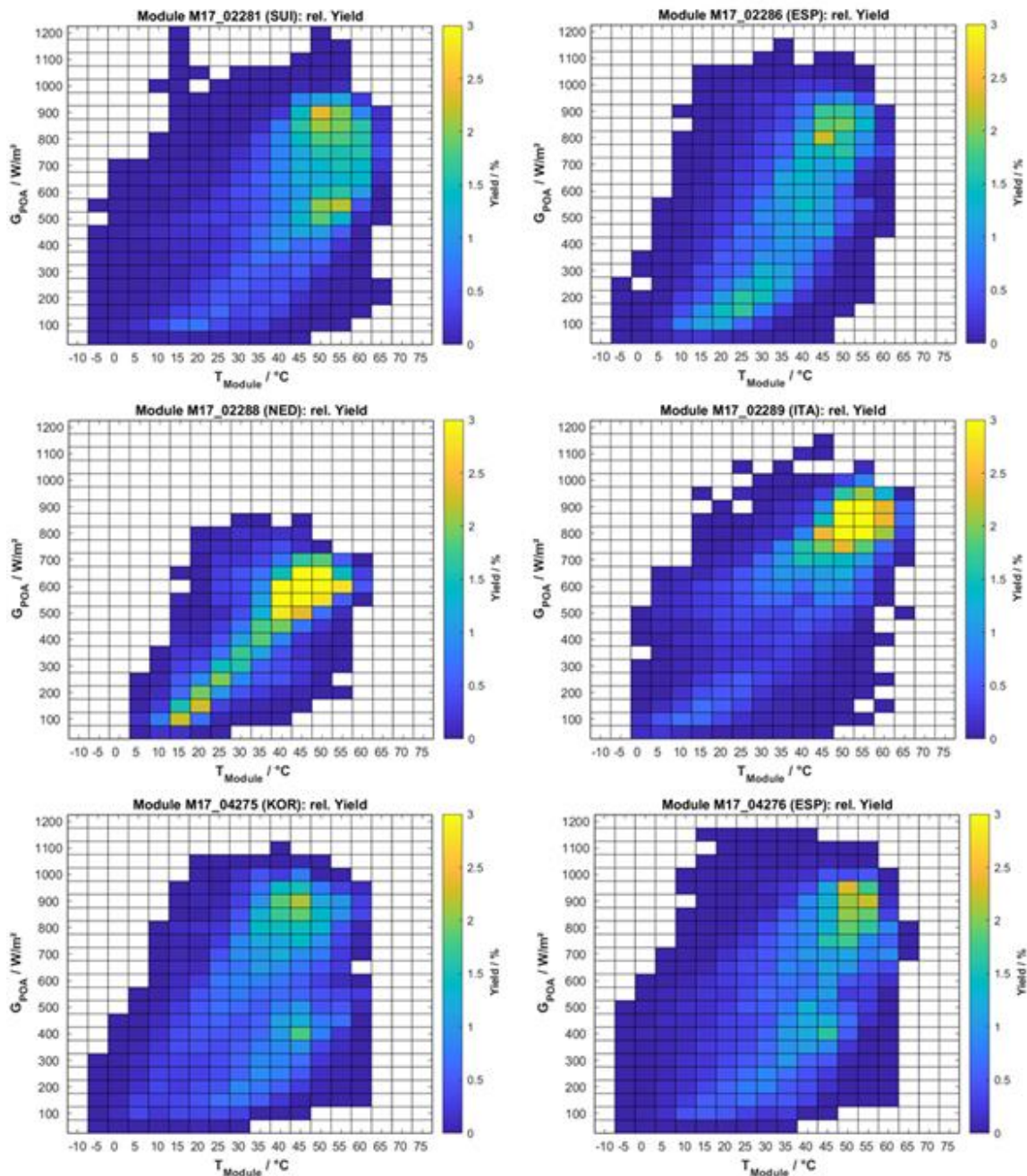
Figure 74: The relative yield of the investigated modules is plotted over the module temperature and the irradiance in 5°C/50 W/m² bins (Source: [52]).

Figure 74 plots the relative yield of the investigated modules is over the module temperature and the irradiance. The colour of every bin represents the relative yield, calculated as yield within one bin divided by the total yield. The sum of all bins represents 100% of the total yield over 12 months. From these matrix-plots, information about the climate as well as the operating conditions of the module can be derived. Of course these matrices are also dependent on the availability of measurement data. It can be observed that five of the six panels have a peak in relative yield at an irradiance of 800 to 950 W/m², while the module temperature is in a range

of 45 to 55 °C. The vertical tilt and south-orientation of the tested modules lead to high irradiation in plane of array from October to March, whereas the irradiation during summer is significantly lower. Therefore, some the modules located in sunny southern regions show a second peak of relative yield at an irradiance of 400 to 600 W/m² and roughly at the same temperature level as the first peak. This leads to the conclusion, that the first peak at around 900 W/m² occurs during the cold part of the year, whereas the other peak is connected to summertime. The manifestation of the two peaks is dependent on the climate in the respective region. Sunny winter months result in a strongly pronounced upper peak, whereas cloudy conditions in winter stress the peak in summer. Module M17_02288_NED does not show a second peak (although the data availability was high for the whole period of the round robin). This is due to the fact, that the test site in the Netherlands is the most northerly located module in this study. In the Netherlands there is 'Temperate Coastal' climate (Cfb) where cold winters are lacking in general. Last winter (in the measurement period of this paper) was even warmer than normal [52].

In a next step, a climate independent Key Performance Indicator (KPI) for BIPV-modules was defined [146]. As this is also the aim of the IEC 61853 standard, an approach that is based on the P_{mpp}-matrix (as a function of G_{POA} and T_{mod}) originating from IEC 61853 was used. As described in [50], for detailed research on BIPV-module performance, a couple of extensions to this P_{mpp}-matrix can be very valuable. This approach was applied for the analysis of the monitoring data of the BIPV test-modules of the Task 15 round robin action. Best practices were adopted to get the most out of the dataset of the Task 15 round robin consisting of more than one-year outdoor monitoring data for seven test sites with a time resolution of at least 5 minutes for each site (and even higher for some sites). This was the first time an IEC 61853 G-T power matrix was performed on BIPV-modules from the same series (identically constructed) distributed and monitored with an accorded methodology over sites all over the world. Moreover, as these modules have been analysed indoors extensively (IV, EL, etc.) in the same laboratory before sending the BIPV-modules to the various test sites and after the end of the outdoor testing, any possible change in the status of the module, like e.g. degradation, pollution, light soaking, etc. could be identified [146].

5.2 Performance of Coloured PV Modules

An increasing number of coloured modules are reaching the market promising added value due to better aesthetics. An overview of the state of the art of coloured BIPV modules and products is given in the technical report prepared within IEA PVPS Task 15 [147]. The report gives also inside into the different colouring techniques, the theoretical background and experimental results. Figure 75 shows some typical examples of coloured modules.

Figure 75: Selection of picture details of coloured PV modules from different manufacturers and R&D projects (top: Smart-Flex [148] , PV Construct [149], bottom: Sunage [150], Hochschule Luzern [151].

Colouring of modules can be achieved through many different techniques (e.g. special anti-reflective coatings, coloured PV layers, encapsulants or backsheets, spectrally selective glass coatings or foils, digital or screen glass prints, glass sandblasting, mineral coatings or email on glass). All techniques lead to a change in spectral response, which leads to a decrease in short circuit current and consequently in STC power. The colour-induced performance loss is significantly changing with customization of the product (layer position, colour/s, uniformity, transparency and opacity). Literature states efficiency losses ranging from 5-50% [152–155]. However, when talking about energy rating it has to be considered that also other module parameters can be influenced by the aesthetical changes. Other parameters typically affected are the operating temperature, measured by the NMOT test, and the angle of incidence response. The temperature coefficient is given by the cell material properties and is therefore not affected by the colour. The main challenge of the developers of coloured modules stays in balancing the aesthetic requirements with the efficiency and energy output of the PV modules and in predicting/modelling the energy yield of coloured PV modules.

To better understand the performance under real operating conditions, coloured modules have to be monitored together with reference modules with an identical bill of materials (BOM) and module architecture but without colour treatment. A study done by SUPSI PVLab et al. [156] presented the first results of a one year measurement campaign on seven different coloured module prototypes. Figure 76 shows a picture of the outdoor test facility installed at SUPSI in Lugano (CH). The colours of the tested modules ranged from red/terracotta to white/grey modules including plain colour and multi-colour devices. The level of cell camouflage (visibility of cells) varied significantly within the modules. A bifacial module and a module with deep structured glass were included as well.

Figure 76: Picture of an outdoor test stand with coloured modules together with some reference modules (Source:[156]). Modules form the left top to the right: textile modules (bifacial), Swiss cantonal flags, deep structured façade module, terracotta module with reference, white module with reference and light grey module with reference.

The energy production of each coloured module is compared to the yield of a specific non-coloured/transparent reference module. For the textile style module, the cantonal flags and the deep structured façade module no original reference module with the same BOM was available and a commercial reference module with the same cell technology was used instead. The textile style bifacial module was compared to a monofacial module with the same cell technology (HJT) and with similar front side cell efficiency. To take into account the fact that the commercial reference modules have a different number of cells in series the direct kWh intercomparison has to be made by normalizing the measured kWh value to the active module area (cells in series*cell area).

Figure 77 shows the results of the 1-year kWh intercomparison (1) for the area-specific yield [kWh/m²] shown here as bars with the original colour of the modules, and (2) for the STC power specific yield [kWh/W] obtained by normalizing the energy to the indoor measured STC power and represented in the figure as orange bars.
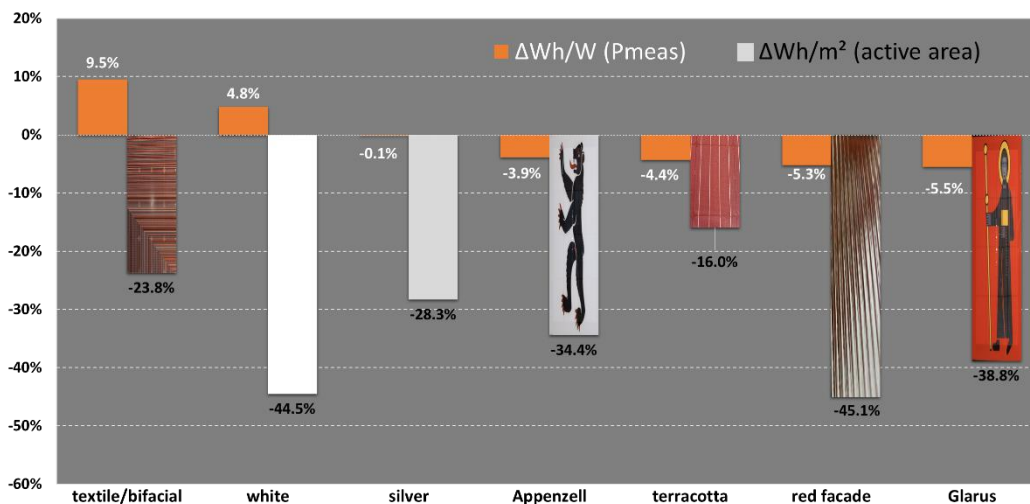

Figure 77: Annual kWh intercomparison between coloured and transparent reference modules normalized to the module active area [kWh/m²] (orange bars) and to the measured STC power [kWh/W$_p$] (bars in original module colour).

Depending on the technology (type and uniformity of colour/s and level of cell camouflage) the coloured modules produce 16-45% less energy in kWh/m² with respect to the reference modules. The difference is the sum of losses or gains which can be estimated from energy rating measurements done in the laboratory under controlled test conditions. All modules have been therefore characterised previously to be installed on the outdoor test facility, starting from the most important tests, the STC power measurement, and the spectral response.

The measurements in the laboratory demonstrated that the reduction of the STC power of the coloured modules is directly related to the change in spectral response and the respective short circuit current loss, obtained by integration of the SR curves of the coloured and its reference module. The effect of the colour on the spectral response is shown in Figure 78a. The losses in short circuit current (I_{sc}) measured at STC are the highest for the modules (1) in which the cells are completely hidden behind the coating and (2) which reflect the highest fraction of light. This is the case for the white module and the terracotta module with deep structured glass (see Figure 76). The smallest difference in performance compared to the reference is observed in the terracotta module, where the coating is so thin that the cells are still visible at a glance. The measured I_{sc} losses explain most of the observed kWh/m² losses depicted in Figure 77, but not all.

The impact of secondary colour induced effects is getting visible in Figure 77 when normalising the produced kWh to the measured STC power. The kWh/W_p difference with respect to the reference module ranges now from a gain of 9.5% to a loss of 5.5%. Secondary effects like the operating module temperature, response to daily and seasonal spectral variations and angular response or irradiance gains due to the use of bifacial cells are determining these numbers, stressing the need for a full characterization of coloured modules according to IEC 61853 Part 1 and Part 2.

The example of the textile module (9.5% kWh/W_p gain compared to the reference module), shows how the use of bifacial cells can be the solution to partially compensate for the efficiency loss due to the front colour printing. The backside of the module is fully transparent leading to a bifaciality factor >1. Precise quantification of the bifacial gains versus colour-induced losses is here not possible due to the non-availability of reference modules with the same BOM.

In the case of the white module (4.8% kWh/W_p gain compared to the reference module), the partial compensation of the STC efficiency loss is attributed to the spectral selective foil, which has the advantage to reflect and diffuse the visible spectrum, while the infrared part is transmitted and converted into electricity. Despite the large loss in I_{sc}, the foil leads on one side to a lower operating temperature of up to 10°C (see Figure 78b), and on the other side to a lower spectral mismatch over the day. The same effect can be seen, although to a minor extent, in the light grey module.

The other modules show a negative effect of the colouring on the kWh/W_p performance of -3.9% to -5.5%, due to thermal and spectral losses. The red façade module reaches the highest cell temperatures due to the very thick glass structure.
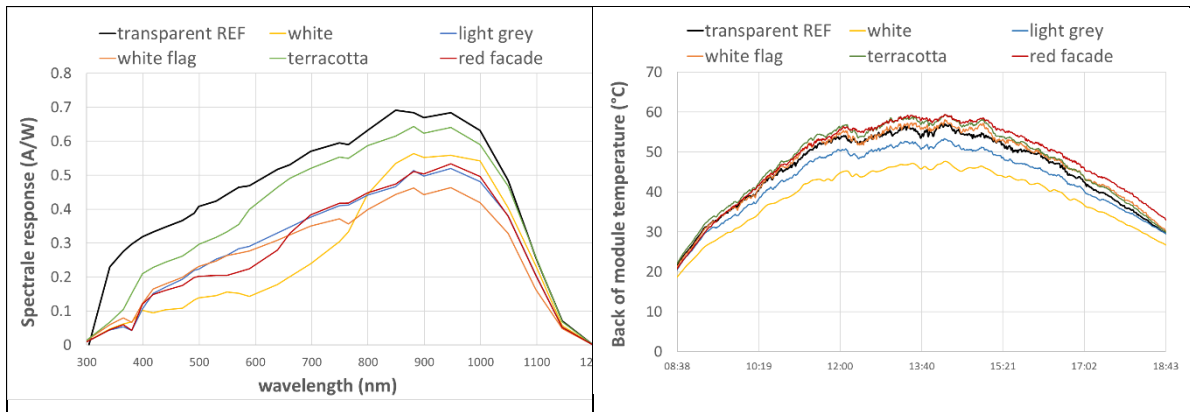
Figure 78: a) Visualisation of spectral response curves of all coloured modules against one of the reference modules. b) Back of module temperature of coloured mono-facial modules for one day in August against one reference module.

In multi-colour modules, a further difference in performance is expected due to the contribution of possible mismatching effects from the designed patterns. But measurements of test modules showed that despite the completely different patterns and colours (two modules from the same manufacturer representing Swiss cantonal flags), a relative difference in the performance of just 5% was found. Careful planning of the artistic design was found to be the key point to minimize the mismatch losses of the modules.

5.3 Uncertainty of Energy Rating

Considering the energy rating methodology described in IEC 61853-3 [5], the retrieved Climate Specific Energy Rating (*CSER*) parameter, like any estimated value has an associated uncertainty derived from both the possible errors (systematic and random) in the determination of the input data used and from the applied calculation models themselves.

Part 1 [3] and 2 [4] of the IEC 61853 standard define the procedures to obtain the input data required by the models described in Part 3 [5], and represent various characteristics of the PV device, such as the temperature and irradiance behaviour or the spectral response. As stated in the first two documents, for every performance test a report has to be prepared including among other details "*a statement of the estimated uncertainty of the calibration and test result (where relevant)*". Similarly, in part 3, a report with the resulting energy ratings shall be prepared. This should include, among other information, "*a statement of the estimated uncertainty of the energy rating results*".

Regarding the input data required for the estimation of the *CSER*, one of the main factors contributing to the differences in the performance between devices is the irradiance dependency which is modelled based on the power matrix measurements [11, 13, 107]. Therefore, it is of high importance to limit the uncertainty of these measurements, which are obtained following the conditions defined in a series of normative references listed in Part 1. Each measurement is subjected to uncertainty, which depends on the applied levels of irradiance and temperature, measuring set-up, procedure, etc. Laboratories performing these kind of power measurements have declared uncertainties for each of those measurements [107, 157], which depending on the specific setup may be correlated to a greater or lesser extent. For example, any error in the calibration of the reference cell for the irradiance level determination will be present in all measurements.

Besides the performance matrix, another important source of uncertainty in the energy rating analysis comes from the measurements required to calculate the two coefficients, (u_0 and u_1)

used to estimate the temperature of the PV module and simulate the thermal performance as a function of the received irradiance, ambient temperature and wind speed [107]. The experimental set-up to define these parameters, described in part 2, is difficult to implement with the subsequent possible measuring errors. At present, the IEC Technical Committee 82 is working on the first amendment to part 2 of the IEC 61853 standard, which may include changes in the determination of both thermal parameters.

Another input data required for the estimation of the *CSER* is the a_r parameter used for the irradiance correction due to the angle of incidence effects. This empirical coefficient is calculated from measurements of the short circuit current of the PV device when illuminated using different incidence angles between the light source and the normal to the module's surface. These measurements, especially those at high incidence angles are subjected to errors from the measurement set-up and the intrinsic PV device response derived from its configuration (anti-reflective coating, structured glass or standard glass). The measurement uncertainty is significant for incidence angles above 50º. The variability in the measurements at 70º and 80º for various silicon-based modules could be 1.5% and 2.4% respectively, as stated by [118]. Moreover, part 2 of the standard, where the a_r setup determination is described, does not specifically indicate the fitting procedure to apply to the experimental data in order to calculate the value of a_r, which results in different a_r values depending on the procedure used.

The spectral correction applied in the IEC 61853-3 methodology uses spectral response values, which should be obtained following the procedure described in IEC 60904-8 [112] and so are also subjected to uncertainty. For example, the set-up applied in [13], has an uncertainty for the raw spectral response measurements of 3.38%. However, this contributes to an uncertainty of 0.124% in the spectral mismatch factor estimation. In addition to this, the fact that the spectrally resolved irradiance data provided in the climatic reference datasets (IEC 61853-4 [6]) is integrated into bands of different width, requires an additional step in the estimation of the spectral correction coefficient. The spectral response value for each of these 29 bands has to be calculated and part 3 does not clearly describe how to estimate these discrete values from the spectral response data measured at small wavelength steps according to [112] on the PV device under test.

The input data used in the IEC 61853-3 methodology regarding solar radiation data and the climatological variables of ambient temperature and wind speed provided in part 4 are fixed reference datasets and therefore are not considered to contribute to uncertainty. The accuracy of the solar resource data and climatological variables are more important for an accurate estimation of the expected energy yield than for an energy rating analysis where the accuracy of the data regarding the PV device is more important. As a result, the accuracy of the energy rating calculation is limited by the uncertainty in the PV module measurements since the methodology and the climatic datasets are predefined and standardized [13].

How the uncertainty in the various input data is transmitted throughout the different steps of the energy rating methodology into the final *CSER* value is not defined nor quantified in the IEC 61853 standard series.

Various studies have quantified the impact of the input data uncertainties on the estimated energy rating, for example [11, 13, 157]. Sources of uncertainty in the power matrix measurement are described [157] and analysed [11, 157], but the energy rating estimation method differs from the one defined in IEC 61853-3. Authors highlight the importance of the STC power value as it is often not a constant value, but it may depend on light and temperature exposure [118]. Uncertainty of STC power may vary between 1.1% and 2% depending on the technology, which for the authors is the most important contributor to the uncertainty in the final energy rating estimation. The estimated uncertainty in the performance estimation ranges from 1.8%

to 3%, including the STC power estimation [11]. Measurement uncertainties often depend on the target conditions of the measurements, which are commonly optimized for STC. As a result, the measurements of the other points of the power matrix of IEC 61853-1, will present higher uncertainty values, as reflected in [107, 118, 157]. Declared uncertainties in the power matrix data ranging from 1.3 to 3.5% result in uncertainties in the final energy rating value of 1.32 to 4.5% depending on the level of correlation assumed between the various power measurements, ranging from fully independent to the worst-case scenario where measurements are considered fully correlated [157]. A complete uncertainty analysis of both the input data and the power output estimation is presented in [107] following the IEC 61853-3 methodology for the energy rating estimation. The final average uncertainty estimated for the *CSER* parameter is 1.9% which is related to an estimated uncertainty of 2.2% in the yearly energy output and 1.9% in the STC power. Authors conclude that the most important sources of error are the irradiance measurement in the power matrix and the determination of the two thermal parameters, u_0 and u_1.

In addition to the uncertainty in the input data, the models integrated in the IEC 61853-3 methodology may not be accurate, to the same extent, for all PV technologies and devices due to their intrinsic characteristics. For example, the model applied for the angle of incidence analysis uses a mathematical expression to adjust the short circuit current measurements to the various incidence angles applied that may not be accurate enough to fit the data at high incidence angles and may behave differently for different devices. The model may not represent to the same extent the behaviour of devices with different optical characteristics using anti-reflecting coatings, structured or standard glass. The effect of different surfaces on the performance of the devices is quantified, following a different model to the one defined in part 3 in [14]. Besides, the assumption of an isotropic distribution of the diffuse irradiance is a simplification of the real solar resource available.

Similarly, the model used to estimate the operating temperature of the PV module may not be able to reflect the thermal behaviour of different encapsulations or module configurations, linked to the module heat capacitance, thermal transients, temperature gradient across the module or the radiative heat transfer that occur on the device.

To estimate the power output, it is necessary to apply interpolation and extrapolation on the measurements of the power matrix defined in part 1. However, as stated in [157], the uncertainty of the interpolated values could be smaller than the uncertainty of the measured points, as long as these are not correlated. Part 3 contains a series of equations describing how to apply the bilinear interpolation and extrapolation. Nevertheless, they are not described in enough detail for all possible situations (defined by the available in-plane irradiance and the module operating temperature) which may lead to different implementations.

In addition to this lack of clarity under certain circumstances, mainly characterized by low irradiance conditions, the bilinear interpolation and extrapolation used in the energy rating standard may lead to deviations from the real behaviour of technologies with significant non-linearities. This may be disadvantageous or beneficial in the power output estimation under certain circumstances, especially under low irradiance levels which are abundant in some of the reference climates. However, deviations at low irradiance levels can be considered not too relevant from the energy production point of view over the complete year analysed in the energy rating standard. Besides, considering nonlinear models at low irradiance levels provided very similar results to linear ones, so the additional complexity may not be required [104].

Various interpolation methods were analysed in [107], where the one used at the IEC 61853 shows one of the lowest bias. Besides, authors concluded that the error and bias derived from the interpolation methodology applied is much lower than the uncertainty introduced by the

input data used throughout the complete energy rating estimation. The higher impact being from the thermal parameters and the irradiance measurements during the power matrix measurement. In this description of uncertainties, we are always considering expanded two sigma values.

5.4 Representative Metadata Analysis of PV Systems

In the early days of photovoltaic deployment, PV systems were installed under optimum conditions for cost reasons: facing South (at the Northern hemisphere) or North (at the Southern hemisphere) at a tilt angle somewhat lower than the location's latitude [158, 159]. In this way, the maximum annual specific yield in kWh per kW$_p$ installed could be achieved. Earlier work of Task 13 members has been focused on the analysis of annual specific yield in various countries (EU, USA, Australia), and it has been reported that annual specific yield is higher for countries with higher irradiance, while the annual system performance ratio is negatively correlated with ambient temperature [160]. Visualization of an updated data set of some 20,000 systems in Netherlands, Germany, Belgium, France, and Italy, based on web-scraping internet sources showed a larger annual specific yield with decreasing latitude [161]. Similar findings have been reported for France [162] and Belgium [163]. These studies usually show average or median values for annual specific yield, sometimes geographically resolved [161], while some attempt to fit a function on the observed distribution of values [162, 163]. Notwithstanding these results, it is unknown how representative the actual systems are for the installed PV based in a country or region: a data-set may contain only roof-mounted systems, or field-based systems, or a mix of these.

With the large decrease in PV system cost, it can be expected that PV systems would be economically attractive at locations with non-optimum azimuth and tilt. While variations indeed are observed in field-based systems [164] especially for residential systems azimuth and tilt variations are inherent to the specific building on which the systems are installed. However, in such urban environments, shading effects of various roof elements and neighbouring buildings will lower performance ratio and annual specific yield. A recent study comparing yield between urban and rural environments in the Netherlands shows that performance ratio, thus accounting for non-optimum azimuth and tilt, indeed is lower in an urban setting [165].

Rather than finding annual yield data, it is suggested to obtain PV system meta-data (tilt and azimuth of modules, installed capacity), and to use representative distributions of that, regionally resolved, to calculate the specific annual yield distributions based on annually varying weather information (irradiance, ambient temperature) [166]. In a concerted effort to collect and process as many performance data as well as metadata (tilt, azimuth, installed capacity and specific annual yield) as possible, Killinger et al. [167] have collected metadata from nearly 3 million PV systems located in Europe, USA, Japan and Australia, representing a total capacity of 59 GWp (14.8% of 2018 installed capacity worldwide [167, 168]. These data have been clustered by two classes of system size (<25 kWp, and >25 kWp), and on a country level. Each metadata parameter in a cluster was approximated by a distribution function. A specific distribution function was found based on the best fit of a selection of 13 functions, such as Weibull [169].

Results show commonalities across all clusters, see Table 19 and Figure 79, for systems with capacity smaller than 25 kWp, thus mostly residential systems). Mean tilt values were reported in a range between 16.1 degrees (Australia) and 35.6 degrees (Belgium), average specific annual yield values occur between 786 kWh/kWp (Denmark) and 1426 kWh/kWp (USA South). The region with smallest median capacity was the UK (2.94 kWp) and the largest was Germany (8.96 kWp). Almost all countries had a mean azimuth angle facing the equator.

Figure 79 shows all metadata collected and fitted with distributions functions that best fitted the data. Data on systems larger than 25 kWp show similar distributions, while average tilt values are larger compared to systems smaller than 25 kWp, and specific yields larger, which evidences that larger installations allow for optimum conditions [167, 168].

Table 19: Mean or median value extracted from the entire data set for several countries for each of the metadata parameters (adapted from Source [168]).

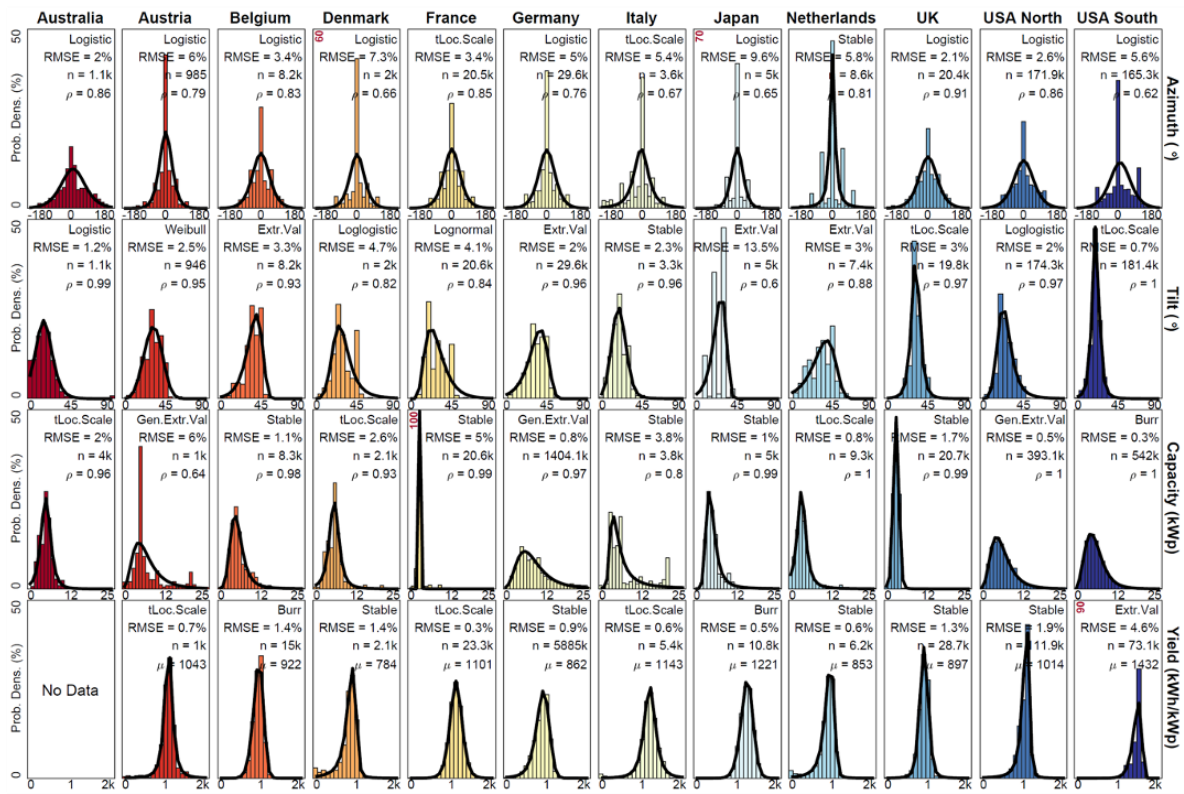| Country	Azimuth (degrees) (mean)	Tilt (degrees) (mean)	Capacity (kWp) (median)	Specific yield (kWh/kWp) (mean)
Australia	8.58	16.1	5.00	-
Austria	-0.34	31.1	5.15	1040
Belgium	-1.69	35.6	5.20	922
Denmark	0.48	30.0	6.00	786
France	-0.28	28.7	2.96	1101
Italy	-15.9	19.8	5.88	1142
Japan	-1.20	23.8	4.92	1222
Netherlands	0.77	32.5	3.30	855
UK	-1.07	31.8	2.94	897
USA North	0.42	25.2	5.81	1005
USA South	9.33	19.9	5.26	1426

Figure 79: Histograms of real data (bar) with approximated probability distributions (line) for the different clusters (columns) and parameters (rows), where capacity is the installed capacity and yield is the specific annual yield. All systems reported here have a capacity smaller than 25 kW$_p$. Within each of the axes is reported the name of the best fitting distribution type, the root mean squared error (RMSE) between the scatter of real data in the histogram against the fitted probability density distribution, the number of data points considered for that cluster (n), and the Pearson correlation coefficient (ρ) of the linear regression. The mean value μ is shown in place of ρ for Yield. All y-axes are scaled between 0% and 50% probability except where a bold red value is assigned to the individual axis (Source: [168], reproduced with permission from Elsevier).

Azimuth data is best fitted for nearly all countries by a logistic probability distribution function, while no such correspondence is observed for tilt, capacity nor annual yield. The tilt angle distributions differ quite a lot seven different distribution types have been found. The tilt angle increases somewhat with latitude. The physical roof angle is dictating the tilt angle of the PV system, while on flat roofs, tilt angles typically are kept low to keep wind forces low. Interestingly, Belgium and the Netherlands share similar climate and latitude yet have different tilt distributions, most probably due to nationally differing architectural roof styles. The distributions for the installed capacity lead to a similar average capacity, with a clear deviation in the case of France which shows a peak at 3 kW$_p$. This was due to regulations [162]. Histograms of specific annual yield data are much smoother than other metadata histograms, which is due to larger sample size and digital recording of data instead of manual human error-prone data reporting. Results of mean annual yields are similar to the earlier reported ones, while also differences can be observed, most probably related to the representativeness differences in datasets.

Having established a set of representative distributions for azimuth, tilt and capacity, they can be used in regional, or national, PV power modelling approaches, such as suggested by Saint-Drenan et al. [166]. Killinger et al. [167] suggest using the fitted distributions to randomly sample the desired metadata of a portfolio of systems in a specific cluster. The reported distribution functions should not be used generally, but only for specific clusters, or for clusters not analyzed here that have similar climates, latitudes and support policies or subsidies. To illustrate this, PV power generation in Germany for systems smaller than 25 kW$_p$ can be derived as follows, based on the distributions.

First, as the installed capacity, geographic location and a specific annual yield of all PV systems is known, it should not be sampled if one wishes realistic outputs, though it may be sampled for theoretical reasons.

Second, for each PV system, tilt and azimuth are assigned to that system by sampling the fitted distribution. For the azimuth, a logistic distribution is used with locations coefficient of −0.1366 and a scale parameter of 23.0048, and for the tilt, an extreme value distribution is used with a mean of 38.0648 and a standard deviation of 9.6547 [168]. The capacity can either be the actual capacity of a system, or can be taken from the distribution (in this case a general extreme value distribution with a shape of 0.1143, a scale of 3.5745, and a location of 6.2413 as parameters.

Third, for each PV system energy yield can be simulated using appropriate models, geographic location and meteorological data. The generated PV energy in Germany can then be derived by aggregating the simulated energy from all systems. If the number of PV systems is too large, one can also use an approach to randomly choose PV systems and subsequently up-scale the results in order to limit computational effort. Rather than a simulation of energy yields, actual yield, as collected and fitted here, could be used. However, energy yield is an output value, which is based on static metadata and dynamic weather data. Also, if one wants to calculate daily or monthly energy generation, the only simulation possible is based on the metadata distribution functions. Here, the use of a performance ratio, or rather a distribution of performance ratio values per cluster that are derived from specific annual yield values may be worthwhile [167]. This was suggested earlier to visualize regional differences in annual yield using a single performance ratio of 0.85, thus assuming all PV systems are performing well [170].

5.5 Long-Term Degradation Rates: Case Study of a Small System in Bangkok, Thailand

One of the biggest questions is what kind of information the energy rating has in the long run for a photovoltaic technology, and even more for an installation. Perhaps to clarify this it is necessary to understand the differences between energy rating, energy yield, and long-term performance.

The energy rating, what has been the focus of this report is described in the series of standards IEC 61853 and evaluates the PV module performance based on power (watts), energy (watt-hours), and performance ratio. The energy yield is an exposition of the technology for at least one year, monitoring the performance of the PV technology [171]. The long-term performance assessment is representative measurement for periods of several years of operations.

These differences are summarized in Table 20.

Table 20: Comparison: Energy rating, energy yield and long-term performance assessment.

	PV Energy Rating	PV Energy Yield	Long-term Performance Assessment
Basis	pure calculation under standardized conditions	measurement under real operating conditions	Real-operating conditions
Duration	-	1 year	Years of operation
Goal	Assess expected performance based on 1-year data sets covering different climatic regions	Assess real performance at one specific location for one year	Assess real performance at one specific location for the long-term
Standards/Practices	series of standards IEC 61853	PV module characterization based on IEC standards (e.g., IEC 60904-x, IEC 61853-x) Measurements of IV curves, MPP and environmental data (IEC 60904-1 , IEC 61829, IEC 61724-1)	PV module characterization based on IEC standards (e.g., IEC 60904-x, IEC 61853-x). Measurements of IV curves, MPP and environmental data (IEC 60904-1 , IEC 61829, IEC 61724-1) Inspections, continuo monitoring, cleaning procedures, re-testing

Even by recognizing that several factors are associated with the energy yield performance, the long-term performance remains unclear. The relatively high maturity and market share of crystalline silicon modules allow performance studies of up to 20 years or more to be found in the literature [73, 172]. Less studies are found for thin-film technologies [173, 174]. Among these studies, it is important to distinguish the performance degradation of PV modules from the degradation of the PV system. For PV systems, the degradation is considerably higher due to the inclusion of losses of other components, the so-called system balance (BOS).

Although c-Si is a mature technology, not all failures are 100% known, as time advances new phenomena appear and will continue to appear in the long term - especially in more recent technologies such as PERC, n-pert, bifacial - which will involve the search for new solutions.

This chapter will open the arising problem of long-term degradations of (PV Modules) through a case study in the location of Thailand.

5.5.1 Introduction to the case study

PV systems have been in Thailand for several decades starting from 1970s [175]. Early adoptions were mostly stand-alone systems used for telecommunication applications. In 1980s, off-grid systems became widespread in rural areas including systems for schools, water pumping systems, and centralized battery charging stations. In 1990s, PV and balance of system (BOS) domestic manufacturing were founded. A rapid growth was observed in 2000s because of the Solar Home Project (SHP), a government subsidy program. Domestic PV and BOS testing

laboratories have also been established for product quality control. The growth continues as the Thai government initiated the adder and feed-in tariff programs with the accumulated capacity of 2.9 GW in 2018 [176]. The majority of installations are utility-scaled PV projects. Solar power is also included in the Thailand Power Development Plan (PDP2018) with a target of 10 GW in 2037 [177].

Currently, many systems over 10 years old have exhibited degradation and failures in both PV panels and BOS equipment. Researchers from the National Science and Technology Development Agency (NSTDA) have reported degradation rates for poly-Si modules of 0.5%/yr in a 3-year old system installed in a hot and humid climate [178]. The CES Solar Cells Testing Center (CSSC) has reported degradation rates for mono-Si and poly-Si modules, installed for 13 years near the gulf of Thailand, at 1.14%/yr and 1.41%/yr, respectively [179, 180].

PV system reliability is strongly influenced by the degradation of PV modules. An investigation of cause and effect is important for both preventive and corrective actions. Electrical degradation and physical module deterioration have been addressed previously [179]. In this case study, we investigated a 15-year old system using annual visual inspection results and electroluminescence images, as well as measured weather, system performance ratio, and module performance.

5.5.2 Background system information

The system under study is a 3.12 kW$_p$ free-standing flat roof PV grid-connected system of 32 modules in two strings. It is located at 13°34' N and 100°26' E, in a tropical hot and humid climate in the southern Bangkok area, Thailand near the sea. It was installed in 2003 and is still functioning. All modules are crystalline silicon. Half of the modules were locally assembled (mono or poly?) and half were imported (mono or poly?). The monitoring system was installed in 2010. Meteorology data such as in-plane solar irradiance, ambient and module temperature, wind speed and direction, and relative humidity are measured.

5.5.3 Data monitoring

The measurements are performed according to the IEC 61724 standard [141] with a sampling interval of 30 seconds. The monitored parameters are as follows.

1. Meteorology parameters: in-plane global irradiance at S-facing, 14 degree tilt (W/m^2), ambient temperature (^{o}C) using T-type thermocouple and wind speed (m/s**).**
2. Photovoltaic array parameters: the output DC voltage (V), the output DC current (A) are measured at PV string by DC meter before the inverter input and the back-of-module temperature (^{o}C) using T-type thermocouple.
3. Output parameters from the inverter: the utility grid AC voltage (V), the AC current to the utility grid (A) and the AC active power to the utility grid (kW).

5.5.4 PV module testing

All 32 modules are tested according to IEC 61215 [181] every year at CSSC, an ISO/IEC17025 accredited laboratory. The tests include (1) visual inspection, (2) performance at standard test condition (STC; 1000 W/m^2, AM. 1.5, 25 °C), (3) insulation, and (4) electroluminescence. Related electrical parameters are the maximum power (P_{max}), shot-circuit current (I_{sc}), current at maximum power (I_{mp}), and open-circuit voltage (V_{oc}). The degradation rates are calculated and measurements are compared with the corresponding nameplates.

5.5.5 Meteorology result

The in-plane solar irradiation of the system was between 1,810 and 2,005 kWh/m²/yr. From system monitoring data during 2012 - 2018, the 50th percentile of in-plane daily solar irradiation was 5.30 kWh/m²/day. Figure 80 presents (a) probability density function (PDF) and (b) cumulative distribution function (CDF) of in-plane solar irradiation. The average of in-plane solar irradiation was about 1,891 kWh/m²/year.
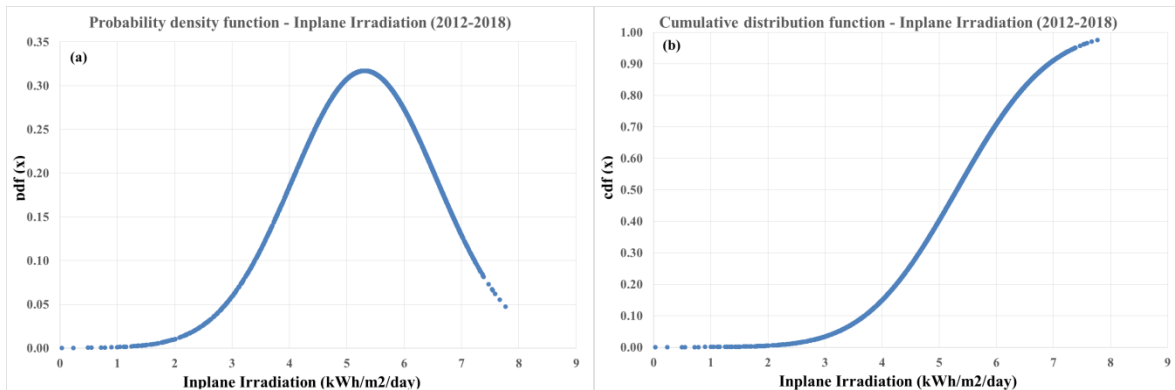
Figure 80: In-plane irradiation a site station which continue record from 2012 to 2018; (a) probability density function (PDF) and (b) cumulative distribution function (CDF) Mean = 5.31 (kWh/m²/day) and STDEV = 1.26 (kWh/m²/day).

Figure 81 presents the average monthly temperatures at the site. From the measurement data in 2012-2016, the average ambient (include night time) temperature is 29.1°C. The maximum temperature is 36.0°C in April and the minimum is 20.0°C in January. The average module temperature is 33.3°C. The maximum module temperature is 67.4°C in September because of the cumulative heat content from high solar irradiance in winter. The minimum module temperature is at 20.0°C, which is the same as the ambient temperature in January. The largest difference between the ambient and module temperatures is at 47.0°C in September. The average relative humidity is about 78%. The recorded values of module temperature are in the range of 19.6 – 67.4°C.

Figure 81: The average monthly ambient (left) and module (right) temperature between 2010 and 2018.

Performance ratio of the system

The performance ratio is evaluated from 2012-2019 as shown in Table 20. The evaluation is according to IEC 61724.

Table 21: PV system performance (Installation capacity is 3.12 kWp).

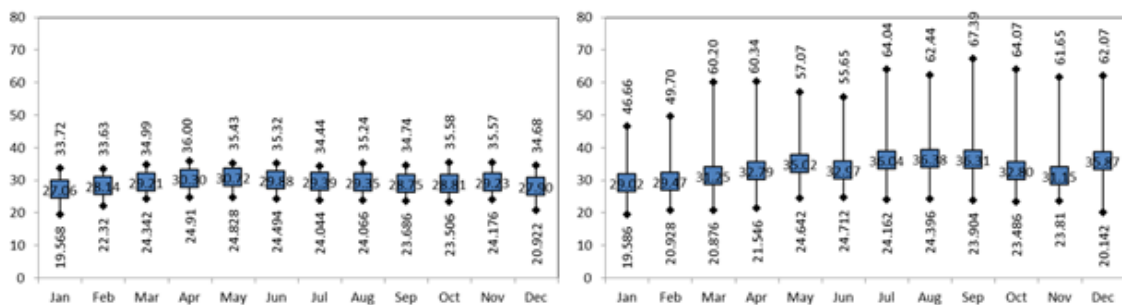| Year	In plane solar irradiation (kWh/m²/year)	AC energy (kWh/year)	Yield (kWh/kWp)	PR (%)	Remark
2012	1,888	3,859	1,237	66	arranged the position of PV modules by Isc
2013	1,810	3,992	1,279	71	Irradiation 2013 (data from 22 – 30 Apr 2013 were evaluated)
2014	1,929	4,000	1,282	66	-
2015	1,963	3,971	1,273	65	-
2016	2,005	3,282	1,052	62	-
2017	1,818	3,033	972	53	System disconnected for 2 months
2018	1,821	3,641	1,167x	64	Arrange and re-installation

5.5.6 Electrical degradation

All 32 modules have been measured since 2010 annually for performance at standard test conditions (STC) according to IEC61215:2005. Electrical parameters, consisting of current-voltage characteristic (I-V curves), short-circuit current (I_{sc}), open-circuit voltage (V_{oc}), current at maximum power point (I_{mp}), the voltage at maximum power point (V_{mp}), power at maximum power point (P_{mp}), fill factor (FF), were measured by CSSC at STC. The uncertainty of measurement for performance at STC is 2.24%.

Parameters obtained by IV characteristics at STC are evaluated for the annual degradation and depicted in Figure 82. Here the annual degradation rate of each I-V parameter compared to the nominal (nameplate) is shown. The power output of poly-Si modules decreased with a slope -0.06, also revealed in the I_{mp} and V_{mp} which slopes -0.04 and -0.03 respectively. The output power results of mono-Si modules and their plausibility is still being analysed.
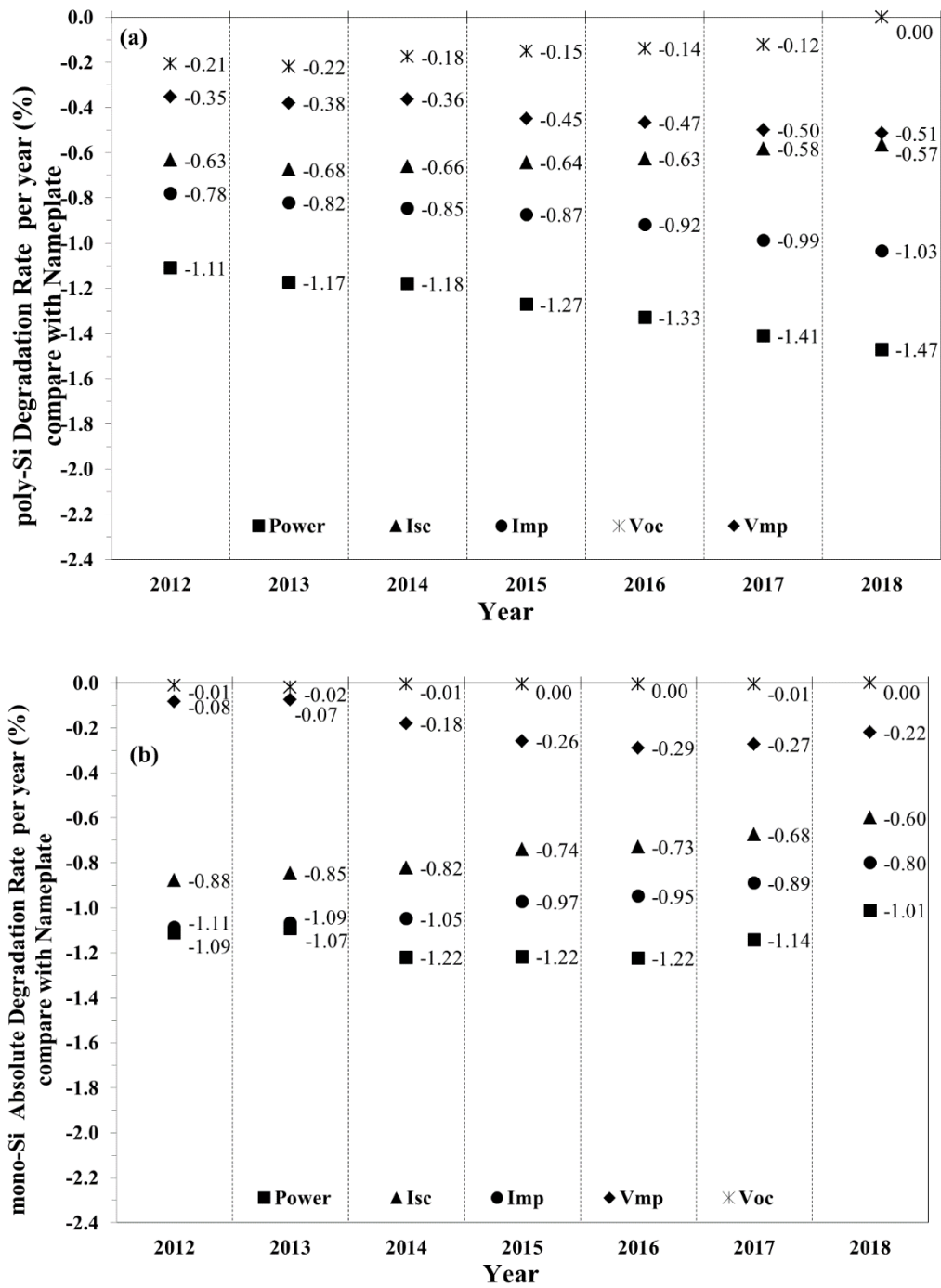
Figure 82: Electrical parameter degradation compared with nameplate; (a) poly-Si modules and (b) mono-Si modules.

2010   **2013**   **2015**   **2016**   **2017**   **2018**
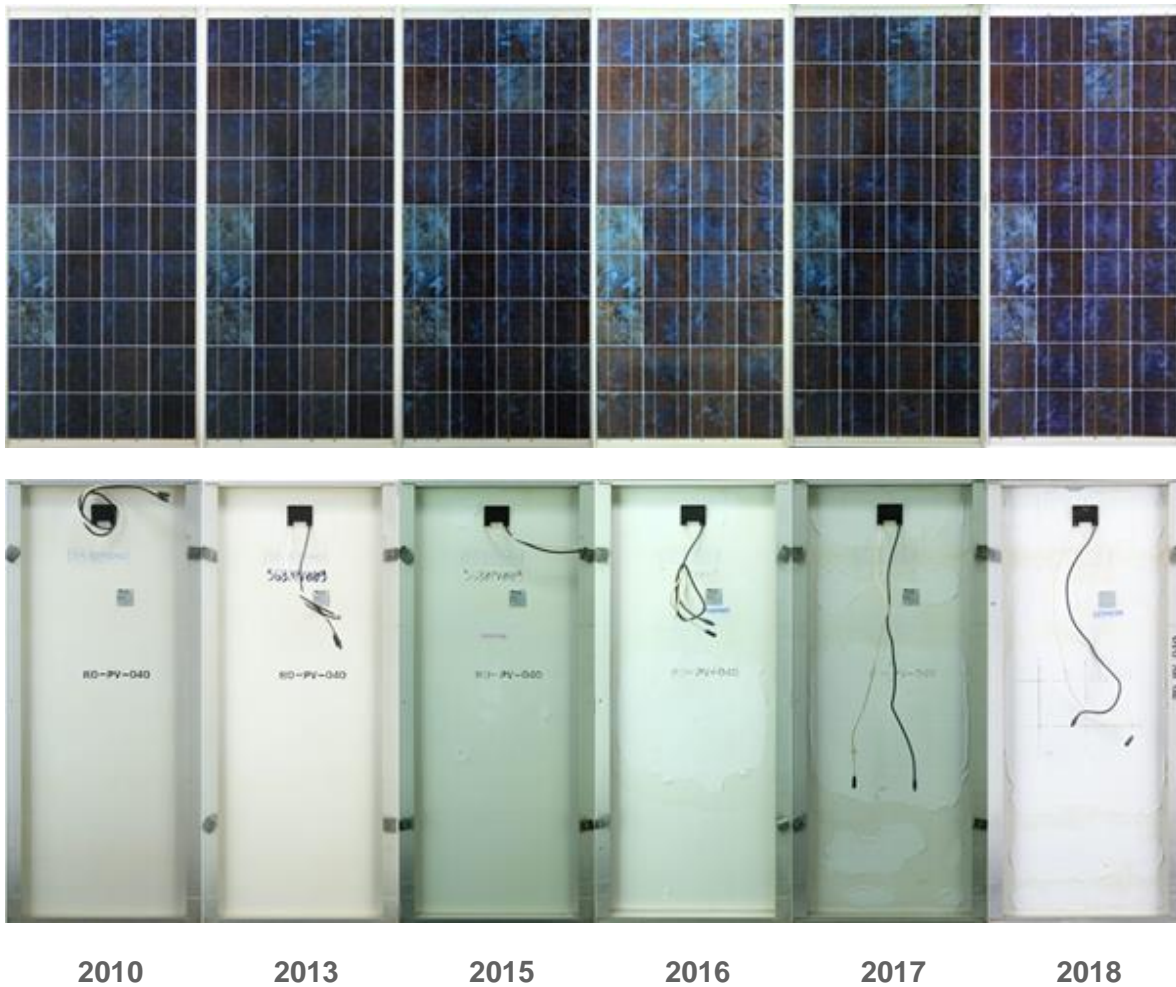
Figure 83: Front and rear sides of example poly-Si module from 2010 to 2018.

a)   b)
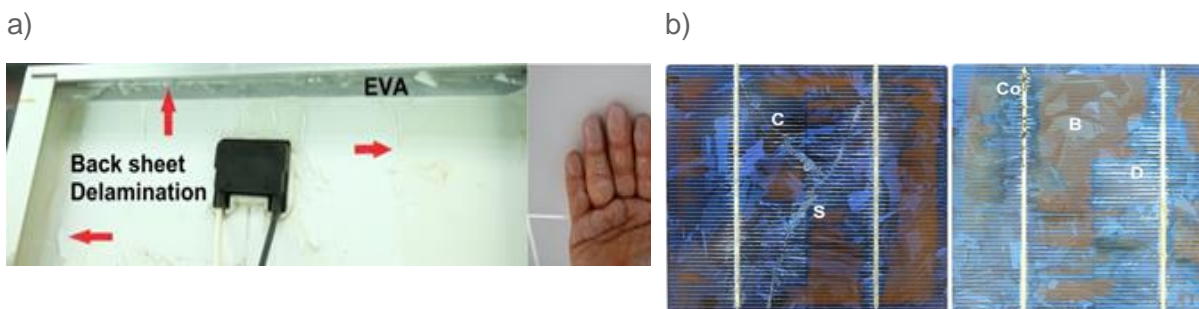
Figure 84: (a) Back-sheet delamination and chalking (b) Visual defects consist of Browning (B), Crack (C), Corrosion (Co), Delamination (D) and Snail trails (S). Source: [182].

After electrical characterization, electroluminescence images were taken. The poly-Si modules exhibited the following failures: crystal dislocations, edge wafer, finger failure, crack and micro-crack [183]. Figure 85 presents EL images of the same poly-Si module from 2016 to 2018. The mono-Si modules only exhibited shunt faults on cells as shown in Figure 86.
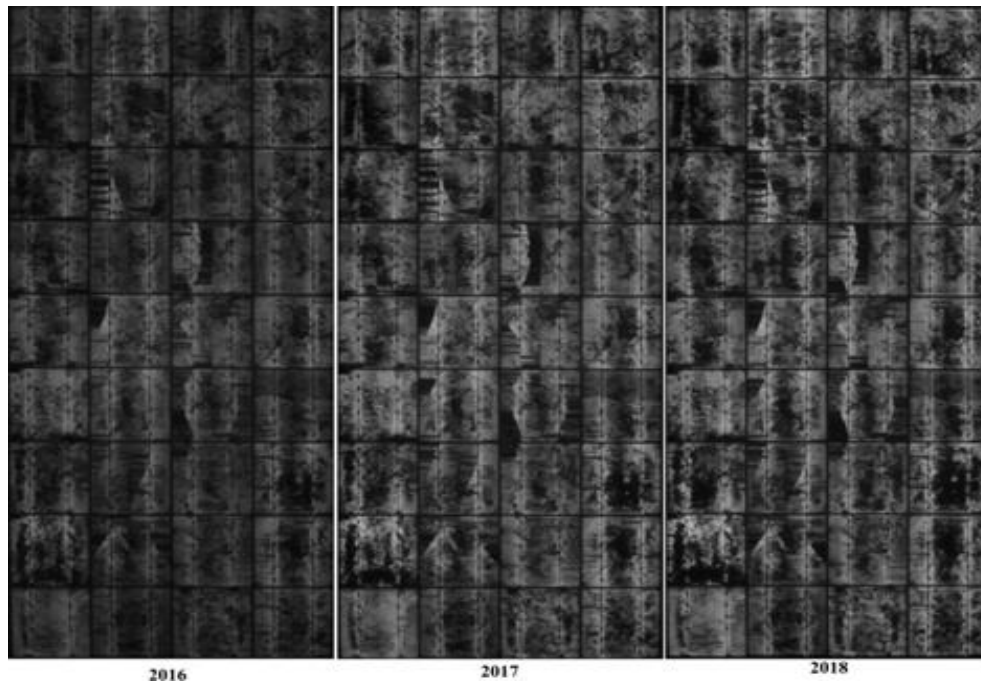
Figure 85: EL images of example poly-Si module during 2016 to 2018.
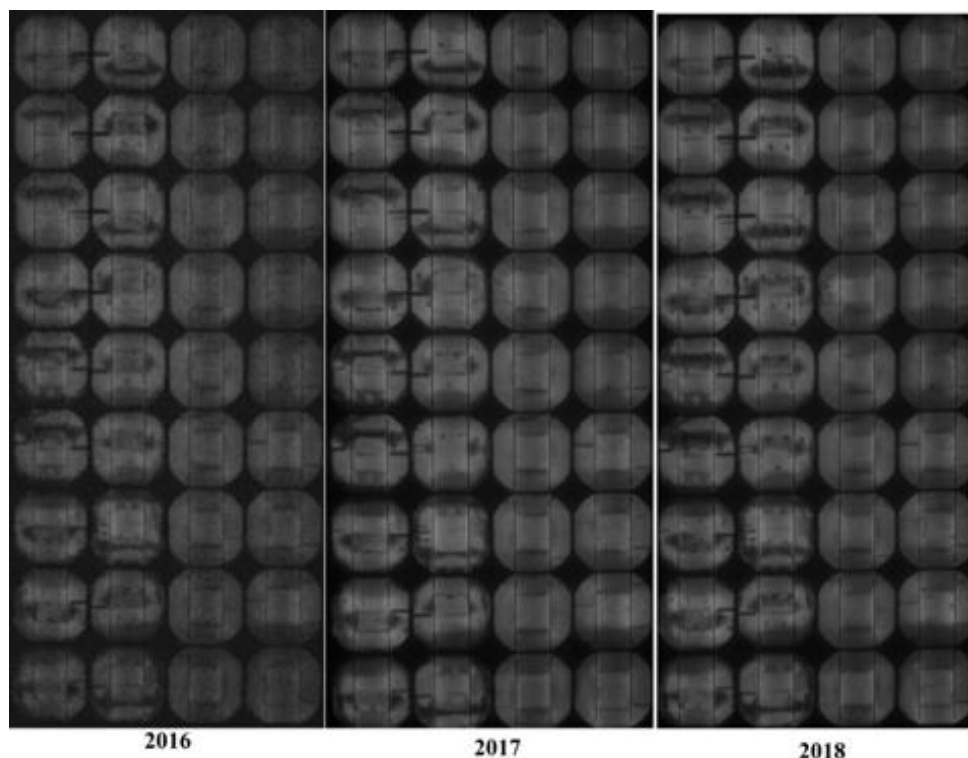
Figure 86: EL images of example mono-Si module from 2016 to 2018.

5.5.7 Conclusion

Module degradation which affects the system performance has been observed on the PV modules under study. In this study, the power degradation rate of poly-Si modules is -1.47% per year and for mono-Si modules the results and their plausibility are still being analysed. When

observed each year, the physical degradation is increasing, for example, the delamination areas, corrosion areas and the level of browning. These defects have an impact on the performance of the modules that were quantified. We plan to continue our work on finding the correlation of climate factors and module degradation by using the monitoring data compared with the annual time series of visual defects and electrical performance. In near future, we plan to analyse a monitoring degradation of this system with the correlation of PV performance degradation by STC result.

6 CONCLUSIONS

The IEC Standard series 61853 "Photovoltaic (PV) module performance testing and energy rating" (Part 1 to 4) provides a methodology to obtain a simple but realistic estimate of the performance of a PV module in different climatic conditions. The final output is the so-called Climate Specific Energy Rating (CSER) parameter. The CSER is equivalent to the performance ratio of the PV module for a complete year and allows to compare the performance of different PV technologies or modules under real working conditions. If the CSER is one, this means that the average efficiency of the photovoltaic module is equal to its efficiency in STC. If yield losses are dominant, CSER will take values lower than one.

As an input to the calculation of the CSER, module characteristics include the performance under variable irradiance and module temperature (G-T matrix), its angular responsivity (AR), the spectral responsivity (SR), and the nominal module operating temperature (NMOT) of PV modules. The measurement procedures for these are described in Part 1 and 2 of the IEC series.

Part 3 lays down a methodology for the calculation of the CSER value, which additionally to the results of the first two parts incorporates the reference climate data sets from Part 4 as input data. Currently the user can choose from six climate data sets (continental temperate, coastal temperate, tropical humid, arid subtropical, coastal subtropical, high altitude), all of which comprise a time series of hourly data of meteorological parameters for a full year. The climate data sets also contain solar spectral irradiance data, which are not presented in a high resolution but in a low-resolution format with 29 data points in the total wavelength range 300 nm to 4000 nm. The wavelength intervals for averaging solar spectral irradiance are also known as Kato-bands.

With regard to Part 1 and Part 2, this report provides the information for indoor and outdoor characterization, pointing out the objective of these measurements and the main advantages and disadvantages of the two approaches (laboratory and outdoor). In addition, the exemplary results of these measurements have been examined in detail.

Since talking about energy yield of PV modules is also setting climatic data sets, the climate classification plays an important role. This report has examined global approaches, as the PVCZ scheme aims to understand the degradation of PV modules based on the Arrhenius law, and the KGPV scheme extends the KG climate classification by including irradiation as a new layer of the map. Climate classification presents a multifaceted problem, in which solutions have to balance specificity, accuracy, simplicity, and applicability. Efforts have been made, but still, the correlation with field-observed degradation modes are needed.

Currently, the scope of the IEC 61853 energy covers single-junction monofacial devices. If in the future, other devices such as bifacial or multi-junction devices are to be considered, the standard datasets may have to be modified or extended. The new variables will depend on the methodology used to model the performance of the new devices and the availability of data at global scale.

Another limitation of the IEC energy rating standard regards the technologies with significant non-linearity in the characteristics modelled, such as the performance at low irradiance levels.

This report also examines the approaches of accredited laboratories and institutions to energy rating. Experimental results have also been shown for relatively new technologies and other PV solutions, such as bi-phase, colour and BIPV modules. For these approaches and results, as well as for the IEC 61853 method, the uncertainty in the PV rating shall be considered. As

in any other estimation model, possible systematic and random errors may occur in the input data used and in the applied calculation models themselves, as they may not be robust and representative, to the same extent, for all PV technologies and devices. Therefore, results should be taken with caution, due to the different effects taken into consideration, for devices whose efficiency is affected by long-term exposure to outdoor conditions, as results may be misleading. Devices lacking long-term stability would obtain overestimated ratings with regard to real lifetime performance. These and other possible sources of uncertainties are also discussed.

The search for higher efficiencies and lower LCOEs in the PV industry, has made that the concept of energy instead of power is becoming more and more important and with this, the development of new and better energy rating methods has started on a promising path.

REFERENCES

[1]   E. Dunlop, A. Gracia Amillo, E. Salis, T. Sample, and Taylor, N., *Transitional methods for PV modules, inverters and systems in an Ecodesign Framework*. EUR 29513 EN, ISBN: 978-92-79-98284-2 (online), doi: 10.2760/496002. Luxemburg, 2019.

[2]   D. Moser, S. Lindig, M. Richter, J. Ascencio Vásquez, I. Horvath, B. Müller, M. Green, J. Vedde, M. Herz, B. Herteleer, K.A. Weiß, and B. Stridh, "Uncertainties in Yield Assessments and PV LCOE: Report IEA-PVPS T13-18:2020," IEA Report Photovoltaic Systems Programme, International Energy Agency.

[3]   *IEC 61853-1: Photovoltaic (PV) module performance testing and energy rating - Part 1: Irradiance and temperature performance measurements and power rating*, 1.0th ed., International Electrotechnical Commission, 2011.

[4]   *IEC 61853-2: Photovoltaic (PV) module performance testing and energy rating - Part 2: Spectral responsivity, incidence angle and module operating temperature measurements*, 1.0th ed., International Electrotechnical Commission, 2016.

[5]   *IEC 61853-3: Photovoltaic (PV) module performance testing and energy rating - Part 3: Energy rating of PV modules*, 1.0th ed., International Electrotechnical Commission, 2018.

[6]   *IEC 61853-4: Photovoltaic (PV) module performance testing and energy rating - Part 4: Standard reference climatic profiles*, 1.0th ed., International Electrotechnical Commission, 2018.

[7]   T. Huld, A. Gracia Amillo, T. Sample, E. D. Dunlop, E. Salis, and R. Kenny, "The completed IEC 61853 standard series on PV module energy rating, overview, applications and outlook," in Proc. 35th Eur. Photovolt. Sol. Energy Conf. Exhib. (EUPVSEC) pp. 1113–1118. Brussels, Belgium, 2018.

[8]   C. Reise, B. Müller, D. Moser, A. Driesse, G. Razongles, and M. Richter, "Uncertainties in PV System Yield Predictions and Assessments," Report IEA-PVPS T13-12:2018, International Energy Agency, Paris, France, 2018.

[9]   M. Schweiger, J. Bonilla, W. Herrmann, A. Gerber, and U. Rau, "Performance stability of photovoltaic modules in different climates," *Prog. Photovolt: Res. Appl.*, vol. 25, no. 12, pp. 968–981, 2017, doi: 10.1002/pip.2904.

[10]   B. Marion, B. Kroposki, K. Emery, J. del Cueto, D. Myers, and C. Osterwald, "Validation of a Photovoltaic Module Energy Ratings Procedure at NREL," *NREL Technical Report*, NREL/TP-520-26909, 1999, doi: 10.2172/12187.

[11]   D. Dirnberger, B. Müller, and C. Reise, "PV module energy rating: opportunities and limitations," *Prog. Photovolt: Res. Appl.*, vol. 23, no. 12, pp. 1754–1770, 2015, doi: 10.1002/pip.2618.

[12]   A. Louwen, A. C. de Waal, R. E. I. Schropp, A. P. C. Faaij, and W. G. J. H. M. van Sark, "Comprehensive characterisation and analysis of PV module performance under real operating conditions," *Prog. Photovolt: Res. Appl.*, vol. 25, no. 3, pp. 218–232, 2017, doi: 10.1002/pip.2848.

[13]   T. Huld, E. Salis, A. Pozza, W. Herrmann, and H. Müllejans, "Photovoltaic energy rating data sets for Europe," *Solar Energy*, vol. 133, pp. 349–362, 2016, doi: 10.1016/j.solener.2016.03.071.

[14]   M. Schweiger, W. Herrmann, A. Gerber, and U. Rau, "Understanding the Energy Yield of Photovoltaic Modules in Different Climates by Linear Performance Loss Analysis," *IET Renewable Power Generation*, vol. 11, 2017, doi: 10.1049/iet-rpg.2016.0682.

[15]   B. Bora, R. Kumar, O. S. Sastry, B. Prasad, S. Mondal, and A. K. Tripathi, "Energy rating estimation of PV module technologies for different climatic conditions," *Solar Energy*, vol. 174, pp. 901–911, 2018, doi: 10.1016/j.solener.2018.09.069.

[16]   M. Kottek, J. Grieser, C. Beck, B. Rudolf, and F. Rubel, "World Map of the Köppen-Geiger Climate Classification Updated," *Meteorologische Zeitschrift*, vol. 15, pp. 259–263, 2006, doi: 10.1127/0941-2948/2006/0130.

[17]   F. R. M. Kottek, *World map of the köppen-geiger climate classification.* [Online]. Available: http://koeppen-geiger.vu-wien.ac.at/

[18]   D. Dirnberger, B. Müller, and C. Reise, "On the uncertainty of energetic impact on the yield of different PV technologies due to varying spectral irradiance," *Solar Energy*, vol. 111, pp. 82–96, 2015, doi: 10.1016/j.solener.2014.10.033.

[19]   M. Bliss, T. R. Betts, and R. Gottschalg, "Indoor measurement of photovoltaic device characteristics at varying irradiance, temperature and spectrum for energy rating," *Measurement Science and Technology*, vol. 21, no. 11, p. 115701, 2010, doi: 10.1088/0957-0233/21/11/115701.

[20]   T. Huld, G. Friesen, A. Skoczek, R. P.Kenny, T. Sample, M. Field, E. Dunlop, "A power-rating model for crystalline silicon PV modules," *Solar Energy Materials and Solar Cells - SOLAR ENERG MATER SOLAR CELLS*, vol. 95, pp. 3359–3369, 2011, doi: 10.1016/j.solmat.2011.07.026.

[21]   R. P. Kenny, D. Viganó, E. Salis, G. Bardizza, M. Norton, H. Müllejans,and W. Zaaiman, "Power rating of photovoltaic modules including validation of procedures to implement IEC 61853-1 on solar simulators and under natural sunlight," *Prog. Photovolt: Res. Appl.*, vol. 21, no. 6, pp. 1384–1399, 2013, doi: 10.1002/pip.2365.

[22]   D. Dirnberger, G. Blackburn, B. Müller, and C. Reise, "On the impact of solar spectral irradiance on the yield of different PV technologies," *Solar Energy Materials and Solar Cells*, vol. 132, pp. 431–442, 2015, doi: 10.1016/j.solmat.2014.09.034.

[23]   G. Kleiss, H. Schülbe, and B. Nacke, "Energy rating of crystalline solar modules: investigation of uncertainties due to binning in mass production," in Proc. 32nd Eur. Photovolt. Sol. Energy Conf. Exhib. (EUPVSEC), ISBN: 3-936338-41-8 pp. 2244 - 2247. Munich, Germany, 2016.

[24]   B. Müller, L. Hardt, A. Armbruster, K. Kiefer, and C. Reise, "Yield predictions for photovoltaic power plants: empirical validation, recent advances and remaining uncertainties," *Prog. Photovolt: Res. Appl.*, vol. 24, no. 4, pp. 570–583, 2016, doi: 10.1002/pip.2616.

[25]   S. Ransome and J. Sutterlueti, "Degradation analysis of PV technologies using NREL and Gantner Instruments outdoor data," in *2016 IEEE 43rd Photovoltaic Specialists Conference (PVSC)*, 2016, pp. 3441–3446.

[26]   I. Geisemeyer, N. Tucher, B. Müller, H. Steinkemper, J. Hohl-Ebinger, M. C. Schubert and W. Warta, "Angle Dependence of Solar Cells and Modules: The Role of Cell Texturization," *IEEE Journal of Photovoltaics*, vol. 7, no. 1, pp. 19–24, 2017, doi: 10.1109/JPHOTOV.2016.2614120.

[27]   B. Müller, P. Bostock, B. Farnung, and C. Reise, Eds., "A Framework to Calculate Uncertainties for Lifetime Energy Yield Predictions of PV Systems,"

[28]   J. Polo, M. Alonso-Abella, J. A. Ruiz-Arias, and J. L. Balenzategui, "Worldwide analysis of spectral factors for seven photovoltaic technologies," *Solar Energy*, vol. 142, pp. 194–203, 2017, doi: 10.1016/j.solener.2016.12.024.

[29]   S. Ransome, "Validating Energy Yield Modelling with the NREL Outdoor Dataset," in *2018 IEEE 7th World Conference on Photovoltaic Energy Conversion (WCPEC) (A Joint Conference of 45th IEEE PVSC, 28th PVSEC & 34th EU PVSEC)*, 2018, pp. 2713–2718.

[30]   M. Richter, "Reducing uncertainty in PV yield assessments," *PV Tech Power*, no. 14, pp. 50–56, 2018.

[31]   B. Hüttl, L. Gottschalk, S. Schneider, D. Pflaum, and A. Schulze, "Accurate performance rating of photovoltaic modules under outdoor test conditions," *Solar Energy*, vol. 177, pp. 737–745, 2019, doi: 10.1016/j.solener.2018.12.002.

[32]   S. Ransome and J. Sutterlueti, "How to Choose the Best Empirical Model for Optimum Energy Yield Predictions," in *2017 IEEE 44th Photovoltaic Specialist Conference (PVSC)*, 2017, pp. 652–657.

[33]   S. Ransome and J. Sutterlueti, "Checking the new IEC 61853.1-4 with high quality 3rd party data to benchmark its practical relevance in energy yield prediction," in *2019 IEEE 46th Photovoltaic Specialists Conference (PVSC)*, 2019, pp. 2229–2234.

[34]   S. Ransome and J. Sutterlueti, "Quantifying long term PV performance and degradation under real outdoor and IEC 61853 test conditions using high quality module iv measurements," in Proc. 36th Eur. Photovolt. Sol. Energy Conf. Exhib. (EUPVSEC), ISBN: 3-936338-60-4 pp. 1640 - 1645. Marseille, France, 2019.

[35]   T. Karin, C. B. Jones, and A. Jain, "Photovoltaic climate zones: The global distribution of climate stressors affecting photovoltaic degradation," in Proc. 36th Eur. Photovolt. Sol. Energy Conf. Exhib. (EUPVSEC) pp. 825-834. Marseille, France, 2019.

[36]   T. Karin, C. B. Jones, and A. Jain, "Photovoltaic Degradation Climate Zones," in *2019 IEEE 46th Photovoltaic Specialists Conference (PVSC)*, 2019, pp. 687–694.

[37]   J. Ascencio-Vásquez, I. Kaaya, K. Brecl, K.-A. Weiss, and M. Topič, *Global Climate Data Processing and Mapping of Degradation Mechanisms and Degradation Rates of PV Modules,* 1996-1073, doi: 10.3390/en12244749, 2019.

[38]   J. Ascencio-Vásquez, K. Brecl, and M. Topič, "Methodology of Köppen-Geiger-Photovoltaic climate classification and implications to worldwide mapping of PV system performance," *Solar Energy*, vol. 191, pp. 672–685, 2019, doi: 10.1016/j.solener.2019.08.072.

[39]   *IEC 60904-9: Photovoltaic devices - Part 9: Classification of solar simulator characteristics*, 3.0th ed., International Electrotechnical Commission, 2020.

[40]   M. Schweiger, "Performance of PV modules with different technologies and the impact on energy yield in four climatic zones," Ph.D. dissertation, RWTH Aachen University, Aachen, Germany, 2017. [Online]. Available: http://publications.rwth-aachen.de/record/711967/files/711967.pdf

[41]   *IEC 60904-3: Photovoltaic devices -Part 3: Measurement principles for terrestrial photovoltaic (PV) solar devices with reference spectral irradiance data*, 4.0th ed., International Electrotechnical Commission, 2019.

[42]   *IEC 60904-7: Photovoltaic devices - Part 7: Computation of the spectral mismatch correction for measurements of photovoltaic devices(PV) solar devices with reference spectral irradiance data*, 4.0th ed., International Electrotechnical Commission, 2019.

[43]   W. Herrmann, M. Schweiger, L. Rimmelspacher, "Solar Simulator Measurement Procedures for Determination of the Angular Characteristic of PV Modules," in Proc. 29th Eur. Photovolt. Sol. Energy Conf. Exhib. (EUPVSEC), ISBN: 3-936338-34-5 pp. 2403 - 2406. Amsterdam, Niederlande, 2019.

[44]   B. H. King, C. W. Hansen, D. Riley, C. D. Robinson and L. Pratt, "Procedure to Determine Coefficients for the Sandia Array Performance Model (SAPM)," Sandia National Laboratories, 2016. [Online]. Available: https://prod-ng.sandia.gov/techlib-noauth/access-control.cgi/2016/165284.pdf

[45]   D. L. King, W. E. Boyson, J. A. Kratochvil, "Photovoltaic Array Performance Model," Sandia National Laboratories, 2004. [Online]. Available: https://prod-ng.sandia.gov/techlib-noauth/access-control.cgi/2016/165284.pdf

[46]   W. De Soto, S.A. Klein, and W.A. Beckman, "Improvement and validation of a model for photovoltaic array performance," *Solar Energy*, vol. 80, no. 1, pp. 78–88, 2006, doi: 10.1016/j.solener.2005.06.010.

[47]   B. H. King, D. Riley, C. D. Robinson, and L. Pratt, "Recent advancements in outdoor measurement techniques for angle of incidence effects," in *2015 IEEE 42nd Photovoltaic Specialist Conference (PVSC)*, 2015, pp. 1–6.

154

[48]   N. Martin and J. M. Ruiz, "Calculation of the PV modules angular losses under field conditions by means of an analytical model," *Solar Energy Materials and Solar Cells*, vol. 70, no. 1, pp. 25–38, 2001, doi: 10.1016/S0927-0248(00)00408-6.

[49]   D. L. King, J. A. Kratochvil, and W. E. Boyson, "Measuring solar spectral and angle-of-incidence effects on photovoltaic modules and solar irradiance sensors," in *1997 IEEE 26th Photovoltaic Specialists Conference (PVSC)*, 1997, pp. 1113–1116.

[50]   R.M.E. Valckenborg, B. Van Aken, "Outdoor Performance Quantification and Understanding of Various PV Technologies using the IEC 61853 Matrix," in Proc. 36th Eur. Photovolt. Sol. Energy Conf. Exhib. (EUPVSEC), ISBN: 3-936338-60-4 pp. 880 - 886. Marseille, France, 2019.

[51]   P. Illich, G.C. Eder, K.A. Berger, G. Újvári, P. Gaisberger, D. Moor, M. Aichinger, S. Boddaert, R.M.E. Valckenborg, J. van den Brand, P. Bonomo, F. Frontini, C.S. Polo López, M. Del Buono, A.G. Imenes, N. Martín Chivelet, F. Chenlo, A. Sanz Martinez, M. Machado, J.-T. Kim, A. Masolin and M. Ritzen, "Comparative Performance Measurements of Identical BIPV-Elements in Different Climatic Environments - A Round Robin Action within the IEA PVPS Task 15 Collaboration," in Proc. 35th Eur. Photovolt. Sol. Energy Conf. Exhib. (EUPVSEC), ISBN: 3-936338-50-7 pp. 1794 - 1800. Brussels, Belgium, 2017.

[52]   L. Gaisberger, P. Rechberger, G. Eder, K. Berger, Ú. Gusztáv, P. Illich, D. Moor, S. Boddaert, R. Valckenborg, P. Bonomo, C. Polo, M. Del Buono, N. Martin Chivelet, E. Mejuto, A. Sanz, M. Machado, J-T. Kim and M. Ritzen, "BIPV Round-Robin Action of IEA PVPS Task 15," in Proc. 35th Eur. Photovolt. Sol. Energy Conf. Exhib. (EUPVSEC), ISBN: 3-936338-50-7 pp. 1794 - 1800. Brussels, Belgium, 2017.

[53]   A. F. Souka and H. H. Safwat, "Determination of the optimum orientations for the double-exposure, flat-plate collector and its reflectors," *Solar Energy*, vol. 10, no. 4, pp. 170–174, 1966, doi: 10.1016/0038-092X(66)90004-1.

[54]   *PV Performance Modeling Collaborative | An Industry and National Laboratory collaborative to improve Photovoltaic Performance Modeling.* [Online]. Available: https://pvpmc.sandia.gov/pv-research/pv-lifetime-project/pv-lifetime-modules/ (accessed: Oct. 8 2020).

[55]   *IEC TS 60904-1-2: Photovoltaic devices - Part 1-2: Measurement of current-voltage characteristics of bifacial photovol-taic (PV) devices*, 1.0th ed., International Electrotechnical Commission, 2019.

[56]   *Measurement procedures for current-voltage characteristics of bifacial photovoltaic (PV) modules*, 2018.

[57]   J. S. Stein, "Characterizing and modeling the performance of bifacial photovoltaic modules and systems," in 7th PVPMC Workshop on Energy Rating and Module Performance Modeling, ISBN: SAND2017-3088 C. Lugano, Switzerland, Mar. 30 2017.

[58]   R. Valckenborg, "[Duplikat] Characterizing and modeling the performance of bifacial photovoltaic modules and systems: Application of IEC 61853 matrix to bifacial PV," in bifiPV workshop. Lugano, Switzerland, 16-18 September, 2019.

[59]   F. Rubel and M. Kottek, "Comments on: "The thermal zones of the Earth"" by Wladimir Köppen (1884)," *Meteorologische Zeitschrift*, vol. 20, pp. 361–365, 2011, doi: 10.1127/0941-2948/2011/0285.

[60]   R. Geiger, *Landolt-Börnstein: Zahlenwerte und Funktionen aus Physik, Chemie, Astronomie, Geophysik und Technik: Ch. Klassifikation der Klimate nach W. Koppen*. Berlin, 1954.

[61]   F. Rubel and M. Kottek, "Observed and projected climate shifts 1901-2100 depicted by world maps of the Köppen-Geiger climate classification," *Meteorologische Zeitschrift*, vol. 19, pp. 135–141, 2010, doi: 10.1127/0941-2948/2010/0430.

[62]   F. Rubel, K. Brugger, K. Haslinger, and I. Auer, "The climate of the European Alps: Shift of very high resolution Köppen-Geiger climate zones 1800–2100," *Meteorologische Zeitschrift*, vol. 26, pp. 115–125, 2017, doi: 10.1127/metz/2016/0816.

[63]   M. C. Peel, B. L. Finlayson, and T. A. McMahon, "Updated world map of the Köppen-Geiger climate classification," *Hydrology and Earth System Sciences*, vol. 11, no. 5, pp. 1633–1644, 2007, doi: 10.5194/hess-11-1633-2007.

[64]   D. J. Kriticos, B. L. Webber, A. Leriche, N. Ota, I. Macadam, J. Bathols and J. K. Scott, "CliMond: global high-resolution historical and future scenario climate surfaces for bioclimatic modelling," *Methods in Ecology and Evolution*, vol. 3, no. 1, pp. 53–64, 2012, doi: 10.1111/j.2041-210X.2011.00134.x.

[65]   H. E. Beck, N. E. Zimmermann, T. R. McVicar, N. Vergopolan, A. Berg, and E. F. Wood, "Present and future Köppen-Geiger climate classification maps at 1-km resolution," *Scientific Data*, vol. 5, no. 1, p. 180214, 2018, doi: 10.1038/sdata.2018.214.

[66]   J. R. Russell, *Dry Climates of the United States: I Climatic Map*: Publications in Geography, 1931.

[67]   Y. Wang, W. Huang, A. Fairbrother, L. S. Fridman, A. J. Curran, N. R. Wheeler, S. Napoli, A. Hauser, S. Julien, X. Gu, G. Obrien, K. T. Wan, L. Ji, M. Kempe, K. Boyce, R. French and L. Bruckman, "Generalized Spatio-Temporal Model of Backsheet Degradation From Field Surveys of Photovoltaic Modules," *IEEE Journal of Photovoltaics*, vol. 9, pp. 1–8, 2019, doi: 10.1109/JPHOTOV.2019.2928700.

[68]   S. Julien, M. Kempe, J. Eafanti, J. Morse, Y. Wang, A. Fairbrother, S. Napoli, A.W. Hauser, L. Ji, G. O'Brien, X. Gu, R. French, L. Bruckman, K.T. Wan and K. Boyce, "Characterizing photovoltaic backsheet adhesion degradation using the wedge and single cantilever beam tests, Part I: Field Modules," *Solar Energy Materials and Solar Cells*, vol. 215, p. 110669, 2020, doi: 10.1016/j.solmat.2020.110669.

[69]   Y. Lyu, A. Fairbrother, M. Gong, J.H. Kim, X. Gu, M. Kempe, S. Julien, K. T.Wan, S. Napoli, A. Hauser, G. O'Brien, Y. Wang, R. French, L. Bruckman, L. Ji and K. Boyce, "Impact of environmental variables on the degradation of photovoltaic components and perspectives for the reliability assessment methodology," *Solar Energy*, vol. 199, pp. 425–436, 2020, doi: 10.1016/j.solener.2020.02.020.

[70]   Y. Lyu, A. Fairbrother, M. Gong, J. H. Kim, A. Hauser, G. O'Brien and X. Gu, "Drivers for the cracking of multilayer polyamide-based backsheets in field photovoltaic modules: In-depth degradation mapping analysis," *Prog. Photovolt: Res. Appl.*, vol. 28, no. 7, pp. 704–716, 2020, doi: 10.1002/pip.3260.

[71]   D. A. Gordon, W.-H. Huang, D. M. Burns, R. H. French, and L. S. Bruckman, "Multivariate multiple regression models of poly(ethylene-terephthalate) film degradation under outdoor and multi-stressor accelerated weathering exposures," *PloS one*, vol. 13, no. 12, e0209016, 2018, doi: 10.1371/journal.pone.0209016.

[72]   K. Boyce, S. Merzlic, A. Fairbrother, X. Gu, S. Julien and K.T. Wan, L. Ji, A. Lefebvre, G. O'Brien, Y. Wang, L. Bruckman, R. French and M. Kempe, *Degradation analysis of field-exposed photovoltaic modules with non-fluoropolymer-based backsheets*, doi: 10.1117/12.2272488, 2017.

[73]   D. C. Jordan, S. R. Kurtz, K. VanSant, and J. Newmiller, "Compendium of photovoltaic degradation rates," *Prog. Photovolt: Res. Appl.*, vol. 24, no. 7, pp. 978–989, 2016, doi: 10.1002/pip.2744.

[74]   M. Koehl, M. Heck, and S. Wiesmeier, "Categorization of weathering stresses for photovoltaic modules," *Energy Science & Engineering*, vol. 6, no. 2, pp. 93–111, 2018, doi: 10.1002/ese3.189.

[75]   G. C. Eder, Y. Voronko, S. Dimitriadis, K. Knöbl, G. Újvári, K. A. Berger, M. Halwachs, L. Neumaier, and C. Hirschl, "Climate specific accelerated ageing tests and evaluation of ageing induced electrical, physical, and chemical changes," *Prog. Photovolt: Res. Appl.*, vol. 27, no. 11, pp. 934–949, 2019, doi: 10.1002/pip.3090.

[76]   I. Kaaya, M. Koehl, A. P. Mehilli, S. d. C. Mariano, and K. A. Weiss, "Modeling Outdoor Service Lifetime Prediction of PV Modules: Effects of Combined Climatic Stressors on PV Module Power Degradation," *IEEE Journal of Photovoltaics*, vol. 9, no. 4, pp. 1105–1112, 2019, doi: 10.1109/JPHOTOV.2019.2916197.

[77]   Bekeley Lab, *PVTOOLS.* [Online]. Available: https://pvtools.lbl.gov/pv-climate-stressors (accessed: Oct. 28 2020).

[78]   R. J. Wieser, A. Xin, R. French, and L. Bruckman, "Evaluation and Prediction of Koeppen Geiger Climate Zone Based off of Real-World Satellite Weather Data," in PVSC 47. Virtual: IEEE. [Online]. Available: https:// www.ieee-pvsc.org/virtual/index.php?page=presentation&session_id=126&presentation_id=527##, 2020.

[79]   B. Chelsey, N. R. Wheeler, F. Rubel, and R. French, *Package 'kgc'-Kgc: Koeppen-Geiger Climatic Zones.* [Online]. Available: ttps://cran.r-project.org/package=kgc.

[80]   J. Ascencio Vasquez, *Data for: Methodology of Köppen-Geiger-Photovoltaic climate classification and implications to Worldwide Mapping of PV System Performance: Mendeley Data*. doi: 10.17632/z3byd8jyfn.1. [Online]. Available: https://data.mendeley.com/datasets/z3byd8jyfn/1

[81]   T. Ishii, K. Otani, A. Itagaki, and K. Utsunomiya, "A simplified methodology for estimating solar spectral influence on photovoltaic energy yield using average photon energy," *Energy Sci Eng*, vol. 1, no. 1, pp. 18–26, 2013, doi: 10.1002/ese3.3.

[82]   N. Lindsay, Q. Libois, J. Badosa, A. Migan-Dubois, and V. Bourdin, "Errors in PV power modelling due to the lack of spectral and angular details of solar irradiance inputs," *Solar Energy*, vol. 197, pp. 266–278, 2020, doi: 10.1016/j.solener.2019.12.042.

[83]   D. Moser, M. Del Buono, U. Jahn, M. Herz, M. Richter, and K. de Brabandere, "Identification of technical risks in the photovoltaic value chain and quantification of the economic impact," *Prog. Photovolt: Res. Appl.*, vol. 25, no. 7, pp. 592–604, 2017, doi: 10.1002/pip.2857.

[84]   P. M. Rodrigo, E. F. Fernández, F. M. Almonacid, and P. J. Pérez-Higueras, "Quantification of the spectral coupling of atmosphere and photovoltaic system performance: Indexes, methods and impact on energy harvesting," *Solar Energy Materials and Solar Cells*, vol. 163, pp. 73–90, 2017, doi: 10.1016/j.solmat.2017.01.018.

[85]   C. Jardine, T. Betts, R. Gottschalg, D. G. Infield and K. Lane, "Influence of spectral effects on the performance of multijunction amorphous silicon cells," in Proc. of PV in Europe: From PV Technology to Energy Solutions Conf. and Exh., 2002.

[86]   N. Pooltananan, P. Sripadungtham, A.Limmanee and E. Hattha, "Effect of spectral irradiance distribution on the outdoor performance of photovoltaic modules," in *ECTI-CON2010: The 2010 ECTI International Confernce on Electrical Engineering/Electronics, Computer, Telecommunications and Information Technology*, 2010, pp. 71–73.

[87]   M. Schweiger, M. Ulrich, I. Nixdorf, L. Rimmelspacher, U. Jahn and W. Herrmann, "Spectral Analysis of Various Thin-Film Modules Using High Precision Spectral Response Data and Solar Spectral Irradiance Data," in Proc. 27th Eur. Photovolt. Sol. Energy Conf. Exhib. (EUPVSEC), ISBN: 3-936338-28-0 pp. 3284 - 3290. Frankfurt, Germany, 2012.

[88]   J. Chantana, Y. Imai, Y. Kawano, Y. Hishikawa, K. Nishioka and T. Minemoto, "Impact of average photon energy on spectral gain and loss of various-type PV technologies at different locations," *Renewable Energy*, vol. 145, pp. 1317–1324, 2020, doi: 10.1016/j.renene.2019.06.139.

[89]   K. Passow and M. Lee, "Effect of spectral shift on solar PV performance," in *2016 IEEE Conference on Technologies for Sustainability (SusTech)*, 2016, pp. 246–250.

[90]   T. Minemoto, Y. Nakada, H. Takahashi and H. Takakura, "Uniqueness verification of solar spectrum index of average photon energy for evaluating outdoor performance of photovoltaic modules," *Solar Energy*, vol. 83, no. 8, pp. 1294–1299, 2009, doi: 10.1016/j.solener.2009.03.004.

[91]   M. Tsuji, M. M. Rahman, Y. Hishikawa, K. Nishioka, and T. Minemoto, "Uniqueness verification of solar spectrum obtained from three sites in Japan based on similar index of average photon energy," *Solar Energy*, vol. 173, pp. 89–96, 2018, doi: 10.1016/j.solener.2018.07.039.

[92]   L. Mutiara, K. Pegels, and A. Reinders, "Evaluation of spectrally distributed irradiance in the Netherlands regarding the energy performance of various PV technologies," in *2015 IEEE 42nd Photovoltaic Specialist Conference (PVSC)*, 2015, pp. 1–6.

[93]   J. Chantana, Y. Horio, Y. Kawano, Y. Hishikawa, and T. Minemoto, "Spectral mismatch correction factor for precise outdoor performance evaluation and description of performance degradation of different-type photovoltaic modules," *Solar Energy*, vol. 181, pp. 169–177, 2019, doi: 10.1016/j.solener.2019.01.094.

[94]   B. C. Duck and C. J. Fell, "Comparison of methods for estimating the impact of spectrum on PV output," in *2015 IEEE 42nd Photovoltaic Specialist Conference (PVSC)*, 2015, pp. 1–6.

[95]   G. Belluardo, G. Barchi, D. Baumgartner, M. Rennhofer, P. Weihs, and D. Moser, "Uncertainty analysis of a radiative transfer model using Monte Carlo method within 280–2500nm region," *Solar Energy*, vol. 132, pp. 558–569, 2016, doi: 10.1016/j.solener.2016.03.050.

[96]   T. Huld and A. Gracia Amillo, "Estimating PV Module Performance over Large Geographical Regions: The Role of Irradiance, Air Temperature, Wind Speed and Solar Spectrum," *Energies*, vol. 8, pp. 5159–5181, 2015, doi: 10.3390/en8065159.

[97]   M. Langenhorst, B. Sautter, R. Schmager, J. Lehr, E. Ahlswede, M. Powalla, U. Lemmer, B. S. Richards and U. W. Paetzold, "Energy yield of all thin-film perovskite/CIGS tandem solar modules," *Prog. Photovolt: Res. Appl.*, vol. 27, no. 4, pp. 290–298, 2019, doi: 10.1002/pip.3091.

[98]   H. Liu, Z. Ren, Z. Liu, A. G. Aberle, T. Buonassisi, and I. M. Peters, "Predicted outdoor energy yield of Si based tandem solar cells," in doi: 10.1109/PVSC.2016.7749759, pp. 992–996.

[99]   R. Moreno Sáez, M. Sidrach-de-Cardona, and L. Mora-López, "Data mining and statistical techniques for characterizing the performance of thin-film photovoltaic modules," *Expert Systems with Applications*, vol. 40, no. 17, pp. 7141–7150, 2013, doi: 10.1016/j.eswa.2013.06.059.

[100]   M. Piliougine, D. Elizondo, L. Mora-López and M. Sidrach-de-Cardona, "Multilayer perceptron applied to the estimation of the influence of the solar spectral distribution on thin-film photovoltaic modules," *Applied Energy*, vol. 112, pp. 610–617, 2013, doi: 10.1016/j.apenergy.2013.05.053.

[101]   J. Del Campo-Ávila, M. Piliougine, R. Morales-Bueno, and L. Mora-López, "A data mining system for predicting solar global spectral irradiance. Performance assessment in the spectral response ranges of thin-film photovoltaic modules," *Renewable Energy*, vol. 133, pp. 828–839, 2019, doi: 10.1016/j.renene.2018.10.083.

[102]   J. M. Ripalda, J. Buencuerpo, and I. García, "Solar cell designs by maximizing energy production based on machine learning clustering of spectral variations," *Nature Communications*, vol. 9, no. 1, p. 5126, 2018, doi: 10.1038/s41467-018-07431-3.

[103]   T. Huld, E. Dunlop, H. G. Beyer, and R. Gottschalg, "Data sets for energy rating of photovoltaic modules," *Solar Energy*, vol. 93, pp. 267–279, 2013, doi: 10.1016/j.solener.2013.04.014.

[104]   A. Kimber, T. Dierauf, L. Mitchell, C. Whitaker, T. Townsend, J. NewMiller, D. King, J. Granata, K. Emery, C. Osterwald, D. Myers, B. Marion, A. Pligavko, A. Panchula, T. Levit-sky, J. Forbess, F. Talmud, "Improved test method to verify the power rating of a photovoltaic (PV) project," in *2009 34th IEEE Photovoltaic Specialists Conference (PVSC)*, 2009, pp. 316–321.

[105]   W. Köppen, Ed., *Das geoghaphisca System der Klimate*. Berlin: Gebrüder Borntraeger, 1936. [Online]. Available: http://koeppen-geiger.vu-wien.ac.at/pdf/Koppen_1936.pdf

[106]   K. Scharmer *et al., The European Solar Radiation Atlas Vol.2: Database and exploitation software*, 2000.

[107]   J. C. Blakesley T. Huld, H. Müllejans, A. Gracia-Amillo, G. Friesen,T.R. Betts and W. Hermann, "Accuracy, cost and sensitivity analysis of PV energy rating," *Solar Energy*, vol. 203, pp. 91–100, 2020, doi: 10.1016/j.solener.2020.03.088.

158

[108]   A. Marzo, P. Ferrada, F. Beiza, P. Besson, J. Alonso-Montesinos, J. Ballestrín, R. Román, C. Portillo, R. Escobar, E.Fuentealba, "Standard or local solar spectrum? Implications for solar technologies studies in the Atacama desert," *Renewable Energy*, vol. 127, pp. 871–882, 2018, doi: 10.1016/j.renene.2018.05.039.

[109]   J.-F. Lelièvre, E. Cabrera, B. Hladys, N. Pinochet, V. Gutierrez, A. Marzo, P. Ferrada, D. Muñoz and A. Derrier, "Development of Ultra-Accelerated Ageing Tests for Improved Reliability and Durability of Bifacial Photovoltaic Modules in Harsh Desert Conditions," in Proc. 36th Eur. Photovolt. Sol. Energy Conf. Exhib. (EUPVSEC). Marseille, France, 2019.

[110]   R. N. Dows and E. J. Gough, "PVUSA procurement, acceptance, and rating practices for photovoltaic power plants," report, University of North Texas, United States, 1995. [Online]. Available: https://digital.library.unt.edu/ark:/67531/metadc621398/

[111]   N. Martin Chivelet and J. M. Ruiz, "Corrigendum to "Calculation of the PV modules angular losses under field conditions by means of an analytical model" [Sol. Energy Mater. Sol. Cells 70 (1) (2001) 25–38]," *Solar Energy Materials and Solar Cells*, vol. 110, p. 154, 2013, doi: 10.1016/j.solmat.2012.11.002.

[112]   *IEC 60904-8: Photovoltaic devices – Measurement of spectral responsivity of a photovoltaic (PV) device*, 3.0th ed., International Electrotechnical Commission, 2014.

[113]   D. Faiman, "Assessing the outdoor operating temperature of photovoltaic modules," *Prog. Photovolt: Res. Appl.*, vol. 16, no. 4, pp. 307–315, 2008, doi: 10.1002/pip.813.

[114]   M. Koehl, M. Heck, S. Wiesmeier, and J. Wirth, "Modeling of the nominal operating cell temperature based on outdoor weathering," *Solar Energy Materials and Solar Cells*, vol. 95, no. 7, pp. 1638–1646, 2011, doi: 10.1016/j.solmat.2011.01.020.

[115]   G. Bardizza, E. Salis, and E. D. Dunlop, "Power matrix of OPV mini-module under steady conditions of temperature and irradiance at large-area solar simulator," *Solar Energy*, vol. 204, pp. 542–551, 2020, doi: 10.1016/j.solener.2020.04.067.

[116]   T. Huld, R. Gottschalg, H. G. Beyer, and M. Topič, "Mapping the performance of PV modules, effects of module type and data averaging," *Solar Energy*, vol. 84, no. 2, pp. 324–338, 2010, doi: 10.1016/j.solener.2009.12.002.

[117]   T. Huld *et al.,* "A power-rating model for crystalline silicon PV modules," *Solar Energy Materials and Solar Cells*, vol. 95, no. 12, pp. 3359–3369, 2011, doi: 10.1016/j.solmat.2011.07.026.

[118]   C. Monokroussos, X. Y. Zhang, M. Schweiger, D. Etienne, S. Liu, A. Zhou, V. Feng, Y. Zhang and C. Zou, "Energy rating of c-Si and mc-Si commercial PV modules in accordance with IEC 61853-1,-2,-3 and impact on the annual yield," in Proc. 33rd Eur. Photovolt. Sol. Energy Conf. Exhib. (EUPVSEC), ISBN: 3-936338-47-7 pp. 1438 - 1444. Amsterdam, Netherlands, 2017.

[119]   P. Vourlioti, T. Huld, A.M. Gracia Amillo, M. Norton, "Geospatial Mapping of Spectral Mismatch of Multi-Junction Photovoltaic Modules Using Satellite-Retreived Spectral Irradiance Data," in Proc. 31st Eur. Photovolt. Sol. Energy Conf. Exhib. (EUPVSEC), ISBN: 3-936338-39-6 pp. 2017 - 2021. Hamburg, Germany, 2015.

[120]   M.R. Vogt, S. Riechelmann, A.M. Gracia Amillo, A. Driesse, A. Kokka, K. Maham, P. Kärhä, R.P. Kenny, C. Schinke, K. Bothe, J.C. Blakesley, E. Music, F. Plag, G. Friesen, G. Corbellini, N. Riedel-Lyngskær, R.M.E. Valckenborg, M. Schweiger, and W. Herrmann, "Interlaboratory Comparison of the PV Module Energy Rating Standard IEC 61853-3," 4BO.13.2, in Proc. 38th Eur. Photovolt. Sol. Energy Conf. Exhib. (EUPVSEC). EU PVSEC 2020, 2020.

[121]   A. Driese, *PV Performance Labs Tools for Python*: GitHub repository, 2020. [Online]. Available: https://github.com/adriesse/pvpltools-python

[122]   *IEC 60904-10: Photovoltaic devices - Part 10: Methods of linear dependence and linearity measurements*, 3.0th ed., International Electrotechnical Commission, 2020.

[123]   C. Monokroussos, H. Müllejans, Q. Gao, and W. Herrmann, "I-V translation procedure for higher accuracy and compliance with PERC cell technology requirements," 4AV.2.19, in Proc. 38th Eur. Photovolt. Sol. Energy Conf. Exhib. (EUPVSEC). EU PVSEC 2020, 2020.

[124]   *IEC 60891 (Draft) Photovoltaic devices - Procedures for temperature and irradiance corrections to measured I-V characteristics.*, 3.0th ed., International Electrotechnical Commission.

[125]   S. Ransome and J. Sutterlueti, "A Systematic Comparison of 12 Empirical Models Used for Energy Yield Predictions vs PV Technology," in Proc. 33rd Eur. Photovolt. Sol. Energy Conf. Exhib. (EUPVSEC), ISBN: 3-936338-47-7 pp. 1445 - 1450. Amsterdam, Netherlands, 2017.

[126]   W. Herrmann, S. Zamini, F. Fabero, T. Betts, N. van der Borg, K. Kiefer, G. Friesen, H. Müllejans, H.-D. Mohring, M.A. Vazquez, D. Fraile Montoro, "PV Module Output Power Characterisation in Test Laboratories and in the PV Industry - Results of the European PERFORMANCE Project," in Proc. 25th Eur. Photovolt. Sol. Energy Conf. Exhib. (EUPVSEC), ISBN: 3-936338-26-4 pp. 3879 - 3883. Valencia, Spain, 2010.

[127]   E. Salis, D. Pavanello, M. Field, U. Kräling, F. Neuberger, K. Kiefer, C. Osterwald, S. Rummel, D. Levi, Y. Hishikawa, K. Yamagoe, H. Ohshima, M. Yoshita, and H. Müllejans, "Improvements in world-wide intercomparison of PV module calibration," *Solar Energy*, vol. 155, pp. 1451–1461, 2017, doi: 10.1016/j.solener.2017.07.081.

[128]   C.W. Hansen, K.A. Klise, J.S. Stein, Y. Ueda, K. Hakuta, "Calibration of Photovoltaic Module Performance Models Using Monitored System Data," in Proc. 29th Eur. Photovolt. Sol. Energy Conf. Exhib. (EUPVSEC), ISBN: 3-936338-34-5 pp. 3472 - 3476. Amsterdam, Netherlands, 2014.

[129]   C. W. Hansen, K. A. Klise, and J. S. Stein, "Data requirements for calibration of photovoltaic system models using monitored system data," in *IEEE 42nd Photovoltaic Specialist 2015*, doi: 10.1109/PVSC.2015.7356173, pp. 1–5.

[130]   *Method of testing to determine the thermal performance of solar collectors*, ASHRAE-93-1986/XAB, 1.0th ed., American Society of Heating, Refrigerating and Air-Conditioning Engineers (ASHRAE), 1985.

[131]   B. H. King and C. D. Robinson, "Simplifying methods to calibrate the Sandia Array Performance Model," in 6th PV Performance Modeling Workshop. [Online]. Available: https://www.osti.gov/servlets/purl/1404812 Freiburg, Germany, 25 October, 2016.

[132]   R. Singh *et al.,* "Analyses of measurement parameters for laboratory characterization of the operating temperature coefficients of CI(G)S PV modules," in *2016 IEEE 43rd Photovoltaic Specialists Conference (PVSC)*, 2016, pp. 3095–3099.

[133]   Internationale Elektrotechnische Kommission, "Photovoltaic (PV) module performance testing and energy rating: IEC 61853-1," Geneva, International standard / International Electrotechnical Commission, 2011.

[134]   Internationale Elektrotechnische Kommission, "Photovoltaic (PV) module performance testing and energy rating: IEC 61853-4," Geneva, International standard / International Electrotechnical Commission IEC 61853-4, 2018.

[135]   N. Martín and J. M. Ruiz, "A new model for PV modules angular losses under field conditions," *International Journal of Solar Energy*, vol. 22, no. 1, pp. 19–31, 2002, doi: 10.1080/01425910212852.

[136]   Internationale Elektrotechnische Kommission, "Photovoltaic (PV) module performance testing and energy rating: IEC 61853-2," Geneva, International standard / International Electrotechnical Commission IEC 61853-2, 2016.

[137]   Internationale Elektrotechnische Kommission, "Photovoltaic (PV) module performance testing and energy rating: IEC 61853-3," Geneva, International standard / International Electrotechnical Commission IEC 61853-3, 2018.

[138]   W. Heydenreich, B. Müller, and C. Reise, "Describing the World With Three Parameters: A New Approach to PV Module Power Modelling," 2008, doi: 10.4229/23RDEUPVSEC2008-4DO.9.4.

[139]   A. Driesse, *PV Performance Labs Tools for Python*. GitHub repository. [Online]. Available: https://github.com/adriesse/pvpltools-python

[140]   A. Driesse and J. Stein, "From IEC 61853 power measurements to PV system simulations: SANDIA REPORT," Sandia National Laboratories, 2020.

[141]   *IEC 61724-1: Photovoltaic system performance – Part 1: Monitoring*, 1.0, International Electrotechnical Commission, 2017.

[142]   J. Blakesley, J. Holder, G. Koutsourakis, S. Douglas, R. Abrams, F. Mukadam, D. Ruiz, "Spectrally corrected albedo," in bifiPV workshop. Amsterdam, Netherlands, 2019.

[143]   C. Monokroussos, Q. Gao, X.Y. Zhang, E. Lee, Y. Wang, C. Zou, L. Rimmelspache, J. Bonilla Castro, M. Schweiger, W. Herrmann, "Rear-side spectral irradiance at 1 sun and application to bifacial module power rating," *Prog. Photovolt: Res. Appl.*, vol. 28, no. 8, pp. 755–766, 2020, doi: 10.1002/pip.3268.

[144]   M.R. Vogt, T. Gewohn, K. Bothe, C. Schinke, R. Brendel, "Impact of Using Spectrally Resolved Ground Albedo Data for Performance Simula-tions of Bifacial Modules," in Proc. 35th Eur. Photovolt. Sol. Energy Conf. Exhib. (EUPVSEC), ISBN: 3-936338-50-7 pp. 1011 - 1016. Brussels, Belgium, 2018.

[145]   G.C. Eder, K. Knöbl, L. Maul, M. Aichinger, G. Peharz, W. Nemitz, K.A. Berger, "Designed BIPV-Elements with Printed Front-Glass: Simulation and Experimental Evaluation of the Effect of Printing on the Electrical Performance," (Poster), in Proc. 33rd Eur. Photovolt. Sol. Energy Conf. Exhib. (EUPVSEC), ISBN: 3-936338-47-7. Amsterdam, Netherlands, 2017.

[146]   R.M.E. Valckenborg, B. Van Aken, "IEC61853-Matrix Analysis of PVPS Task 15 BIPV Round-Robin for more than one year at seven test sites over the world," in Proc. 37th Eur. Photovolt. Sol. Energy Conf. Exhib. (EUPVSEC). (Virtual), 2020.

[147]   G.C. Eder, G. Peharz, P. Bonomo, E. Saretta, F. Frontini, C. Polo, H. Wilson, J. Eisenlohr, N. Martin, S. Karlsson, N. Jakica, A. Zanell, D. Moor, T. Kolas and M. Van der Donker, "Coloured BIPV : Market, Research and Development," Report IEA-PVPS T15-07: 2019, International Energy Agency, Feb. 2019.

[148]   SMART-FLEX project, *Demonstration at industrial scale of the FLeXible manufacturing of SMART multifunctional photovoltaic building elements: Project ID: 322434*. Funded by European Union's Seventh Framework Programme, 2013-2016. Accessed: November 29th, 2017. [Online]. Available: http://www.smartflexsolarfacades/

[149]   CONSTRUCT PV Project, *Constructing buildings with customizable size PV modules integrated in the opaque part of the building skin: FP7-ENERGY-2011-2, ENERGY.2011.2.1-4*. European Union Seventh Framework Programme (FP7), 2013-2018. [Online]. Available: www.constructpv.eu

[150]   Sunage SA, *Photovoltaic PV module manufacturer Werbsite.* Accessed: November 14th, 2020. [Online]. Available: www.sunage.ch

[151]   Hochschule Luzern. Envelopes and Solar Energy Competence Centre within the Hochschule Luzern. Accessed: November 14th, 2020. [Online]. Available: https://www.hslu.ch/en/lucerne-school-of-engineering-architecture/research/competence-centers/gebaeudehuelleundingenieurbau/gebaeudehuelle/envelopes-and-solar-energy/

[152]   G.C. Eder, K. Knöbl, L. Maul, M. Aichinger, G. Peharz, W. Nemitz, K.A. Berger, "Designed BIPV-Elements with Printed Front-Glass: Simulation and Experimental Evaluation of the Effect of Printing on the Electrical Performance," 6BV.3.57, in Proc. 33rd Eur. Photovolt. Sol. Energy Conf. Exhib. (EUPVSEC), ISBN: 3-936338-47-7. Amsterdam, Netherlands, 2017.

[153]   F. Frontini, P. Bonomo, E. Saretta, T. Weber, J. Berghold, "Indoor and Outdoor Characterization of Innovative Colored BIPV Modules for Façade Application," in Proc. 32nd Eur. Photovolt. Sol. Energy Conf. Exhib. (EUPVSEC), ISBN: 3-936338-41-8 pp. 2498 - 2502. Munich, Germany, 2016.

[154]   C. Tzikas, R.M.E. Valckenborg, M. Dörenkämper, M.N. van den Donker, D. Duque Lozano, A. Bognar, R. Loonen, J.L.M. Hensen, W. Folkerts, "Outdoor Characterization of Colored and Textured Prototype PV Façade Elements," in Proc. 35th Eur. Photovolt. Sol. Energy Conf. Exhib. (EUPVSEC), ISBN: 3-936338-50-7 pp. 1468 - 1471. Brussels, Belgium, 2018.

[155]   G. Peharz and A. Ulm, "Quantifying the influence of colors on the performance of c-Si photovoltaic devices," *Renewable Energy*, vol. 129, pp. 299–308, 2018, doi: 10.1016/j.renene.2018.05.068.

[156]   R. R. Molinero, G. Friesen and M. Caccivio, "ENHANCE: Next Generation Photovoltaic Performance: Final Report," University of Applied Sciences and Arts of Southern Switzerland (SUPSI), Canobbio, Nov. 2019. [Online]. Available: https://www.aramis.admin.ch/Default.aspx?DocumentID=64923&Load=true

[157]   B. Mahiylov, M. Bliss, T.R. Betts, R. Gottschalg, "Uncertainty in photovoltaic module energy rating," in *Proceedings of the 11th Photovoltaic Science, Applications and Technology Conference C97 (PVSAT-11).* [Online]. Available: https://hdl.handle.net/2134/17784

[158]   S. Pfenninger and I. Staffell, "Long-term patterns of European PV output using 30 years of validated hourly reanalysis and satellite data," *Energy*, vol. 114, pp. 1251–1265, 2016, doi: 10.1016/j.energy.2016.08.060.

[159]   M. Šúri, T. A. Huld, and E. D. Dunlop, H. A. Ossenbrink, "Potential of solar electricity generation in the European Union member states and candidate countries," *Solar Energy*, vol. 81, no. 10, pp. 1295–1305, 2007, doi: 10.1016/j.solener.2006.12.007.

[160]   W. van Sark, T. Nordmann, L. Clavadetscher, and M. Green, *Analysis of Long-Term Performance of PV Systems Different Data Resolution for Different Purposes*2014.

[161]   B. Kausika, P. Moraitis, and W. van Sark, "Visualization of Operational Performance of Grid-Connected PV Systems in Selected European Countries," *Energies*, vol. 11, p. 1330, 2018, doi: 10.3390/en11061330.

[162]   J. Leloux, L. Narvarte, and D. Trebosc, "Review of the performance of residential PV systems in France," *Renewable and Sustainable Energy Reviews*, 2012, doi: 10.1016/j.rser.2011.10.018.

[163]   J. Leloux, L. Narvarte, and D. Trebosc, "Review of the performance of residential PV systems in Belgium," *Renewable and Sustainable Energy Reviews*, 2012, doi: 10.1016/j.rser.2011.07.145.

[164]   N. H. Reich, B. Mueller, A. Armbruster, W. G. J. H. M. van Sark, K. Kiefer, and C. Reise, "Performance ratio revisited: is PR > 90% realistic?," *Prog. Photovolt: Res. Appl.*, vol. 20, no. 6, pp. 717–726, 2012, doi: 10.1002/pip.1219.

[165]   P. Moraitis, B. Kausika, N. Nortier, and W. van Sark, "Urban Environment and Solar PV Performance: The Case of the Netherlands," *Energies*, vol. 11, p. 1333, 2018, doi: 10.3390/en11061333.

[166]   Y.-M. Saint-Drenan, L. Wald, T. Ranchin, L. Dubus, and A. Troccoli, "An approach for the estimation of the aggregated photovoltaic power generated in several European countries from meteorological data," *Advances in Science and Research*, vol. 15, pp. 51–62, 2018, doi: 10.5194/asr-15-51-2018.

[167]   S. Killinger *et al.,* "On the search for representative characteristics of PV systems Data collection and analysis of PV system azimuth, tilt, capacity, yield and shading," *Solar Energy*, vol. 173, pp. 1087–1106, 2018, doi: 10.1016/j.solener.2018.08.051.

[168]   J. Bright and S. Killinger, "Corrigendum to "On the search for representative characteristics of PV systems: Data collection and analysis of PV system azimuth, tilt, capacity, yield and shading" [Sol. Energy 173 (2018) 1087-1106]," *Solar Energy*, vol. 187, pp. 290–292, 2019, doi: 10.1016/j.solener.2019.04.030.

[169]   M. Matlab, *Fit probability distribution object to data - MATLAB fitdist.* [Online]. Available: https://nl.math-works.com/help/stats/fitdist.html#btu538h-distname

[170]   W.G.J.H.M. van Sark, L. Bosselaar, P. Gerrissen, K. Esmeijer, P. Moraitis, M. van den Donker, G. Emsbroek, "Update of the Dutch PV Specific Yield for Determination of PV Contribution to Renewable Energy Production: 25% More Energy!," in *Proc. 29th Eur. Photovolt. Sol. Energy Conf. Exhib. (EUPVSEC)*, pp. 4095–4097.

[171]   G. Friesen and W. Herrmann, G. Belluardo, B. Herteleer, J. Sutterlütti A. Driesse, K, Emery, M.Schweiger, "Photovoltaic Module Energy Yield Measurements: Existing Approaches and Best Practice: IEA PVPS T13-11," Report IEA-PVPS T13-12:2018, International Energy Agency, Paris, France, 2018.

[172]   J. Bonilla Castro, "Electrical Stability of PV Modules Operating in Various Open-Air Climates," Master Thesis, Colgone University of Applied Sciences (TH Kön), Cologne, Germany, 2016.

[173]   D. C. Jordan and S. R. Kurtz, "Thin-film reliability trends toward improved stability," in *2011 37th IEEE Photovoltaic Specialists Conference*, 2011, pp. 827–832.

[174]   C. Radue and E.E. van Dyk, "Degradation analysis of thin film photovoltaic modules," *Physica B: Condensed Matter*, vol. 404, no. 22, pp. 4449–4451, 2009, doi: 10.1016/j.physb.2009.09.011.

[175]   K. Kirtikara, "Lessons learnt from using PV standalone systems to provide a better quality of life for rural people," 4-3, 2004.

[176]   DEDE, "Thailand PV status report 2018: Department of Alternative Energy Development and Efficiency," Ministry of Energy, 2019.

[177]   Ministry of Energy, "PDP: National Electricity Generation Development Plan: VER 2018-2580," Ministry of Energy, Thailand, 2018. [Online]. Available: https://www.egat.co.th/images/businessop/PDP2018-apr2019.pdf

[178]   A. Limmanee, N. Udomdachanut, S. Songtrai, S. Kaewniyompanit, Y. Sato, M. Nakaishi, S. Kittisontirak, K. Sriprapha, and Y. Sakamoto, "Field performance and degradation rates of different types of photovoltaic modules: A case study in Thailand," *Renewable Energy*, vol. 89, pp. 12–17, 2016, doi: 10.1016/j.renene.2015.11.088.

[179]   Y. Sangpongsanont, C. Limsakul, M. Seapan, B. Muenpinij, T. Chenvidhya, C. Jiva-cate, D. Chenvidhya, and K. Kirtikara, "Long-Term Monitoring of a Small Residential Rooftop Pv Gird-Connected System in Thailand," in *23rd Photovoltaic Science and Engineering Conf.*

[180]   Y. Sangpongsanont, D. Chenvidhya, S. Chuangchote, M. Seapan, K. Kirtikara, P. Parinya, C. Limsakul, T. Chenvidhya, and B. Muenpinij, "Thirteen-year Long-term Monitoring and Reli-ability of PV Module Degradation in Thailand," in *26th Photovoltaic Science and Engineering*.

[181]   *IEC 61215-1-1: Terrestrial photovoltaic (PV) modules - Design qualification and type approval - Part 1-1: Special requirements for testing of crystalline silicon photovoltaic (PV) modules*, 1.0, International Electrotechnical Commission, 2016.

[182]   Y. Sangpongsanont, D. Chenvidhya, S. Chuangchote, and K. Kirtikara, "Corrosion growth of solar cells in modules after 15 years of operation," *Solar Energy*, vol. 205, pp. 409–431, 2020, doi: 10.1016/j.solener.2020.05.016.

[183]   M. Köntges, S. Kurtz, C. Packard, U. Jahn, K. A. Berger, K. Kato, T. Friesen, H. Liu, M. Van Iseghem, J. Wohlgemuth, D. Miller, M. Kempe, P.H., F. Reil, N. Bogdanski, W. Herrmann, C. Buerhop-Lutz, G. Razongles, Friesen, G, "Review of Failures of Photovoltaic Modules: Report IEA-PVPS T13-01:2014," IEA Report Photovoltaic Systems Programme, International Energy Agency.

ANNEX 1 MODELLING VALIDATION DATA SET

This Annex 1 describes some data files containing measured module data of a standard crystalline silicon module. The intention is to provide an open source data set that contains all of the necessary input data to calculate the energy yield of a module together with 1 year of real outdoor data for comparison. The data sets have been made available on the PV Performance Modelling Collaborative website [54].

The data set is divided into two parts, which includes:

A.   Module characterisation data

- P_{max}, I_{sc}, and V_{oc} matrix
- Temperature coefficient α, β and δ
- Spectral response curve
- Angular loss curve
- Thermal coefficients U0 and U1

B.   1 year real operating data (5 minute intervals)

- P_{max}, I_{sc} and V_{oc} extracted from I-V curves
- Module temperature T_{mod}
- In plane irradiance G_{poa}
- Horizontal irradiance G_{hor}
- Diffuse irradiance G_{diff}
- Ambient temperature T_{amb}
- Wind speed ws

Module characterisation

The module characterisation according IEC 61853-1:2011 [3] and IEC 61853-2:2016 [4] is performed by SUPSI PVLab, an ISO 17025-accredited test lab. The measurement uncertainties of the single measurements are included in the data files. The module was stabilised prior characterisation.

The I-V curves at different irradiances (100 - 1100 W/m²) and temperatures (15°C - 75°C) are measured with a Class A+A+A+ PASAN IIIB solar simulator equipped with different neutral density filters for the adjustment of irradiance and a thermal box for the regulation of temperature.

The spectral response, used also for the spectral mismatch correction of the I-V curves, is measured on the same solar simulator, but by placing 28 narrow band-pass filters from 360 to 1200 nm in front of the light source.

The angle of incidence (AOI) dependency is measured on the same set-up, by rotating the module from 0 - 85° in front of the solar simulator and by shading a single cell to obtain the change of I_{sc} for a single cell. The approach follows the non-destructive procedure developed and validated by Herrmann et al. in [43].

The thermal coefficients (U0 andU1) are measured outdoors on an open-rack equipped with maximum power point trackers (MPPT). The module temperature (T_{mod}) is monitored in five second intervals simultaneously to the wind speed (ws), ambient temperature (T_{amb}) and in-plane irradiance (G_{poa}).

Module energy yield measurements

The energy yield of the module is monitored for one year. The I-V curves are recorded at intervals of five minutes together with the module temperature (T_{mod}) and the irradiance. Following irradiance values are measured: horizontal global (G_{hor}), diffuse irradiance (G_{diff}) and in-plane global (G_{poa}) and spectral irradiance (G_{spec}). The in-plane irradiance is measured with a calibrated Kipp&Zone CMP21 pyranometer and an EKO MS-710/712 (350-1700nm) spectroradiometer. Wind speed (ws) and wind direction (wd), ambient temperature (T_{amb}) and humidity (hum) is monitored separately through the meteo tower located in close proximity to the energy yield test stand.